The Effects of Sulforaphane on Normal and Cancerous epithelial Cells

Yaser Eidah Alqurashi

A thesis submitted in fulfilment of the requirements for the degree of Doctor of Philosophy

School of Biological Sciences

University of East Anglia

September 17

Abstract

The cytoskeleton plays vital roles in many cell functions and any disorder could lead to different diseases such as cancer, which causes uncontrolled cell division, cell motility and invasion. Cell migration is important for developmental morphogenesis, tissue repair and tumour metastasis. During the migration process, microtubule organisation and dynamics play important roles, and are regulated by Plus-end Tracking (+TIP) proteins. A better understanding of cell migration mechanisms could lead to an efficient treatment for invasive cancer cells such as pancreatic cancer. Sulforaphane (SFN) is a potential treatment for different cancer types with various possible means of action. Studies have indicated that SFN has the potential to slow down the progression of cancer, promote apoptosis and suppress cell proliferation. However, how SFN affects microtubule dynamics, stability and organisation is poorly understood.

This project investigated the effect of SFN on microtubule organisation and dynamics and the impact on cell migration. Certain pancreatic cancers show up-regulation of the end-binding protein EB2 and the tubulin deacetylase HDAC6 which both influence microtubule dynamics and stability and thus also cell migration. Other cancers such as breast cancer have reported an up-regulation in EB1. This project therefore focused on the effects of SFN on EB1, EB2 and HDAC6 expression and localisation and the consequences for cell migration.

The impact of SFN on normal (ARPE-19) and cancerous (Panc-1) epithelial cell migration was assessed by live time-lapse imaging of sparsely seeded cells. Microtubule and actin filament organisation was assessed to observe the effects of SFN on the treated cells. The impact of SFN on EB and HDAC6 localisation and expression was determined by immuno-labelling. Experiments involving SFN treatment with or without functional inhibition of HDAC6 (with the HDAC6 inhibitor tubacin) were carried out and their effect on cell migration was investigated. The effect of SFN on microtubule dynamics and stability was assessed by analysing live time-lapse GFP-CLIP-170 dynamics. Microtubule post-

translational modifications were studied by immuno-labelling in SFN treated cells. Focal adhesion area and dynamics were also assessed by FRAP and immuno-labelling in SFN treated cells.

SFN treatment caused a dramatic decrease in the speed of random migration and cell area in ARPE-19 cells. A marked co-alignment between microtubules and actin filaments, increased EB1 decoration of the microtubule lattice and an apparent increase in cytoplasmic EB2 were also observed upon SFN treatment. However, SFN treated Panc-1 cells revealed no significant decrease in the speed of random cell migration. Interestingly, a combination of tubacin and SFN caused a significant decrease in the speed of cell migration. Analysis of microtubule dynamics in GFP-CLIP-170 expressing cells revealed that SFN treated cells possessed less dynamic microtubules. There was also evidence of SFN inducing microtubule stability.

The results suggest that SFN or a combination of tubacin and SFN could be promising treatments for cancer. Moreover, these results can provide a better understanding of the effects of SFN on the organisation of the cell cytoskeleton. Treatment with SFN resulted in interesting changes in EB and HDAC6 localisation, which may provide potential targets for effective cancer treatments.

Acknowledgements

In the name of Allah, the most gracious, the most merciful

First and foremost, I give praise, hour and glory to Allah the Lord of the universe, without his bounty, grace and blessings this work would never have been accomplished.

I would like to express my heartfelt gratitude to my supervisor Dr. Mette Mogensen for her professional guidance and support during all stages of this research journey. Mette was not only my supervisor but also my mentor. I am most indebted to her patience and invaluable advice that inspired me to see things positively, and felt honoured with her confidence and trust in my ability. Thank you Mette, for giving me the opportunity to work with you. I would like also extend my sincere thanks and appreciation to Dr. Paul Thomas and Dr. Elizabeth Lund for all constructive advice, support and suggestion. I would like to thank all the current and former lab members; Tope Amodu, James, Ben, Julia, Debbie and Jonathan for providing help, advice and support.

I am grateful to the Saudi Government, the ministry of High Education, for the full scholarship and for giving me this opportunity to join the University of East Anglia, and gain unmatched educational experience in one of the best universities in the world. I am also grateful for the great atmosphere and studying conditions that the School of Biological Sciences and the BMRC provided, and big thanks go to all the staff, it was grate to work with you.

Last but not least, I owe my loving thanks to my mum Aljohara, my beloved wife Dr.Tahani, my son Sultan, my daughter Yasmin, and my whole family, for their love, unremitting prayers, support and encouragement throughout my study. Without endless support I would not have made it to this point. I hope that I have made you proud.

DEDICATION

To my dear mother and father, my beloved wife, son, daughter,

brothers and sisters

with honest love and respect…

Table of Contents

Abstract ..... **II**

Acknowledgements ..... **IV**

DEDICATION ..... **V**

Table of Contents ..... **VI**

List of Figures ..... **XII**

List of Tables ..... **XVII**

List of Abbreviations ..... **XVIII**

Chapter I: Introduction **1**

1.1 Sulforaphane and the cytoskeleton **2**

1.2 The Cytoskeleton and Cancer **2**

1.2.1 Pancreatic cancer 4

1.3 The Cytoskeleton **8**

1.3.1 Actin 8

1.3.1.2 Intermediumte filaments 12

1.4 Microtubules **13**

1.4.1 Microtubule structure 13

1.4.2 Microtubule nucleation 18

1.4.3 Microtubule minus-end associated proteins and microtubule anchorage 21

1.4.4 Post-translational modifications 22

1.4.4.1 The detyrosination/tyrosination cycle 23

1.4.4.2 Acetylation 24

1.4.4.3 Other post-translational modification 28

1.5 Microtubule Dynamics and Microtubule-associated Proteins **29**

1.5.1 Dynamic instability 29

1.5.2 Polymerases and depolymerases 30
1.5.3 Microtubule plus-end tracking proteins (+TIP) 31
1.5.3.1 The end binding proteins 32
1.5.3.2 Cytoskeleton-associated protein Gly-rich (CAP-Gly) proteins 37
1.5.3.3 Other +TIPs 38
1.6 Cell Migration 40
1.6.1 Cytoskeletal organisation in migrating cells 43
1.7 Sulforaphane (SFN) 53
1.8 Summary 59
1.9 Hypothesis and Aims 61

Chapter II: Materials & Methods 62

2.1 Cell culture 63
2.1.1 Maintenance of cell lines 63
2.1.1.1 Passaging of cell lines 64
2.1.1.2 Freezing and thawing cells 64
2.1.1.3 Cell counting 65
2.1.2 Seeding cells 65
2.2 Drug treatments 66
2.2.1 Sulforaphane (SFN) 66
2.2.2 Tubacin 66
2.3 Cell viability assay (MTT assay) 67
2.4 Transfection of plasmids 68
2.5 Fixation 69
2.6 Immunolabelling 69
2.7 Western blotting 73
2.7.1 Cell lysis 73
2.7.2 Protein quantification 73
2.7.3 SDS-PAGE electrophoresis 74

2.7.3.1 Protein transfer 74
2.7.4 Protein detection 75
2.7.4.1 Antibody probing 75
2.7.4.2 Immuno-detection 75
2.7.4.3 Re-probing 76
2.7.5 Fluorescence Western Blot - Odyssey 76
2.8 Microscopy 77
2.8.1 Widefield fluorescence 77
2.8.2 Live imaging of migrating cells 77
2.8.3 Live imaging of CLIP-170 dynamics 78
2.8.4 Confocal microscopy and FRAP of focal adhesion 78
2.9 Random cell migration 79
2.10 Cold treatment 79
2.11 Analysis of microtubule acetylation 80
2.12 Analysis of area and shape of EB1 and lattice intensity 81
2.13 Analysis of CLIP-170 comet dynamics 82
2.14 FRAP analysis 82
2.15 Statistical analysis 83

Chapter III: Characterisation of Model Cell lines 84
3.1 Overview 85
3.2 Introduction 85
3.3 Results 88
3.3.1 Characterisation of ARPE-19 and PANC-1 cells 88
3.3.2 Microtubule organisation and tubulin modifications 88
3.3.3 Actin organisation 89
3.3.4 End-binding protein expression and localisation 90
3.3.5 HDAC6 localisation and expression 91

3.4 Discussion 92

Chapter IV: Effects of Sulforaphane on Random Cell Migration 112

4.1 Overview 113

4.2 Introduction 113

4.3 Results 115

4.3.1 SFN concentrations greater than 30 µM dramatically decrease cell viability in AREP-19 and PANC-1 cells 115

4.3.2 SFN treatment causes distinct morphological changes 116

4.3.3 SFN treatment causes a decrease in the migration speed of ARPE-19 cells 117

4.3.4 SFN treatment alters microtubule organisation and leads to the formation of distinct bundles 119

4.3.5 Actin filaments co-aligned with microtubules in SFN treated ARPE-91 cells 120

4.3.6 EB1 is expressed along the microtubule lattice in SFN treated ARPE-19 and PANC-1 cells 121

4.3.7 EB2 is localised along microtubules and is free in the cytoplasm in SFN treated ARPE-19 and PANC-1 cells 123

4.3.8 HDAC6 is mainly localised in the cytoplasm in SFN-treated ARPE-19 and PANC-1 cells 124

4.3.9 Tubacin treatment has no effect on cell viability in ARPE-19 and PANC-1 cells 125

4.3.10 Inhibition of HDAC6 with tubacin causes cell spreading in ARPE-19 and PANC-1 cells 126

4.3.11 Tubacin induces a marked increase in acetylated microtubules in ARPE-19 and PANC-1 cells 127

4.3.12 A combination of tubacin and SFN causes a significant reduction in cell migration speed 128

4.3.13 Treatment with tubacin on its own has no effect on EB1 localisation and expression in ARPE-19 and PANC-1 cells 129

4.3.14 Tubacin only treatment has no effect on EB2 localisation and expression in ARPE-19 and PANC-1 cells 131

4.3.15 Tubacin treatment does not lead to co-localisation of HDAC6 and microtubules 132

4.4 Discussion 138

4.4.1 SFN caused an increase in cell area in ARPE-19 and PANC-1 cells 138

4.4.2 SFN caused a dramatic decrease in ARPE-19 cell migration 139

4.4.3 SFN altered microtubule and actin organisation and resulted in EB1 decorating the microtubule lattice while EB2 became cytoplasmic 140

4.4.4 SFN treatment caused loss of HDAC6 localisation along microtubule lattices in ARPE-19 and PANC-1 cells 142

4.4.5 Combination treatments of tubacin and SFN inhibited PANC-1 cell migration 142

Chapter V: Sulforaphane Treatment and Microtubule Dynamics and Stability 189

5.1 Overview 190

5.2 Introduction 190

5.3 Results 195

5.3.1 SFN treated ARPE-19 but not PANC-1 cells express more acetylated microtubules 195

5.3.2 SFN treated ARPE-19 but not PANC-1 cells reveal an increase in detyrosinated tubulin 197

5.3.3 SFN treatment affects microtubule dynamics in ARPE-19 cells 197

5.3.4 SFN treatment increases focal adhesion area AREP-19 cells 199

5.3.5 SFN treatment and focal adhesion dynamics in ARPE-19 and PANC-1 cells 200

5.4 Discussion 204

5.4.1 SFN increases acetylated and detyrosinated microtubules and inhibits microtubule dynamics in ARPE-19 but not in PANC-1 cells 204

5.4.2 SFN treatment leads to increased focal adhesion area and size in ARPE-19 but not in PANC-1 cells 206

5.4.3 SFN treatment did not inhibit focal adhesion turnover 207

Chapter VI: General Discussion 228

6.1 Introduction 229

6.1.1 Research findings 231

6.2 General discussion 232

6.3 Future work 239

Appendices 241

Appendix A: Reagents and Solutions 242

Appendix B: Supplementary Data 247

References 255

List of Figures

Chapter I

Figure 1.1 Anatomy of the pancreas……7

Figure 1.2 Actin filament structure……9

Figure 1.3 Microtubule Structure……16

Figure 1.4 Microtubule assembly and disassembly……17

Figure 1.5 Microtubule nucleation by γ-tubulin complexes……20

Figure 1.6 HDACs, Phylogenetic tree and HDAC6 domains……26

Figure 1.7 Domain structures of +TIP proteins……34

Figure 1.8 Cell migration mechanism……42

Figure 1.9 Cytoskeletal organisation in cell migration……45

Figure 1.10 Schematic representation of stress fibers types……46

Figure 1.11 Cell adhesion composition……50

Figure 1.12 Sulforaphane (SFN)……54

Chapter III

Figure 3.1 ARPE-19 and PANC-1 cell morphology……96

Figure 3.2 Microtubule organisation in ARPE-19 cells……97

Figure 3.3 Microtubule organisation in PANC-1 cells……98

Figure 3.4 Tubulin modifications in ARPE-19 cells……99

Figure 3.5 Tubulin modifications in PANC-1 cells……100

Figure 3.6 Actin organisation in ARPE-19 cells……101

Figure 3.7 Actin organisation in PANC-1 cells……102

Figure 3.8 Actin organisation in PANC-1 cells……103

Figure 3.9 EB1 localisation in ARPE-19 cells……104

Figure 3.10 EB1 localisation in PANC-1 cells……105

Figure 3.11 EB3 localisation in ARPE-19 cells……106

Figure 3.12 EB3 localisation in PANC-1 cells……107

Figure 3.13 EB2 localisation in ARPE-19 cells……108

Figure 3.14 EB2 localisation in PANC-1 cells……109

Figure 3.15 HDAC6 localisation in ARPE-19 cells……110

Figure 3.16 HDAC6 localisation in PANC-1 cells……111

Chapter IV

Figure 4.1 SFN ≥ 30µM decreases cell viability in AREP-19 and PANC-1 cells……147

Figure 4.2 SFN at 10 and 15µM affects cell area and morphology in ARPE-19 and PANC-1cells……148

Figure 4.3 Single cell tracking of ARPE-19 cells……149

Figure 4.4 Single cell tracking of PANC-1 cells……150

Figure 4.5 SFN causes decreased speed of random migration in ARPE-19 cells……151

Figure 4.6 SFN did not affect the speed of random migration in PANC-1 cells……152

Figure 4.7 SFN affects microtubules organisation in ARPE-19……153

Figure 4.8 SFN affects microtubules organisation in PANC-1……154

Figure 4.9 SFN causes actin filaments disorganisation and co-alignment with microtubules in ARPE-19 cells……155

Figure 4.10 Stress fibers organisation in SFN treated ARPE-19 cells……156

Figure 4.11 Effects of SFN on actin organisation in PANC-1 cells……157

Figure 4.12 Stress fibres organisation in SFN treated PANC-1 cells……158

Figure 4.13 EB1 localisation in SFN treated ARPE-19 cells……159

Figure 4.14 EB1 expression and comets analysis in SFN treated ARPE-19……160

Figure 4.15 EB1 localisation in SFN treated PANC-1 cells……161

Figure 4.16 EB1 localisation in SFN treated PANC-1 cells……162

Figure 4.17 EB1 expression and comets analysis in PANC-1 cells……163

Figure 4.18 EB2 localisation in SFN treated ARPE-19 cells……164

Figure 4.19 EB2 localisation in SFN treated ARPE-19 cells……165

Figure 4.20 EB2 localisation in SFN treated PANC-1 cells……166

Figure 4.21 EB2 expression in SFN treated ARPE-19 and PANC-1 cells……167

Figure 4.22 HDAC6 localisation in SFN treated ARPE-19 cells……168

Figure 4.23 HDAC6 localisation in SFN treated ARPE-19 cells……169

Figure 4.24 HDAC6 localisation in SFN treated PANC-1 cells……170

Figure 4.25 HDAC6 localisation in SFN treated PANC-1 cells……171

Figure 4.26 Combination of tubacin and SFN has no effect on cell viability in AREP-19 and PANC-1 cells……172

Figure 4.27 Relative area of ARPE-19 and PANC-1 cells in the absence of active HDAC6……173

Figure 4.28 The effect of tubacin on microtubule acetylation in ARPE-19……174

Figure 4.29 The effect of tubacin om microtubule acetylation in PANC-1……175

Figure 4.30 The effect of tubacin and a combination of tubacin and SFN on microtubule acetylation in ARPE-19 and PANC-1 cells……176

Figure 4.31 A combination of tubacin and SFN causes a reduction in speed of cell migration in ARPE-19 and PANC-1 cells……177

Figure 4.32 EB1 localisation in tubacin and combination of tubacin and SFN treated ARPE-19 cells……178

Figure 4.33 EB1 expression and comets analysis in tubacin and a combination of tubacin and SFN treated ARPE-19 cells……179

Figure 4.34 EB1 localisation in tubacin treated PANC-1 cells……180

Figure 4.35 EB1 expression and comets analysis in tubacin and a combination of tubacin and SFN treated PANC-1- cells……181

Figure 4.36 EB2 localisation in tubacin treated in ARPE-19 cells……182

Figure 4.37 EB2 localisation in tubacin treated in PANC-1 cells……183

Figure 4.38 EB2 expression in tubacin treated in PANC-1 cells……184

Figure 4.39 HDAC6 localisation in tubacin treated ARPE-19 cells……185

Figure 4.40 HDAC6 localisation in tubacin treated ARPE-19 cells……..……..186

Figure 4.41 HDAC6 localisation in tubacin treated PANC-1 cells……..……187

Figure 4.42 HDAC6 localisation in tubacin treated PANC-1 cells……..……..188

Chapter V

Figure 5.1 SFN treated ARPE-19 cells express acetylated tubulin along microtubules..208

Figure 5.2 SFN increases acetylated microtubules in ARPE-19 cells……..……..209

Figure 5.3 SFN stabilised microtubules against cold in ARPE-19 cells ……..……...210

Figure 5.4 SFN treated PANC-1 cells express acetylated tubulin ……..……...211

Figure 5.5 SFN treated PANC-1 cells shows no significant increase in acetylated microtubules expression……..…..212

Figure 5.6 SFN treated PANC-1 cells shows no marked increase in stable microtubules against cold treatment……..……..213

Figure 5.7 SFN treated ARPE-19 cells express detyrosinated tubulin in microtubule bundles……..……214

Figure 5.8 Detyrosinated tubulin is not expressed in PANC-1 cells ……..……..215

Figure 5.9 Microtubule dynamics tracking of ARPE-19 cells……..…..216

Figure 5.10 SFN treatment leads to decrease CLIP-170 comets velocity and growth events in ARPE-19 cells……..……..217

Figure 5.11 Microtubule dynamics tracking of PANC-1 cells……..218

Figure 5.12 SFN treatment did not showed changes in focal adhesion appearance in PANC-1 cells……..……...219

Figure 5.13 SFN treatment leads to spread more focal adhesion in ARPE-19 cells……220

Figure 5.14 SFN treatment and focal adhesion localisation in PANC-1 cells…..……..221

Figure 5.15 SFN treatment leads to increase adhesion area and area in ARPE-19 cells……..……..222

Figure 5.16 SFN treatment shows no effect on adhesion area or area in PANC-1 cell……..223

Figure 5.17 FRAP of GFP-paxillin at focal adhesion in ARPE-19 cells……224

Figure 5.18 FRAP of GFP-paxillin at focal adhesion in PANC-1 cells……225

Figure 5.19 FRAP analyses of GFP-paxillin in ARPE-19 cells……226

Figure 5.20 FRAP analyses of GFP-paxillin in PANC-1 cells……227

Chapter VI

Figure 6.1 Model for SFN effects on cell migration……237

List of Tables

Table 1: List of cell lines and medium……63

Table 2: Constructs details……69

Table 3: Details of primary antibodies ……71

Table 4: Details of secondary antibodies……72

Table 5: Chapter IV summary……134

Table 6: Chapter V summary……202

List of Abbreviations

+TIP	plus-end tracking protein
ACF7	Actin cross-linking factor-7
ADP	Adenosine-5’-diphosphate
APC	Adenomatous polyposis coli
Arp	Actin related protein
ARPE	Retinal pigment epithelial
ATP	Adenosine-5’-triphosphate
BCA	Bicinchoninic Acid
BFP	Blue fluorescent protein
BSA	Bovine serum albumin
Ca2+	Calcium ions
CAP-Gly	Cytoskeleton-associated Protein Glycine-rich
CHD	Calponin homology domain
CHO	Chinese hamster ovary
CLASP 1/2	Cytoplasmic linker associated protein 1/2
CLIP-170/115	Cytoplasmic linker protein 170/115
COOH	Carboxy terminal
DAPI	4',6-diamidino-2-phenylindole
DHC	Dynein heavy chain
DIC	Dynein intermediumte chain
DLC	Dynein light chain
DLIC	Dynein light intermediumte chain
DMEM	Dulbecco's modified eagle medium
DMSO	Dimethyl sulfoxide

EB1/2/3	End binding protein 1/2/3
GAP	GTPase activating proteins
GDI	RhoGDP dissociation inhibitor
GDP	Guanosine-5'-diphosphate
Glu tub	Detyrosinated tubulin
HEPES	N-2-Hydroxyethylpiperazine-N-2-Ethanesulfonic Acid
HDAC	Histone deacetylase
HDAC6	Histone deacetylase 6
IQGAP 1/2/3	IQ motif containing GTPase activating protein 1/2/3
Lys-40	N-terminus of α-tubulin on lysine 40 (
MAP	Microtubule associated protein
MDCK	Madin darby canine kidney
MTOC	Microtubule organising centre
PBS	Phospho buffered saline
PCM	Pericentriolar matrix
SDS	Sodium dodecyl sulphate
SFN	Sulforaphane
SIRT2	Human Sir2
TTL	Tubulin tyrosine ligase
T	Tubacin
Tx100	Triton X100
Tyr tub	Tyrosinated tubulin
αTAT1	α-tubulin acetyltransferase 1
γ-TuRC	gamma tubulin ring complex
γ-TuSC	gamma tubulin small ring complex
v/v	Volume/volume
w/v	Weight/volume

Chapter I: Introduction

1.1 Sulforaphane and the cytoskeleton

High consumption of cruciferous vegetables, such as broccoli, is associated with a lower risk of cancer, in for example, the breast, colon, prostate and pancreas. There is preliminary evidence that sulforaphane (SFN) may prevent or slow the development of cancer (Fimognari and Hrelia, 2007). SFN has heterogeneous biological activities involving cell cycle arrest and apoptosis (Jackson and Singletary, 2004, Pledgie-Tracy et al., 2007, Dickinson et al., 2015). It seems that SFN is able to prevent, delay or reverse malignant neoplasm, and it thus holds the potential to be a therapeutic agent (Fimognari and Hrelia, 2007). However, the mechanisms behind its effects are not fully defined and this is especially so with regards to its effects on the cytoskeleton. The cytoskeleton plays vital roles in many cell functions and it has been linked to different diseases, including cancer. Microtubules are one of the main targets for anti-cancer chemotherapy due to their vital roles in cell activities including cell division, differentiation and migration. The exact effects of SFN on microtubules and their associated functions are not fully understood. It is therefore important to provide a better understanding of the effect of SFN on microtubules in normal and cancerous cells.

1.2 The Cytoskeleton and Cancer

This study is focused on the cytoskeleton in disease, and in particular the microtubule cytoskeleton and its role in the migration of pancreatic cancer cells. Cancer is a major health problem in the world, where the lifestyle and environment in the developed world increase the risk of developing the disease. In addition, improved healthcare leads to an increased aging population, and it is likely to increase the number of people becoming affected. In the UK, it has been reported that pancreatic adenocarcinoma is the fifth leading cause of cancer-related

mortality and the eighth most common cancer death worldwide (Bond-Smith et al., 2012, Torre et al., 2015).

The cytoskeleton is a highly flexible filamentous network composed of three components: actin filaments, intermediumte filaments and microtubules. The cytoskeleton is vital to cell function, and without it, cells are not viable. Additionally, the cytoskeleton has been associated with various diseases, in particular with cancer, with cancers causing uncontrolled cell division, cell motility and invasion. Microtubules and associated proteins play an important part in these cellular processes (Frixione, 2000). The exact mechanisms of these processes are not fully understood, so it is therefore vital to provide a better understanding of microtubule functions under normal situations, and then examine the effect of cancer.

Microtubules are an important target for anti-cancer chemotherapy; in the 1980s, taxol, including its derivatives, became a widely used cancer drug for breast, ovarian and lung cancer, as it binds to microtubules and influences microtubule dynamics. Taxol causes microtubules to form bundles, and stabilises the microtubule lattice and stimulates polymerisation. Consequently, this will block cell division and promote apoptosis, and ultimately impede tumour growth – all of this is achieved by preventing microtubule dynamics that are required for successful mitotic spindle formations and function. Vinca alkaloids are also important anti-cancer agents that target microtubule dynamics and thus affect spindle microtubules (Jordan et al., 1991, Jordan and Wilson, 2004).

Recent studies have identified abnormal expression levels and distribution patterns of important microtubule plus-end binding proteins in cancer such as EB1 and EB2. EB1 overexpression has been reported in some cancers, such as glioblastoma, breast, colorectal, esophageal squamous cell carcinoma, hepatocellular carcinoma and oral cancer (Dong et al., 2010, Berges et al., 2014, Kumar et al., 2016). It has

been reported that EB1 regulates cancer cell sensitivity to the anti-microtubule agent (paclitaxel), with EB1 increasing the ability of paclitaxel to bind microtubules and promotes tubulin polymerisation and stabilisation in breast cancer cells (Luo et al., 2014, Thomas et al., 2015). In addition, EB2 overexpression has been associated with increased pancreatic cancer invasion (Abiatari et al., 2009). EB1 overexpression induces microtubule bundling in human breast cancer cells (MCF7), thus, having a role in microtubule assembly and reorganisation, which is an important process in cancer (Bu and Su, 2001). These findings suggest that further investigations are needed into EBs as potential targets for anti-cancer treatments (Bhat and Setaluri, 2007).

1.2.1 Pancreatic cancer

Pancreatic cancer is a highly aggressive malignancy and is the most complex epithelial cancer to treat, where strong resistance to existing treatments are evident (Bardeesy and DePinho, 2002, Wang et al., 2011). It remains the fifth leading cause of cancer-related deaths in the United Kingdom, fourth in the United States, and the eighth globally with only about 5% of pancreatic cancer patients expected to survive for five years after diagnosis (Siegel et al., 2016). In general, pancreatic cancer seldom occurs before the age of 40, but most cases of pancreatic adenocarcinoma occur in those over the age of 70 in both genders (Bardeesy and DePinho, 2002).

The pancreas regulates two major functions, digestion and glucose metabolism. The exocrine pancreas comprises acinar and duct cells, where acinar cells are organised in a grape-like shape and produce digestive enzymes including trypsinogen, chymotrypsinogen, elastase, carboxypeptidase, pancreatic lipase, nucleases and amylase. The ducts add mucus and bicarbonate to the enzymes and

empty into the duodenum. The acinar cells play a vital role in regulating blood sugar by producing insulin (Figure 1.1) (Bardeesy and DePinho, 2002).

There are various types of pancreatic cancer, and the most common one, accounting for about 85% of cases, is pancreatic ductal adenocarcinoma. This cancer begins in the ducts that transport enzymes from acinar cells, and more than 60% of this cancer occurs in the 'head' of the pancreas near the duodenum (Bardeesy and DePinho, 2002).

There are a number of risk factors regarding pancreatic cancer, including cigarette smoking. Studies estimate that cigarette smoking doubles the risk of pancreatic cancer, and it is believed that about 25% of cases of pancreatic cancer are due to smoking. Other identified risk factors include diets high in meat and fat, obesity, diabetes mellitus, chronic pancreatitis and inherited predisposition, which accounts for about 10% of pancreatic cancer (Bardeesy and DePinho, 2002, Hezel et al., 2006, Maitra and Hruban, 2008).

Cancer develops through the accumulation of genetic mutations leading to the activation of cancerous genes and inactivation of tumour suppressor genes. Multiple combinations of mutations can cause the development of pancreatic adenocarcinoma, including KRAS gene (K-ras or Ki-ras), TP53 (tumour protein p53) (known as p53 protein), CDKN2A (cyclin dependent kinase inhibitor 2A) (encoding p16) and SMAD4 (mother against decapentaplegic homology 4) (also known as DPC4, deleted in pancreatic cancer 4). KRAS relates to growth increasing signals from the cell surface to the nucleus. It functions as binary molecular switches (on/off), where it is a member of the GTP (guanosine triphosphate) binding proteins. KRAS proteins interact with signalling molecules that regulate cell activities, including proliferation, differentiation, apoptosis, and cell migration. Mutations in KRAS decrease GTP hydrolysis and, thus, causes KRAS to remain active (Moore et al., 2003, di Magliano and Logsdon, 2013).

DPC4 is a tumour suppressor gene that is mutated in pancreatic cancer. It is important in signalling, where it plays a vital role in the transduction of TGF-β (transforming growth factor β) signalling from the cell surface to the nucleus (Moore et al., 2003, Li et al., 2004, Deer et al., 2010). In addition, p53 is mutated in pancreatic cancer cells, where in normal cells it functions as tumour suppressor conserving stability by stopping genome mutation. Mutations in p53 could lead to abnormal cell proliferation resulting in cancer and more than 50% of human late stage cancers, and 26% of primary stage cancers revealing mutations in p23 gene (Moore et al., 2003). Interestingly, most pancreatic cancer cell lines (> 95%) have defective p53, including the PANC-1 cell line. Additionally, mutations in p53 and p16 play important roles in the cell cycle and the maintenance of the genome after DNA damage (Moore et al., 2003, Maitra and Hruban, 2008, Deer et al., 2010).

The relationship of these mutations to the phenotype of pancreatic cancer is still unclear, as a few studies have indicated that there is no correlation with either the grade of differentiation, or biological behaviour and mutational status of pancreatic cancer cells. However, it has been suggested that genotype and phenotype may be correlated, and reported that metastatic activities were linked to p53 mutation *in vivo* (Deer et al., 2010).

Perineural invasion of tumour cells is one of the characteristic features of human pancreatic cancer, which involves growth along pancreatic nerves and this is a likely cause of recurrence of the disease. Upregulation in genes including the MAPRE (microtubule-associated protein RP/EB) gene family (MAPRE 1, 2 and 3), which function as microtubule-plus-end associated proteins (EB1, EB2 and EB3) have been associated with cancer. It has been demonstrated that MAPRE2 (EB2) levels are higher in pancreatic cancer cells (PANC-1) compared to normal cells; this observation suggests that EB2 might be involved in increased migration of pancreatic cancer cells (Abiatari et al., 2009).

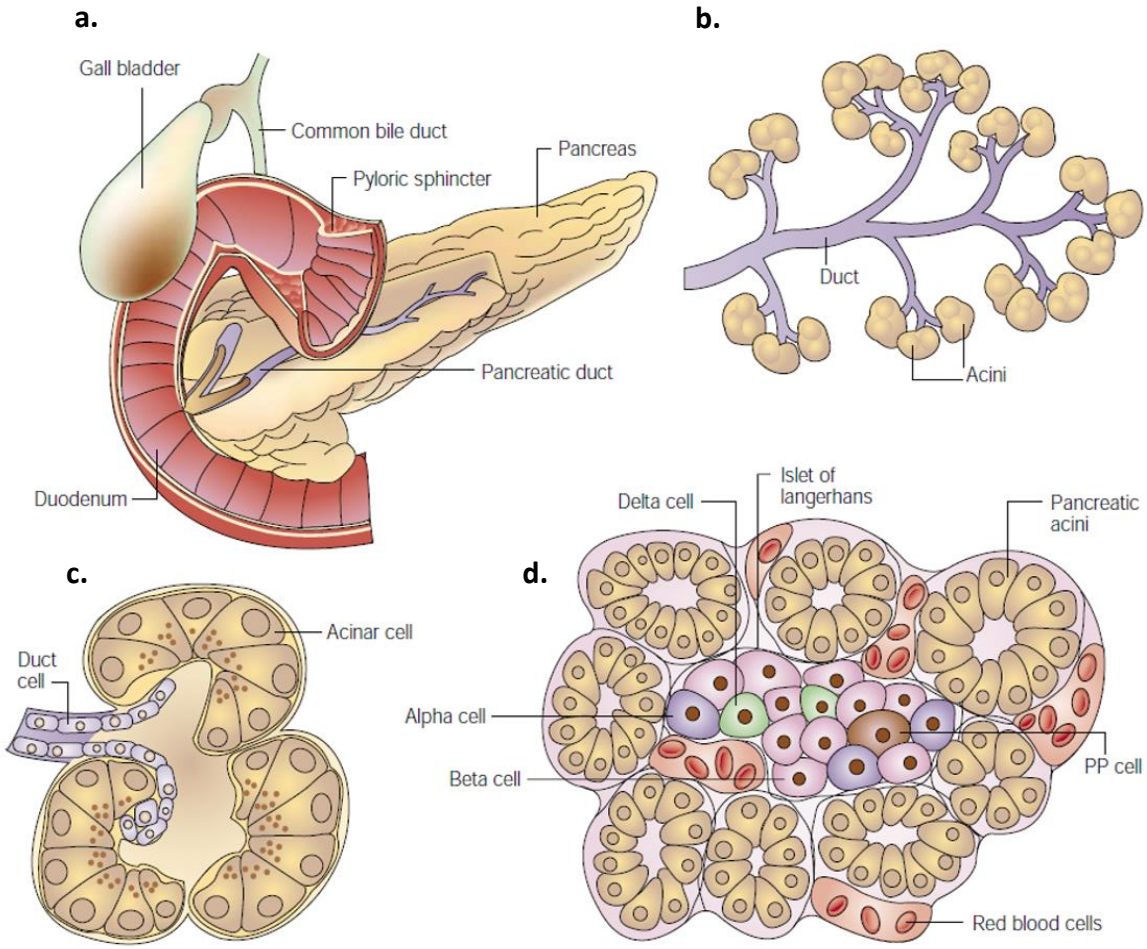

Figure 1.1 Anatomy of the pancreas
a) Anatomy of the pancreas: the pancreas is comprised of different functional parts, which control two main processes, digestion and glucose metabolism. b) The exocrine pancreas; composes acinar and duct cells. c) Single acinus: the acinar cells produce insulin and are organised in grape-like structures. d) Exocrine tissue consists of four cell types, which are organised into compact islets embedded in acinar tissue, within acinar, secreting hormones into the bloodstream. Adapted from Bardeesy and DePinho (2002).

1.3 The Cytoskeleton

The cytoskeleton is vital for cell survival. The ability of cells to arrange into a variety of shapes, organise the many components in their interior, and interact mechanically with the environment depends on the cytoskeleton. The cytoskeleton also facilitates cell movement, proliferation and differentiation. The advent of the electron microscope in the 1930s allowed for the observation of the cytoskeleton, and lately fluorescence microscopy allows advanced investigations of cytoskeletal fibres. The cytoskeleton has three major networks of filaments: actin filaments, intermediumte filaments and, of main interest to this study is the microtubules. Each type of filament has distinct mechanical properties and is made from a different subunit, and these filaments associate with various accessory proteins and give them dynamic structure (Brinkley, 1985, Frixione, 2000).

1.3.1 Actin

Actin was first noticed as a filament combined with myosin motors in the myofibrils responsible for mammalian muscle contraction (Straub, 1943, Szent-Györgyi, 1953, Frixione, 2000). The actin cytoskeleton has a fundamental role in many cell biological processes, including cell migration, morphogenesis, cytokinesis and endocytosis, which depend on dynamic actin filaments (Lappalainen, 2016). Actin is the smallest in terms of diameters of the cytoskeletal filaments with a diameter around 5–9 nm. Each filament is a twisted chain of identical globular subunits (G-actin), a 42-kDa protein, arranged in a head tail mode. Actin filaments have a distinct polarity, called the plus-ends and the minus ends (Figure 1.2). This polarity is important in assembly and disassembly although both ends can grow, the plus-end grows faster than the minus end (Dominguez and Holmes, 2011).

Actin filament structure

a) Actin filaments

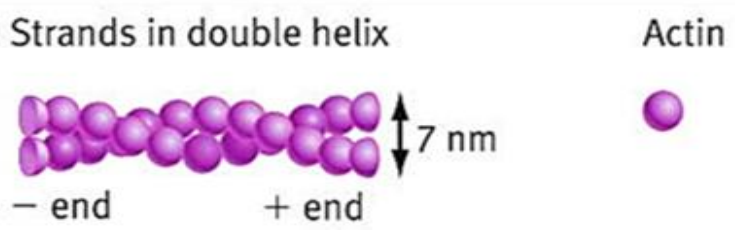

b) Actin Treadmilling

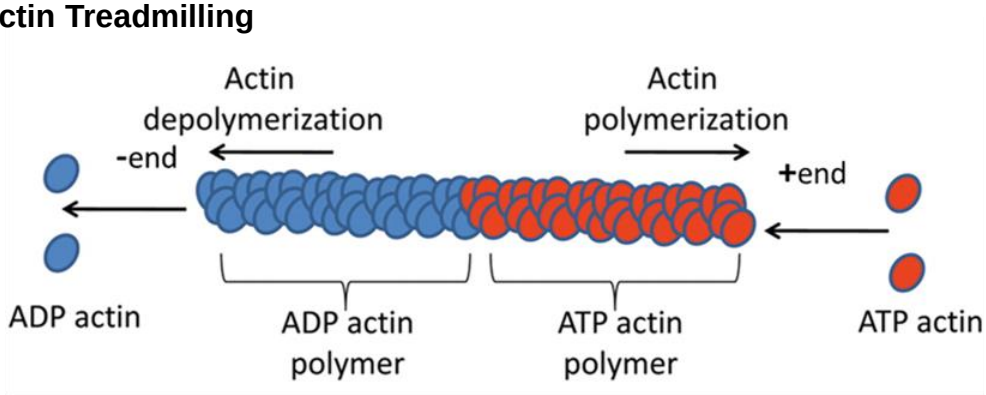

c) Actin branching

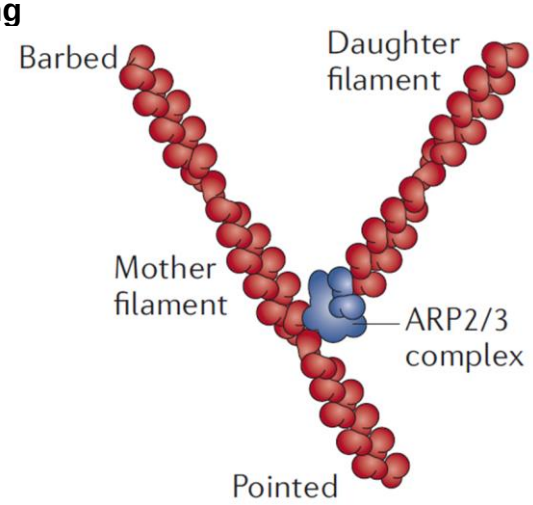

Figure 1.2 Actin filament structure
a) Actin filaments consist of two-twisted strands with organisational polarity, plus and minus ends, and diameter around 7nm. b) Actin Treadmilling, at the plus-end, actin monomers bound to ATP and added to the growing filament. Meanwhile, at the minus end, actin–ADP monomers are lost causing disassembly of actin filaments. c) Actin branching: ARP2/3 binds to the sides of an actin filament, helping nucleation of a new actin filament and starting a new actin network. Adapted from Goley and Welch, (2006).

Assembly of actin filaments (F-actin) occurs when actin monomers bound to ATP (Adenosine Tri-Phosphate) are added to the plus-end – this stage is called polymerisation. Shortly after polymerisation, the ATP is hydrolysed to ADP (Adenosine Diphosphate); the actin–ADP subunit is unstable in the filament, causing actin filament disassembly (Chhabra and Higgs, 2007, Dominguez and Holmes, 2011). .

Actin filaments can assemble into different organisations, such as lamellipodia, filopodia and stress fibres, which perform different functions within the cell. Lamellipodia are dynamic membrane protrusions, which occur at the leading edge of migrating cells and consist of a meshwork of actin filaments that pushes the membrane of the cell and drives the cell forward (Dominguez and Holmes, 2011). Actin filaments also assemble into stress fibres, consisting of an array of F-actin linked to myosin II and their interaction provides tension, where they associate with focal adhesions (Pollard and Borisy, 2003, Vinzenz et al., 2012, Blanchoin et al., 2014).

Actin filament assembly and disassembly are governed by actin binding proteins (ABPs), which can bind to actin filaments in different ways, either at the ends or along the filament side. Some proteins form a cap at the end of the filament to prevent further addition or loss of actin subunits, such as CapZ. In addition, there are some proteins responsible for depolymerisation and turnover of actin filaments, including the ADF/cofilin family. Cofilin can bind to actin filaments and increases the dissociation rate of actin monomers at the minus ends, where cofilin binds to G-actin-ADP and this prevents the filaments from assembling; this effect can be reversed by profilin. Profilin induces the exchange of bound ADP for ATP, which dissociates cofilin from monomers and then leads to filament assembly. Cofilin and profilin with other binding proteins can act together to increase the rapid turnover of actin filaments and reorganise the actin cytoskeleton, which is important for cell

movements and changes of cell shape (Chhabra and Higgs, 2007, Pollard and Cooper, 2009, Dominguez and Holmes, 2011).

There are several essential nucleation proteins, including the ARP2/3 complex and formins, where the actin network within lamellipodia is driven by ARP2/3 nucleation (Vinzenz et al., 2012). Actin nucleation usually occurs at the cell cortex, and it is catalysed by the actin-like ARP2/3 complex. The ARP2/3 proteins act as nucleation sites to initiate the assembly of new filaments and regulate the actin cytoskeleton by binding to the minus ends of actin. ARP2/3 can also be found at the sides of pre-existing actin filaments, causing the formation of a branched actin network (Figure 1.2, c) (Goley and Welch, 2006, Pollard and Cooper, 2009, Chhabra and Higgs, 2007, Vinzenz et al., 2012). Formins are a group of actin-binding proteins that play a role in increasing actin filament assembly when needed. Formins have essential functions in cytokinesis and cell polarisation, actin assembly at the adherent junctions and formation of filopodia. They associate with the plus-end and nucleate and promote actin filament elongation and actin bundles. These proteins can also control actin assembly at the advancing front of migrating cells (Chhabra and Higgs, 2007, Dominguez and Holmes, 2011, Nurnberg et al., 2011, Blanchoin et al., 2014).

Generally, actin filaments are assembled into two types of structures, termed ‘actin bundles’ and ‘actin networks’. In actin bundles the actin filaments are cross-linked into closely packed parallel arrays as found in microvilli, which are found at surface projections. In actin networks, the actin filaments are loosely cross-linked orthogonal arrays that form three-dimensional meshwork. These structures are regulated by a variety of actin binding proteins such as fimbrin and filamin, where fimbrin binds actin filaments and holds two parallel filaments close together. While, filamin forms cross-links between orthogonal actin filaments, and creates a loose three-dimensional meshwork. (Chhabra and Higgs, 2007, Dominguez and Holmes, 2011, Blanchoin et al., 2014).

The actin network can link to the plasma membrane by binding to spectrins and ERM proteins (ezrin, radixin and moesin), that bind membrane associated proteins directly to cortex actin filaments (Fehon et al., 2010). Spectrin is related to filamin protein, and forms a spectrin–actin network in red blood cells (Louvet-Vallée, 2000). The activity of actin can be controlled by the Rho GTPases Cdc42, Rac and Rho. These proteins act as molecular switches; when bound to GTP they are considered active, and when GTP is hydrolysed to GDP, they are inactive. Active Cdc42, Rac and Rho have been linked to filopodia, lamellipodia and focal contact formation receptively (Burridge and Wennerberg, 2004).

1.3.1.2 Intermediumte filaments

Intermediumte filaments provide mechanical strength and the capability to resist external stresses and have a diameter of about 10 nm. In humans, intermediumte filaments are diverse with more than 90 genes expressed in a tissue specific manner. For example, keratins are expressed in epithelial cells, and vimentins are found in mesenchymal cells while lamins are present in the nucleus of all cells (Fuchs and Weber, 1994).

The different types of intermediumte filaments are structurally similar, and are assembled to form parallel polymers consisting of two different α-helical monomers to form a nonpolar coiled-coil structure. In addition, between two and four protofibrils twist into the final lattice of intermediumte filament. Intermediumte filaments obtain their strength and flexibility from the large number of polypeptides (Fuchs and Weber, 1994, Herrmann and Aebi, 2004).

The head and tail domains play an important role in the differences between the intermediumte filaments. This allows intermediumte filaments to associate with different structures, including other cytoskeleton filaments and junctional components at the plasma membrane. In addition, this variety of binding proteins

associate the intermediumte filament networks with their tissue environment – for example, epithelial tissues are linked to each other, and to the basal lamina, by the intermediumte filament networks through specialist junctions, and this gives more strength across the tissue via integrity. However, mutations in intermediumte filaments and in associated proteins cause disruption of intermediumte filaments and many diseases, which lead to the loss of mechanical functions, and skin blistering (Lane et al., 1992, Fuchs and Cleveland, 1998, Haines and Lane, 2012).

1.4 Microtubules

Microtubules have many vital functions in biological processes, including: cell division, cell morphology by providing internal structure and support, cell polarity, and cell motility, which is of particular interest to this project (Vasiliev et al., 1970, Drubin and Nelson, 1996, Mitchison and Salmon, 2001, Hawkins et al., 2010). Moreover, microtubules provide tracks for the transport for of organelles, vesicles, and signalling molecules (Cole and Lippincott-Schwartz, 1995).

1.4.1 Microtubule structure

Microtubules are tubular structures that exist in all eukaryotic cells. As shown in figure 1.3, a microtubule is assembled from polymers, which are made of α-tubulin and β-tubulin heterodimers assembled into polarised protofilaments. A microtubule is usually arranged in thirteen parallel protofilaments, which form a hollow rigid tube approximately 25 nm in diameter. However, the number of protofilaments may vary in certain differentiated cells, such as the pillar cells in the inner ear, where many of the microtubules have15 protofilaments. Protofilaments can assemble into B-type lattice, by which subunits of protofilaments associate in α-α and β-β manner. The polymerisation in microtubules is a head-to-tail process, starting with initial

nucleation and then elongation, thus dictating the polarity of the microtubule. As a result, the two ends of the microtubule are termed the 'plus-end' or 'fast-growing end', which is terminated by β-tubulin, and the 'minus end' or 'slow-growing end', which is terminated by α-tubulin (Desai and Mitchison, 1997, Howard and Hyman, 2003, Conde and Caceres, 2009).

Microtubules can be assembled and disassembled. However, the minus-end is often stabilised and anchored at the centrosome, whereas the plus-ends elongate towards the cell periphery. This elongation requires energy from the adding of GTP-tubulin (Akhmanova and Hoogenraad, 2005). The disassembly of microtubules is known as depolymerisation, and causes the shortening of microtubules (Desai and Mitchison, 1997, Nogales, 2000, Nogales and Wang, 2006). Both α and β tubulins are able to bind GTP, but GTP can only be hydrolysed on β-tubulin. Therefore, heterodimer addition occurs specifically at the β-tubulin exposed growing microtubule plus-ends. The nucleotide status of tubulin heterodimers in the microtubule lattice determines the level of curvature in the protofilament. GTP-tubulin subunits are bound as a cap at the growing end of a microtubule, which gives longitudinal strength and encourages straight protofilaments. Thereby, this GTP-cap provides enough energy in the lattice to enable further tubulins to be added to the growing microtubule. The hydrolysis of GTP to GDP on β-tubulin causes a conformational change, where the protofilaments curve outwards, generating a lateral pulling that enhances depolymerisation of the microtubule (Nogales and Wang, 2006, Howard and Hyman, 2007, Rice et al., 2008) (Figure1.4). Two models have been suggested which depend on the relationship between GTP and conformational change in αβ-tubulin, the allosteric model and the lattice model. The allosteric model proposes that, α/β tubulin heterodimers are curved when GDP is bound, and when GTP binds the dimer straightens out and allows lateral incorporation onto microtubule. This model relies on observations that straighter microtubules elongate from GTP bound αβ-tubulin, and curve from

GDP αβ-tubulin (Müller-Reichert et al., 1998, Wang and Nogales, 2005). The lattice model indicates that conformational alterations with straightening are a consequence of microtubule assemble. It also suggest that the GTP acts to increase recruitment and that straightening is due to lateral associations. A study that supports the lattice model shows that γ and αβ-tubulin rearrangements did not occur in response to GTP binding (Wang and Nogales, 2005, Nogales and Wang, 2006, Rice et al., 2008).

Microtubule Structure

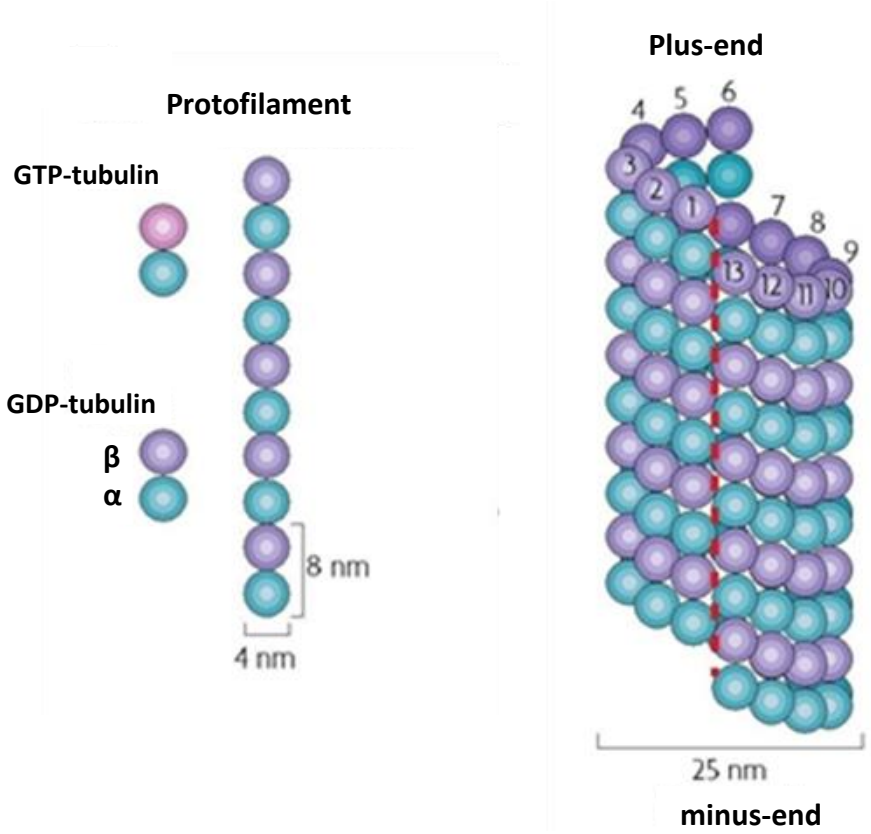

Figure 1.3 Microtubule Structure
Microtubules consist of α- and β-tubulin heterodimers, which form protofilaments. 13-protofilaments assemble laterally in a non-symmetrical helix to form a hollow tube 25 nm in width, which rises by three monomers every turn. Note the seam in the microtubule wall, and the polarity of the filament. Adapted from Akhmanova and Steinmetz (2008).

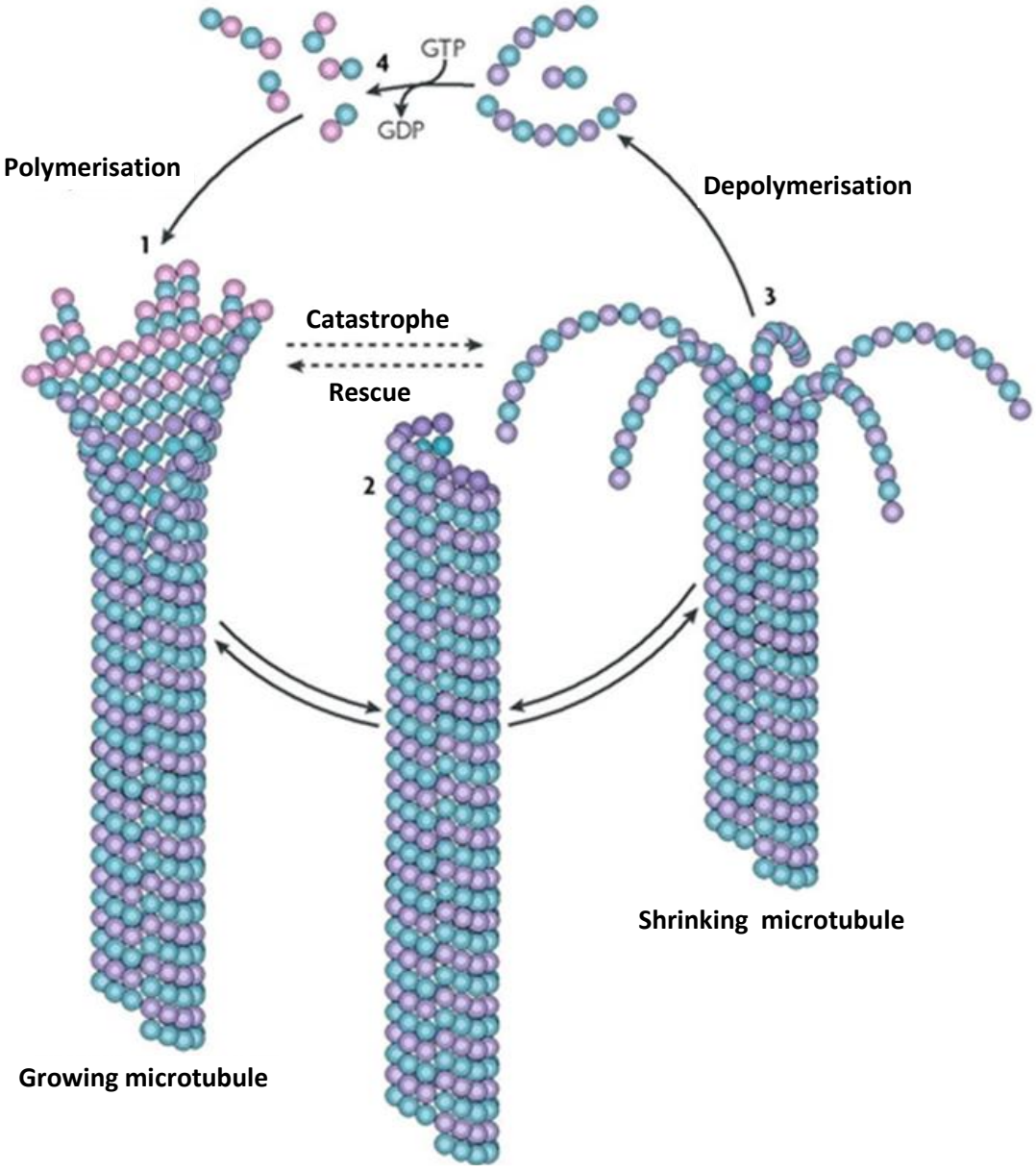

Figure 1.4 Microtubule assembly and disassembly
Microtubules can switch rapidly between phases of growth and shrinkage. Growing microtubules possess a GTP-tubulin cap. Protofilaments are straight and the lattice stable, allowing incorporation of GTP-tubulin heterodimers at the plus end. Hydrolysis of GTP in β-tubulin in the cap causes protofilaments to curve and peel away, and the microtubule to shrink. Adapted from Akhmanova and Steinmetz (2008).

1.4.2 Microtubule nucleation

The process in which various αβ-tubulins interact to form a microtubule seed, termed 'microtubule nucleation', controls the number of microtubules formed and enables microtubules to extend in the cytoplasm (Kellogg et al., 1994, Job et al., 2003). Microtubule nucleation is organised by the microtubule organisation centre (MTOC). In eukaryotic cells, it is often the centrosome while the fungal spindle pole body (SPB) is a MTOC in fungae. Despite morphological differences between MOTCs they share functional nucleating complexes, which contain γ-tubulin and several γ-tubulin complex proteins (GCPs). In the centrosome, the nucleating complex consist of the small γ-tubulin complex (γTuSC), associated with one molecule each of GCP2 and GCP3 (Figure 1.5, a). Several copies of γ-TuSC and linked by additional accessory proteins (GCP2, GCP3, GCP4, GCP5 and CGP6) are arranged into the more potent γ-tubulin ring complex (γTuRu) (Figure 1.5, b) (Raynaud-Messina and Merdes, 2007, Kollman et al., 2011).

Two models for γ-TuRC-based microtubule nucleation have been proposed: the protofilament model and the template model. The protofilament model proposes that γ-TuRCs interact with each other longitudinally and encourage the lateral addition of αβ-tubulin heterodimers. The template model suggests that γ-TuRCs form a cap that surrounds the minus ends of the microtubule, where γ-tubulin subunits are laterally organised and longitudinally contact with α-tubulin (Figure 1.5, c and d). Most of the evidences support the template model (Wiese and Zheng, 2006, Kollman et al., 2011). It is still unclear how the template model could nucleate the thirteen protofilaments of microtubules, as an even number of γ-tubulins (12 or 14) would have to be combined into the γTuRC through six or seven of γ-TuSC complexes. A study showed that thirteen γ-tubulin are present in the γTuRC, where the first and seventh γTuSC overlap. This may be controlled by lateral interactions between GCP proteins, as GCP4, 5 and 6 are directly combined into the ring without acting as a scaffold for γTuSC subunits. This allows the half

overlap and possibly direct the position of the microtubule seam (Kollman et al., 2011).

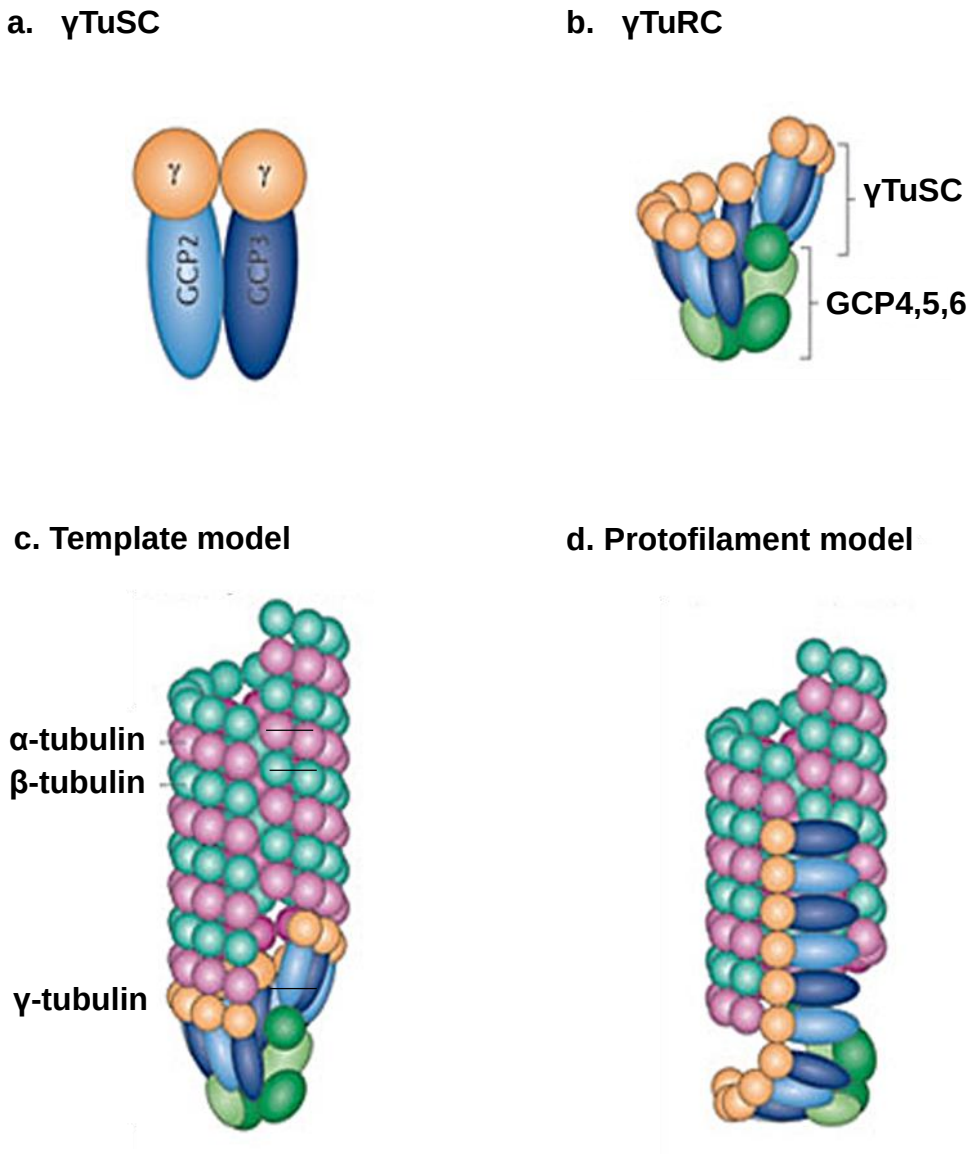

Figure 1.5 Microtubule nucleation by γ-tubulin complexes
a) γ-Tubulin small complex (γ-TuSC) consists of two molecules of γ-tubulin associated with one molecule each of GCP2 and GCP3. b) γ-TuRC, large complex or γ-tubulin ring complex, consists of multiple γTuSCs assembled with GCP4, GCP5, and GCP6 into the γ-tubulin ring complex (γTuRC). c) The template model: the γTuRC acts as a template, creating a ring of γ-tubulins that make longitudinal contact with αβ-tubulin. d) The protofilament model: the γTuRC attaches to present a γ-tubulin protofilament, which nucleates through lateral contacts with αβ-tubulin. Adapted from Kollman et al. (2011).

1.4.3 Microtubule minus-end associated proteins and microtubule anchorage

A centrosome-focused radial array facilitates cytoplasm organisation keeping organelles in position and providing tracks for vesicular traffic (Cole and Lippincott-Schwartz, 1995). Centrosomes consist of many ring structures formed from γ-tubulin and several γ-tubulin complex proteins (GCPs), which are the nucleation site for the assembly of one microtubule (Mogensen et al., 1997). The αβ-tubulin dimers are added to the nucleation site in a specific orientation with the minus end of each microtubule embedded in the centrosome and the plus-end growing outwards into the cytoplasm. In addition, the centrosome in most animal cells contains a pair of centrioles made of a cylindrical array of short microtubules and pericentriolar material (PCM) (Kaverina et al., 2002). The centrioles have no direct role in the nucleation of microtubules in the centrosome; however, they aid in organising the PCM around them (Bobinnec et al., 1998, Mogensen, 1999)

Many differentiated epithelial cells can assemble a non-centrosomal microtubule array, such as the skin, gastrointestinal tract, kidney, retina and cochlea (Furness et al., 1990, Mogensen et al., 1997, Mogensen, 1999). The mechanism that controls the organisation and behaviour of microtubule minus-ends remain unclear. However, there are several minus-end proteins that play vital roles in stabilising the apico-basal non-centrosomal microtubule array, such as ninein and CAMSAPs (1, 2 and 3). It has been indicated that, in the inner ear CAMSAP3, which is a minus end-binding protein, may help to establish and protect the non-centrosomal site (Zheng et al., 2013). Ninein has been referred to as responsible for microtubules anchorage at both the centrosome and at non-centrosomal sites (Moss et al., 2007, Goldspink et al., 2017). It accumulates at the mother centrosome and associates with minus-ends of microtubules. Importantly, in cochlea pillar cells, ninein is located at the apical non-centrosomal sites, where minus-ends of microtubules

array are located. Ninein is released and travels along microtubules to these apical sites, and it stabilises the minus-ends of the microtubules. Therefore, ninein is vital for the successful anchorage and apical-basal array (Moss et al., 2007, Goldspink et al., 2017).

1.4.4 Post-translational modifications

Different subtypes of microtubules exist through the expression of different tubulin isotypes (7α and 8β tubulin present in the human genome) and post-translational modification, such as detyrosination and acetylation. Together this is referred to as the 'tubulin code', which result in unique microtubule interaction with associated proteins which has functional implications (Sirajuddin et al., 2014, Yu et al., 2015). For example, detyrosinated microtubules enhance the traveling of some motor proteins along them, such as kinesin motors (kinesin 1 family). Moreover, CLIP-170 and $p150^{Glued}$ could recognise and bind to tysosinated microtubules, and affect their dynamics (Hammond et al., 2008, Garnham and Roll-Mecak, 2012, Sirajuddin et al., 2014).

Post-translational modifications generally occur on the C-terminal tail domains of α and β-tubulin, which are exposed on the outer face of the polymer. This location provides a 'code' for suitable MAP recruitment, hence affecting the microtubule properties, in particular stability. This allows specific microtubules with dissimilar properties to perform particular roles within the microtubule networks. Alternatively different modifications can occur along the length of the microtubules (Verhey and Gaertig, 2007, Garnham and Roll-Mecak, 2012, Yu et al., 2015). The post-translational modifications include detyrosination, acetylation, phosphorylation, glutamylation and glycylation. Additionally, further post-translational modifications, such as polyamination, β-tubulin acetylation and succination have recently been discussed (Li and Yang, 2015).

1.4.4.1 The detyrosination/tyrosination cycle

Tyrosination was the first modification identified in the early 70s, and it consists of the removal of a C-terminal tyrosine to expose a glutamine (Barra et al., 1973, Hallak et al., 1977). The C-terminal of α-tubulin undergoes a cycle of loss and re-addition of tyrosine, known as the tyrosination–detyrosination cycle. The removal of the tyrosine exposes a glutamic acid residue at the C-terminus, termed 'Glu-tubulin', and modifies tubulin to detyrosintion, which accumulates only in stable microtubules. Whereas the specific carboxypeptidase enzymes responsible for detyrosination have yet to be recognised (Janke and Bulinski, 2011, Garnham and Roll-Mecak, 2012, Yu et al., 2015), the re-addition of tyrosine involves tubulin-tyrosine ligase (TTL). This enzyme requires ATP to function and works to re-tyrosinate soluble heterodimers. The tyrosination–detyrosination cycle is reversible. Detyrosinated tubulin at the C-terminus can be further modified by removing the last glutamic acid residue and ends with irreversible Δ2-tubulin (Janke and Bulinski, 2011, Yu et al., 2015).

In undifferentiated cells, there are two distinct populations of tubulin at interphase and most are tyrosinated; however, there is a small subgroup of detyrosinated microtubules (Gundersen et al., 1984). This subgroup has been linked with stable, long-lived microtubules, while most of the microtubules are dynamic (Webster et al., 1987). Detyrosinated tubulin (Glu-tubulin) is used as a marker for microtubule stability (Peris et al., 2009).

On the other hand, it has been reported that detyrosination of the lattice inhibits the binding of depolymerising motors for microtubules (MCAK and KIF2A) (Peris et al., 2009). Moreover, these associations of motor proteins and detyrosinated microtubules have been shown to cross-link microtubules with vimentin intermediumte filaments. Meanwhile tyrosinated tubulin has been shown to enhance microtubule dynamics by binding +TIP, such as CLIP-170 and $p150^{Glued}$

which contain a CAP-Gly domain. However, EB1 binds plus-ends of microtubules independent of tubulin tyrosnation. Consequently, defective tyrosination and detyrosination have been involved in diseases that link to the reduction of TTL and decreased tubulin tyrosination, such as disorganisation of neuronal networks, and cancer tumorigenesis and invasion (Hammond et al., 2008, Garnham and Roll-Mecak, 2012).

1.4.4.2 Acetylation

Tubulin is a major target for acetylation at the N-terminus of α-tubulin on lysine 40 (Lys-40). Acetylation was first discovered in the late 1960s on histones, and in the 1970s and 1980s was noticed on different non-histone proteins such as α-tubulin. In the last decade, acetylation was identified in post-translational modifications with about 2000 acetylation proteins. Acetylation is reversible and requires several acetyltransferase enzymes to be activated, including Mec-17 (mechanosensory abnormality protein 17) and αTAT1 (α-tubulin acetyltransferase 1). The effect of tubulin acetylation on microtubule dynamics is still not fully understood; however, it is known to be linked to stable microtubules (long-lived microtubules) but does not significantly influence polymerisation or depolymerisation. In mice lucking αTAT1 and acetylated microtubules, the microtubules were sensitive to nocodazole, thus, suggesting decreased stability (Kalebic et al., 2013). Acetylation affects protein interaction with microtubules. Some studies showed that acetylated tubulin increases kinesin-1 binding to microtubules (Reed et al., 2006, Dompierre et al., 2007, Rymut and Kelley, 2015, Yu et al., 2015), it has also been shown that acetylated tubulin interacts with membranes and provides tracks for movement (Janke and Bulinski, 2011, Garnham and Roll-Mecak, 2012). Two tubulin deacetylases have been identified: histone deacetylase 6 (HDAC6), which co-localises with the microtubule network (Hubbert et al., 2002), and Sirtuin 2

(SIRT2). Deacetylation occurs on tubulin dimers (North et al., 2003, Rymut and Kelley, 2015).

HDACs associate with different non-histone substrates to regulate various cellular activities such as cell division, cell movement and angiogenesis. There are two different phylogenetic classes for HDAC: class I and class II, where class I comprises HDAC 1, 2, 3 and 8, and they are generally close to yeast, and class II consists of HDAC 4, 5, 6, 7, 9 and 10. Most HDACs are located in the nucleus, including class I; however, HDAC3 can also localise to the cytoplasm. Class II can be found in the nucleus and cytoplasm due to their ability to shuttle in and out of the nucleus (Figure 1.6, a) (De Ruijter et al., 2003)

Studies have shown that histone deacetylase 6 (HDAC6) is a unique enzyme in HDACs due to the fact that it has a minimal effect on cell cycle-related gene expression and cell proliferation. HDAC6 can be found in the cytoplasm, although in the nucleus it associates with HDAC11, and functions as α-tubulin deacetylase, regulating microtubule-dependent cell motility. HDAC6 has been noted to be a microtubule-associated protein, which deacetylates α-tubulin and regulates microtubule dynamics (Huo et al., 2011). It was observed, *in vivo*, that HDAC6 plays an important role in regulating stability and dynamics of microtubules, where depolymerised tubulin is quickly deacetylated, whereas acetylated tubulin occurs in polymerised microtubules (Hubbert et al., 2002, Matsuyama et al., 2002, Zhang et al., 2003). Furthermore, HDAC6 can participate in a varied range of cellular processes, and interacts with microtubule-associated proteins at the microtubule plus-end (De Ruijter et al., 2003, Clarke et al., 2011, Ding et al., 2014, Li et al., 2014). HDAC6 consists of two deacetylation domains and binds tubulin via these domains (Zhang et al., 2003), while the N- and C-terminals are responsible for HDAC6 associating with EB1 (the end binding protein 1), Arp1 (actin related protein 1) and CLIP-170, with no overlapping with domains involved in tubulin binding (Zilberman et al., 2009, Li et al., 2011, Li et al., 2014) (Figure 1.6, b).

a) Phylogenetic tree of HDACs

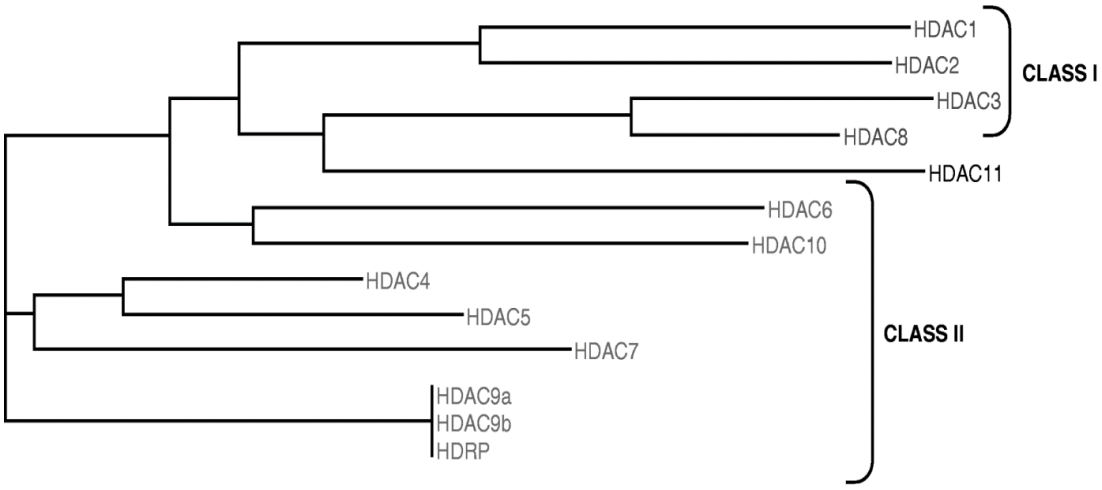

b) HDAC6 domains

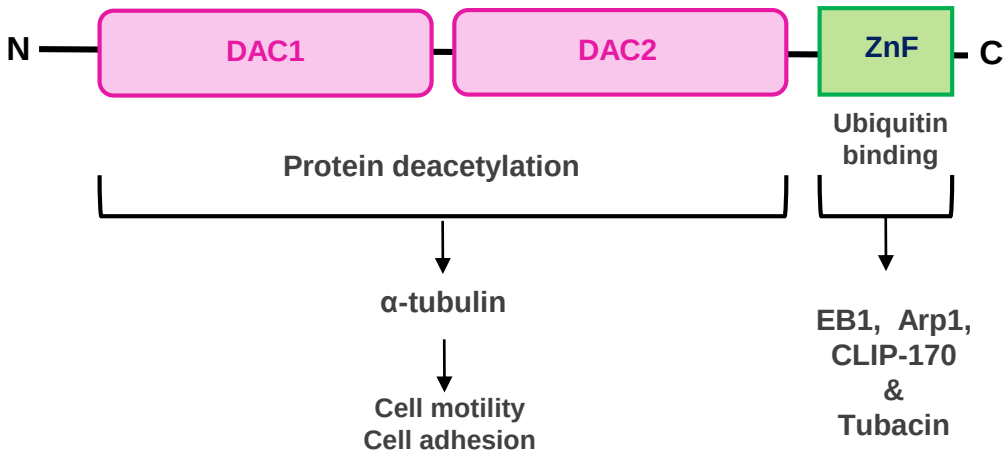

Figure 1.6 HDACs, Phylogenetic tree and HDAC6 domain
a) Phylogenetic tree of HADCs have two classes, I and II. Class I contains HDAC 1, 2, 3 and 8. Class II contains HDAC 4, 5, 6, 7, 9 and 10.
b) HDAC6 domains comprise two deacetylation domains and bind tubulin through these domains, whereas C-terminals are responsible for HDAC6 associated with EB1 (the end binding protein 1), Arp1 (actin-related protein 1) and CLIP-170 without overlapping with domains involved in tubulin binding. Moreover, tubacin inhibiter binds HDAC6 via C-terminal. Adapted from Zhang et al. (2003).

Overexpression of HDAC6 causes complete deacetylation of microtubules and promotes cell migration of many cancer cells, including pancreatic cancer, ovarian cancer and prostate cancer cell (Hubbert et al., 2002, Yang and Seto, 2008, Huo et al., 2011, Li et al., 2014, Rymut and Kelley, 2015). It has been indicated that HDAC6 activity can be inhibited by several HDAC6 inhibitors, such as trichostatin A (TSA, a non-specific inhibitor of HDAC6), tubacin (tubulin acetylation inducer) and tubastatin A (a specific inhibitor of HDAC6). Tubacin is a specific inhibitor of the deacetylation of α-tubulin with no effect on the level of histone acetylation and gene expression of cell cycle processing, where it interacts with one of deacetylate domains of HDAC6 at the C-terminal (Haggarty et al., 2003). It has been reported that treating cells with tubastatin A, TSA or tubacin dramatically increases α-tubulin acetylation, efficiently increasing the amount acetylation microtubules (Zilberman et al., 2009, Asthana et al., 2013). Inhibition of HDAC6 with TSA and tubacin or tubastatin A leads to an increase in microtubule acetylation and this decreases microtubule dynamics, meanwhile genetic knockout and RNAi-mediumted knockdown increases acetylated tubulin but does not affect microtubule dynamics (Zilberman et al., 2009, Asthana et al., 2013) . In addition, TSA and tubastatin A increase the co-alignment between HDAC6 and microtubule lattice in MCF7 treated cells with 240nM of TAS or 30μM tubastatin A for 24 hour (Asthana et al., 2013). So HDAC6 has been used as a target for cancer drugs (Hubbert et al., 2002, Haggarty et al., 2003, Zilberman et al., 2009, Li et al., 2014). Ziberman et al. (2009) suggested that HDAC6 makes a cap at the plus-end of microtubules, and under normal conditions the HDAC6 cap quickly deacetylates α-tubulin and is removed from the microtubule end. Thus, the capping activity has a very quick effect on microtubules and should not impede microtubule dynamics, while the overexpression of HDAC6 influences microtubule dynamics and increases cell movement. Moreover, the HDAC6 cap tracks EB1 and Arp1, and this facilitates the interaction of HDAC6 with the microtubule plus-ends. While inhibition of HDAC6 activity decreases microtubule dynamics by affecting the microtubule

plus-end proteins. For example, it has been found that inhibition of HDAC6 activity leads to a reduction in the length of EB1 comet tail, and decreases microtubule dynamics. However, HDAC6 knockdown has no effect on EB1 comet length, which suggests that HDAC6 is associated with EB1 and Arp1 and affects their localisation at microtubule ends (Zilberman et al., 2009).

Inhibition of HDAC6 activity by tubacin and TSA impairs cell migration, and TSA (but not with tubacin) increases CLIP-170 acetylation in pancreatic cells (Li et al., 2014). At the same time, inhibition of HDAC6 activity by tubacin in mouse embryonic fibroblast cells increases the total area of adhesion and decreased adhesion turnover, which then rapidly suppressed cell motility (Tran et al., 2007).

1.4.4.3 Other post-translational modification

Polyglutamylation and polyglycylation are types of translational modifications found in the axonemes of cilia and flagella. They consist of adding one or more glutamate and glycine to side chains on one or more of the glutamates in the C-terminal domains of both α and β tubulins by tubulin tyrosine ligase-like (TTLL) family enzymes. Polyglutamylation has vital roles in control of transport within cilia and flagella, which allow fine-tuning of motor activity (Janke et al., 2005, Janke and Bulinski, 2011, Yu et al., 2015).

Phosphorylation can also occur on microtubules at serine and tyrosine residues near the C-terminal. α-Tubulin is phosphorylated on tyrosine residue by kinases, such as Cdk1, CK2 and CamkII and Scr, while β-tubulin is phosphorylated on serine residues, which inhibits polymerisation. In general, phosphorylation of tubulin has been poorly studied and little is known about the process (Janke and Bulinski, 2012, Yu et al., 2015).

1.5 Microtubule Dynamics and Microtubule-associated Proteins

1.5.1 Dynamic instability

A fundamental characteristic of microtubules is their ability to be highly dynamic. Microtubules can switch rapidly between phases of growth, pause and shrinkage at the microtubule plus-end; this behaviour is called dynamic instability. Dynamic instability allows the microtubules to explore the cytoplasm and make contact with cellular structures such as kinetochores or the cell cortex (Galjart and Perez, 2003, Galjart, 2010). This helps microtubule networks to rapidly rearrange in response to cellular function. The alteration from growth to shrinkage is termed 'catastrophe', and the conversion from shrinkage to growth is termed 'rescue' (Mitchison and Kirschner, 1984, Howard and Hyman, 2003, Akhmanova and Steinmetz, 2015).

The dynamic property of microtubules is based on the GTP-cap model; in the presence of this cap a microtubule continues to grow and becomes elongated. On the other hand, loss of the GTP-cap by hydrolysing to GDP causes rapid microtubule shrinkage, where the hydrolysis of GTP to GDP on β-tubulin depolymerised microtubules (Howard and Hyman, 2007, Akhmanova and Steinmetz, 2015). A tight lattice is generally organised by growing microtubules that are bound to GTP, and this affects microtubule structure and stability. However, unstable microtubules bound to GDP undergo disassembly at the end of the filament, and the microtubule begins to depolymerise. In this phase, unstable microtubules experience catastrophe and begin to shrink. Rescue can occur in the shrinking microtubules, enabling them to start growing again (Desai and Mitchison, 1997, Akhmanova and Steinmetz, 2015). The actual growth rate of an individual microtubule can differ over time and relies on the length of the GTP-cap at the microtubule plus-end. Dynamic instability is influenced by a variety of

microtubule-associated proteins (MAPs) that tightly control the changes between phases of growth and shrinkage. Post-translation modification of tubulin also affects dynamics. However, regulation of microtubule dynamics remains unclear (Howard and Hyman, 2009, Akhmanova and Steinmetz, 2015).

1.5.2 Polymerases and depolymerases

Polymerases and depolymerases facilitate and regulate microtubule plus-end switching between growth and shrinkage. Microtubule depolymerisation factors are kinesin families, kinesin-8, kinesin-13 or kinesin-14. Kinesin-13 family proteins such as MCAK have been identified as regulating microtubule disassembly. MCAK requires ATP hydrolysis to function, in order to remove terminal subunits from microtubule ends. Kinesin-8 can destabilise the GTP cap on microtubules by using their ability to walk along the microtubule to plus-ends and remove the subunits. Furthermore, they accumulate at the end of longer microtubules and depolymerise them. Additionally, these kinesin families can disassemble stabilised microtubules (Howard and Hyman, 2007, Howard and Hyman, 2009, Akhmanova and Steinmetz, 2015).

The polymerase XMAP215 (human homologue chTOG, gene CKAP5) has been well studied and identified as a polymerase, where it promotes the growth rate of microtubules up to ten times, thus, accelerating the regrowth of microtubules. TOG domains are important for increasing regulating microtubule growth. It has been suggested that there are two ways in which XMAP215 might catalyse polymerisation. XMAP215 could act as an adaptor and bring multiple tubulin monomers to growing microtubule ends, or modify the structure of growing microtubule ends to facilitate tubulin binding (Howard and Hyman, 2007, Akhmanova and Steinmetz, 2015).

1.5.3 Microtubule plus-end tracking proteins (+TIP)

Microtubule plus-end tracking proteins (+TIPs) are a varied group of microtubule-associated proteins that track the plus-end of growing microtubules. They are highly diverse proteins that include microtubule-dependent motors and non-motor proteins. Microtubule +TIPs can be distinguished from other microtubule-associated proteins by their specific accumulation at the plus-ends of growing microtubules. However, investigating +TIPs is complex, due to their interactions with each other and binding to the plus-end of microtubules (Galjart and Perez, 2003, Galjart, 2010). +TIPs have an important function, by which they contribute to regulating the dynamic behaviour of microtubules, which affects the shape of the microtubule network, and thus cell functions such as cell division and motility. They also have a role in cargo capture through interactions with motors and facilitate interactions of microtubule ends with various cellular components, such as the cell cortex and kinetochores (Akhmanova and Hoogenraad, 2005, Galjart, 2005, Galjart, 2010, Akhmanova and Hoogenraad, 2015).

It has been demonstrated that there are three mechanisms by which +TIPs associate with microtubule plus-ends, including treadmilling, hitchhiking and motor transport. Treadmilling is the most studied mechanism and was described using live imaging of GFP-CLIP-170. The +TIPs lasts only for a short time and dissociates at the microtubule plus-ends, and this +TIP does not move along the microtubule lattice. The addition and loss of +TIP molecules from the microtubule ends is not fully understood; however, some +TIPs, such as CLIP-170 and $p150^{Glued}$, may co-assemble with tubulin heterodimers, and when phosphorylated increase the release from the microtubule. Other treadmilling +TIPs such as the end binding proteins (EBs) may use different mechanisms, by recognising the structural features or affinity for the GTP-cap at tubulin, EB1 binds to a stabilised microtubule in the presence of the GTP-cap. Hitchhiking is similar to treadmilling, as it involves transient binding to the microtubule via other +TIPs (Carvalho et al., 2003, Galjart

and Perez, 2003, Galjart, 2010, Akhmanova and Steinmetz, 2015). The budding yeast protein Kar9p is a well-studied example, where a relative homologue of the mammalian tumour suppressor protein, adenomatous polyposis coli (APC), depends on EB1 homology Bim1p for recruitment to the microtubule plus-end. The final mechanism depends on motor transport; some +TIPs, including APC, are transported to the plus-ends of the microtubule by kinesin family motor proteins (Carvalho et al., 2003, Akhmanova and Steinmetz, 2015). So the +TIPs can use a single mechanism or combinations of mechanisms, as demonstrated for APC (Carvalho et al., 2003). APC can associate with microtubules by three different methods: direct binding to microtubules through their microtubule binding domain by hitchhiking through EB1 or by transport via a kinesin motor (Carvalho et al., 2003).

1.5.3.1 The end binding proteins

The most prominent group of +TIPs are the end binding (EB) proteins. Mammalian cells have three highly conserved proteins: EB1, EB2 and EB3, encoded by three separate genes MAPRE 1, 2 and 3. EB1 is considered to be the master controller of +TIPs, due to its ability to independently recognise and bind to the plus-ends of growing microtubules. EB1 was first discovered as an APC (adenomatous polyposis coli) binding partner in a yeast two-hybrid screen, and its gene located to human chromosome 20q11.2, which is called MAPRE 1 (Su et al., 1995). It was later shown that the EB1 organisation revealed an association with microtubules in both interphase and mitosis, independently from its interaction with APC (Morrison et al., 1998). In humans two more genes were identified: MAPRE 2 on chromosome 18q12.1 (encoding EB2) and MAPRE 3 on chromosome 2q23.3-p23.1 (encoding EB3) (Su and Qi, 2001).

EBs are small proteins with a molecular weight of around 30–39 kDa, and consist of an N-terminal calponin homology (CH domain), which is followed by a

changeable linker region, and a coiled-coil domain followed by the C-terminal acidic tail region. The CH domain in the linker region is necessary to specifically recognise and track growing microtubule ends. The linker region is composed of Ser, Thr and Tyr residues, which contribute to the phosphorylation of EB function during the cell cycle (Akhmanova and Steinmetz, 2015). The coiled-coil domain extends into an end-binding homology (EBH) domain and a C-terminal EEY/F acidic tail region. It has been suggested that the coiled-coil domain has a role in controlling the direct binding to GTP-tubulin, while the C-terminal domain tail region interacts with various +TIPs (Akhmanova and Steinmetz, 2008, Akhmanova and Steinmetz, 2015). It has been revealed that the capability of the EB proteins to dimerise through the EBH domain is crucial for their plus-end tracking ability (Slep and Vale, 2007). The C-terminal acidic tail has also shown to be important as a self-inhibitor of EB activity, beside its main function as a location for protein binding (Figure 1.7, a) (Hayashi et al., 2005, Akhmanova and Steinmetz, 2008, Akhmanova and Steinmetz, 2015).

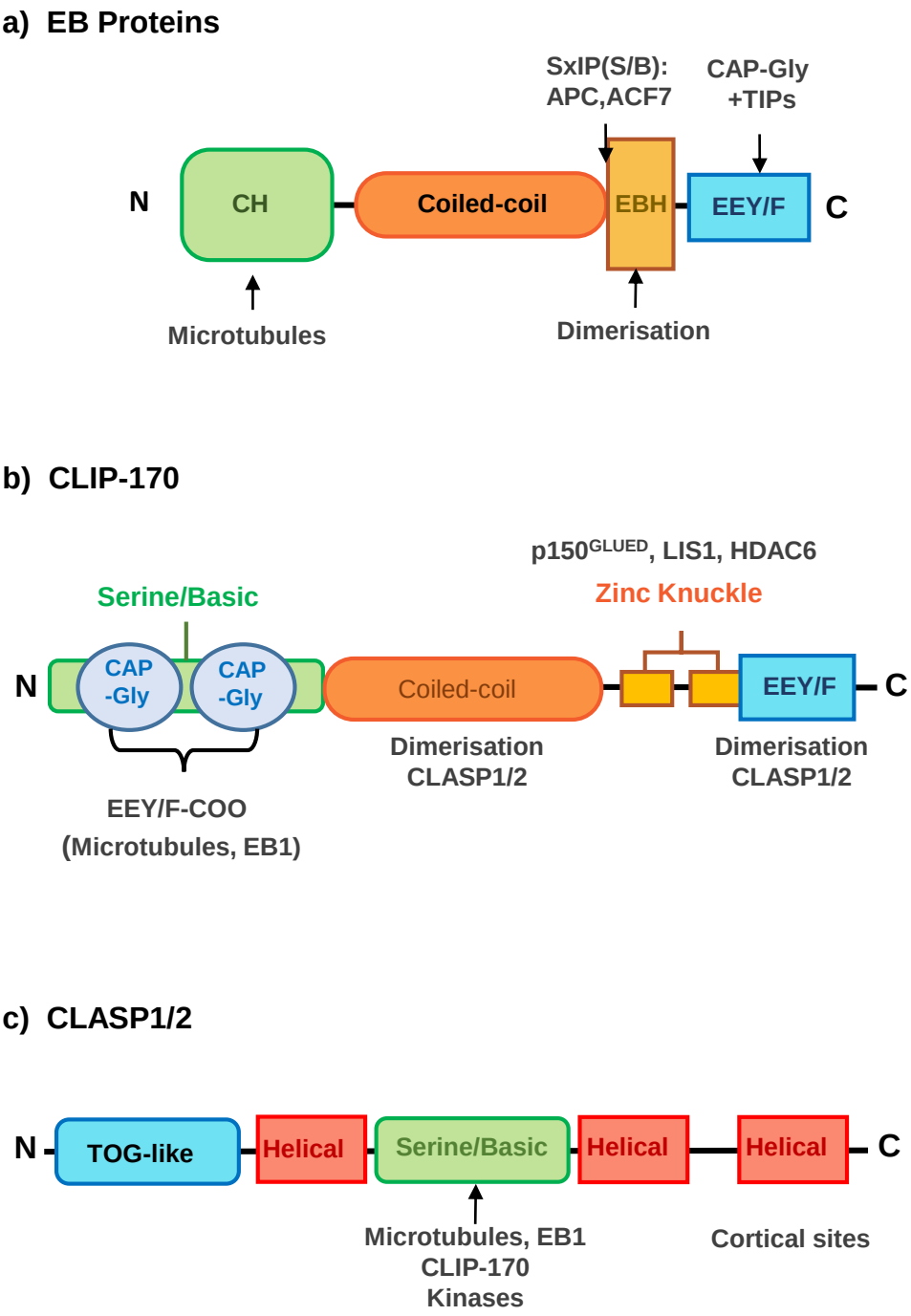

Figure 1.7 Domain structures of +TIP proteins
a) The EBs bind microtubules through their N-terminal CH domain. They bind CAP-Gly+TIPs via the C-terminal acidic tail domain and recognise serine/basic regions through the EBH region. They dimerise via a central coiled-coil region. b) CLIP-170 recognises the C-terminal tail of EB1 and microtubules through N-terminal CAP-Gly domains. CLIP-170 can also bind further +TIPS through additional sites, and can self-inhibit via its own C-terminal tail region. c) CLASP1/2 recognise EB1, microtubules and CLIP-170 through serine/basic. Adapted from Akhmanova and Steinmetz (2008).

Several models have been proposed to explain how the CH domain of EBs recognises the growing ends of the microtubules. EBs may distinguish extended sheets of tubulin at the growing ends, or may bind an A-lattice conformation similar to that found in a microtubule seam. The most well-studied model is its recognition of the GTP tubulin cap, a model proposed in which the EBs may recognise the GTP and GDP nucleotide status of the microtubule (Akhmanova and Steinmetz, 2011). It has been demonstrated that EBs (EB1 and EB3) recognise the end of growing microtubules due to their high affinity for the specific structural conformation exhibited by the GTP tubulin cap, or probably by the GTP hydrolysis processing at this end site. This was shown by using microtubules incorporating GTPγS (a slowly hydrolysable analogue of GTP) (Maurer et al., 2011, Maurer et al., 2012). Interestingly, it has been discovered that remnants of GTP tubulin along the mature microtubule lattice may act as switch points for rescuing depolymerising microtubules (Cassimeris, 2009). Despite the binding to the plus-end of microtubules, all three EB members can also associate along the entire microtubule lattice, as a result of their transient overexpression, they switch to distribution along the lattice (Bu and Su, 2001).

EB1 has been described as the 'master controller' of +TIPs (Vaughan, 2005), because of its ability to track the plus-end of growing microtubules, and interact with most other +TIPs including CLIPs (Lansbergen et al., 2006, Dixit et al., 2009), CLASPs and APC (Mimori-Kiyosue et al., 2005). EB1 and EB3, but not EB2, have an essential role in the regulation of interactions at the plus-end of the microtubule, by facilitating microtubule connections with internal cell structures, such as the cortex, organelles and kinetochores, and also with the actin cytoskeleton (Vaughan, 2005, Lansbergen and Akhmanova, 2006). Furthermore, EB1 is also an active component in the centrosome (Louie et al., 2004), where it has been implicated in spindle formation (Rehberg and Gräf, 2002). It has also been reported to play a role in a microtubule minus end anchoring complex (Yan et al., 2006). EBs affect the

dynamic instability of microtubules, which is an important process for microtubule apico-basal reorganisation during epithelial differentiation. EB1 has been shown to modify microtubule dynamics *in vitro* and *in vivo*, and it is also involved in the accurate chromosome separation during mitosis and in polarisation of the microtubule cytoskeleton in migrating cells (Bu and Su, 2001).

The importance of the role of EBs lies in the regulation of microtubule dynamics, but the exact mechanisms by which they directly perform this function are not fully understood. It has been suggested that EB1 catalyses the rescue phases of microtubule dynamics (Bieling et al., 2007, Vitre et al., 2008), or by suppressing the catastrophe phase (Manna et al., 2008). However, some studies showed no effect at all on both phases; it seems that the EB1 role is to stimulate microtubule growth by impeding catastrophe, which was reported *in vivo* in *Xenopus* and the fission yeast homologue Mal3 (Busch and Brunner, 2004). Structural studies showed EB1 binding between protofilaments and suggest that EB1 discourages the peeling away of protofilaments from the microtubule, which occurs in the catastrophe phase and thus promotes growth (Sandblad et al., 2006, des Georges et al., 2008, Maurer et al., 2012). Additionally, recent studies have shown that the length of the EB1 comet reflects the area of the GTP tubulin cap (Seetapun et al., 2012, Duellberg et al., 2016).

It has also been shown how the domains of the EB family members influence their ability to govern microtubule growth. It was found that EB1 and EB3, but less so EB2, were needed for enhancing microtubule growth, and also suppressing catastrophe, instead of directly promoting growth rate or rescue. From the structural point, the C-terminal acidic tail is not required for the growth, but the EBH domain has the ability to dimerise. EB2 was found to have less ability to compete with other family members for contact with microtubule ends. Phosphorylation of EB2 leads to dispersal in the cytoplasm instead of localisation along the microtubule lattices, which causes a delay in cell mitosis (Iimori et al., 2016). Consequently, EB1 and

EB3 comets appeares as classic +TIP firework shapes, while EB2 is more associated along the microtubule lattice with little accumulation at the plus-ends in interphase cells. This is due to the difference between EB2, EB1 and EB3 amino acids, which are clustered at important CH domain residues (Komarova et al., 2009). Recently, Goldspink et al. suggested that EB2 is expressed during the early stages of differentiation, thus keeping a dynamic microtubule population, which is vital for cell-to-cell junction formation and initial microtubule reorganisation (Goldspink et al., 2013). A recent study showed that overexpression of EB2 is involved in the invasion of pancreatic cancer (Abiatari et al., 2009). Moreover, it has been suggested that EB2 associates with HAX1 (HCLS1-asociated protein X-1) and plays a vital role in focal adhesion turnover and cell migration, where interaction between EB2 and HAX1 in skin epidermal cells promotes focal adhesion turnover while their knockdown results in focal adhesion stability and impair cell migration (Liu et al., 2015). It has also been reported that EB2 associates with MAP4K4 and increases focal adhesion turnover and cell migration (Yue et al., 2014). In addition, CK2 (casein kinase II) has been shown to decrease cell adhesion under shear stress in endothelial cells by phosphorylating EB2 at residue serine 236 (Stenner et al., 2013).

1.5.3.2 Cytoskeleton-associated protein Gly-rich (CAP-Gly) proteins

This group of proteins includes two major +TIPs; the cytoskeletal linker protein (CLIP-170 and CLIP-115), and $p150^{Glued}$, a subunit of dynactin. They can bind to the C-terminal of EBs via their CAP-Gly domains at the N-terminal regions. CAP-Gly domains are globular components that specifically distinguish the acidic C-terminal EEY/F tail motif that is found in EBs, microtubules and CLIP-170 itself (Akhmanova and Steinmetz, 2008, Manna et al., 2008, Honnappa et al., 2009, Komarova et al., 2009, Akhmanova and Steinmetz, 2015).

CLIPs and $p150^{Glued}$ are structurally similar, containing two microtubule-binding domains in the N-terminus, CAP-Gly domains, followed by coiled-coil regions that allow them to form parallel dimers, and Zinc metal motif in the C-terminus that associates with other +TIPs. CLIP-170 can fold back on itself due to the existence of CAP-Gly (Figure 1.7, b) (Akhmanova and Steinmetz, 2008, Akhmanova and Steinmetz, 2015).

CLIP-170 was the first +TIP to be identified, as comets at the plus-end of microtubules in living cells (Perez et al., 1999). It has also been observed that there are two CLIP proteins in mammals, although lower eukaryotes only have one CLIP (Dzhindzhev et al., 2005). Studies have shown that CLIP-170 moves with the growth end of microtubules in living cells. Therefore, it has been suggested that CLIP-170 and CLIP-115 may act as rescue factors, as they were observed in the rescue phase of microtubules, but not in the catastrophe. CLIP proteins are dependent on EBs, in particular EB1 and EB3; depletion of both EB1 and EB3 decreases the level of associated CLIPs with microtubule plus-ends, and can be rescued by transfection of an EB1 construct (Komarova et al., 2005). Moreover, CLIP-170 can interact with HDAC6 via coiled coil domain and Zinc finger, and this interaction functions to stimulate the cell migration of pancreatic cancer (Li et al., 2014).

1.5.3.3 Other +TIPs

Many other +TIPs found on microtubules can be characterised by their unique structures. For instance, cytoplasmic linker-associated proteins (CLASPs) are an important class of microtubule-associated proteins (MAPs) and +TIPs. Two members of the CLASP family, CLASP1 and CLASP2, are associated with multiple cellular functions. They contribute to the organisation of subcellular structures by linking microtubules to organelles, and are required for proper spindle assembly during mitosis (Lansbergen et al., 2006, Mimori-Kiyosue et al., 2006,

Wilbur and Heald, 2013). In the interphase cell, CLASPs are involved in forming polarised microtubule arrays and can bind directly to distal microtubule ends and stabilise microtubules by increasing pause and suppress shrinkage in association with EB1 (Mimori-Kiyosue et al., 2005). In particular, CLASP2 links microtubules to the cell cortex via its COOH-terminal domain, and is involved in stabilising microtubules (Mimori-Kiyosue et al., 2005). CLASPs can promote interactions between the microtubule plus-end and the cell cortex via two CLASP partners, LL5β and ELKS, which form a microtubule-independent membrane bond complex, and can bind to EB1 and EB3, and recognise the growing plus-end of microtubules (Mimori-Kiyosue et al., 2005, Lansbergen et al., 2006).

CLASP proteins structurally consist of conserved TOG-like (TOGL) domains and SR-rich domains, which are regions with stretches of sequences rich in serine, proline and arginine. *S. cerevisiae Stu1*, *S. pombe Cls1*, and *C. elegans Cls2* have two TOGL domains, and *D. melanogaster* MAST/orbit and human CLASP1 and CLASP2 have three TOGL domains in their C-terminals (Al-Bassam et al., 2010, Al-Bassam and Chang, 2011). Studies have shown that CLASP proteins enhance microtubule rescue and suppress microtubule catastrophe. These functions are related to the structure of the CLASPs, wherein conserved TOG domains are used to attract tubulin dimers to microtubules by binding a single αβ-tubulin dimer through two sets of TOG domains, and binding to the microtubule lattice through two S/R-rich domains without releasing its bound tubulin dimer (Figure 1.7, c) (Al-Bassam and Chang, 2011).

The polymerase XMAP15 is characterised as a +TIP that binds microtubules via several N-terminal TOG domains (Slep and Vale, 2007). There are different microtubule motors that can accumulate at microtubule ends, and thus can be defined as +TIPs, which bind through multiple tubulin-binding TOG domains. These include dynein and kinesin MCAK, the depolymerised protein, containing

basic/serine SxlP regions, which can bind to EB1 (Akhmanova and Steinmetz, 2015).

1.6 Cell Migration

Migration of single and sheets of cells is vital during embryonic development, and remains essential in the mature organism. Cell migration is required for developmental morphogenesis, tissue repair, regeneration and tumour metastasis. Generally, migration consist of a repetition of four basic steps: a) protrusion, (b) adhesion, (c) contraction, and (d) retraction (Figure 1.8) (Vicente-Manzanares et al., 2005, Tschumperlin, 2013). These different steps have to occur without any disorder, and need to be coordinated in time and space. The four migration steps consist firstly of membrane protrusion at the leading edge leading to the formation of lamellipodia and filopodia. These extensions at the leading edge then attach to the extracellular matrix (ECM) by focal adhesions and via integrins. This attachment to the ECM of the internal cytoskeleton allows movement by myosin II activity to pull the cell over the matrix. In the final step, retraction occurs at the cell rear with disassembly of focal adhesions to allow a new cycle to start again (Figure 1.8) (Etienne-Manneville, 2013, Tschumperlin, 2013).

The migration steps are controlled by many different proteins and especially the Rho family of GTPases (RhoA, Rac1 and Cdc42), which interact with actin filaments, microtubules and focal adhesions during cell movement. Generally, RhoA is considered to influence actin contraction and retraction, and Rac to encourage lamellipodium extension and actin polymerisation while Cdc42 is assumed to enhance filopodia elongation and inhibit actin depolymerisation. The active GTP-bound forms of Rac and Cdc42 accumulate at the front edge of the cells and promote protrusion and initiate adhesion. Meanwhile, at the back of the cell

body Rho activity is important of the maturation of focal adhesions and for cell contraction.

Serious consequences may occur during disorganised migration processes, including intellectual disability, vascular disease, tumour and metastasis. Moreover, a better understanding of cell migration mechanisms could lead to effective treatment for diseases such as invasive cancer cells (Lauffenburger and Horwitz, 1996, Horwitz and Webb, 2003, Parsons et al., 2010, Etienne-Manneville, 2013).

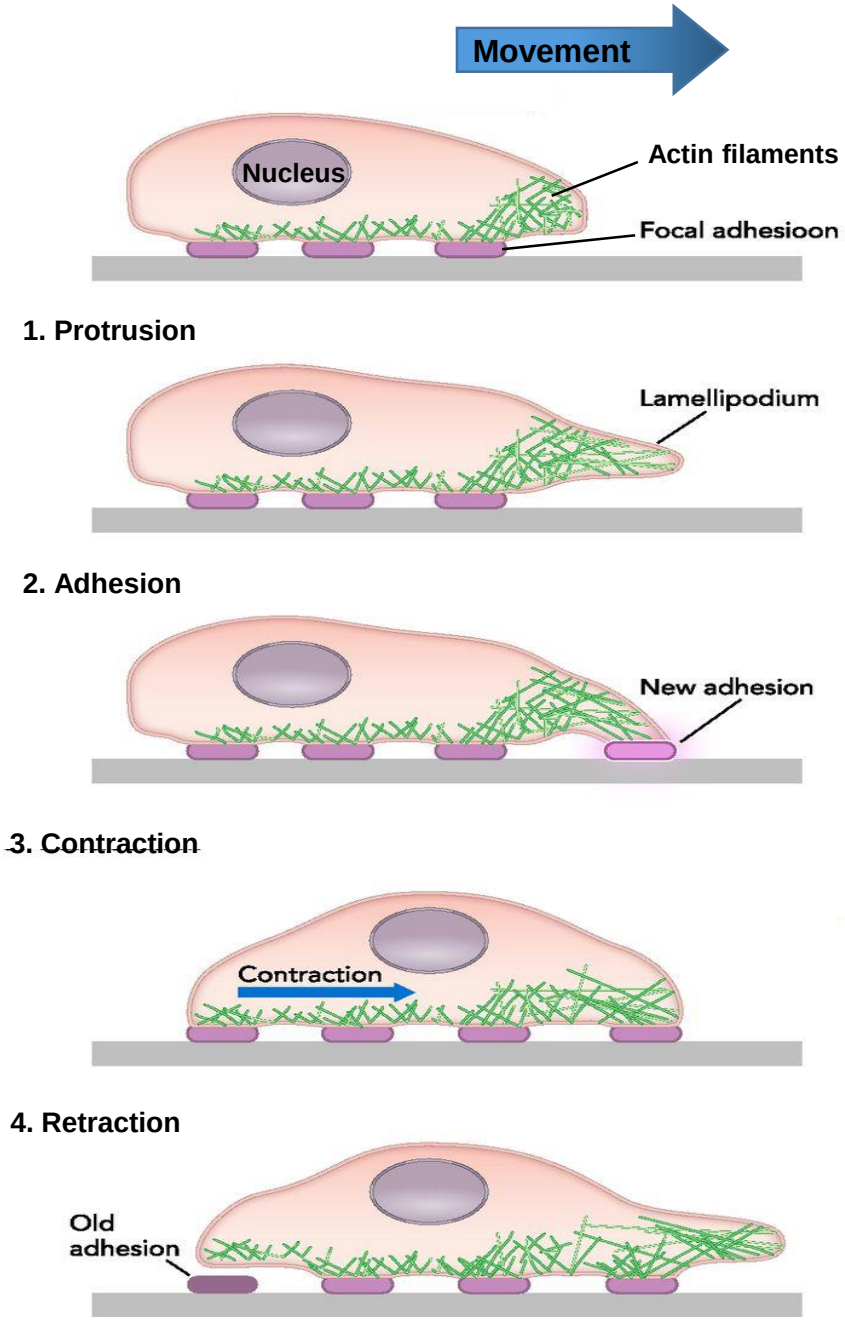

Figure 1.8 Cell migration mechanism

Schematic representation of the steps in cell migration. 1. Extension of a protrusion at the leading edge forming the lamellipodium. 2. Formation of new adhesions that attach the cell to the ECM, which allows the cell to crawl over the matrix. 3. Contraction at the rear area and 4. De-adhesion at the trailing edge to start a new cycle again. Adapted from (Tschumperlin 2013)

1.6.1 Cytoskeletal organisation in migrating cells

The cytoskeleton consist of actin filaments, intermediate filaments and microtubules that play an essential role in cell migration. The cytoskeleton needs rearrangements in order to produce the force to perform the required movement. Generally, the leading edge of a migrating cell extends to form a lamellipodium that is characterised by an extensive actin network. This actin network pushes forward the membrane with myosin II and actin stress fibres contracting at the back of the cell. At the same time, the centrosome and Golgi apparatus relocate to a location in front of the nucleus. Meanwhile, microtubules are required for the direction of migration. Microtubules act to suppress regional remodelling of cell morphology and thus specify the direction of migration. In migrating cells, lamellipodia extend at the front area with some stable microtubules, resulting in inhibition of lamellipodium retraction in that region. Microtubules aid in the delivery of vesicles that help to maintain the growth of the leading edge, and therefore prioritise the lamellipodium to establish the leading edge. At the same time, the rear area of the cell is rich in dynamic microtubules, which cause high turnover of focal adhesions at the back of the cell but little turnover at the front (Pollard and Borisy, 2003, Goley and Welch, 2006, Ganguly et al., 2012, Vinzenz et al., 2012, Etienne-Manneville, 2013).

Actin filaments play essential roles in cell migration, where they are involved in all processes of migration, protrusion, adhesion, contraction, and retraction. At the leading edge of migrating cells, an actin network provides forces through the formation of lamellipodium, which derives from retrograde actin flow and myosin generated tension. Actin filaments are nucleated by ARP2/3 complex at the front of the cells with most of their plus-ends close to the plasma membrane. Filopodia consist of actin filaments, which are finger-like structures found at the advance front of the leading edge where the plus-ends of the actin bundle point outward. The actin bundle within filopodia are nucleated by formins that associate with the

plus-end of actin filaments to promote assembly. Moreover, filopodia are vital for the directional response of the migrating cell. Actin filaments also create contractile stress fibres (actin and myosin II), which are responsible for contraction of the cell body and retraction of the trailing edge, and also for contacting focal adhesions (Figure 1.9, a) (Pollard and Borisy, 2003, Blanchoin et al., 2014). There are different types of stress fibre, ventral stress fibres, which are anchored at each end by focal adhesions, and dorsal stress fibres, which are anchored at one end by a small focal adhesion behind the leading edge. Dorsal stress fibres extend towards the nucleus and link with transverse arcs. Arcs consist of a bundle of actin filaments and little or no myosin II that form behind the front of migrating cell or spreading cells and are generated by the ARP2/3 complex. They act as connectors for the the ventral adhesion with the dorsal contractile actin network (Figure 1.10) (Burridge and Guilluy, 2016).

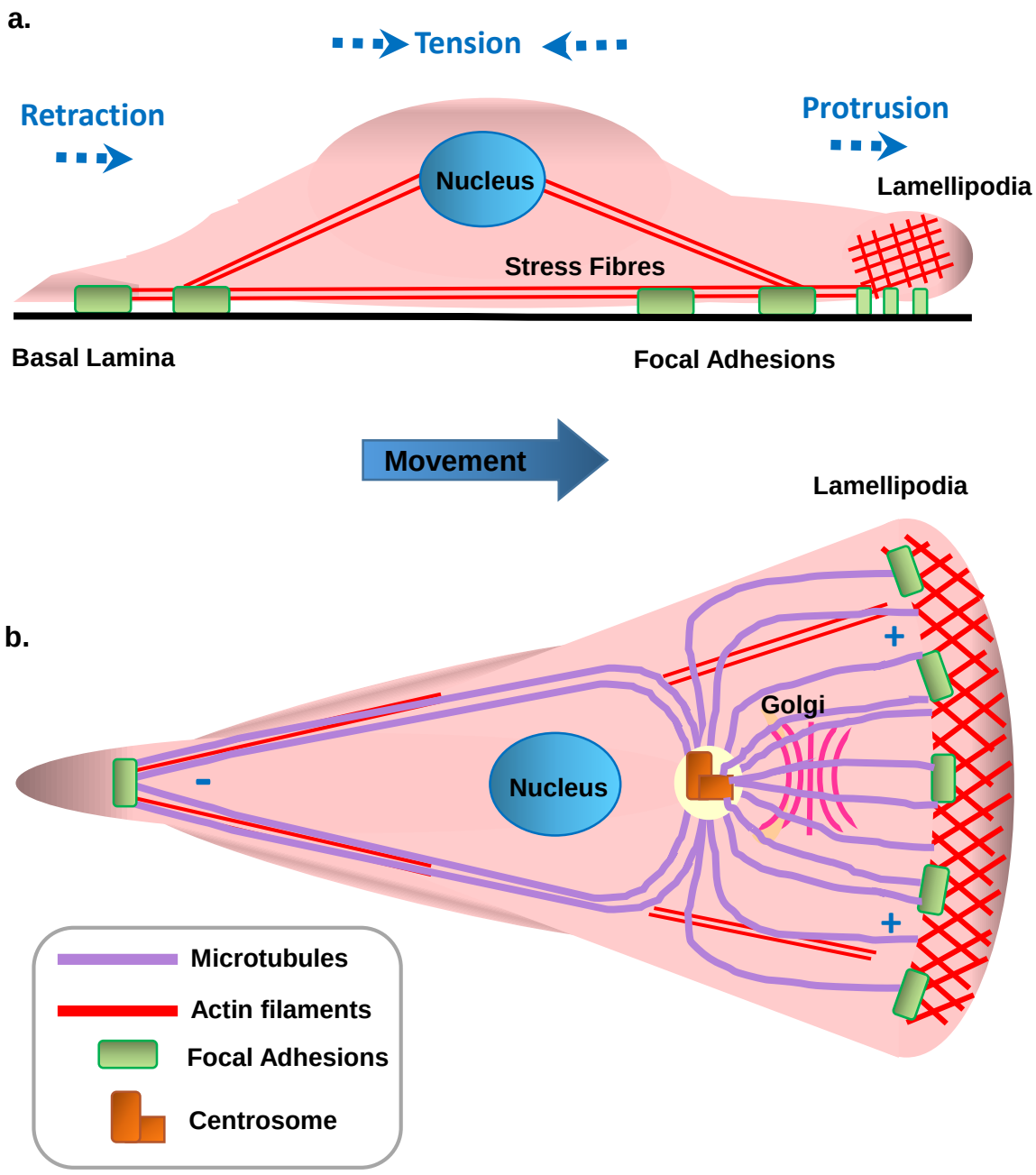

Figure 1.9 Cytoskeletal organisation in cell migration
a) A migrating cell undergoes different actin related processes. During migration, polymerised actin filaments in Lamellipodia push forwards the plasma membrane at the leading edge. Focal adhesions are attached to the ECM, allowing tension exerted by actomyosin contraction in stress fibres to pull the cell forward. Finally, focal adhesions turnover and the rear of the cell retracts. b) Microtubules reorganise during cell migration. The centrosome and Golgi apparatus relocates to the front of the nucleus facing the leading edge, where stable microtubules extend to the leading edge. Dynamic microtubules also extend to the rear of the cell. Adapted from (Lauffenburger and Horwitz, 1996; Ridley et al. 2003).

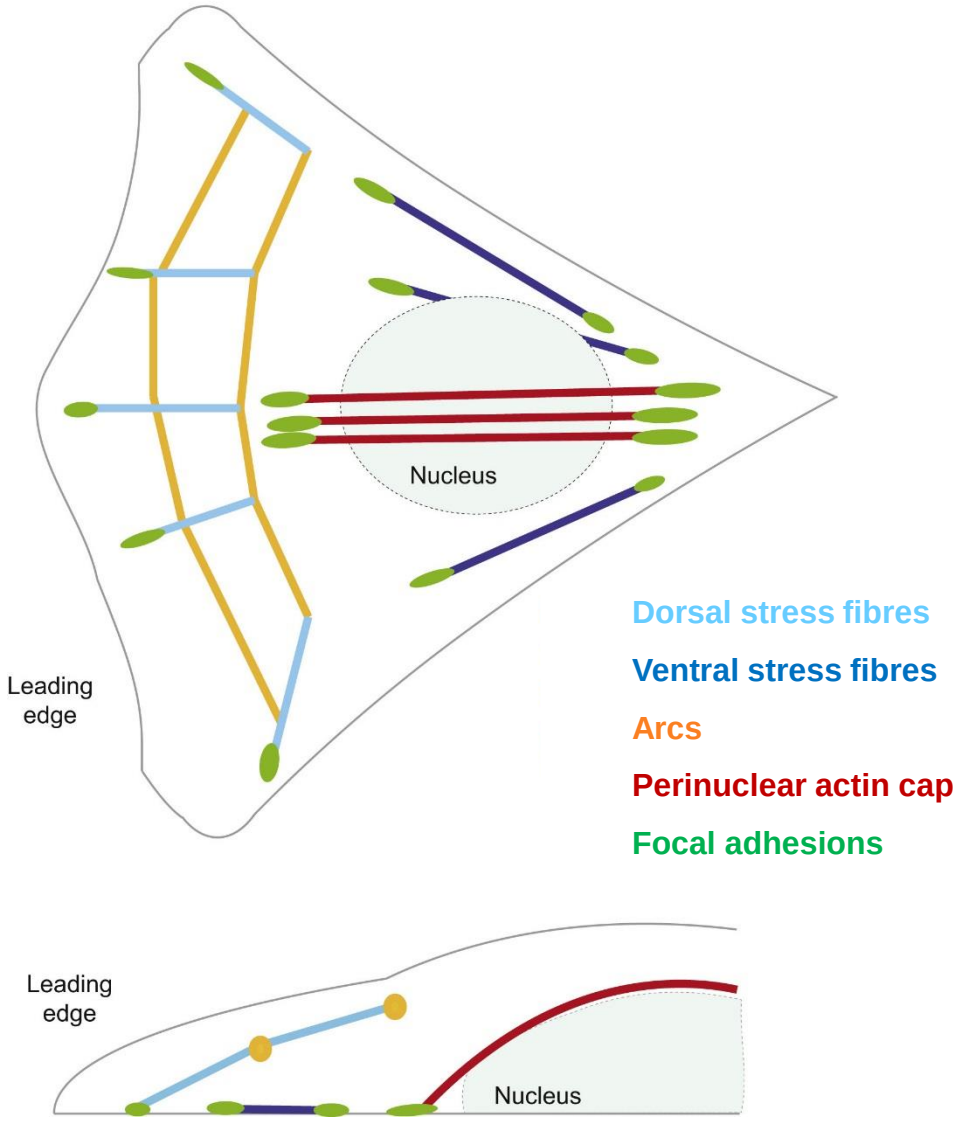

Figure 1.10 Schematic representation of stress fibres types

Four different types of stress fibre in migrating cells, dorsal stress fibres that are anchored at one end by focal adhesion close to the cell front edge. Ventral stress fibres anchored at the both ends by focal adhesion. Arcs are formed behind the leading edge of spreading cells of migrating cells, and they are not directly linked by focal adhesion. Fourth type is the perinuclear actin cap, which is consisted of ventral stress fibres that wrap over the nucleus and anchor to elongated focal adhesions, which associate focal adhesion from at each end. Adapted from (Burrindge and Guilluy, 2016).

Migrating cells are controlled by the Rho GTPase family of proteins, including RhoA, Rac and Cdc42. They play important roles in cell migration by regulating the changes in the cytoskeleton and in adhesions to establish movement. In general, Rho family protein activity is important for regulating adhesions sites and have major roles in modulating microtubule stability (Wojnacki et al., 2014). The activity of Rho family proteins is regulated by GTP-binding, exchanging GDP to GTP by GEFs (guanine nucleotide exchange factors) that activate Rho family. GAPs (GTPase-activating proteins) are inactivators that prevent the activity of Rho family proteins and hydrolyse GTP to GDP. Rac can also be activated by tyrosine receptors or G-protein couple receptors, and also by integrin (Raftopoulou and Hall, 2004, Etienne-Manneville, 2013).

Actin filaments are the main target for Rho family proteins. Rho family proteins play different important roles in actin filament regulation during cell migration. RhoA has a critical role in regulating the formation of stress fibres and regulates cell body contraction by controlling myosin II. Meanwhile, the formation of the lamellipodium can be promoted by Rac1 via stimulation of actin polymerisation, where it has been found that inhibition of Rac can suppress cell migration. Rac can also stimulate actin polymerisation by interaction with WASp and N-WASp that leads to activation of the ARP2/3 complex (Raftopoulou and Hall, 2004). Cdc42 is another Rho family protein that induces filopodia formation and acts at the advancing front of migrating cells to control the direction (Ridley, 2001, Burridge and Wennerberg, 2004, Raftopoulou and Hall, 2004, Etienne-Manneville, 2013).

Adhesion formation is an important step toward cells migration. It occurs during the binding of adhesion receptors to ECM via integrins along the cell periphery. The attachment between cell and ECM generates the required force for crawling over the matrix, which relies on the ability of the cells to dynamically remodel adhesion sites. Small focal adhesions can be located in the lamellipodium, and they are referred to as focal complexes, and allow the cell to generate traction and then

rapidly turnover. In contrast, focal complexes can mature into focal adhesions, which are stable large complexes, and associate the ends of stress fibres (Wolfenson et al., 2009, Danen, 2013). Several large proteins have been defined at focal adhesions, due to different interaction partners that allow the cell to construct many signalling complexes with different behaviours. These proteins include paxillin, vinculin, FAK (focal adhesion kinase) and ILK (integrin-linked kinase), along with ingegrin subunits, such as α-V and β-3 (Figure 1.11) (Wozniak et al., 2004). Integrins mediate cell adhesion with the extracellular matrix (ECM) and have vital roles in cell survival, differentiation and migration. Integrins are heterodimers consisting of α and β subunits, with different types determining the receptor specificity for the different ECM molecules. For example, human retinal pigment epithelial cells (ARPE-19) expresses integrin α5 that interact with fibronectin (Hynes, 1992, Elner and Elner, 1996, Proulx et al., 2004). There is little information of integrins in PANC1 cells but one study seems to indicate that α2 β1 which interacts with collagen1 is expressed in these pancreatic cells (Arao et al., 2000).

In migrating cells, a dissociation occurs to the small adhesions near the cell leading edge that allows the cell to detach from ECM and then re-attach again at different spots. While the mature focal adhesion anchors stress fibres to generate contraction forces and also to stop the cell movement (Parsons et al., 2010). The connection between focal adhesions and actin filaments is obtained by adaptor proteins, such as talin and tensin. This allows new focal adhesions to grow and mature and then provide forward traction forces with actin filaments and myosin II. These processes are governed by Rac1 that is vital for actin filament growth in lamellipodium that lead to promote adhesions growth, with Cdc42 contribution to Rac activation or localisation at the leading edge (Ridley, 2001). Focal adhesions have to disassemble in the cell body and in the rear of the cell in order to allow the cell to move forward, and this requires dynamic microtubules. To complete the migration cycle integrin mediumted focal adhesions connect the actin filaments and allow cells to crawl on

the extracellular matrix during migration. However, focal adhesions can increase cell adhesion with ECM, and thus decrease cell migration, where RhoA controls focal adhesion turnover (Wozniak et al., 2004, Parsons et al., 2010, Etienne-Manneville, 2013, Danen, 2013, Burridge and Guilluy, 2016).

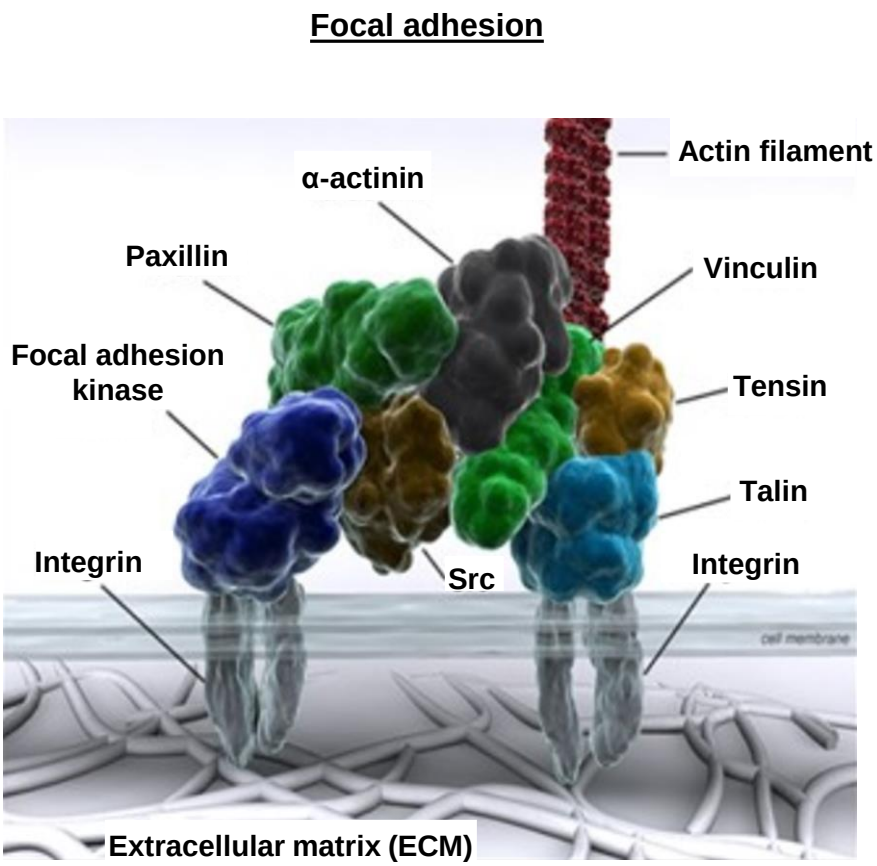

Figure 1.11 Cell adhesion composition
Mature stable focal complexes termed focal adhesions. Focal adhesions are large and consists of a large number of proteins, including paxillin, vinculin and two integrins α-V and β-3. Adhesion complexes link with actin filaments via different proteins, such talin and tensin. Adapted from Wozniak et. al., 2004.

Microtubule dynamics have critical roles in cell migration, where the microtubules act differently at the front and the rear of migrating cells. During cell migration, stabilised microtubules enable the centrosome to reorient towards the leading edge, which causes a polarised microtubule array that facilitates cell movement. Basically, migrating cells relay on both actin filaments and microtubules to generate required forces in protrusions. Stable microtubules contribute to the generation of pushing forces needed for the lamellipodium with a few microtubules interacting with actin filaments near the leading edge. These microtubules are referred as pioneer microtubules and are found in the lamellipodium . Stable microtubules also target and interact with young adhesions to deliver additional components or to dissolve adhesions at the front to maintain the cycle. Meanwhile, more dynamic microtubules found at the cell rear influence focal adhesion turnover to start the contraction at the cell rear (figure 1.9, b) (Kaverina and Straube, 2011, Etienne-Manneville, 2013, Akhshi et al., 2014, Charafeddine et al., 2016). Microtubules also play an indirect role in cell protrusion by regulating signalling proteins and impact on the activity of RhoGTPases and locally increasing actin polymerisation. Rac is mainly active at the cell front, thus induces actin filament assembly, and RhoA is mainly active at the cell rear to induce myosin II contraction and focal adhesion turnover. Both proteins are regulated by dynamic microtubules, with stable microtubules at the cell front regulating Rho activity by sequestering the Rho effector GEF-H1 from microtubules but dynamic microtubules at the rear area release Rho GEF-H1 to activate Rho and cause focal adhesion turnover and influence myosin II contraction (Stehbens and Wittmann, 2012, Akhshi et al., 2014). It has been shown that, nocodazole treatment activates RhoA signalling through ROCK (Rho-associated kinase) to trigger the release of Rho effector GEF-H1 from microtubules and activate Rho (Chang et al., 2008). Rac is inactive at the cell rear and binds cytoplasmic tubulin, however, it is active at the cell front and causes an increase in focal adhesion growth and polymerises actin filaments (Akhshi et al., 2014, Charafeddine et al., 2016).

Dynamic microtubules promote focal adhesion turnover by delivering important proteins for disassembly with +TIPs contribution. Recently, it has been reported that EB2 increases focal adhesion turnover via association with essential protein kinase kinase kinase 4 (MAP4K4, disassembly protein) (Yue et al., 2014). Furthermore, EB2 associates with HAX1 to increase focal adhesion turnover and promotes migration, while knockout will impair cell migration (Liu et al., 2015). Moreover, depleting EB2 can inhibit microtubule dynamics and result in co-alignment between microtubules and actin filaments with EB1 and ACF7 associated along the lattice, which leads to impair migration (form unpublished data from our lab) (Goldspink et al., 2013). APC can increase protrusions in migrating cells by promoting the growth of microtubules and decreasing shrinkage (Carvalho et al., 2003, Kroboth et al., 2007, Komarova et al., 2009). It has been shown that microtubule associated protein CLIP-170 binds closely to formins to increase actin filament elongation. Thus, dynamic microtubules are required for rapid actin filament assembly (Stehbens et al., 2014, Henty-Ridilla et al., 2016). ACF7, CLIP-170 and ACP are localised at the growing microtubule ends via an interaction with EB1 and this contributes to microtubule organisation and stabilisation near the leading edge and also localise focal adhesion sites in migrating cells (Stehbens and Wittmann, 2012, Akhmanova and Hoogenraad, 2015). Moreover, microtubule associated motors can deliver β-actin and ARP2/3 complexes to influence actin polymerisation (Vinzenz et al., 2012, Etienne-Manneville, 2013). Many +TIPs (including APC, CLIPs and CLASPs) can also interact with Rac and Cdc42 via IQGAP1. In addition, ACF7 has been linked to the disassembly of focal adhesions, where it associates with EB1 at the plus-end of microtubules and help to guide along actin filaments (Wu et al., 2008, Kaverina and Straube, 2011).

1.7 Sulforaphane (SFN)

Several natural components in our diet have been found to have an inhibitory influence on tumorigenesis. Isothiocyanates (ITCs) are produced in plants and specifically in cruciferous vegetables, and the most characterised component is sulforaphane (SFN). It has been documented that SFN has various possible mechanisms to prevent cancerous activity and slow progression of the disease (Fimognari and Hrelia, 2007). However, the molecular mechanisms of the effects of SFN in many cancer diseases has not been fully clarified and especially its effect on microtubules.

Cruciferous vegetables, for instance broccoli, cauliflower, cabbage and kale, have been associated with cancer protection. Studies showed that 67% of investigations on the consumption of these vegetables and cancer risk reported an inverse relation between consumption and risk of cancer. Furthermore, the studies found the greatest inverse associations between the consumption of broccoli/brassica and risk of different cancers, such as lung, stomach, prostate and pancreatic cancer (Verhoeven et al., 1996, Cohen et al., 2000).

Crucifers contain various bioactive components, including flavonoids, minerals (selenium) and vitamins (vitamin C); however, the bioactive compounds connected with cancer protection are glucosinolates (GLS). GLS is a chemical compound that consists of a β-D-thioglucose group (a sulfonated oxime group and a side chain comes from methionine, phenylalanine), tryptophan or branched-chain amino acids. Glucosinolates have to be hydrolysed to become bioactive and are then called isothiocyanate (ITC). Isothiocyanate is released when the cell wall is ruptured during chewing, producing an enzymatic reaction between the myrosinase enzyme and glucosinolates (Figure 1.12) (Fimognari and Hrelia, 2007, Houghton et al., 2013).

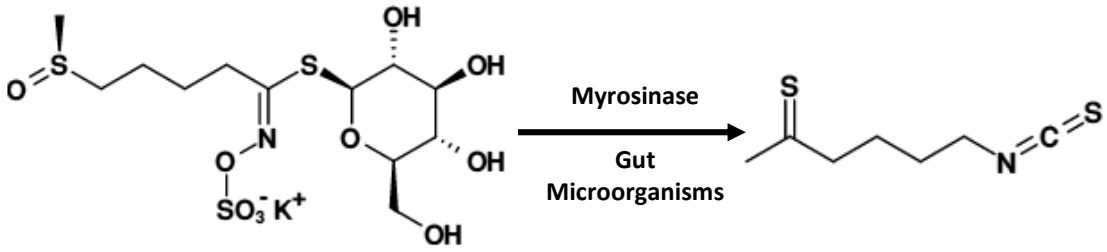

Glucoraphanin **Sulforaphane**

Figure 1.12 Sulforaphane (SFN)

Isothiocyanate (ITC) released when the cell wall is ruptured during chewing, produces an enzymatic reaction between the myrosinase enzyme and glucoraphanin. The most characterized broccoli-derived isothiocyanate is sulforaphane (SFN). SFN comprises [1-isothiocyanato-4-(methylsulfiny) butane], and it is highly concentration in broccoli. Adapted from (Fimognari and Hrelia, 2007).

In humans, high concentrations of isothiocyanate can be established in the diet by ingesting crucifers, where the highest SFN concentrations of ~2-3 μM in plasma, serum and erythrocytes are achieved one hour after ingestion of broccoli or sprouts containing 200 μM equivalents of isothiocyanates (Gasper et al., 2005). It has been reported that super broccoli has approximately 2.5 μmol of glucoraphanin per gram (Traka et al., 2013). This will equate to 2.5 μmol of SFN/gram if fully converted, so it can suggest that to get a concentration of 23 μmol/L we would need to eat 1Kg/ broccoli.

Studies have shown that there are several different possible mechanisms of SFN in preventing cancer, including the inhibition of carcinogen-activating enzymes, such as the cytochrome P450 isoenzyme 2E1, the induction of conjugating enzymes, such as glutathione S-transferases, the reduction of the DNA binding ability of nucleus and the inhibition of histone deacetylase (HDAC) activity *in vitro* and *in vivo*. SFN can also induce apoptotic cell death by significantly reducing the viability, as found in breast cancer cells. It seems that SFN induces apoptosis through the mitochondrial pathway, where cytochrome c is released and activates caspases (degrades proteins) (Pledgie-Tracy et al., 2007, Dickinson et al., 2015). In addition, SFN is known to affect microtubule polymerisation in cancerous cells, inhibiting cell proliferation and initiating apoptosis, thus retarding or eliminating neoplastic cells and inhibiting the progression of benign tumours into malignant tumours, and metastasis formation. Therefore, it seems SFN is capable of preventing, delaying or reversing the formation of a malignant neoplasm, as well as having the ability to act on cancerous cells, and thus holds the potential to be a therapeutic agent (Fimognari and Hrelia, 2007).

Studies suggest that SFN plays a significant role as an anti-proliferative agent in cancer. Jackson and Singletary (2004) showed that 15 μM SFN for 48 h induces mitotic arrest in the breast cancer cells (MCF7 cell line). They also showed that SFN simulated cell death *in vitro* and *in vivo*, and disrupted microtubule dynamics

at the mitotic stage. However, high concentrations of SFN inhibit tubulin polymerisation *in vitro* (Jackson and Singletary, 2004). Similarly, in bovine aortic endothelial cells (BAE cell line), SFN disturbed microtubule polymerisation and inhibited the mitotic cell cycle when treated with 15 μM for 48 hour (Jackson et al., 2007).

Gamet-Payrastre et al. (2000) investigated the effect of SFN in growth and viability in a human colon cancer (HT29 cell line), where SFN induced cell cycle arrest, followed by cell death via an apoptotic process. The effect of 96 hours of SFN on cell viability was studied by using an MTT assay and SFN at 15 μM was shown to significantly decrease cell viability with inhibition in growth rate and increase in apoptosis. It also notice that after 48 incubation SFN with ≤ 20 μM dramatically inhibits cell viability (Gamet-Payrastre et al., 2000).

A critical property of microtubules is their dynamic instability, and the central mechanism of anti-cancer treatments is to suppress this dynamic activity, such as the chemotherapy agents, taxanes (for prostate cancer) and the vinca alkaloids. It has been found that a concentration of SFN of 15 μM for 20 hours inhibits microtubule dynamic instability and reduces microtubule turnover in human breast cancer adenocarcinoma cells (MCF7 cells). Specifically, this concentration decreased the shortening rate by 50% and the shortening length by 57%. It also suppressed the growth rate and the length of growth to around 30 and 49%, respectively, and reduced the total dynamics by 53%. Additionally, the durations of individual growth and shortage events were decreased. However, only four microtubules were used to analyse dynamic instability (Azarenko et al., 2008).

SFN also causes an increase in acetylation of microtubules in human breast cancer with 15 and 25 μM SFN, compared with untreated cells. At high concentrations of up to 50 μM, microtubules were mostly depolymerised and remaining microtubules became completely stable and highly acetylated. (Azarenko et al., 2008). Therefore,

from these observations, SFN causes changes in microtubule post-translational modifications, where it increases tubulin acetylation, which is known to be linked with stable microtubules. Similarly, it has been noticed that tubulin acetylation was increased in prostate cancer cells treated with 15 µM SFN (Gibbs et al., 2009, Clarke et al., 2011).

Interestingly, recent studies reported that SFN decreased the level of acetylated tubulin; this was observed *in vitro* in skin human keratinocytes (HaCaT) after treatment with 15 µM SFN for a 48 hour incubation. A reduction was only observed in the level of HDAC6 (Dickinson et al., 2015).

HDAC6 activity functions as α-tubulin deacetylase and regulates microtubule-dependent cell motility. Inhibitors of HDAC have become interesting as novel chemoprotective agents, as they target genetic events that can occur at different stages of cancer development. The effect of SFN on HDAC activity was investigated in a variety of human breast cancer cell lines, such as MDA-MB-231, MDA-MB-468, MCF-7 and T47D. These cell lines were treated with a range of SFN concentrations (5, 15 and 25 µM) and incubated for 48 hours, then the activity of HDAC was measured using an HDAC activity assay, *in vitro*. It was found that SFN significantly inhibited HDAC activity in breast cancer cell lines. Moreover, no significant changes were observed in the acetylation global histone H3 or H4 in cells treated with SFN up to 25 µM. HDAC6 inhibitor trichostantin A (TSA) was used as a positive control for 48 hours; results showed that the inhibition of HDAC6 leads to the accumulation of acetylated tubulin in breast cancer cells (Pledgie-Tracy et al., 2007). Recent studies showed that SFN for 48-hour incubation decreases HDAC6 level but not the nuclear HDACs. It has been suggested that this difference in SFN effect on HDACs may be due to the serum in the culture medium, where serum has a different effect on signalling that may impact on SFN function (Dickinson et al., 2015).

In human prostate cancer cells the effect of SFN on HDAC activity was investigated. Two prostate cancer cell lines were used, LnCaP and PC-3. Treating prostate cancer cells with 15 μM SFN for 48 hours inhibited HDAC6 activity. Whereas immunoblotting confirmed that SFN increased the amount of acetylated histone H3 and H4 in prostate cancer cells, with reduction on HDAC activity (Myzak et al., 2006, Clarke et al., 2011). The reduction in HDAC6 level was also observed in prostate cancer cells after long incubation with SFN (Gibbs et al., 2009).

The expression of HDAC6 in human pancreatic cancer (PANC-1) was examined, and it has been found that HDAC6 is overexpressed, which may induce cell migration (invasion and growth). The inhibition of HDAC6 activity decreases its expression and thus impairs the movement of cancerous pancreatic cells, where overexpression of HDAC6 showed enhancement of cell motility (Li et al., 2014). It seems that overexpression of HDAC6 in pancreatic cancer cells may rescue the HDAC6 level from SFN treatment, which deacetylates microtubules (Gibbs et al., 2009).

1.8 Summary

The microtubule cytoskeleton plays essential roles and it has the ability to reorganise with a variety of cellular functions. Microtubules are highly dynamic and this is very important for their ability to reorganise and perform different roles, such as cell division, trafficking, polarisation and migration. These functions require association with multiple proteins, in particular +TIPs such as the end-binding proteins, which influence their dynamics and stability. The end binding proteins influence microtubule dynamics at the growing end, and their expression level and localisation cause changes in microtubule states. Furthermore, HDAC6 has a role in tubulin deacetylation and that influences cell migration.

In many animal cells, microtubules are arranged in a radial array with the minus-ends anchored at the centrosome and the plus-ends directed towards the cell periphery. In general, microtubules contribute to cell migration by regulating actin polymerisation, transporting membrane vesicles to the leading edge, and facilitating the turnover of focal adhesions. Most anti-cancer treatments target microtubule dynamics to suppress their roles in different cellular functions.

SFN is a natural product present in, for example, broccoli and it is particularly interesting as a chemo-preventive agent. SFN has various possible mechanisms to prevent cancerous activity and slow progression of the disease. SFN is known to affect microtubule polymerisation, inhibit cell proliferation and initiate apoptosis, thus retarding or eliminating neoplastic cells and inhibiting the progression of benign tumours into malignant tumours and metastasis formation. It has been suggested to affect microtubule dynamics by increasing their stability, and to inhibit HDAC6 activity.

This study aims to examine whether the migration of epithelial cells and in particular pancreatic cancer cells, can be affected by SFN. The investigation is

focused on the effects that may occur on microtubules and actin filament organisation. In addition, analysis of whether SFN may affect the expression and localisation of EBs and HDAC6.

1.9 Hypothesis and Aims

We hypothesise that relatively high concentrations (≥10μM) of SFN will increase microtubule stability while also decreasing dynamic activity and cause a reduction in the speed of migration.

SFN has been reported to affect microtubule behaviour, cell migration and mitosis. Understanding these actions will lead to more effective drug use. The aim of this study is to investigate the effects of SFN on microtubule organisation, dynamics and stability, and particularly with regard to cell migration in normal and cancerous cells. The impact on end-binding proteins (EBs) and HDAC6 will also be studied.

Objectives:

To achieve these aims the cell models (ARPE-19 and PANC-1) to be used in this project first will need to be characterised. This will involve characterising the organisation of microtubules and actin filaments in ARPE-19 and PANC-1 cells and determined the expression and localisation of EBs and HDAC6. The next objective is to study the effects of SFN on cell migration using different SFN concentrations for 48 hour. In addition, immuno-labelling will be perform to determine microtubule modifications and to observe microtubule and actin filament organisation and EBs and HDAC6 localisation in SFN treated cells compare with untreated and DMSO treated cells. HDAC6 is highly expressed in PANC1 cells, a further objective is therefore to use a specific inhibiter of HDAC6 (tubacin) to examine the effect of its inhibition on cell migration and microtubule and actin filament organisation. In addition, the effects of combinations of tubacin and SFN will also be investigated. A further objective is to study the direct effect of SFN on microtubules dynamics and stability and the consequences for focal adhesion dynamics and turnover.

Chapter II: Materials & Methods

2.1 Cell culture

2.1.1 Maintenance of cell lines

All work in tissue culture for this project were performed under sterile conditions in a Class II laminar flow tissue culture hood. Cells were grown in 75cm^2 culture flasks (Nunc) with a vented cap and membrane to allow sterile gas exchange. Cell lines were maintained at 37ºC in a humid atmosphere containing 5% CO_2. Cell lines were grown in appropriate medium containing the indicated supplements (Table 1).

Table 1: List of cell lines and medium.

Cell Line	Medium	Supplements	Antibiotics
ARPE-19	DMEM/F:12 (1:1) (High Glucose, +NEAA)	10% FBS 1% L-Glutamine 2% Sodium bicarbonate 0.1µg/ml gentamicin	Gift: Julie Sanderson (UEA)
PANC-1	DMEM (High Glucose, +NEAA)	10% FBS 1% L-Glutamine 100U/ml penicillin 0.1 mg/ml streptomycin	ATCC
DMEM, DMEM/F: 12 (Invitrogen, Paisley, Scotland). Penicillin, streptomycin, L-Glutamine (Sigma, Poole, Dorset). FBS (PAA Laboratories, Yeovil, Somerset).			

2.1.1.1 Passaging of cell lines

Cells were passaged twice a week to maintain an exponential growth phase until they reached 80% confluency. All reagents were warmed to 37ºC using a water bath prior to use. For subculture of a flask, the medium was removed and the cells were washed with 0.25% trypsin/1mM ethylenediaminetetraacetic acid (EDTA) (Sigma, Poole, Dorset) to remove any traces of medium that could interfere with cell detachment from the plastic. After removal of this wash, cells were incubated in 5ml of 0.25% trypsin/EDTA at 37ºC, 5% CO_2 for five minutes until the cells had detached from the tissue culture plastic. Afterwards, the trypsin was neutralised by adding 5ml of medium containing 10% foetal bovine serum (FBS) (Invitrogen). The suspended cells were then pelleted in sterile tubes by centrifugation at 1000rcf for five-minutes at room temperature. After the supernatant was removed, the cell pellet was resuspended in relevant fresh medium. Finally, resuspended cells were diluted into new 75cm^2 culture flasks (T75) in a total volume of 10ml medium.

2.1.1.2 Freezing and thawing cells

Cell lines in low passage were stocked in a liquid nitrogen dewar to avoid potential phenotypic changes associated with high passage numbers. To freeze cells, firstly, a flask was passaged until the cell pellet was ready for resuspension, with the pellet resuspended in appropriate medium with 10% dimethylsulphoxide (DMSO) to act as a cryopreservant. This was aliquoted into several cryovials (Corning, Amsterdam, Netherlands) and immediumtely transferred to a freezing box containing isopropanol (Mr Frosty™) before being gradually frozen at -80°C. For long-term storage, cryovials were placed in liquid nitrogen dewars.

To thaw cell lines from frozen the cryovials were quickly heated in a 37°C water bath, after which the cells were immediumtely transferred to a sterile tube containing pre-warmed 10ml of medium and centrifuged for five-minutes at 800rcf

to remove the DMSO. The cell pellet was resuspended in 5ml of medium and transferred into a 25cm^2 culture flask. The medium in these flasks was changed every other day until the cells reached 80% confluency. Once the cells reached this level, they were passaged as per standard maintenance procedures, which helped the cells to settle before use in any experiments.

2.1.1.3 Cell counting

The cells were counted during cell passaging with a haemocytometer before the centrifugation stage. The haemocytometer chamber was mounted with a coverslip, allowing the medium containing the cells to enter the chamber by capillary action. In the chamber there was a large 4x4 square grid, and the number of cells within a single square was used to determine the cell concentration by multiplying this number by 1x10^4, which provided a final cell concentration per ml. To ensure a correct cell count, the number of cells in four squares was counted and the mean was used to estimate the concentration of cells.

2.1.2 Seeding cells

Cells were seeded onto appropriate surfaces for experiments as needed, including multiwell plate plastic surfaces (Nunc, Penfield, New York, USA), 13mm diameter glass coverslips (No. 0 thickness) (VWR International, Lutterworth, Leicestershire) and glass-bottomed dishes (MatTek, Ashland, Massachusetts, USA) for live fluorescence microscopy. Oven baking was used to sterilise glass coverslips at 180°C overnight. For seeding, cells were trypsinised as described above and resuspended in fresh medium. Cell counting was used to determine cell concentration, followed by appropriate dilution of seeds to a specified density. This variety in density depends on different cell types and experimental purposes.

2.2 Drug treatments

2.2.1 Sulforaphane (SFN)

Sulforaphane (SFN) (LKT LABS) was dissolved in DMSO and stock solutions stored at -20°C with a total concentration of 100mM. When required, it is freshly prepared and added to the cell cultures to achieve the indicated final concentrations. The DMSO concentration was 0.005% in the final solutions of the SFN treatment range (0.5, 1, 2, 5, 10, 15, 20, 30 and 40µM), where DMSO alone at 0.01% concentration was found to have no significant effect on cellular function. In our experiments, cells were treated with normal medium containing SFN and DMSO, diluted to a final concentration range to examine appropriate concentration, and incubated for 48 hours at 37°C and 5% CO_2. Different experiments were applied to investigate the effect of SFN on cancerous and normal epithelial cells, including live imaging, immunolabelling, Western blotting and MTT assay (these methods are described later in this chapter).

2.2.2 Tubacin

Tubacin (Sigma, Poole, Dorset) was dissolved in DMSO with a final concentration of 10mM, with stock solutions freshly prepared each time and added to the cell medium to obtain the indicated final concentrations (2, 5 and 10 µM). The concentration of DMSO was 0.01% and the tubacin concentration was 10µM in the final solution. Cell lines were treated with different concentrations of tubacin (2, 5 and 10 µM) and incubated for various timepoints throughout the treatment in a 37°C, 5% CO_2 incubator. MTT assay was applied to determine the effects of tubacin on cell viability, followed by investigation of effects on cell migration, microtubules and associated proteins by immunolabelling.

Combinations treatment of 10 and 15µM SFN and 10µM tubacin were used in our experiments. Cells were treated with a combination of SFN and tubacin and incubated in, then used in a variety of experiments, including live imaging, immunolabelling, Western blotting and MTT assay.

2.3 Cell viability assay (MTT assay)

Cytotoxicity has been assessed by using an MTT assay (Sigma, UK) to determine the effect of a drug on cellular viability. The MTT (3-[4,5-dimethylthiazol-2-yl]-2,5 diphenyl tetrazolium bromide) assay is based on the conversion of the tetrazolium salt MTT, a yellow solution, into purple formazan crystals in living cells. The principle of the MTT assay is that the activity of mitochondria in most viable cells is stable, thus an increase or decrease in the number of living cells is related to mitochondrial activity. These changes in living cell numbers can be detected by measuring formazan concentration using a plate reader at 750nm (van Meerloo et al., 2011). The MTT assay is largely utilised to measure the cytotoxic effects of drugs on cell lines *in vitro*, then compare the treated cells to DMSO control cells.

Cells were seeded in 96-well microplates in triplicate to minimise the variability of the results, and then incubated for 24 hours at 37°C with 5% CO_2. After incubation, the medium was removed and replaced in quadruplicate with fresh medium containing the drugs, SFN, tubacin, or a combination of them, and incubated again for 48 hours. Following this, 10µl MTT agent was added to each well and the plate was agitated for one minute on a plate-shaker in slow mode, and then incubated for four-hours. Afterwards, 100µl crystal dissolving solution was added to each well and then the plate was left to rest for ten-minutes before measuring. The cellular homogenate was measured at 570nm using the plate reader. Cell viability results

were compared to DMSO treated cells and expressed as the mean of three independent experiments using GraphPad Prism 5.0 software.

2.4 Transfection of plasmids

Transformation of all used plasmids in experiments was in the DH5α *Escherichia coli* cells. The DH5α cells were defrosted on ice for about 20 minutes, and then 1µl of plasmid (20µg/ml) was added to 50µl of DH5α cells and left on ice for another 15 minutes. The cells were heat shocked at 42ºC for two-minutes and placed back on ice for one-minute. Sterile Lysogeny broth (500µls) was added to the cells and incubated for one-hour at 37ºC under gentle agitation. Cells were then spread onto agar and sealed with a lid, then incubated overnight at 37ºC. The following day, a medium aread colony was picked from the agar plates and placed into 10 ml of LB starter culture containing the appropriate selective antibiotics and incubated for 6-8 hours at 37°C under gentle agitation. One ml of the cells was placed into 250 mls of LB plus antiobiotics and placed at 37°C under gentle agitation overnight. Cells were harvested by centrifugation at 6000g for 15 minutes at 4°C. The constructs were then isolated and purified from the *E.coli* cells using a high-speed midi kit (Qiagen), according to manufacturer's instructions and stored in TE buffer. The concentration of the cDNA was measured using nano-drop (LabTech, Ringmer East Sussex, UK) and stored at -20ºC. The constructs were amplified in bacteria and purified before use in cell transfection. Table 2 shows a list of constructs used in this study.

Table 2: Constructs details

Construct	Marker	Source
GFP-CLIP-170		N.Galjart
GFP-Paxillin		Addgene

2.5 Fixation

Cells grown on coverslips were all fixed in methanol at -20°C, however, an alternative methanol-formaldehyde fix has been used where the protocol has been modified from the Rogers protocol (Rogers et al., 2002). The method in this protocol gave a better quality of labelling for proteins localised along microtubules such as EB2. A formaldehyde solution was prepared by diluting a 37.5% formaldehyde stock solution on ice-cold methanol.

2.6 Immunolabelling

The fixation techniques used in these experiments were dependent on the antibody being labelled. Cells were seeded on coverslips at $5x10^3$ cells in a 3cm Petri dish and incubated for 24 hours. Methanol was used as the standard fixative for five-minutes at -20ºC. Samples were also fixed by methanol-formaldehyde. After fixation, the cells were washed three times in 1% goat serum (Sigma-Aldrich) in PBS (Oxoid, Basingstoke, Hampshire) and placed in a PBS blocking buffer with 10% goat serum for 30 minutes to prevent non-specific binding of antibodies. For the methanol-formaldehyde fixed samples the blocking solution contained 0.1% Triton X-100.

All primary antibodies used in this study are listed in Table 3. The antibodies were diluted in PBS with 1% goat serum then added to the cells. A 50µl spot of primary antibody was used for each coverslip. Coverslips were gently inverted onto the antibody spot, cell side down, and incubated at room temperature for one hour. Excess primary antibodies were removed by washing the cells in PBS with 1% goat serum six times every five-minutes. All secondary antibodies were diluted in PBS with 1% goat serum.

The secondary antibodies used are listed in Table 4. Coverslips were again inverted onto secondary antibody spots and incubated for 30 minutes in the dark at room temperature. The cells were then placed in PBS with 1% goat serum for three washes of ten minutes to remove any excess secondary antibodies. If a nuclear stain was required, the cells were stained using DAPI (Sigma, Poole, Dorset) diluted in PBS (1:2000) for ten-minutes, followed by three washes in PBS for ten-minutes. Coverslips were mounted cell side up onto glass slides using hydro-mount (National Diagnostics), DABCO was added to reduce photobleaching of fluorophores, and a long glass coverslip (0.13-0.17mm thickness) was then gently lowered to cover the coverslips. Finally, the samples were incubated overnight at 4°C to set before imaging.

Combinations of primary antibodies were used depending on the species it was raised in (mouse, rat and rabbit). Basically, rat and rabbit or mouse and rabbit antibody combinations were mixed when diluting the primary, and convenient secondary antibodies were used. Importantly, all primary antibodies have been previously validated to check specificity.

Table 3: Details of primary antibodies.

Primary antibody	Raised in	Source	Dilution*
Acetylated tubulin	Mouse	Sigma (T6793)	IF: 1:100, WB: 1:500
α-tubulin	Rabbit	Abcam (ab15246)	IF: 1:100, WB: 1:1000
Tyrosinated tubulin (YL1/2)	Rat	AbD Serotec (Kidlington, Oxfordshire) (MCA77G)	IF: 1:200, WB: 1:200
Detyrosinated tubulin	Rabbit	Abcam (ab48389)	IF: 1:200, WB: 1:500
Vinculin	Mouse	Abcam (ab18058)	1:200
β-actin	Rabbit	Abcam (ab8227)	IF: 1:1000, WB: 1:10000
EB1	Mouse	BD Biosciences (610535)	1:500
EB1	Rabbit	Abcam (ab50188)	1:200
EB2 (KT52)	Rat	Abcam (ab45767)	1:200
EB3	Mouse	Abcam (ab45855)	1:200
γ-tubulin	Rabbit	Abcam (ab16504)	1:1000
γ-tubulin	Mouse	Abcam (ab11316)	1:1000
HDAC6	Rabbit	Abcam (ab1440)	1:200
FAK	Rabbit	Cell Signalling (9330)	IF: 1:100, WB: 1:1000
Paxillin	Rabbit	Sigma-Aldrich	1:200
***IF= Immunofluorescence, WB= Western Blot**			

Table 4: Details of secondary antibodies

Secondary antibody	Raised against	Dilution	Source
	Anti-RAT IgG		
	Anti-RABBIT IgG		
	Anti-MOUSE IgG		
	Anti-RAT IgG		
	Anti-RABBIT IgG		
	Anti-MOUSE IgG		
	Anti-RAT IgG		
	Anti-RABBIT IgG		
Cy5	Anti-MOUSE IgG	1:500	Jackson (Stratech, Newmarket, Suffolk)
	Goat anti-MOUSE IgG	1:3000	
	Goat anti-RABBIT IgG	1:1000	
	Goat anti-RAT IgG	1:3000	
IRDye 800CW	anti-MOUSE	1:50000	
IRDye 680RD	anti-RABBIT	1:50000	
Note: all secondary antibodies were raised in goat.			

2.7 Western blotting

2.7.1 Cell lysis

Cells grown in multiwell plates (of 6-wells) or tissue culture flasks were washed with ice cold PBS, then lysed for 30 minutes with 100x Halt Protease/Phosphatase inhibitor (Pierce, Cramlington, Northumberland), diluted into cell lysis buffer (Appendix A). A tissue culture flask, T75, needs 500µl lysis buffer, where 100µl is enough for a six-well plate. Cells were scraped every 15 minutes during lysis and the lysates transferred to an Eppendorf tube. Samples were centrifuged at 13000rpm at 4°C for ten minutes and the pellet was discarded, then stored in a fresh Eppendorf at -20°C.

2.7.2 Protein quantification

Protein quantification was carried out using a BCA™ (Bicinchoninic Acid) protein assay kit (Pierce, Cramlington, Northumberland). This is based on preparing several bovine serum albumin (BSA) standards ranging from 0-2000µg/ml in concentration, diluted in ddH_2O. A 96-well plate was used to quantify proteins, with 40µl water added to each well followed by 10µl of each standard and each sample to be analysed in triplicate. Next, 200µl of the protein assay reagent (reagent A: reagent B, 50:1) was added to each well and the plate incubated for one hour at 37ºC. Absorbance readings at 550nm were measured using a spectrophotometer and the BSA values were used to generate a standard curve, from which the protein concentrations of the cell lysates were estimated.

2.7.3 SDS-PAGE electrophoresis

Using the standard curve from the concentrations calculated in the BCA assay, 20µg of protein content (diluted in ddH_2O) for each sample and 10µl of 5X sample buffer (Appendix A) containing 12.5% β-mercaptoethanol were added, and the tubes heated at 95ºC in a heat block for two-minutes.

Gels were made between spaced glass plates by adding a 8-10% lower resolving gel (Appendix A) and left to set for about 30 minutes. Upper gel was added using a spacing comb, which was removed once the upper gel had set. These gels were transferred to a Mini Protean II tank (BioRad, Hemel Hempstead, Hertfordshire), which was filled with 1X SDS running buffer, diluted in ddH2O from a 10X stock (Appendix A). The prepared samples and protein ladder (BioRad, Hemel Hempstead, Hertfordshire) were loaded into separate wells of the gel. The electrophoresis was performed using 30mA per gel until the sample buffer had migrated towards the bottom of the gel, taking approximately 35-45 minutes.

2.7.3.1 Protein transfer

Once electrophoresis was complete, the gel was placed into transfer buffer (Appendix A), along with a nitrocellulose membrane (BioRad, Hemel Hempstead, Hertfordshire) and two sheets of extra thick blot paper (BioRad, Hemel Hempstead, Hertfordshire), which was left for 15 minutes to equilibrate. Proteins were transferred using the semi-dry transfer system (BioRad, Hemel Hempstead, Hertfordshire). In the transfer stage the sheets, gel and membrane were assembled as follows: thick blot paper at the bottom, the nitrocellulose membrane, the gel, and thick blot paper on the top. Proteins from the gel were transferred to the nitrocellulose membrane at 15V for 35 minutes.

2.7.4 Protein detection

After protein transfer, the nitrocellulose membrane was processed for immunoblotting. The membrane had a quick wash in 0.5% (w/v) dried milk powder (Oxoid, Basingstoke, Hampshire) in PBS-0.05%Tween-20 (Appendix A), followed by incubation in 5% (w/v) milk PBS-T (blocking) on a rocker for either two hours at room temperature, or overnight in the cold room.

2.7.4.1 Antibody probing

Primary antibodies were diluted in 1ml of 0.5% milk PBS-T (Table 3), and added to the membrane (after blocking) in a plastic bag and incubated overnight on a cold room rocker. The next day, the membrane was placed on the rocker at room temperature and washed for ten minutes, three times, with 0.5% milk PBS-T. Secondary antibodies (HRP conjugated) were used and diluted in 10ml of 0.5% milk PBS-T, then added to the membrane for one hour on the rocker at room temperature. Excess secondary antibodies were removed from the membrane then washed with 0.5% milk PBS-T for 30 minutes, with regular changes in the wash over ten-minutes on the rocker at room temperature.

2.7.4.2 Immuno-detection

The membrane was incubated with a custom-made in the laboratory electrochemical luminescence solution (ECL), consisting of ECL reagent A and B, for one-minute. Excess solution was removed and the membrane placed into a cassette lined with cling-film. In the dark room, Hyperfilm ECL photographic film (Amersham, Little Chalfont, Buckinghamshire) was placed side up in prepared cling-film for an appropriate exposure time and developed in a Xenograph.

2.7.4.3 Re-probing

Membranes were stripped and re-probed to examine levels of an additional protein, β-actin, most commonly used as a loading control. To strip, 10X re-blot solution (Chemicon, Watford, Hertfordshire) was diluted in ddH_2O and added to the membranes for 10-15 minutes on a rocker. Following this, the solution was removed then membrane washed by adding 0.5% milk PBS-T three times for five-minutes. Finally, primary antibodies were added and then the protocol followed as per the first probing.

2.7.5 Fluorescence Western Blot - Odyssey

This method depends on fluorescent detection using secondary antibodies labelled with infrared fluorescent dyes instead of enzymes, and on multiplex detection of multiple protein targets without stripping and re-probing. The protocol for this technique is similar to the Western blot that has been previously described, with several differences at particular stages.

After transfer, the membrane was processed for immunoblotting and washed in PBS-T (T20, 0.05%) (Appendix A), followed by incubation in PBS-T (T20, 0.05%) and 5% goat serum (blocking) on the rocker overnight in the cold room. Primary antibodies were diluted in 1ml of 0.5% PBS-T and 2% goat serum, and added to the membrane and incubated for one hour at room temperature.

After the primary antibodies were incubated, the membrane was washed three times for five minutes with 0.5% PBS-T. Secondary antibodies (IRDye 800 or IRDye 680) were used and diluted in 10ml of 0.1% SDS, 2% goat serum and 0.05% PBS-T, then added to the membrane for one-hour on the rocker at room temperature. The membrane washed with 0.05% PBS-T for five minutes, where a final wash with PBS alone. Finally, digital imaging was obtained by using an Odyssey

scanner, with the membrane placed face-down and on the bottom left-hand side of the grid. The scanner revealed target protein signals with high sensitivity.

2.8 Microscopy

2.8.1 Widefield fluorescence

Fixed cells were imaged on a widefield upright Zeiss Axiovert 200M microscope using a monochrome CCD camera (immunofluorescence) to capture the images. The fluorescence of immunolabelled cells was detected using a 100W mercury lamp and dichroic mirror filter set. Axiovision software (Zeiss) was used to create multi-channel images, with Photoshop CS2/7.0 (Adobe) used for further image improvement.

2.8.2 Live imaging of migrating cells

A Zeiss Axiovert inverted microscope was used for performing live time-lapse imaging, with samples maintained in a sealed chamber containing 5% CO_2 at 37°C on a heated stage. Axiovision (Zeiss) software was used to set up time-course experiments and images were captured using a monochrome CCD camera.

For migration experiments cells were seeded in multiwell plates (24 well), with different conditions of treatment and phase images captured every ten-minutes over the experimental time-period of 16 hours from different positions. The objective used was x10. For each condition, an individual cell position was tracked at each time-point in Image J, which was also used to combine tracking traces representing all paths tracked for each condition analysed. The average velocity was also

calculated for each cell. Graph and data analysis preparation was completed in Prism GraphPad software.

2.8.3 Live imaging of CLIP-170 dynamics

For live imaging of microtubule dynamics (GFP-CLIP-170 expressing), ARPE-19 and PANC-1 cells treated with different conditions were grown in glass-bottomed 3cm dishes (MatTek, Ashland, Massachusetts, USA), using a x63 objective lens, a 100W mercury lamp and dichroic mirror filter sets for fluorescence. DMEM/F12 medium without phenol red (Invitrogen, Paisley, Scotland) was used to image cells. Cell images were captured at set exposure levels every three-seconds over a three-minute period, with different areas imaged for each condition. A high-powered LED light was used to excite the GFP, with the ability to switch on and off with no need to open and close the light shutter.

2.8.4 Confocal microscopy and FRAP of focal adhesion

Immunolabelled cells were imaged using an inverted Zeiss LSM510 META scanning confocal microscope. An appropriate laser was required to excite the samples: Enterprise UV (364nm) for DAPI, Argon (488nm) for Alexa 488 fluorophores, Helium/Neon (HeNe1, 543nm) for Alexa 568 fluorophores, and HeNe2 (633nm) for Alexa 647/Cy5 fluorophores. The Argon laser (488) was utilised at 4% intensity for image acquisitions, where focal adhesion was selected and photobleached at 30-40 iterations at 100% intensity.

Analysis of focal adhesion recovery was performed by fluorescence recovery after photobleaching (FRAP). This method relies on powerful and focused light to bleach florescence in selected areas of a living cell. Following observation and

analysis of the fluorescence time needed to return to the first state. In our experiment, GFP-paxillin-expressing ARPE-19 and PANC-1 cells treated with different conditions were grown in glass-bottomed 3cm dishes (MatTek, Ashland, Massachusetts, USA), using a x63 objective lens, a powerful and focused fluorescence light (for bleaching) and a100W mercury lamp and dichroic mirror filter sets for fluorescence. DMEM/F12 medium without phenol red (Invitrogen, Paisley, Scotland) was used to image the cells. Focal adhesion images were captured at set exposure levels, every three-seconds over three-minutes period in selected regions. A high-powered LED light was used to excite the GFP.

2.9 Random cell migration

Cells were seeded sparsely in six-well plates, at 10,000 cells per well, for different treatment conditions. Each condition was imaged by live time-lapse microscopy, where each condition was set for several regions. Images were acquired every ten-minutes over a 16-hour period.

ImageJ software was used to track the position of individual cells across several regions at each time-point. Moreover, it was used to prepare combined tracking traces representing all paths tracked for each condition analysed, and to calculate the average velocity for individual cells. Finally, Prism (Graphpad) software was used to analyse the data and present graphs.

2.10 Cold treatment

Cells were treated with cold medium after seeding and addition of SFN for 48 hours. They were incubated on ice for 15 minutes, 30 minutes and one-hour. Cells were fixed by removing medium and adding methanol at -20°C for five-minutes,

followed by three quick washes in 1% goat serum in PBS. Cells underwent the immunolabelling procedure as described previously with primary antibody α-tubulin.

2.11 Analysis of microtubule acetylation

To analyse the degree of microtubule acetylation in this project, cells were treated and fixed. The microtubules were visualised with rabbit anti-α-tubulin primary (1:100, Abcam) and secondary goat anti-rabbit, Alexa 647 (1:1000, Invitrogen Molecular, Paisley, Scotland). Acetylated microtubules were visualised with mouse anti-α-acetylated tubulin primary antibody (1:100, Sigma) and a secondary goat anti-mouse, Alexa 488 (1:1000, Invitrogen Molecular, Paisley, Scotland). The extent of microtubule acetylation in the absence and presence of SFN treatment was analysed with ImageJ software. Specifically, the fluorescence intensity of acetylated microtubules (green channel) in at least ten interphase cells (PANC-1 and ARPE-19) per condition was analysed. To obtain the percentage of acetylated microtubules area the total area of acetylated tubulin was dividing by the total areas of tubulin. Mitotic cells were not analysed because they were too small and round, with the stain concentrated in a small area.

ImageJ software was used to analyse the area of acetylated tubulin. Firstly, images were exported in two different channels and saved, one for α-tubulin and the other for acetylated tubulin with grey scale (not merged image). During this stage ten cells were used for analysis. Channel properties were changed with length unit micron and pixel width and height to 0.102 micron when a x63 obj lens was used. To prepare for analysis the image background was subtracted and pixels in radius unit adjusted until a satisfactory image was obtained; approximately 80% met the defined criteria. Data were saved to an Excel file, where the total area of acetylated tubulin and α-tubulin was illustrated. Finally, to determine the area of acetylated

tubulin as a proportion of the total tubulin, the total area of acetylated tubulin was divided by the total area of tubulin and multiplied by 100 to get a percentage value.

2.12 Analysis of area and shape of EB1 and lattice intensity

The EB1 comet shape was analysed by measuring the circularity of EB1 at the microtubules plus-end. Macron for comet analysis was applied in ImageJ. Axiovision images (14-bit; i.e., intensity values range from 0 to 16,383) were opened and analysed with ImageJ (Rasband, 1997). Background subtraction (Castle and Keller, 2007) was carried out using a rolling-ball of radius 10 pixels and the images thresholded using the algorithm of Otsu (Otsu, 1979). After background subtraction and thresholding, the intensity (arbitrary Fluorescence Units) and circularity of objects was measured. Objects smaller than 0.12 μm2 (i.e., <12 pixels2) and larger than 3 μm2 (i.e., >300 pixels2) were ignored. This comet analysis code was written by Paul Thomas (Henry Wellcome Laboratory for Cell Imaging, UEA).

For intensity analysis of EB1 along the microtubule lattice, average fluorescence intensity along 2 μm segments at randomly selected regions along the lattice located away from the plus-end (using tubulin channel) was measured from set exposure images (from the same experiment) using ImageJ software, where code was written Paul Thomas (Henry Wellcome Laboratory for Cell Imaging, UEA). Statistical significance was determined using a two-tailed unpaired t-test or one-way ANOVA was performed using Tukey's multiple comparison post-hoc test.

2.13 Analysis of CLIP-170 comet dynamics

To assess the effect of SFN treatment on microtubule dynamics, GFP-CLIP-170 comets were analysed in DMSO and SFN treated cells. Cells were grown in glass-bottomed dishes and incubated overnight. Cells were then treated with 10 and 15 µM SFN and incubated for 48 hours. Thirty-hours after adding the SFN, the cells were transiently transfected with 2µg GFP-CLIP-170 construct for four-hours, where it was delivered using jetPRIME (plasmid kit) (Polyplus) (Akhmanova et al., 2005), then washed with fresh medium and incubated for a total of 48 hours. For each concentration, cells demonstrating GFP-CLIP-170 in microtubules were imaged using live time-lapse fluorescence microscopy for three-minutes, and frames taken every three-seconds, yielding 60 frames in total. The live time-lapse recordings were analysed using the automated tracking software U-Track, originally packaged as plusTipTracker (Applegate et al., 2011). This enabled GFP-CLIP-170 comet paths to be obtained. MATLAB was used to conduct all post-tracking analysis and the microtubule plus-tip tracking package code was written in this program. A series of TIFF files, one for each frame of the recordings were used for the plus-tip tracking to analyse dynamics of the microtubules as described by Applegate et al. (Applegate et al., 2011). Importantly, it must be noted that stable microtubules cannot be identified via this method and GFP-CLIP-170 may cause an increase in microtubule rescue.

2.14 FRAP analysis

Cells were transfected with GFP-paxillin, incubated for four hours, given fresh medium and then incubated for a total of 48 hours. To measure the adhesion dynamics in live cells, after the cells expressing GFP-paxillin, individual focal adhesions were subjected to FRAP (fluorescence recovery after photo-bleaching).

Confocal microscopy was used for the live imaging of GFP-paxillin-expressing cells. FRAP data obtain using the Zeiss LSM 510 META confocal. Images of focal adhesion were collected prior to photobleaching as a measure of the original intensity. The Argon/Ion LASER (488) was utilised at 4% intensity for image acquisitions. The focal adhesion in GFP-paxillin transfected ARPE-19 and PANC-1 cells was selected using the LSM imaging software and photobleached utilising the Argo/Iron laser at 30-40 iterations at 100% intensity. Focal adhesion images were recorded post-bleaching over recovery. GFP-paxillin recovery was determined by measuring the signal intensity of the photobleached over three-minute period (Sprague et al., 2004).

2.15 Statistical analysis

Illustration and preparation of graphs and statistical analysis was performed in GraphPad Prism software. For experiments with multiple groups, one-way ANOVA was performed using Tukey's multiple comparison post-hoc test to assess the significance of any differences between two separate groups within the data set. Differences were regarded as significant when $p<0.05$.

Chapter III: Characterisation of Model Cell lines

3.1 Overview

This chapter characterises the model cell lines utilised in this project. The results illustrate the characteristics of the cell models focussing on the four following aspects: microtubule organisation and tubulin modification, actin organisation, end-binding (EB) protein expression and localisation and microtubule-associated deacetylase 6 (HDAC6) expression and localisation.

3.2 Introduction

The main aim of this project is to investigate whether sulforaphane (SFN) treatment could inhibit cell migration, especially in pancreatic cancer cells. To achieve this target, it is essential to characterise the cell line models, with both normal epithelial cells and pancreatic cancer cell lines being required for this investigation. Normal epithelial cells are required for comparison with the cancerous cells when studying the effect of SFN.

A human retinal pigmented epithelial cell line (ARPE-19) was used as the normal epithelial model. Unfortunately, we were unable to obtain a normal pancreatic cell line for these studies. However, ARPE-19 cells are widely used as a model for undifferentiated epithelial cells. An important feature in this cell line is the organisation of the microtubules, which show a classic radial array with the minus ends anchored at the centrosome and the plus-ends elongating toward the cell periphery. EB proteins, such as EB1, associate at the plus-ends of microtubules and appear as comet-like shapes (Bellett et al., 2009). In addition, ARPE-19 cells are relatively flat, which is ideal for microscopy and analysis of the effects of SFN.

Pancreatic cancer is an aggressive malignancy and it is one of the most difficult types of cancers to treat, as it exhibits resistance to existing treatments. It can also

attack other unaffected parts of the body (Bardeesy and DePinho, 2002, Wang et al., 2011). There are many different types of pancreatic cancers, but the most common is pancreatic ductal adenocarcinoma, and the PANC-1 cell line represents this type of cancer. Gene mutations in PANC-1 cells include p53, which is linked to metastatic activity (Bardeesy and DePinho, 2002, Hezel et al., 2006). In general, the PANC-1 cell line represents undifferentiated epithelial cells that mainly migrate as single cells, which is an interesting feature for studying migration. Cell adhesion is mediumted by contact with the extracellular matrix, and collagen type I is known to stimulate migration. Importantly, the EB2 gene (MAPRE2) is highly overexpressed in PANC-1, and it has been suggested to promote cell migration (Abiatari et al., 2009). EB2 associates along the microtubule lattice and influences microtubule dynamics (Goldspink et al., 2013). HDAC6 is another overexpressed protein in PANC-1 cells. This deacetylates α-tubulin and regulates microtubule dynamics (Huo et al., 2011, Li et al., 2011), and thus, it also promotes cell migration (Li et al., 2014).

The organisation of microtubules is vital for fulfilling their roles in cells. The main functions of microtubules are cell division, cell shape maintenance, intercellular transport, cell polarity and cell migration. This project focus on the effects of SFN on microtubule organisation, modification and dynamics. Many animal cells show microtubules arranged in a radial array, where the minus-ends are anchored at the centrosome, and the plus-ends are elongate toward the cell edge (Cole and Lippincott-Schwartz, 1995, Mogensen, 1999). Disruption in the normal microtubule array formation is likely to contribute to a migration phenotype. Microtubules undergo post-translational modifications, such as acetylation and detyrosination, which affect their properties and may increase stability (Verhey and Gaertig, 2007, Garnham and Roll-Mecak, 2012, Yu et al., 2015). A critical property of microtubules is their dynamic instability, which allows the microtubules to explore the cytoplasm and make contact with other cellular structures, including

the cell cortex (Galjart and Perez, 2003). This dynamics requires a variety of associated proteins to control the alternations between phases of growth and shrinkage, as well as interactions with tubulin modifications that affect the microtubules' stability (Howard and Hyman, 2009). To fully understand the possible effects of any potential disorganisation of microtubules and actin filaments or the redistribution of +TIP in SFN treated normal and pancreatic cancer cells, it must be first understanding of the characterisation of the cell models to be used in this study.

3.3 Results

3.3.1 Characterisation of ARPE-19 and PANC-1 cells

For initial characterisation, ARPE-19 and PANC-1 cell lines were seeded onto glass coverslips and immunolabelled with various antibodies to characterise the cell lines in this project. Cells were stained for microtubules, actin filaments, centrosomal components, EBs and HDAC6 to analyse subsequently the subsequent effect of SFN.

3.3.2 Microtubule organisation and tubulin modifications

The PANC-1 model cell line to be used is a sub-clone of the parental line obtained from ATCC, and it was specifically selected for high EB2 expression. ARPE-19 and PANC-1 cell lines were seeded on glass coverslips and grown overnight to reach about 60% confluence. The cells were fixed for immunolabelling and fluorescence microscopy. Live imaging was used to observe the different morphologies of ARPE-19 and PANC-1 cells, during migration. Live imaging showed that the morphology of ARPE-19 cells were mainly elongated, with thin protrusions around the periphery. The PANC-1 cells appeared rounded with some elongated protrusions (Figure 3.1).

ARPE-19 and PANC-1 cells were fixed and immunolabelled for α-tubulin, γ-tubulin and stained with DAPI for the nucleus. Microscopic images of ARPE-19 cells revealed a classic radial array of microtubules emanating from a centrosome located near the nucleus, with plus-ends elongating out to the cell periphery (Figure 3.2). Although most the microtubules appeared to focus at the centrosome (marked by γ-tubulin), a more disorganised network of microtubules was evident in PANC-1 cells (Figure 3.3). Some microtubules also appeared to be oriented parallel to the

cortex. Interestingly, in some cells, which appeared to display a migratory phenotype, distinct bundles of microtubules were directed towards the leading edge, while other microtubules appeared to form a criss-cross network (Figure 3.7).

ARPE-19 and PANC-1 cells were labelled for tubulin modifications, such as acetylated tubulin, tyrosinated tubulin and detyrosinated tubulin. This was done to determine the extent of these tubulin modifications in the two cell lines. In ARPE-19 cells, most microtubules were tyrosinated, with some acetylated tubulin evident in the central cell area; this formed a bundle, sometimes revealing a curly nature. Detyrosinated tubulin was mainly observed around the centrosomal region, with a few microtubules extending towards the cortex (Figure 3.4). PANC-1 cells showed minimal expression of detyrosinated tubulin. However, most microtubules expressed tyrosinated but also a substantial amount of acetylated tubulin in the central cell areas and near the cell periphery (Figure 3.5).

Overall, ARPE-19 cells presented a classic radial array of microtubules, and most tubulin is tyrosinated, with little detyrosination and acetylation of tubulin. In PANC-1 cells, the microtubule network was more disorganised. Similarly, most of the tubulin was tyrosinated tubulin but extensive acetylated microtubules in the centre and minimal or no expression of detyrosinated tubulin.

3.3.3 Actin organisation

Actin is an essential element of the cell cytoskeleton, and it plays an important role in cell movement and shape; therefore, actin organisation was investigated in this study. An antibody against β-actin was used to investigate the localisation of all actin, whereas phalloidin was used to stain only F-actin (actin filaments).

The results illustrated that, in ARPE-19 cells, actin filaments formed an actin network at the cell periphery, with parallel, thick actin stress fibres in the cell body (Figure 3.6). In PANC-1 cells, peripheral bands of actin filaments were evident in most cells. Distinct dorsal actin filaments were observed in some cells protruding at the front edge (Figure 3.7), while filopodia and microspikes were seen at the very front of the leading edge (Figure 3.8).

3.3.4 End-binding protein expression and localisation

EBs play an important role in the regulation of microtubule dynamics. It is therefore critical to understand the complex molecular processes behind their regulation, with the aim of investigating their regulation in cancer diseases. The localisation and expression of EBs in our cell models were studied, and cells were stained for EBs and microtubules. ARPE-19 and PANC-1 were immunolabelled for EB1 and α-tubulin. In ARPE-19 cells, EB1 was expressed as classic comets at the growing microtubule plus-ends, as is typical (Figure 3.9). In PANC-1 cells, EB1 tended to have a slightly extended tail associated at the plus-ends of microtubule compared to ARPE-19 cells (Figure 3.10).

Interestingly, the level of EB3 expression varied considerably within both ARPE-19 and PANC-1 cells populations. In most ARPE-19 cells EB3 expression was low and tended to be concentrated around the nucleus. EB3 could also be seen along the microtubule lattice and apparently free in the cytoplasm (Figure 3.11). However, sporadic high EB3 expression has previously observed in ARPE-19 cells (Mogensen lab unpublished observations). Varying levels of EB3 expression were also evident in PANC-1 cells (not reported before). Here some cells shared distinct plus-end comets throughout the cell while in others a few comets of EB3 were evident (Figure 3.12).

For localisation of EB2 in ARPE-19 and PANC-1 cells were immunolabelled for EB2 and α-tubulin. In ARPE-19 cells EB2 was found to localise mainly along the microtubule lattice, with some association at the plus-ends (Figure 3.13). EB2 was overexpressed in PANC-1 cells, and it was observed to be punctate in the cytoplasm and along the microtubule lattices (Figure 3.14).

3.3.5 HDAC6 localisation and expression

HDAC6 is a tubulin deacetylase that regulates microtubule dynamics and promotes cell motility. It has been reported that overexpression of HDAC6 leads to significantly increased cell migration in cancerous cells, such as in breast and pancreatic cancer (Li et al., 2014). Due to its important role in microtubule acetylation and cell migration, HDAC6 expression and localisation were studied in our cell line models using immunolabelling. Unfortunately, the antibody did not work in western blotting. So the expression level could not be assessed.

ARPE-19 and PANC-1 cells were immunolabelled for HDAC6 and microtubules. The results illustrated that ARPE-19 cells expressed HDAC6, which was mainly localised in the cytoplasm, but with distinct concentrations around the nucleus and at the leading edge. Staining for acetylated and tyrosinated tubulin did not show an obvious association between HDAC6 and microtubule plus-ends or along the lattice (Figure 3.15). PANC-1 cells were also immunolabelled for HDAC6. The images showed that HDAC6 was mainly free in the cytoplasm, with some concentrations around the nucleus and at the cell periphery (Figure 3.16).

3.4 Discussion

The microtubule cytoskeleton is important for several cell functions, and the precise behaviours and organisation of the microtubules in a cell needs to reflect these functions. Microtubules anchored at the centrosome by minus-ends and the plus-ends elongated and exploring the cellular space to provide support and transport, not least in migration (Cole and Lippincott-Schwartz, 1995, Mogensen et al., 1997, Hawkins et al., 2010). Therefore, disruptions in the microtubule organisation or post-translational modifications may affect their dynamics and stability, as well as their association with +TIPs, and this may lead to loss of function. The results of this study showed that the microtubules in ARPE-19 cells were organised in a classic radial array, with the minus ends anchored at the centrosome and the plus-ends elongating toward the cell periphery. This is an expected result that has been shown previously (Bellett et al., 2009). This makes the ARPE-19 cell line an ideal model, as changes in microtubule organisation can easily be detected following treatment with various compounds, such as SFN.

PANC-1 cells showed a different microtubule organisation. Here microtubules appeared disorganised, although there were still many focussed on the centrosome. Interestingly, bundles of microtubules anchoring at the centrosome and extending to the leading edge were evident on some cells. This would provide a stable system for vesicle transport during migration.

Generally, in undifferentiated cells, in interphase there are two main populations of α-tubulin, a tyrosinated and a small subgroup exhibiting detyrosination (Gundersen et al., 1984). Immunolabelling for tyrosination (YL1/2) and detyrosination (Glu-tubulin) in ARPE-19 and PANC-1 cells showed that most of the microtubules were tyrosinated, suggesting more dynamic microtubules. Tyrosinated tubulin has been showed to recruit some +TIP proteins that are known to influence microtubule dynamics, such as CLIP-19 and $p150^{Glued}$ (Janke and Bulinski, 2011, Garnham and

Roll-Mecak, 2012, Yu et al., 2015). A few detyrosinated microtubules were evident at the cell centre and small segments along the microtubules in ARPE-19 cells, suggesting more stable microtubules; these have been found to prevent the depolymerisation of microtubules with +TIPs, such as MCAK and KIF2A (Peris et al., 2009, Janke and Bulinski, 2011, Yu et al., 2015). However, PANC-1 cells showed very low expression of detyrosinated tubulin.

The effect of tubulin acetylation on the dynamics of microtubules is still not fully clear. However, acetylated tubulin has been used as marker for stable microtubules, and it may affect the microtubule dynamics and increase stability (Palazzo et al., 2003, Dompierre et al., 2007). Moreover acetylated microtubules provide tracks for some motor proteins, including dynein and kinesin-1 (Garnham and Roll-Mecak, 2012, Janke and Bulinski, 2012). Immunolabelling for acetylated tubulin was carried out, and the images illustrated that acetylation occurred along segments of microtubules found in cell body, with some concentrated near the cell centre. These localisations were observed in both cell models.

Actin filaments have a vital role in cell functions, such as cell movement, cell division and structural support. The precise organisation of the actin filaments is important for performing these functions (Lappalainen, 2016). In ARPE-19 and PANC-1 cells, actin filaments were observed around the cell periphery, with some stress fibres mainly running parallel to the cell body near the centre. Dorsal actin arcs were also observed protruding at the front edge in PANC-1 cells and some filopodia and microspikes at the very front edge.

+TIP proteins regulate microtubule dynamics, and this includes the EB proteins (EB1, 2 and 3). EB1 and EB3 have the ability to recognise growing microtubule plus-ends, which are associated with GTP-tubulin and interact with most other +TIPs (Morrison et al., 1998, Lansbergen and Akhmanova, 2006). This ability is important in helping to determine the state of microtubules. EB1 binds to

elongating microtubule plus-ends and it binds between microtubule protofilaments and promotes growth (Sandblad et al., 2006, des Georges et al., 2008, Maurer et al., 2012). Moreover, the length of EB1 comets is an indication of the GTP-tubulin growing tip, which promotes further microtubule polymerisation (Duellberg et al., 2016). A classic EB1 comet-like association at the plus-ends was evident in ARPE-19 cells, while an apparent slightly longer comet tail was present in PANC-1 cells. No EB1 or EB3 microtubule lattice association was observed. Interestingly, sporadic EB3 expression was observed in both ARPE-19 and PANC-1 cells. Further studies of EB3 were therefore not carried out.

EB2 had a different localisation from EB1 and EB3, as it is associated along microtubule lattices and exhibits only a slight accumulation at the microtubule plus-ends. This association along the lattice could possibly prevent EB1 association along the microtubules and thus maintain microtubule dynamics (Goldspink et al., 2013). It has been shown that depletion of EB2 inhibits the dynamics leading to bundles of microtubules co-aligned with actin filaments with EB1 and ACF7 lattice association (Goldspink et al., 2013). However, some EB2 was observed to be free in the cytoplasm of PANC-1 cells, although EB2 is overexpressed in this cell line. Overexpression of EB2 has also been suggested to result in alternating actin filament distribution, as well as the promotion of microtubule dynamics and invasion (Abiatari et al., 2009). Dispersion of EB2 in the cytoplasm may be due to the phosphorylation of EB2 by Aurora B as observed during mitosis (Iimori et al., 2016).

HDAC6 is another protein that is expressed in PANC-1 cells (Li et al., 2014). The results observed here were similar to those of other studies. HDAC6 is mainly found in the cytoplasm of ARPE-19 and PANC-1 cells, with no obvious association with the microtubule lattice or at the plus-ends. Some accumulation at the cell periphery was observed in both cell lines. Previous studies have indicated that HDAC6 is a microtubule-associated protein, functioning as an α-tubulin

deacetylase that regulates microtubule dynamics and influences cell migration (Huo et al., 2011). However, it is mainly found in the cell cytoplasm but can interact with different +TIP proteins, including CLIP-170 and EB1 (Zilberman et al., 2009, Li et al., 2011, Li et al., 2014). Moreover, overexpression of HDAC6 leads to total deacetylation of the microtubules, stimulation of actin polymerisation and promotion of cell migration in many cancer cells (Huo et al., 2011, Li et al., 2014, Ran et al., 2015).

In summary, the results showed that ARPE-19 cells (used here as a normal epithelial cell model) have a classic radial microtubule array, with actin filaments found at the cell periphery and some as central stress fibres. In PANC-1 cells some microtubules were focussed on the centrosome, but a more disorganised network was evident in most cells. Some cells revealed distinct microtubule bundles that targeted the leading edge. Relatively narrow lamellipodia were evident, with microspikes and filopodia, while stress fibres were distinct. The EBs showed a typical plus-end association with microtubules in both cell models. However, HDAC6 did not show any noticeable association with microtubule plus-ends or along the lattice (Huo et al., 2011), rather, it was mainly found in the cytoplasm, with some accumulation in the cell periphery.

ARPE-19

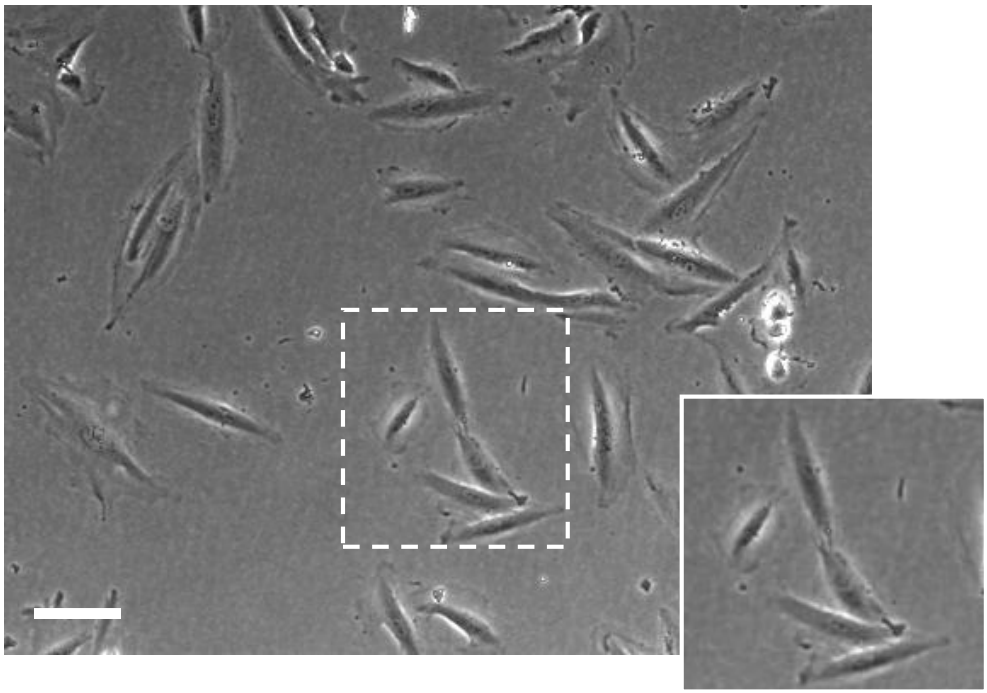

PANC-1

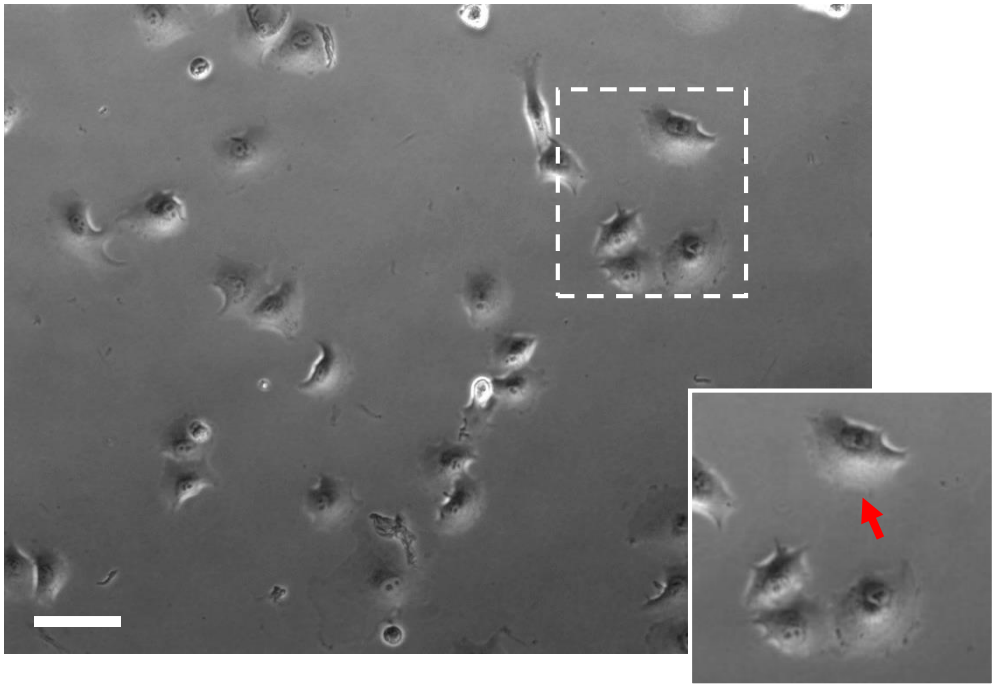

Figure 3.1 ARPE-19 and PANC-1 cell morphology
Frames from live time-lapse imaging of subconfluent ARPE-19 and PANC-1 cells showing different cell morphologies.
ARPE-19 cells appear mainly elongated with thin membrane protrusion around some migrated cells.
The PANC-1 cells look rounded but with relatively large lamellipodia evident in some cells (arrow) with some pointed protrusions. Scale bars = 100µm.

ARPE-19

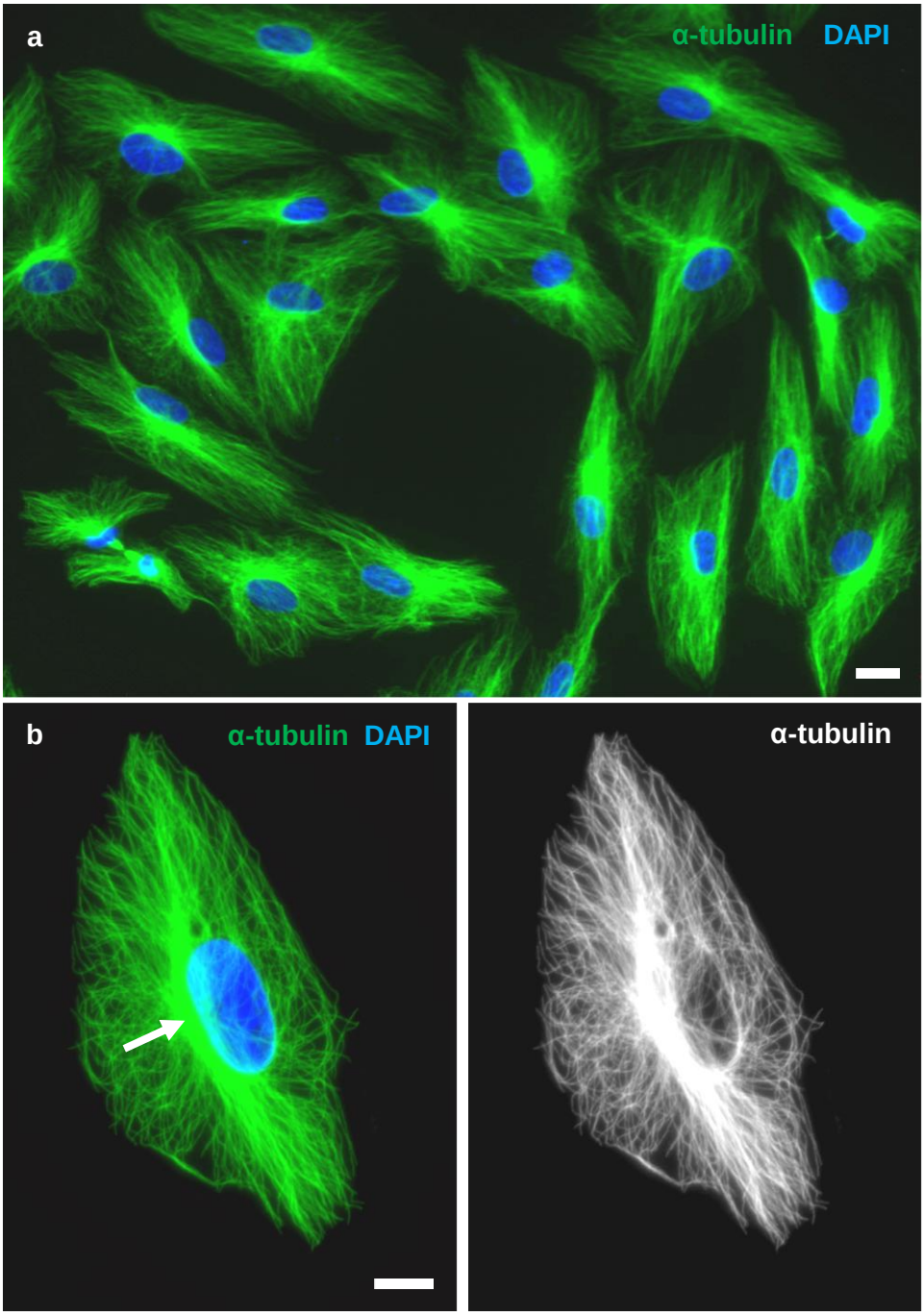

Figure 3.2 Microtubule organisation in ARPE-19 cells
Widefield fluorescent images of cells immuno-labelled for α-tubulin (green) and stained with DAPI (blue). a) A field illustrating subconfluent cells with microtubules arranged in radial arrays. b) A cell highlighting radial organisation with microtubules focused at a point (centrosome) near the nucleus (arrow) and extending towards the cell periphery. Scale bars = 10μm.

PANC-1

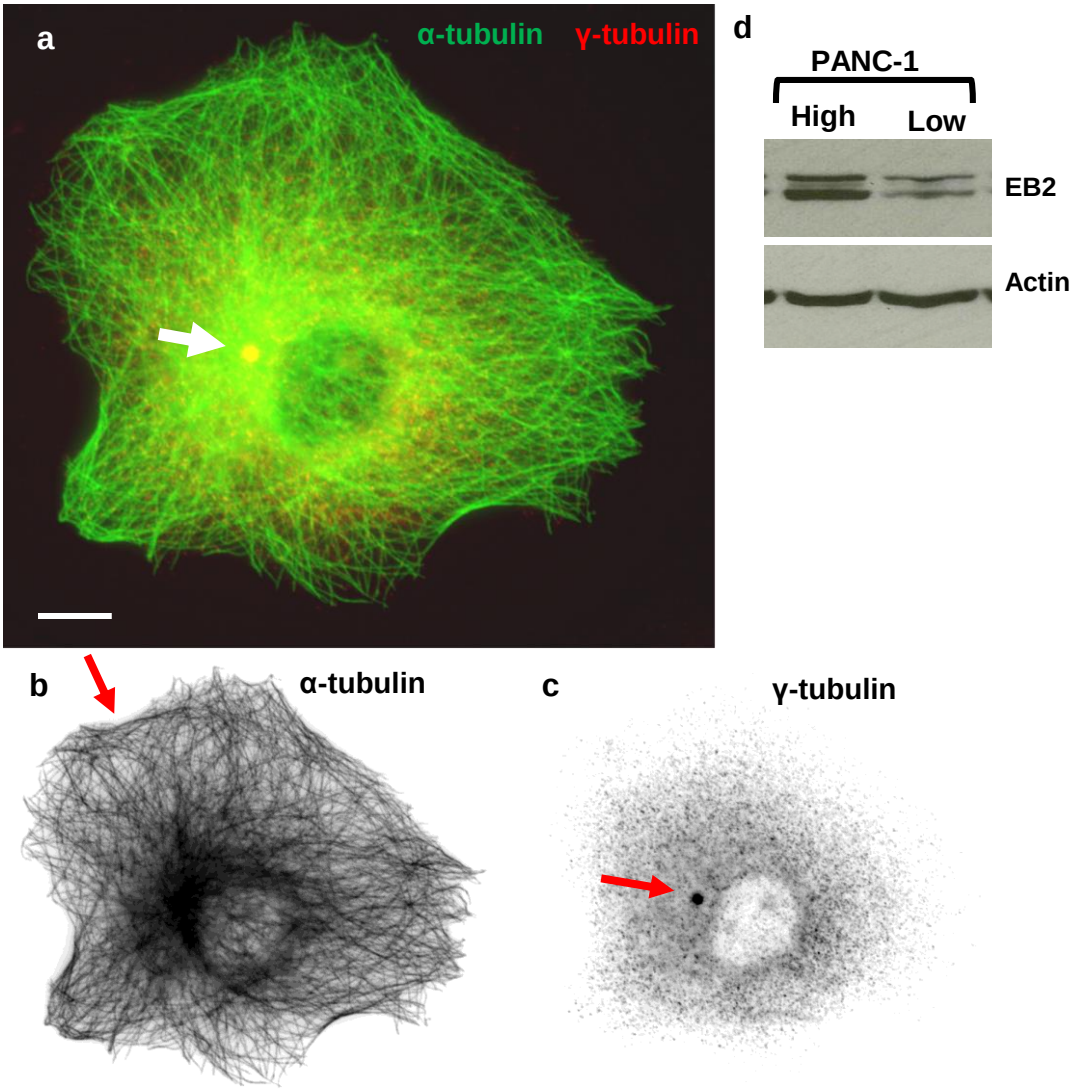

Figure 3.3 Microtubule organisation in PANC-1 cells
Widefield fluorescent images of cells immunolabelled for microtubules (α-tubulin; green/single channel) and γ-tubulin (red/single channel). a and b) Some of the microtubules are focused at the centrosome with the plus ends directed towards the cell periphery but some are arranged parallel to the cortex (arrow). c) High concentration of γ-tubulin is evident at the centrosome (arrow) which is located close to the nucleus. d) Western blot showing EB2 expression in high and low PANC1 sub-clones with the $EB2^{Hi}$ sub-cloned selected as a model cell line for this study. Scale bars = 10µm.

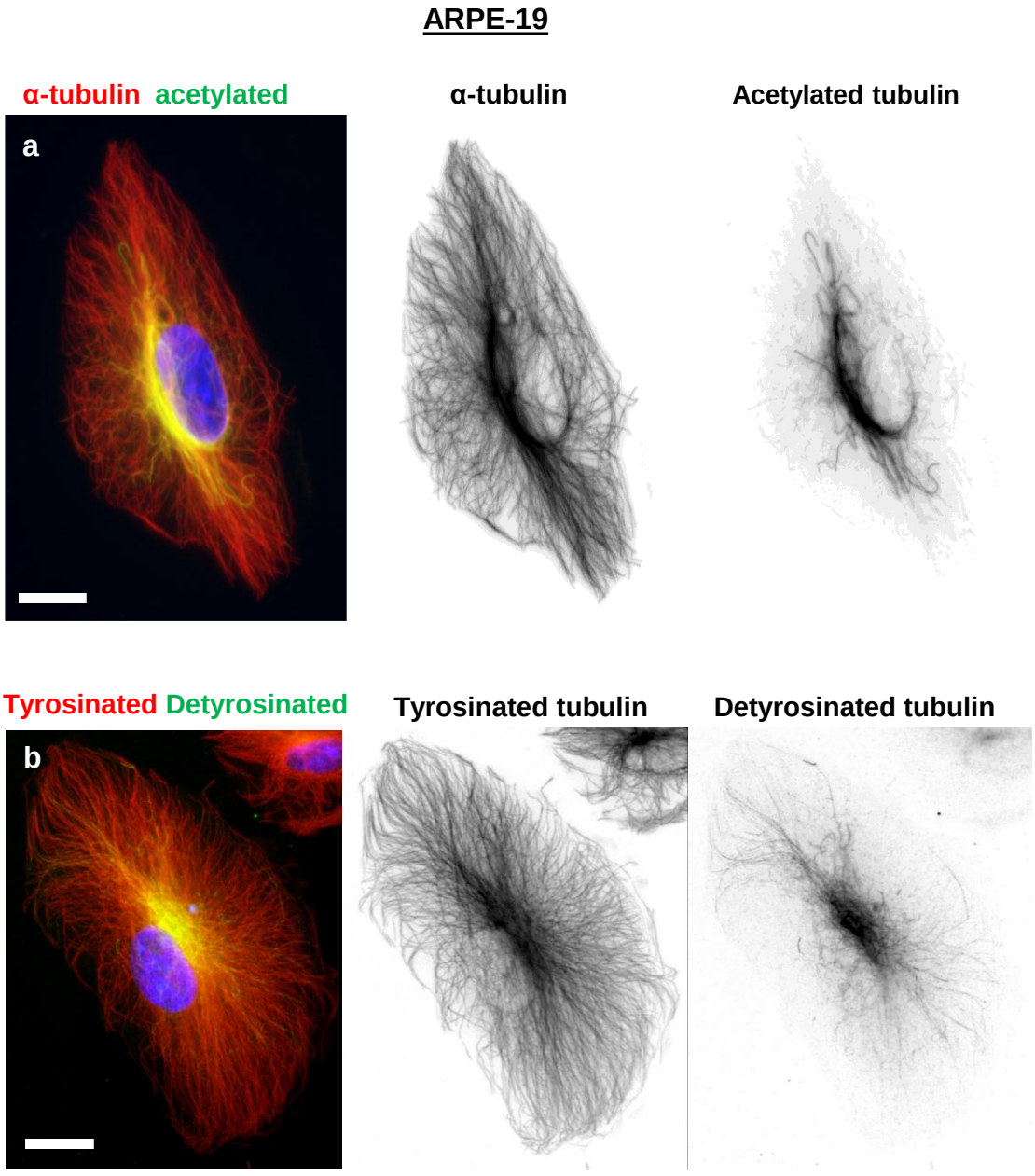

Figure 3.4 Tubulin modifications in ARPE-19 cells
a) Cells were immunolabelled for α-tubulin (red, invert) and acetylated tubulin (green, invert), illustrating a classic microtubule array with some acetylated tubulin at the centre of the cell and few radiating out to the cell edge. b) Immuolabelling for tyrosinated tubulin (YL1/2, red) and detyrosinated tubulin (glu-tubulin, green, invert) showing that most of the microtubules are tyrosinated with some detyrosinated microtubules observed at the central area of the cell, and with small segments along the microtubules. Scale bars = 10µm.

PANC-1

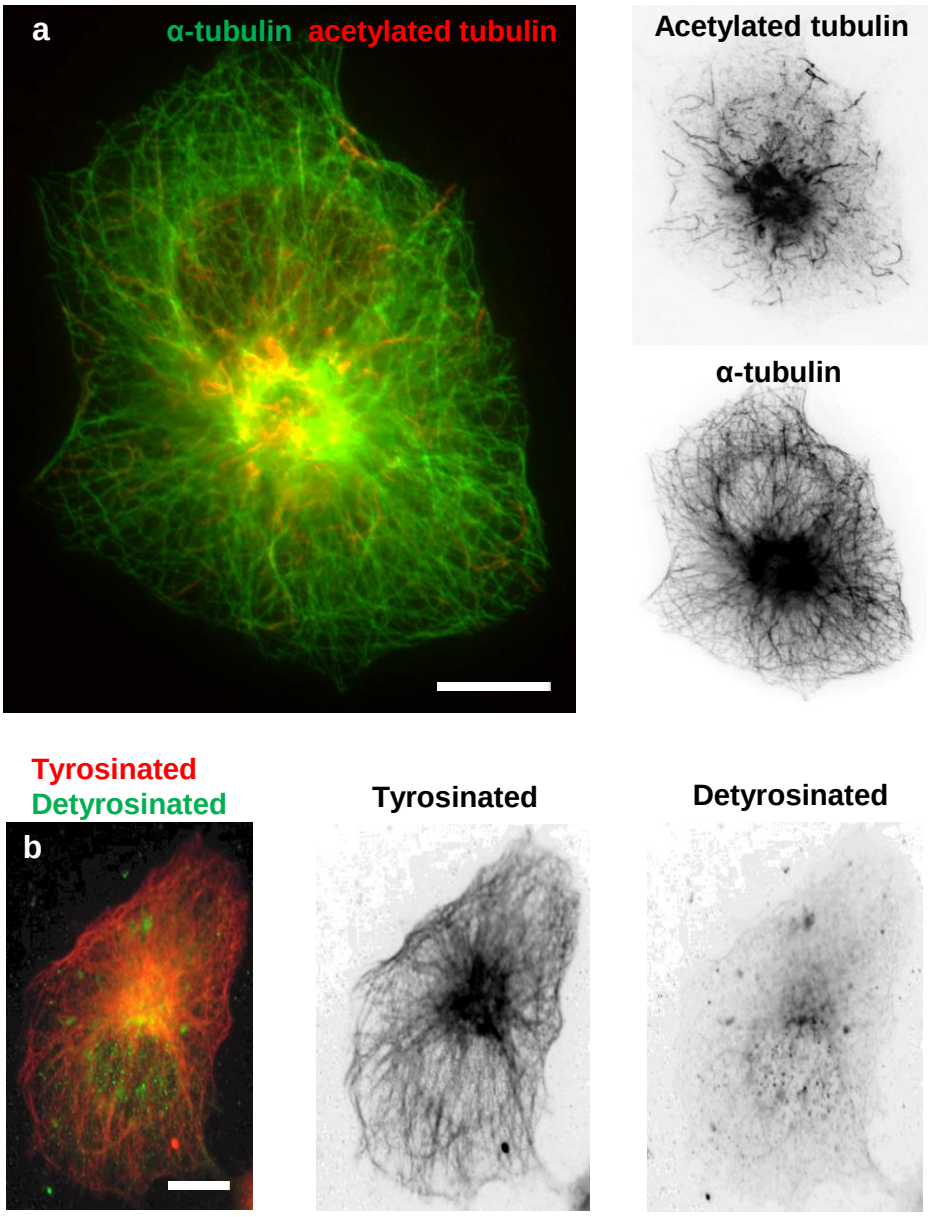

Figure 3.5 Tubulin modifications in PANC-1 cells
a) Cells immunolabelled for acetylated tubulin (red, invert) and α-tubulin (green, invert). The microtubules appear in disorganised network and most of the acetylated microtubules are present in the centre of the cell body and a few close to the cell edges. b) Immuolabelling for tyrosinated tubulin (red, invert), illustrating that many microtubules are tyrosinated with very few detyrosinated microtubules (green, invert).Scale bars = 10µm.

ARPE-19

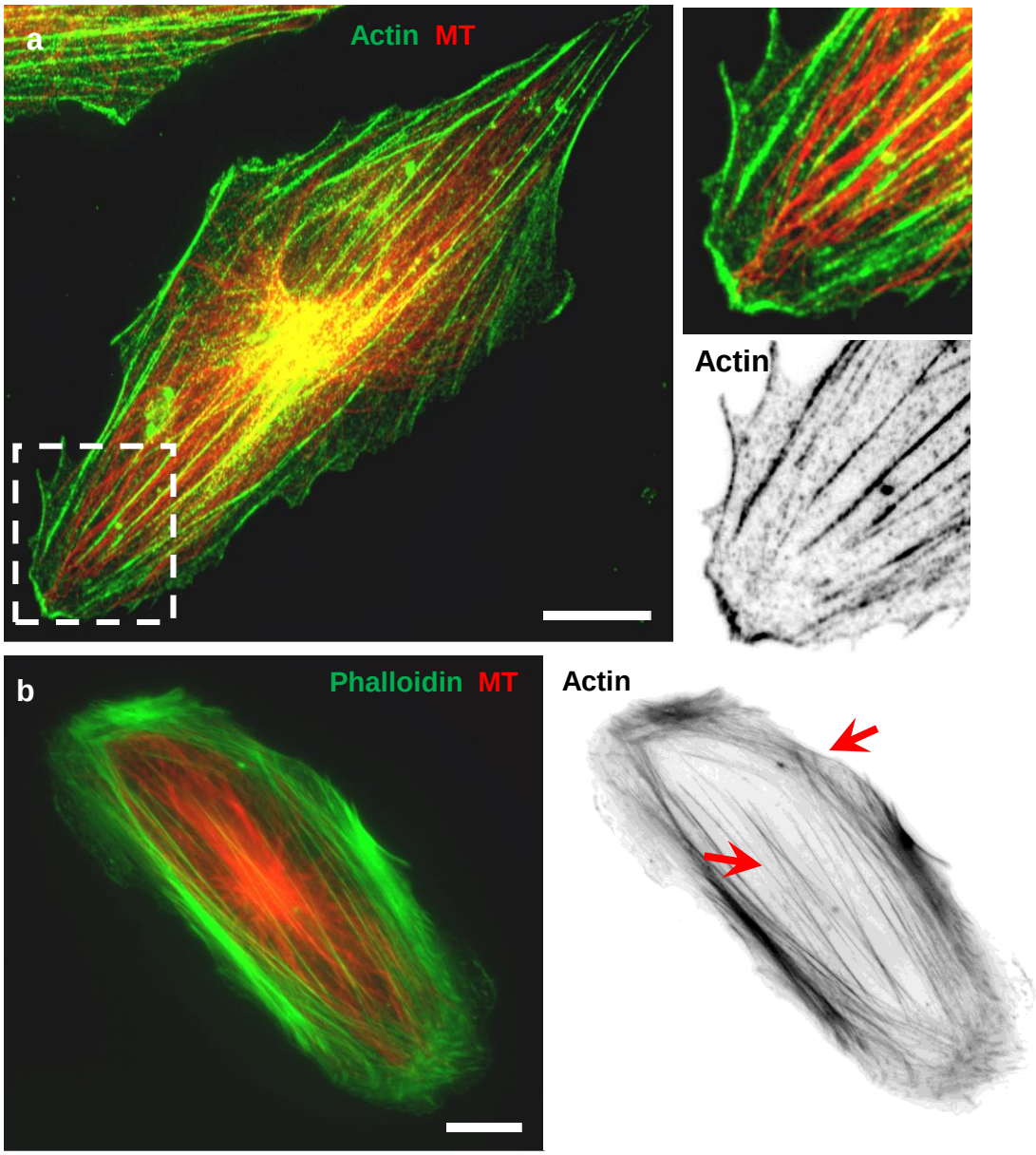

Figure 3.6 Actin organisation in ARPE-19 cells
Cells were immunolabelled for (a) α-tubulin (red) and actin (β-actin; green, invert) illustrating actin organisation and (b) microtubules (red) and actin (Phalloidin; green, invert) showing actin filaments. The actin filament organisation shows a cortical networks and stress fibres in the centre mainly running parallel to the long axis of the cell (enlarged boxed and arrows). Scale bars = 10µm.

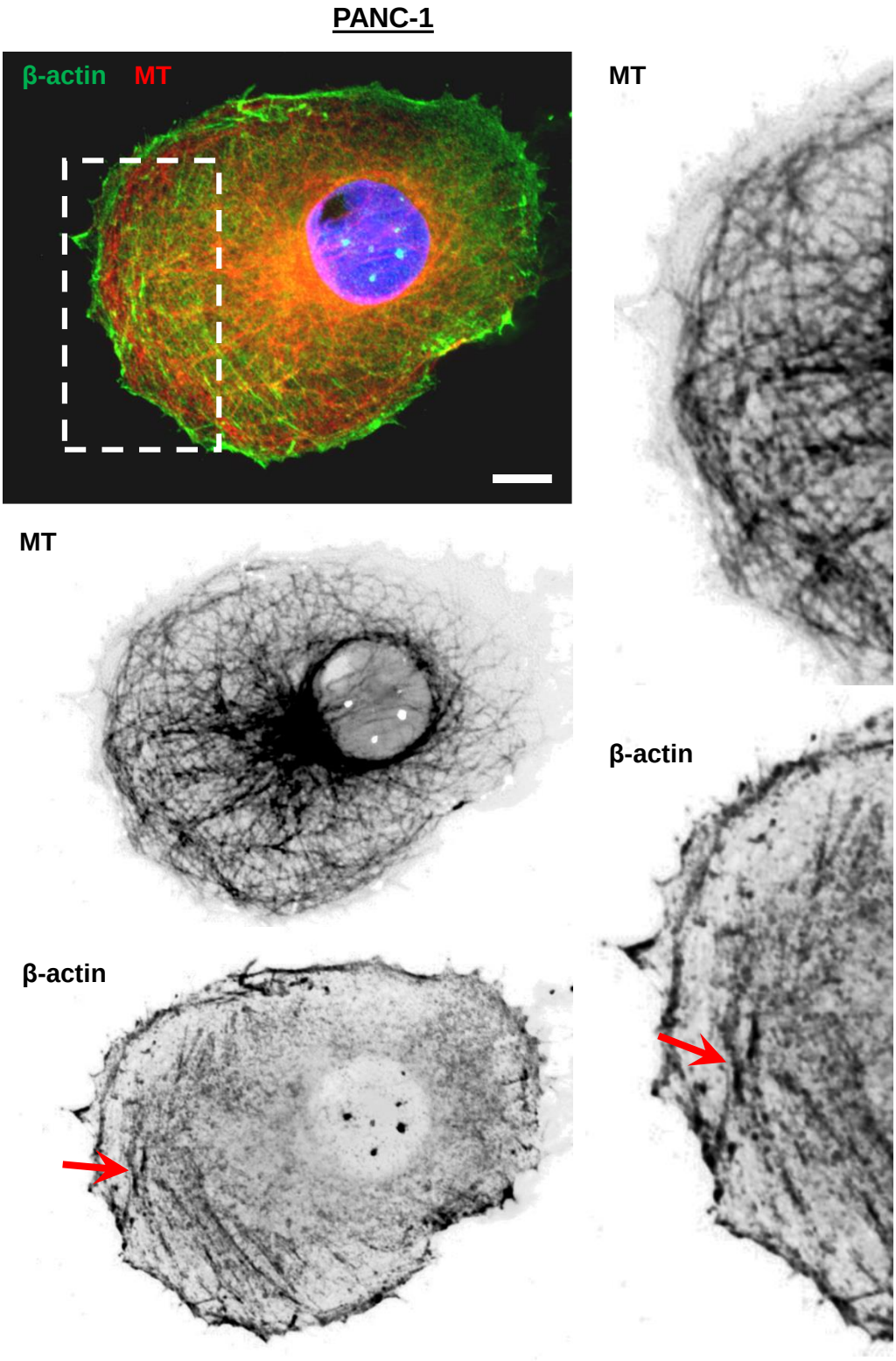

Figure 3.7 Actin organisation in PANC-1 cells
Widefield fluorescent images of cells immunolabelled for α-tubulin (red, invert) and actin (β-actin; green, invert) illustrating parallel actin filaments at the cell edge with dorsal actin filament bundles evident at the front edge (arrows and enlarged boxed). Scale bars = 10µm.

PANC-1

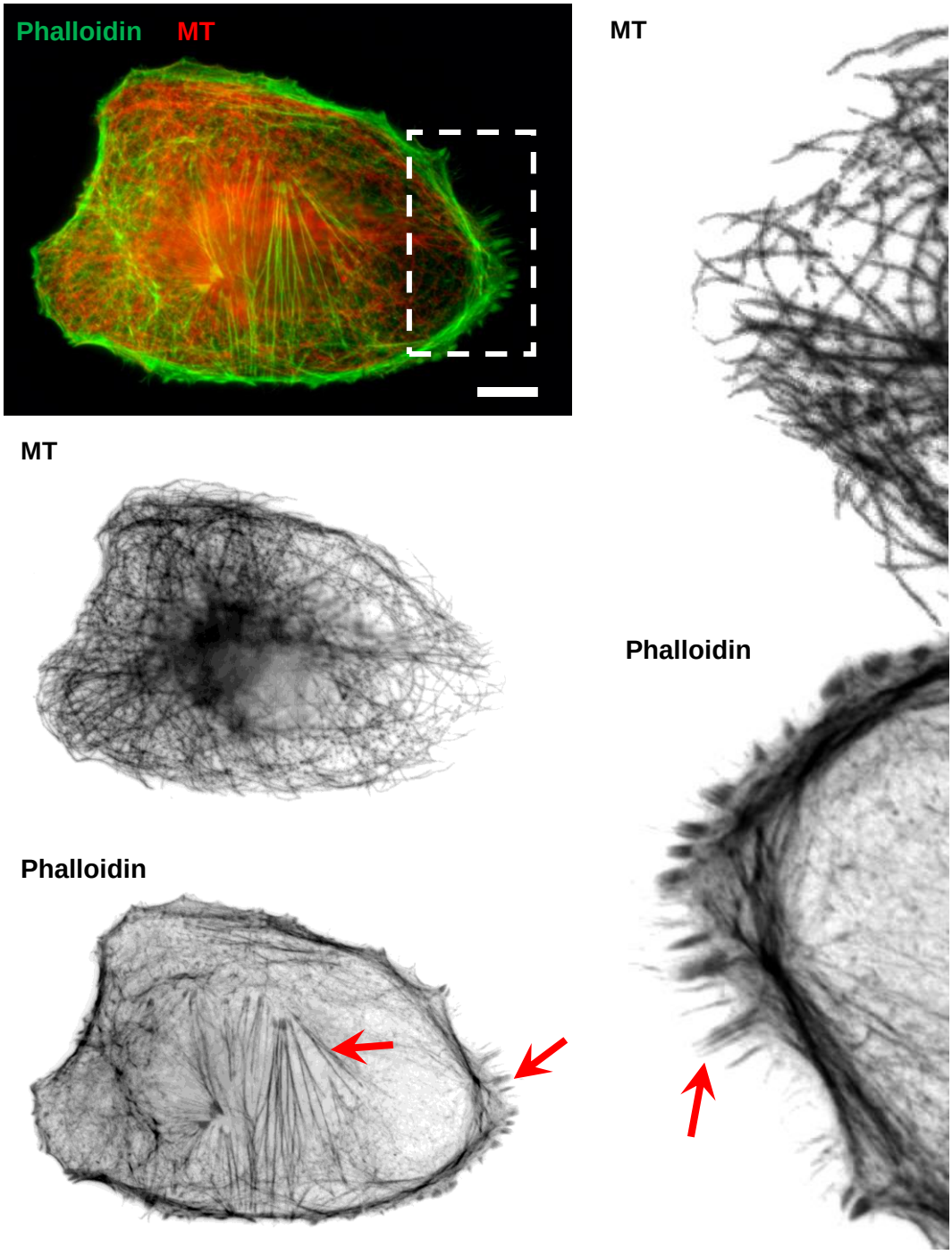

Figure 3.8 Actin organisation in PANC-1 cells
Cells were immune-labedlled α-tubulin (red, invert) and actin (Phalloidin; green, invert). The actin filament organisation shows stress fibres in the cell body (arrow) with filopodia and microspikes at the very front of the leading edge (enlarged boxed, arrows). Scale bars = 10µm.

ARPE-19

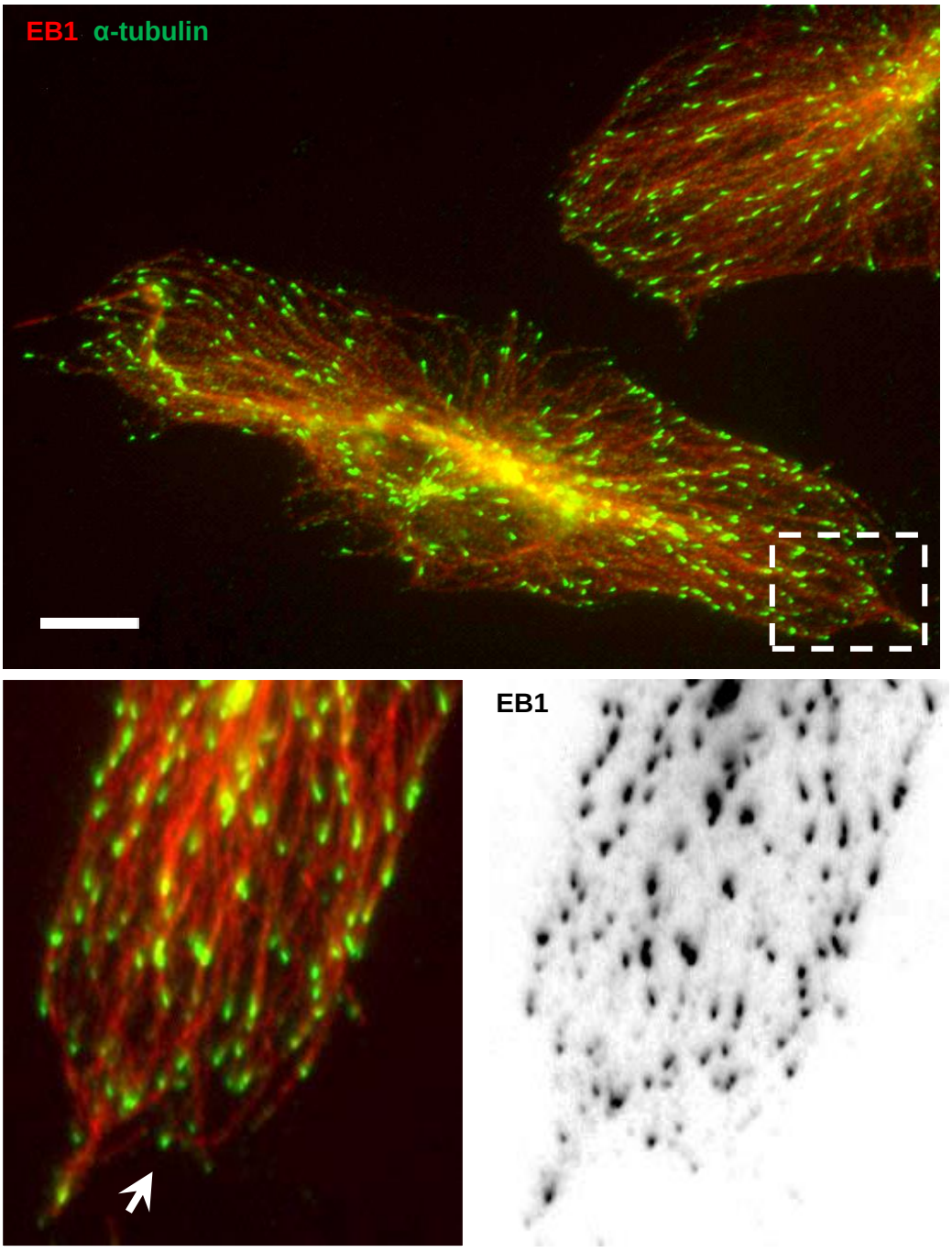

Figure 3.9 EB1 localisation in ARPE-19 cells
Widefield fluorescent images of cells labelled for α-tubulin (red) and EB1 (green, invert). The microtubule network extends forward to the leading edge and EB1 appear as classic comets at the plus-ends. Enlarged region boxed, note EB1 comets at the plus-ends of microtubules (arrowed). Scale bar = 10µm.

PANC-1

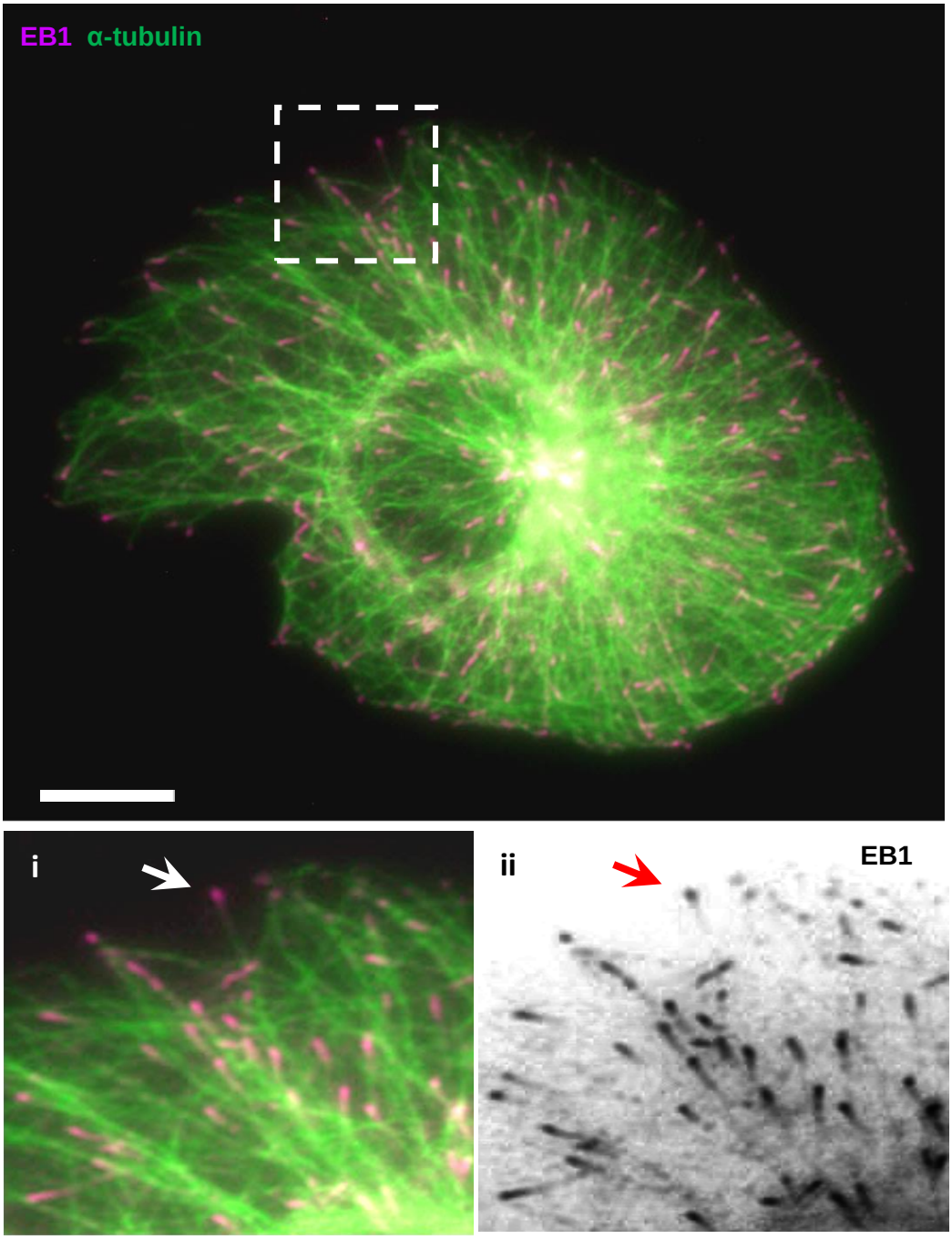

Figure 3.10 EB1 localisation in PANC-1 cells
Widefield fluorescent image of cell immunolabelled for EB1 (purple, invert) and α-tubulin (green) showing the microtubule network extending from the centrosome towards the leading edge with EB1 comets at the plus ends. Enlarged region boxed, showing EB1 comets with a slight extended tail at the plus-ends (arrows). Scale bar =10µm.

ARPE-19

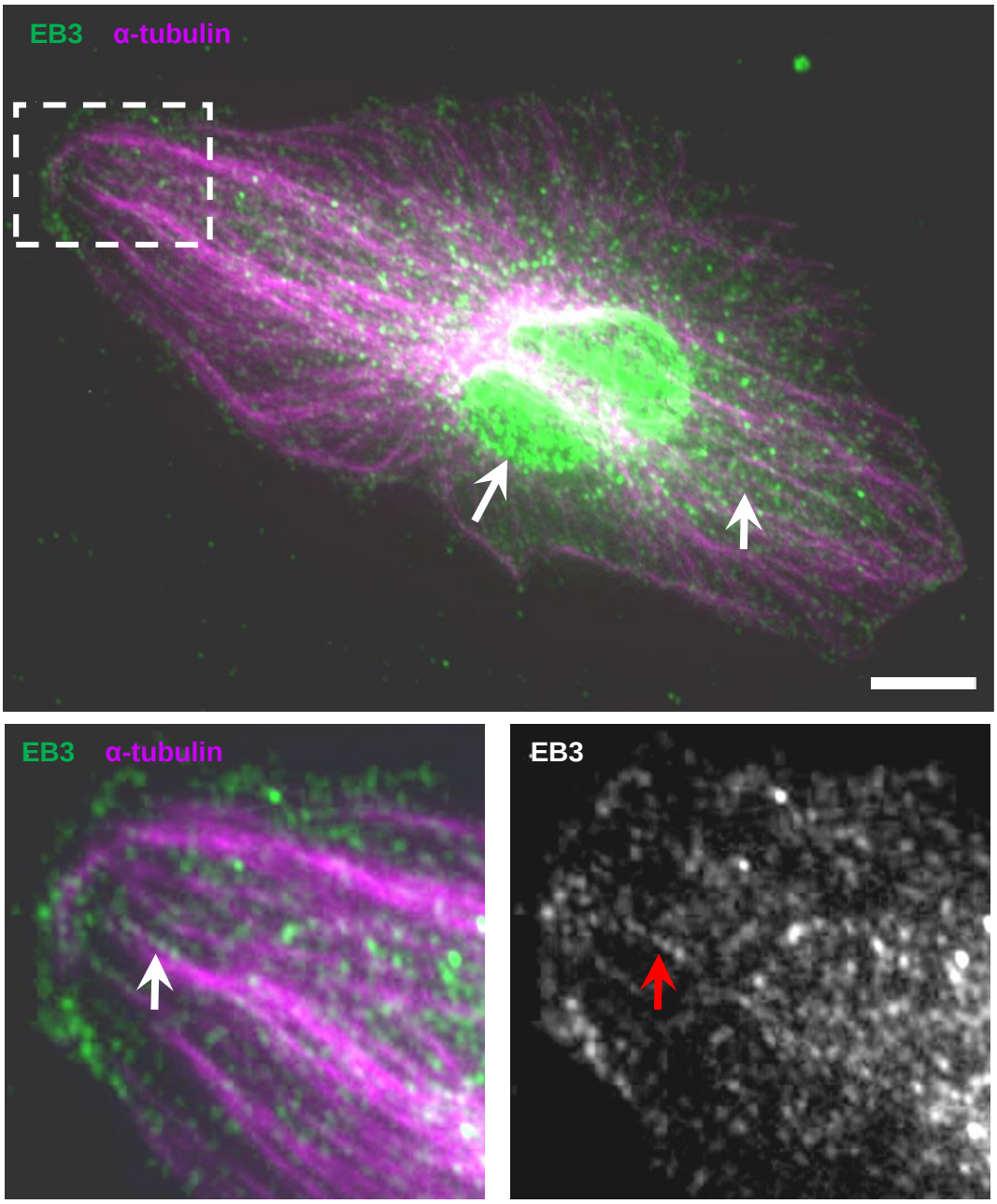

Figure 3.11 EB3 localisation in ARPE-19 cells
Widefield fluorescent image of cell immunolabelled for α-tubulin (purple) and EB3 (green, invert) showing EB3 mainly as punctate in the cytoplasm and concentrate around the nucleus (arrow), but also at plus-end and with some associated along microtubule lattice. Enlarged region boxed showing EB3 along the microtubule lattice and at the plus-ends (arrows). Scale bar = 10µm.

PANC-1

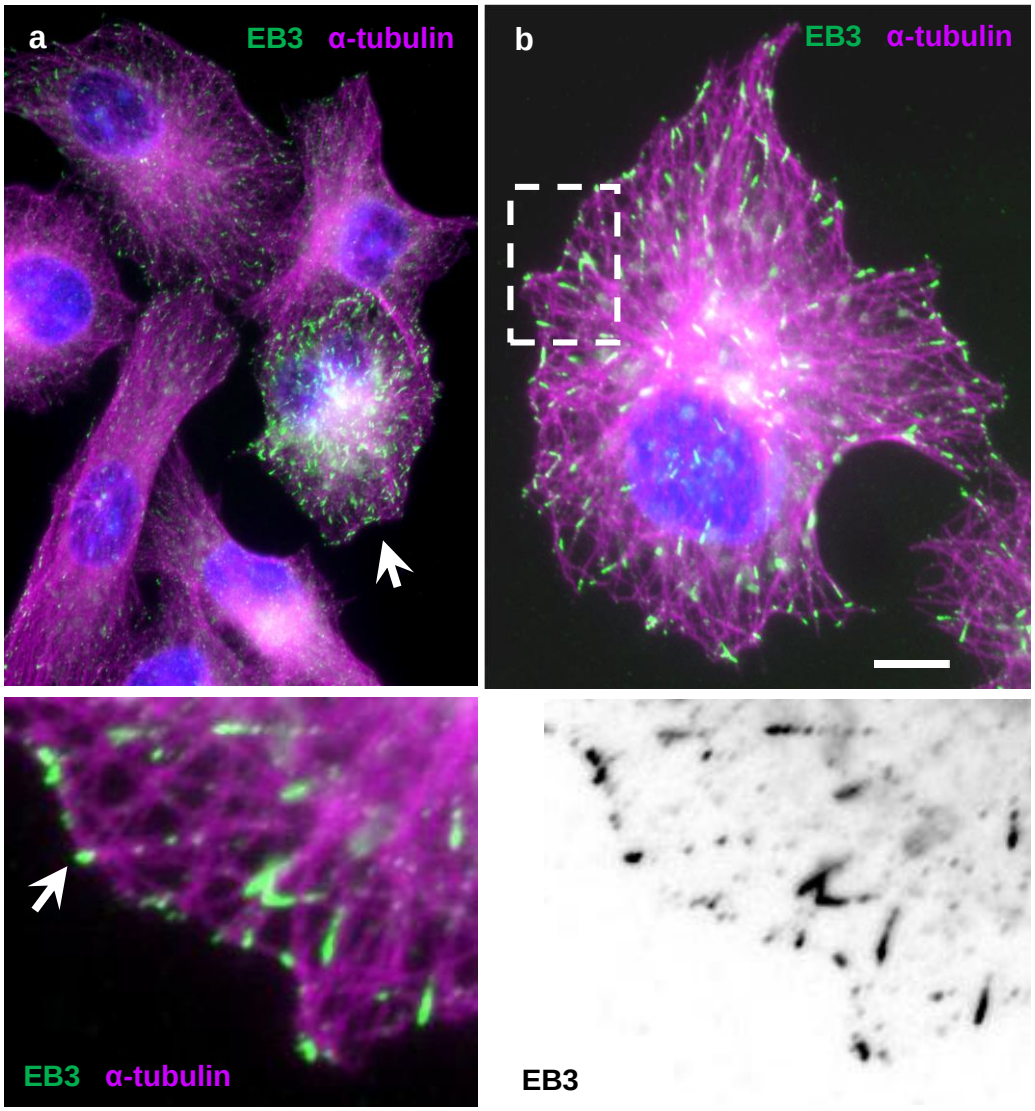

Figure 3.12 EB3 localisation in PANC-1 cells
Cells were immunolabelled for EB3 (green, invert) and microtubules (purple), a) showing EB3 expression is different with some cells appeared highly expressed (arrow) and others with low expression of EB3. b) Cells show microtubules and EB3 with low expression. EB3 localises mainly at the plus-ends of microtubules (enlarged boxed, arrow). Scale bar = 10µm.

ARPE-19

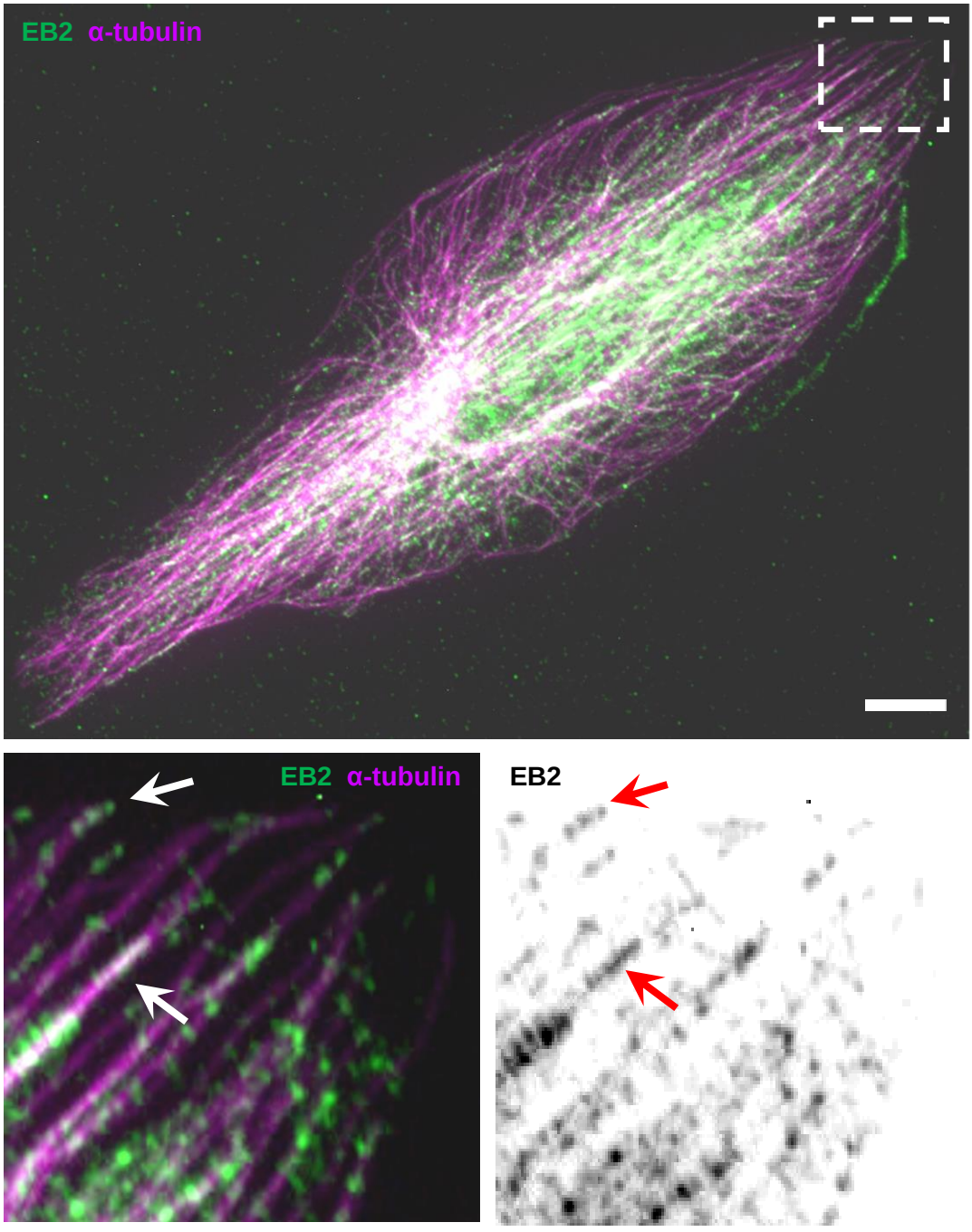

Figure 3.13 EB2 localisation in ARPE-19 cells
Cells were immunolabelled for EB2 (green, invert) and α-tubulin (purple). EB2 is clearly visible along the microtubule lattice as well as some at plus-ends (arrows). Scale bars = 10µm.

PANC-1

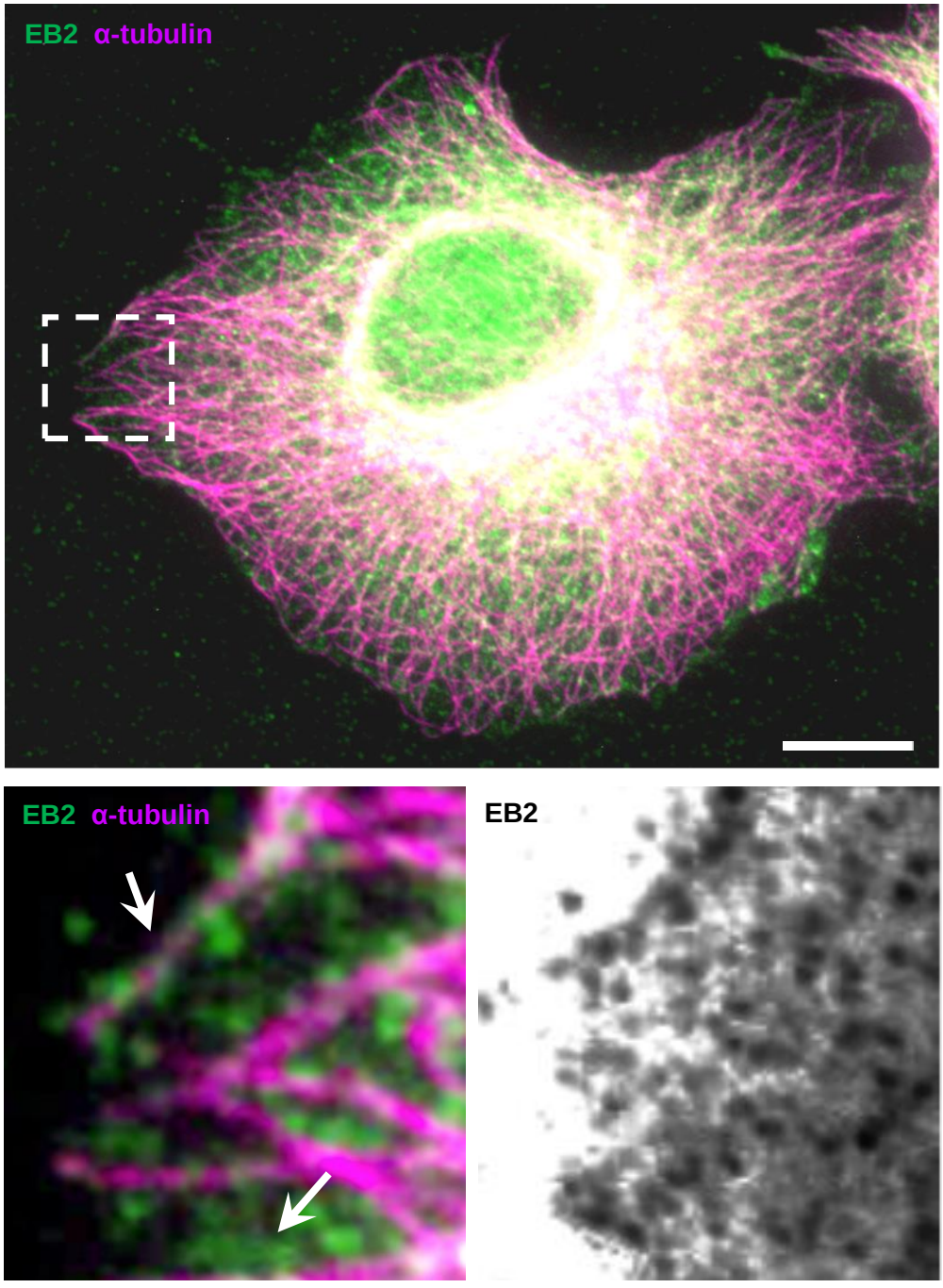

Figure 3.14 EB2 localisation in PANC-1 cells
Widefield fluorescent image of cell immunolabelled for EB2 (green, invert) and α-tubulin (purple). EB2 is mainly punctate in the cytoplasm (arrow) but can also be seen along the microtubule lattice. Enlarged region boxed showing EB2 along the microtubule lattice and the cytoplasm (arrows). Scale bar = 10µm.

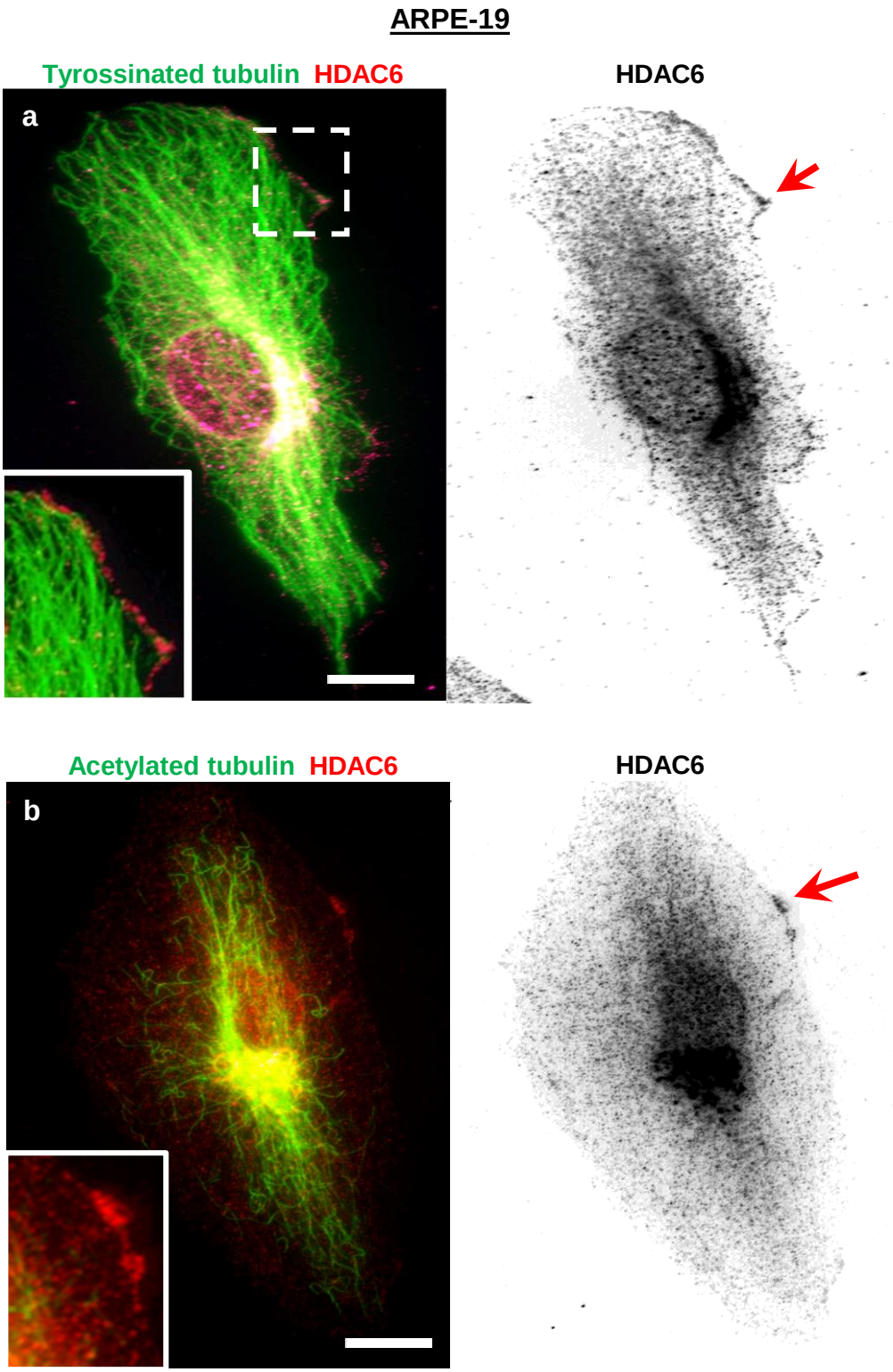

Figure 3.15 HDAC6 localisation in ARPE-19 cells
Widefield fluorescent images of cells immunolabelled for: (a) tyrosinated tubulin (YL1/2, green) and HDAC6 (red, invert). b) Acetylated tubulin (green) and HDAC6 (red, invert). It can be seen that HDAC6 is mainly in the cytoplasm and concentrated around the nucleus, but also accumulating in some areas at the periphery (arrows).Scale bar = 10µm.

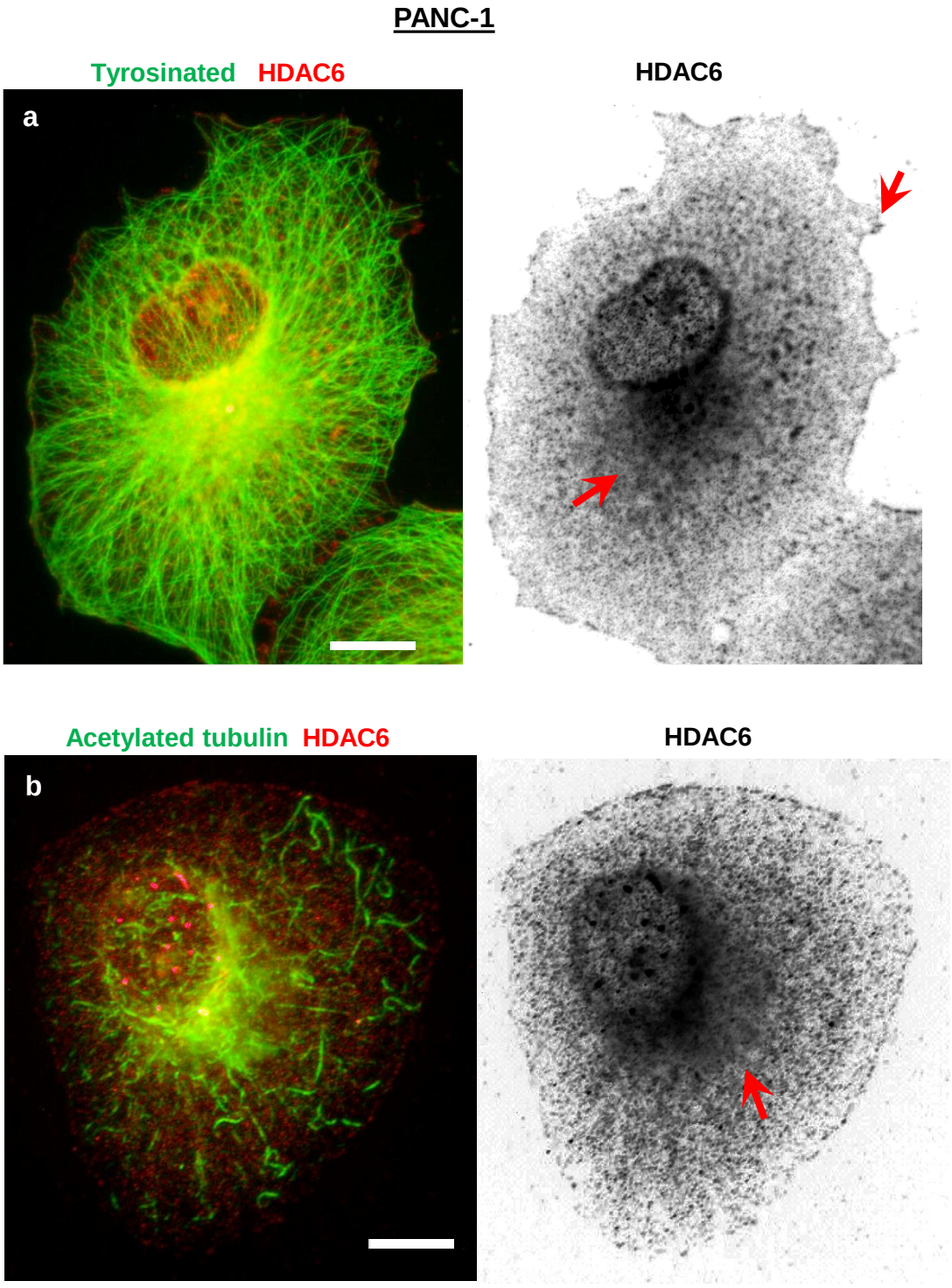

Figure 3.16 HDAC6 localisation in PANC-1 cells
Cells were immunolabelled for: (a) tyrosinated tubulin (YL1/2, green) and HDAC6 (red, invert). b) Acetylated tubulin (green) and HDAC6 (red, invert). HDAC6 is mainly in the cytoplasm, but with some accumulated at the periphery in some cells. Scale bars = 10µm.

Chapter IV: Effects of Sulforaphane on Random Cell Migration

4.1 Overview

This chapter presents the study of the effect of sulforaphane (SFN) on cell migration in pancreatic cancer and normal epithelial cells. The main questions of this study are: Does sulforaphane have an effect on cell migration velocity in normal epithelial and pancreatic cancer cells, and does it influence microtubule and actin organisation? The study also investigates whether SFN affects EB and HDAC6 localisation and expression. In addition, does inhibition of HDAC6 by tubacin, or a combination with SFN and tubacin, affect cell motility and microtubule organisation and EBs localisation?

4.2 Introduction

Cell migration and invasion of tumour cells through tissues to distant sites is a key mechanism in the cancer disease process, known to be responsible for the majority of cancer deaths (Chambers et al., 2002). Pancreatic cancer is one of the most aggressive epithelial cancers. It is the fifth leading cause of death in the United Kingdom, where only 5% patients are expected to survive for only five years after diagnosis. Pancreatic cancer is strongly resistant to current cancer treatment (Bardeesy and DePinho, 2002, Wang et al., 2011).

The cytoskeleton plays an essential role in cell movement by rearranging and producing force in order to initiate this movement. A critical property of microtubules is their dynamic instability; the central mechanism of anticancer treatments is to suppress this instability. It has been reported that SFN suppresses microtubule dynamics in human breast cancer (Azarenko et al., 2008); moreover, excessive microtubule stabilisation has been shown to impede disassembly of focal adhesions which then affect cell migration (Li et al., 2011).

SFN has cancer chemopreventive and therapeutic potential through several possible mechanisms. Accordingly, SFN has been shown to have preventive and therapeutic effects on different cancer types both *in vitro* and *in vivo*. SFN has been reported to affect microtubule polymerisation, inhibit cell proliferation and initiate apoptosis in cancerous cells (Gamet-Payrastre et al., 2000, Jackson and Singletary, 2004). Therefore, SFN may be capable of retarding or eliminating neoplastic cells and inhibiting the progression of tumours into metastasis. It has been reported that SFN reduces cell migration in ovarian cancer cells, but only with cytotoxic concentration (Bryant et al., 2010).

Overexpression of HDAC6, which is evident in a number of cancers, completely deacetylates microtubules (Aldana-Masangkay and Sakamoto, 2010, Li et al., 2014). HDAC6 promotes and regulates cell motility with overexpression of HDAC6 showing enhancement of cell motility, while inhibition impairs cell movement. It has been reported that SFN affects HDAC6 by inhibiting its activity (Pledgie-Tracy et al., 2007). Treating human prostate cancer cells with SFN has been shown to increase tubulin acetylation and inhibit HDAC6 (Myzak et al., 2006). Tubacin (HDAC6-specific activity inhibitor) increases tubulin acetylation and affects microtubule dynamics (Li et al., 2014).

EB proteins have an important role in regulating microtubule dynamics; these proteins interact with various internal cell structures, such as the cortex, organelles and kinetochores, as well as the actin cytoskeleton (Vaughan, 2005, Lansbergen and Akhmanova, 2006). EBs can also associate with the microtubule lattice as a result of overexpression and could affect its dynamics (Bu and Su, 2001).

Further studies are required to understand the effect of SFN, in particular its effect on microtubule and actin filament organisation and associated proteins, such as EBs and HDAC6, and whether such interactions can influence cell migration.

4.3 Results

4.3.1 SFN concentrations greater than 30 µM dramatically decrease cell viability in AREP-19 and PANC-1 cells

The effect of SFN treatment on cell viability was evaluated using an MTT assay. This assay is based on the cleavage of the yellow dye MTT to purple formazan crystals. This occurs only in living cells, due to dehydrogenase activity in mitochondria. Viability was determined by using the MTT assay on SFN-treated ARPE-19 and PANC-1 cells with different levels of SFN for 48 hours. Cells were seeded in a 96-well plate in triplicate for each condition and left overnight to reach confluency. Cells were treated with different levels of SFN 2, 10, 15, 20, 30 and 40 µM or DMSO, or were left untreated and incubated for 48 hours (Gamet-Payrastre et al., 2000, Myzak et al., 2006, Jackson et al., 2007, Pledgie-Tracy et al., 2007, Azarenko et al., 2008, Gibbs et al., 2009, Clarke et al., 2011). Following this, the MTT assay protocol was started with the addition of 10 µl of MTT reagent to each well, followed by incubation for 4 hours. Crystal dissolving solution (100 µl) was added to each well; the cellular homogenate was then measured by recording absorbance at 570 nm in a microtiterplate reader, in order to evaluate drug cytotoxicity (as described in Chapter II, section 2.3). As shown in Figure 4.1, 30 µM and 40 µM SFN showed significantly decreased cell viability in ARPE-19 and PANC-1 cells after a 48-hour incubation. It can also be observed from the results that SFN treatment ranging from 2 to 20 µM had no significant effect on cell viability in either cell line, although there was a noticeable decrease in cell number and morphology with 20 µM SFN. DMSO at 0.01% concentration was used as a vehicle control (the same concentration in which SFN was dissolved) and showed no effect on cell viability.

These results indicate that treatment with SFN at 30 µM or more significantly inhibits cell viability in PANC-1 and ARPE-19 cells. Based on these results, SFN at concentrations of up to 15 µM was used for the experiments in this project to further investigate cell migration.

4.3.2 SFN treatment causes distinct morphological changes

ARPE-19 and PANC-1 cells were seeded to reach subconfluency and grown overnight. The following day, they were treated with different concentrations of SFN (2, 10 and 15 µM) for 48 hours. Samples were fixed for fluorescent imaging while others were used for live time-lapse imaging. Live images of SFN treated cells showed a change in morphology, with treated cells appearing larger in area compared to DMSO control cells. Furthermore, a decrease was observed in the number of cells, along with an accumulation of cells floating in the culture medium, with 30 and 40 µM SFN in both cell lines (data not shown). Frames from the Live-time-lapse imaging were used to analyse cell area. This involved drawing an outline of the cell using ImageJ. Statistical analysis was carried out using one-way analysis of variance (ANOVA) with Tukey's multiple comparison test. The drawback of this method is that the way of measuring cell area relay on the quality of the images, and also on the accurate observation to determine the cell edge.

In ARPE-19 cells, the data revealed a significant increase in the average area of cells treated with 10 and 15 µM, compared to DMSO cells. Untreated and DMSO cells exhibited average cell area of 3395 μm^2 and 3422 μm^2, respectively, compared to 4387 μm^2 in 10 µM SFN and 5284 μm^2 in 15 µM SFN (Figure 4.2, a). Similarly, 10 µM and 15 µM SFN treated PANC-1 cells revealed a dramatic increase in cell area with 4930 μm^2 for 10 µM and 6365 μm^2 in 15 µM SFN compared to 3540 μm^2 in DMSO treated cells. These changes in cell area following SFN treatment

suggest that SFN has an effect on cell adhesion and possibly also cell proliferation, causing cell flattening and increased area.

4.3.3 SFN treatment causes a decrease in the migration speed of ARPE-19 cells

The effect of SFN on random cell migration was analysed in ARPE-19 and PANC-1 cells using 2, 10 and 15 µM SNF as well as untreated cells and DMSO for 48 hours. Cells were seeded in a 24-well plate (four wells per condition) for time-lapse imaging. The 24-well plates were coated with collagen I or fibronectin with a concentration 1 mg/ml before seeding PANC-1 or ARPE-19 cells. It has been suggested that collagen 1 is the ECM component suitable for PANC-1 cells (Wang et al., 2011), whereas fibronectin was examined in our lab and proved better for migration studies in ARPE-19. In ARPE-19 cells, images of representative regions for DMSO, 2 µM, 10 µM and SFN 15 µM SFN treated cells at t=0 illustrated the initial seeding densities for each condition (Figure 4.3 ai, bi, ci, and di). Similarly, DMSO, 2 µM, 10 µM and 15 µM SFN treated PANC-1 cells images showed representative regions at the initial seeding densities (t=0) (Figure 4.4 ai, bi, ci, and di). Separate areas for each condition were imaged live with frames taken every 10 minutes for a 16-hour period, beginning at the 32-hour SFN treatment.

For analysis, eight separate positions were examined for each condition with five cells from each area and total of 40 cells per condition being analysed. imageJ software was utilised to analyse cell movement by using the manual tracking module. To allow for the calculation of speed, the position of each analysed cell was recorded for each frame in the time course. Where a cell underwent mitosis, only one of the resultant daughter cells was followed for the rest of the time-lapse. Data for each cell position was combined in the imageJ to produce a line-tracking trace, showing the paths taken by every cell analysed. Examples of tracking images were illustrated for ARPE-19 cells treated with DMSO (Figure 4.3 aii, Movie S2),

2 SFN µM (Figure 4.3 bii, Movie S3), 10 µM SFN (Figure 4.3 cii, Movie S4) and 15 µM SFN (Figure 4.3 dii, Movie S5). Similarly, examples of tracking images were illustrated for PANC-1 cells treated with DMSO (Figure 4.4 aii, Movie S7), 2 SFN µM (Figure 4.4 bii, Movie S8), 10 µM SFN (Figure 4.4 cii, Movie S9) and 15 µM SFN (Figure 4.4 dii, Movie S10). The dots represent the position of a cell at a particular point in time, whereas the lines represent the path it took over previous frames. These combined tracking traces demonstrate the degree of a cell's movement from its original position, and show the direction of the cell movement, as coloured lines that represent migrating cell track.

It was possible to use the position results of cell tracking traces to calculate the total distance covered by an individual cell over the time course (16 hours), as well as an individual cell's average velocity. The average velocity result for each analysed cell was calculated and presented in a graph to illustrate an overall average velocity for each condition. Statistical analysis was performed by using a one-way ANOVA with Tukey's multiple comparison test. This analysis revealed that SFN treatment has a significant effect on average speed in ARPE-19 cells treated with SFN 10 and 15 µM compared to DMSO control cells (Figure 4.5, a). The average velocity of ARPE-19 cells for each condition showed that untreated cells moved at an average velocity of 0.6328 µm/min and DMSO treated cells with 0.5974 µm/min, while the average velocity for 10 and 15 µM SFN treated ARPE-19 cells were 0.4658 µm/min and 0.2280 µm/min respectively.

However, SFN treatment showed no significant decrease in PANC-1 average cell speed, with 10 and 15 µM SFN treated PANC-1 cells revealing average speeds of 0.5896 µm/min and 0.5807 µm/min respectively, compared to 0.6052 µm/min in DMSO treated cells (Figure 4.6, a).

Migration software was used to show the destination of individual cells during migration, based on the data from cell-tracking traces of migrating cells. Spider

graphs for ARPE-19 cells showed greater distance of migration in DMSO and 2 µM SFN treated cells, compared to treated cells with 10 and 15 µM SFN. At 10 and 15 µM of SFN, most of the cells were concentrated at the centre; this indicates a decrease in distance migrated. Results revealed that DMSO treated cells moved around 563 µm and 2 µM SFN treated cells moved around 526, while 10 µM and 15 µM SFN treated cells moved around 387 µm and 219 µm respectively (Figure 4.5, b).

In PANC-1 cells, spider graphs illustrated no significant difference in migrating cell distance, with most cells reaching around similar distance. Results showed that DMSO treated cells moved around 500 µm, while 2, 10 and 15 µM SFN treated PANC-1 cells moved around 524 µm, 598 µm and 591 µm respectively (Figure 4.5, b).

4.3.4 SFN treatment alters microtubule organisation and leads to the formation of distinct bundles

To investigate the effect of SFN on microtubule organisation, ARPE-19 and PANC-1 cells were seeded on coverslips, coated with collagen I, and treated with 2, 10 and 15 µM SFN and DMSO for 48 hours. Cells were immunolabelled for α-tubulin. DMSO treated ARPE-19 cells showed a classic radial array of microtubules focused in the centre of the cell and the plus-ends spread toward the cell periphery with few microtubule bundles, similar to untreated cells (Chapter III, figure 3.2). The 2 µM SFN treated cells revealed that microtubules were organised in a radial array with few microtubule bundles, and there were no noticeable changes in microtubule organisation compared to DMSO treated cells. The 10 and 15 µM SFN treated ARPE-19 cells showed more microtubule bundles compared to DMSO treated cells (Figure 4.7).

DMSO treated PANC-1 cells revealed microtubules focused in the centre of the cell with a disorganised network elongated towards the cell periphery. This organisation is typical in PANC-1 cells and was also observed in untreated cells (Chapter III, figure 3.3). The 2 and 10 µM SFN treated PANC-1 cells showed no changes in microtubule organisation. However, 15 µM SFN treated cells revealed some alterations in microtubule organisation with some cells containing straight and bundled microtubules, compared to DMSO treated cells (Figure 4.8).

4.3.5 Actin filaments co-aligned with microtubules in SFN treated ARPE-91 cells

Subconfluent cells were immunolabelled for β-actin or phalloidin to observe any changes in the actin filaments relating to the SFN treatment. DMSO treated ARPE-19 cells revealed actin located at the leading edge of the cell and forming lamellipodia with some stress fibres running parallel to long axis of in cell body (Figure 4.9, a and 4.10, a). No obvious changes were observed with 2 µM SFN (Figure 4.9, b and 4.10, b). The 10 µM SFN treated ARPE-19 cells revealed actin filaments co-aligned with microtubules (Figure 4.9, c,) while phalloidin staining showed an increase in stress fibres (Figure 4.10, c). The 15 µM SFN-treated cells revealed actin filaments were co-aligned with microtubules with dotted β-actin appearance that suggests of breakdown of some actin filaments (Figure 4.9, d). Phalloidin staining showed an increased in stress fibres with a decrease of cortical actin in 15 µM SFN treated ARPE-19 cells (Figure 4.10, d).

DMSO treated PANC-1 cells showed β-actin at the periphery with microspikes at the front edge. Stress fibres were observed along the cell body with filopodia and microspikes at the front of the leading edge (Figure 4.11, and 4.12, a). The 10 µM and 15 µM SFN treated PANC-1 cells revealed disorganised actin filaments with a

thin layer of actin at the periphery and some stress fibres in the cell body (Figure 4.11 and 4.12, c and d).

4.3.6 EB1 is expressed along the microtubule lattice in SFN treated ARPE-19 and PANC-1 cells

Cells were treated for 48 hours with DMSO or different concentrations of SFN and then immunolabelled for microtubules and EB1. DMSO treated ARPE-19 cells revealed that EB1 was expressed as classic comets at the microtubule plus-ends (Figure 4.13, a). The 2 µM SFN treated ARPE-19 cells showed EB1 comets at the plus-ends of microtubules, with no change in its localisation compared to DMSO treated cells (Figure 4.13, b). Interestingly, 10 and 15 µM SFN treated ARPE-19 cells revealed an extensive association between EB1 and microtubules lattice, although a distinct accumulation at the plus-end was also evident (Figure 4.13, c, d). Western blots were performed to determine the levels of EB1 expression in untreated, DMSO- and 2, 10 and 15 µM SFN treated ARPE-19 lysates. No change was observed in the levels of EB1 expression in SFN treated cells compared with DMSO treated cell (Figure 4.14, a).

The EB1 comet shape was analysed by measuring the circularity of EB1 accumulation at the plus-end, using ImageJ software for DMSO and 2 µM SFN treated ARPE-19 cells, as well for untreated ARPE-19, as EB1 appeared only at the microtubules plus-ends in these conditions. The results indicated there was no significant difference in comet circularity among all conditions (Figure 4.14, b). Fluorescence intensity analysis was utilised to quantify EB1 lattice association. The intensity of EB1 was measured along 2 µm segments at randomly selected regions along the lattice located away from the plus-end for cells treated with SFN 10 and 15 µM or DMSO. Analysis illustrated a significant increase in intensity along the microtubule lattice in 10 and 15 µM SFN treated ARPE-19 cells, compared to

DMSO treated cells. Significance was assessed by a one-way ANOVA with Tukey's multiple comparison (Figure 4.14, c).

Similarly, PANC-1 cells were immunolabelled for EB1 and α-tubulin. DMSO and 2 and 10 µM SFN treated PANC-1 cells revealed that EB1 was localised mainly as comets at the plus-ends of microtubules but with some association along the lattice around cell centre (Figure 4.15, a and b, and figure 4.16, a). The 15 µM SFN treated PANC-1cells revealed a distinct lattice association of EB1 in many microtubules (Figure 4.16, b). A western blot was performed to investigate the level of EB1 expression under these conditions: untreated, DMSO and 2, 10 and 15 µM SFN treated PANC-1 cells. Again no marked change was observed in the levels of EB1 expression in SFN treated cells compared to DMSO treated cells (Figure 4.17, a).

Furthermore, comet circularity analysis revealed that there was no difference in comet circularity between DMSO and 2 or 10 µM SFN treated PANC-1 cells (Figure 4.17, b). To analyse EB1 lattice association, fluorescence intensity was measured (as previously described) and a significant increase in EB1 intensity along the lattice was evident in 15 µM SFN treated PANC-1 cells (Figure 4.17, c).

EB3 localisation was checked and it was observed that EB3 is sporadically expressed in some PANC-1 cells and concentrated around the centrosome and at the plus-ends of microtubules or with little expression in other cells (data not shown). As expression of EB3 was sporadic, as previously reported for many epithelial cell types, EB3 was not investigated any further.

4.3.7 EB2 is localised along microtubules and is free in the cytoplasm in SFN treated ARPE-19 and PANC-1 cells

In pancreatic cancer cells, it was shown that EB2 is overexpressed in highly invasive cells (Abiatari et al., 2009). ARPE-19 and PANC-1 cells were seeded and treated with different concentrations of SFN or DMSO for 48 hours, immunolabelled for EB2 and α-tubulin and lysates were taken for western blotting. In untreated ARPE-19 and PANC-1 cells, EB2 was localised along the microtubule lattice with some at the plus-ends (Chapter III, Figures 3.13 and 3.14). DMSO-treated ARPE-19 cells showed a typical localisation of EB2 along the lattice with some at the plus-ends of microtubules; a similar observation was made in 2 µM SFN treated ARPE-19 cells (Figure 4.18, a and b). However, 10 and 15 µM SFN treated cells showed more cytoplasmic EB2 with less along the microtubule lattice and at the plus-ends (Figure 4.19, a and b). Western blots were performed to investigate the level of EB2 expression in 2, 10 and 15 µM SFN treated cells and also for untreated and DMSO treated ARPE-19 cells. Results illustrated a slight decrease in the upper band in 10 and 15 µM SFN treated cells compared to DMSO treated cells, but not compared to the untreated cells (Figure 4.21, a).

In PANC-1 cells, the DMSO treated cells showed EB2 was localised along the microtubules with some free EB2 in cell cytoplasm (Figure 4.20, a). However, 10 and 15 µM SFN treated cells revealed more cytoplasmic EB2, with some along the lattice (Figure 4.20, b & c). Western blot results showed no clear evidence of changes in EB2 expression levels in cells treated with 15 µM SFN compared to DMSO treated cells. Further investigations are needed to confirm these results (Figure 4.21, b).

4.3.8 HDAC6 is mainly localised in the cytoplasm in SFN-treated ARPE-19 and PANC-1 cells

HDAC6 is mainly localised in the cell cytoplasm. It has been reported to associate with microtubule plus-ends and functions as an α-tubulin deacetylase, which plays an important role in regulating microtubule dynamics and cell motility (Huo et al., 2011). Pancreatic cancer cells that overexpress HDAC6 may deacetylate microtubules, which promotes cell migration (Li et al., 2014). Importantly, it was shown that SFN inhibits HDAC6 activity in human breast cancer cells (Pledgie-Tracy et al., 2007). Therefore, the effect of SFN on HDAC6 was investigated in our study, in order to observe any impact on HDAC6 localisation. ARPE-19 and PANC-1 cells were seeded and treated with different concentrations of SFN for 48 hours. Both cell lines were immunolabelled for HDAC6 and α-tubulin and fluorescent images were taken using widefield fluorescence microscopy.

DMSO and 2 µM SFN treated ARPE-19 cells revealed HDAC6 localised in a diffuse puncta throughout the cytoplasm and around the nucleus and cell periphery, with some along the microtubule lattice (Figure 4.22, a and b). The 10 and 15 µM SFN treated ARPE-19 cells showed little evidence of HDAC6 along the microtubule lattice; also it showed diffused puncta in the cytoplasm and around the nucleus. The 15 µM SFN treated ARPE-19 cells showed also distinct puncta arrangement (Figure 4.23). Interestingly, filament like association is suggested by the higher dot-like appearance of HDAC6 in ARPE-19 cells treated with 15 µM SFN.

In PANC-1 cells, HDAC6 was found distributed diffusely with puncta around the nucleus and in the cytoplasm, and some lattice association and concentration at periphery in DMSO and 2 µM SFN treated cells (Figure 4.24). The 10 and 15 µM SFN treated PANC-1 cells revealed no association between HDAC6 and

microtubules, and there was also some noticeable accumulation at cell periphery (Figure 4.25).

4.3.9 Tubacin treatment has no effect on cell viability in ARPE-19 and PANC-1 cells

Tubacin a small molecule that binds to the deacetylate tubulin domain of HDAC6 and causes total tubulin acetylation is a specific functional inhibitor of HDAC6 activity (Haggarty et al., 2003). For example, inhibition of HDAC6 with tubacin in human breast cancer cells causes tubulin acetylation and reduces cell movement (Saji et al., 2005). SFN had no noticeable effects on ARPE-19 and PANC-1 cells (Figure 4.20). A combination of two treatments for cancer prevention and therapy has been used in several *in vitro* and *in vivo* cell lines. Each agent may have its own unique targets, but they also share some common targets. Therefore, SFN used in combination with tubacin may provide an advantage over treatment with a single agent only, in terms of therapeutic efficacy.

The effect of tubacin on cell viability was examined using an MTT assay. ARPE-19 and PANC-1 cell lines were seeded in a 96-well plate in triplicate for each condition and incubated overnight (as described in section 4.3.2). Both cell lines were treated with 10 µM tubacin for 48 hours; cells were also treated with combinations of 10 µM tubacin and 10 µM SFN, and 10 µM tubacin with 15 µM SFN, and incubated for 48 hours. The results of the MTT assays showed that there were no significant effects on cell viability (Figure 4.26).

4.3.10 Inhibition of HDAC6 with tubacin causes cell spreading in ARPE-19 and PANC-1 cells

SFN treatment resulted in increased cell area in ARPE-19 and PANC-1. This was statistically confirmed and is illustrated in figure 4.2. Observations on both cell lines showed that there were changes in cell morphology relating to the 10 µM tubacin treatment as well as the combination of SFN (10 and 15 µM) and 10 µM tubacin for 48 hours. 10 µM and 15 µM SFN alone also caused an increase in cell area, as previously illustrated (Figure 4.2). Fluorescent images were used to analyse the effects of tubacin and the combination of tubacin and SFN on cell area. Analysis of the cell area demonstrated that 10 µM tubacin treated ARPE-19 cells showed a significant increase in average cell area compared to DMSO treated cells. Similarly, cells treated with a combination of 10 µM tubacin and 10 µM SFN showed a significant increase in cell area; this was also the case for a combination of 10 µM tubacin and 15 µM SFN (Figure 4.27, a). ImageJ software was used to analyse cell area for 65 cells per condition.

The 10 µM tubacin treated PANC-1 cells revealed a significant increase in cell area, compared to DMSO treated cells. Moreover, the combinations of 10 µM tubacin and 10 µM SFN or 15 µM SFN treated PANC-1 cells revealed a significant increase in cell area in both conditions compared to DMSO treated cells, which seems to be as a result of tubacin treatment with no further increase with the two treatments (Figure 4.27, b). So both separate SFN and tubacin or combined treatments resulted in significant increases in cell area.

4.3.11 Tubacin induces a marked increase in acetylated microtubules in ARPE-19 and PANC-1 cells

The tubacin inhibitor was used to examine whether inhibition of HDAC6 increases the level of tubulin acetylation in the experimental cell lines, ARPE-19 and PANC-1. Both cell lines were treated with 10 µM tubacin as well as with combinations of 10 µM tubacin and 10 µM SFN or 10 µM tubacin and 15 µM SFN, and incubated for 48 hours. Subsequently, they were stained for acetylated tubulin and α-tubulin (total tubulin). In ARPE-91 cells, DMSO treatment showed only that some microtubule segments in the central part of the cell were acetylated, whereas microtubules at the cell periphery lacked acetylated tubulin (Figure 4.28, a); this was also evident in untreated cells (Section 3.3.2, Figure 3.4). In contrast, all microtubules in the 10 µM tubacin treated ARPE-19 cells appeared to be acetylated (Figure 4.28, b). In 10 µM SFN treated ARPE-19 cells acetylated microtubules were concentrated at the central part of the cells except for a few segments near the cell periphery. Similarly, 15 µM SFN treated ARPE-19 cells showed acetylated microtubules in the central part around the nucleus but with several elongated acetylated microtubules reaching the periphery (Figure 4.28, c, d). a combination of 10 µM tubacin and 10 µM SFN or 15 µM SFN showed extensive acetylation of microtubules throughout the cells (Figure 4.28, e, and f). Western blots of ARPE-19 cell lysates revealed that 10 µM tubacin and combinations of 10 µM tubacin and 10 µM SFN or 15 µM SFN caused a marked increase in acetylation. In addition, The SFN treatment alone showed a slight increase in acetylated α-tubulin level compared to DMSO treatment (Figure 4.30).

DMSO treated PANC-1 cells showed some acetylated microtubule segments in the central part of the cell, with a few acetylated microtubules at the cell periphery (Figure 4.29, a); this was also evident in the untreated cells (Figure 3.5). 10 µM tubacin treated PANC-1 cells revealed very extensive microtubule acetylation

throughout the cells (Figure 4.29, b). 10 µM SFN treated PANC-1 cells showed acetylated microtubules in the central part of the cell with some acetylated microtubules extending towards the cell periphery. The 15 µM SFN treated cells showed acetylated microtubules again concentrated around the central part, but with more acetylated microtubules extending towards the periphery (Figure 4.29, c, d). Combined treatments of 10 µM tubacin and 10 µM or 15 µM SFN revealed extensive acetylated microtubules throughout the cells with some bundle formation (Figure 4.29, e, f). Western blots of 10 µM tubacin treated PANC-1 cells showed a significant increase in the levels of acetylated tubulin, as well as in combination of 10 or 15 µM SFN- and 10 µM tubacin treated PANC-1 cells. However, 10 and 15 µM SFN treated PANC-1 cells showed no appreciable changes on acetylated tubulin levels compared to the DMSO treated cells (Figure 4.30).

4.3.12 A combination of tubacin and SFN causes a significant reduction in cell migration speed

The results of the SFN effect on cell migration demonstrated that 10 and 15 µM SFN treatment dramatically reduced the speed of migratory ARPE-19 cells, while no significant reduction was observed in PANC-1 cells (Figure 4.6). Since HDAC6 is highly expressed in pancreatic cancer cells and promotes migration (Li et al., 2014), a combined effect of HDAC6 inhibitor and SFN treatment may affect microtubule dynamics, and as a result, cell migration. Inhibition of HDAC6 activity by tubacin was reported to affect cell migration on cancer cells (Tran et al., 2007). The effect of a combination of tubacin and SFN on cell migration was therefore analysed in ARPE-19 and PANC-1 cells. In the first series of experiments, ARPE-19 and PANC-1 cells were seeded in a 24-well plate and treated with 10 µM tubacin, 10 or 15 µM SFN, and a combination of 10 µM tubacin and 10 µM SFN or 15 µM SFN for 48 hours. Cells were imaged at a rate of one frame every 10

minutes for 16 hours and 10 cells were analysed from 9 separate positions, to give a total of 90 cells for each condition (N=90). Cells were tracked in ImageJ, as described before (Section 4.3.3); again, when cells underwent mitosis, just one of the daughter cells was tracked to the end of the time-lapse.

The position data for each cell was utilised to calculate its average speed of cell movement. Statistically, a one-way ANOVA with Tukey's multiple comparison test was used to analyse the data. In ARPE-19 cells, it was found that tubacin treatment dramatically decreased the cell movement compared to DMSO treated cells (Figure 4.31, a, Movie S11). This was also the case for combinations of 10 and 15 µM SFN and 10 µM tubacin (Figure 4.31, a, Movie S12 and S13). However, 10 µM tubacin treated PANC-1 cells revealed no marked decrease in cell speed, also a combination of 10 µM tubacin and 10 µM SFN showed no reduction in cell speed compared to DMSO treated cells (Figure 4.31, b, Movie S14 and S15). Importantly, 10 µM tubacin and 15 µM SFN treated PANC-1 cells revealed a significant reduction in cell speed compared to DMSO treated cells (Figure 4.31, b, Movie S16).

4.3.13 Treatment with tubacin on its own has no effect on EB1 localisation and expression in ARPE-19 and PANC-1 cells

Our results showed that SFN treatment affects EB1 localisation in ARPE-19 and PANC-1 cells. EB1 appeared to associate with the microtubule lattice in 10 and 15 µM SFN treated ARPE-19 and PANC-1 cells (Figure 4.13 & 4.15). According to Zilberman et al. (2009), inhibition of HDAC6 deacetylase activity by tubacin affects EB1 appearance at the microtubule ends, with the comet tail appearing significantly shorter. We next tested whether tubacin and a combination of SFN

and tubacin could affect the localisation of EB1 at microtubule tips. ARPE-19 and PANC-1 cells were seeded on coverslips and treated with 10 µM tubacin or a combination of 10 µM tubacin and 10 µM SFN or 15 µM SFN for 48 hours. Cells were then labelled for EB1 and α-tubulin. 10 µM tubacin treated ARPE-19 cells revealed classic comets of EB1 at the plus-ends of the microtubules, similar to DMSO-treated cells (Figure 4.32, a and b). A combination of 10 µM tubacin and 10 µM SFN or 15 µM SFN treated ARPE-19 cells showed extensive association of EB1 with the microtubule lattice as also found for 15 µM SFN alone (Figure 4.32 c and d). Interestingly, there appeared to be a reduction in plus-end comets in combined treatments of tubacin and SFN. The western blot of cell lysates revealed that 10 µM tubacin treated ARPE-1 cells showed no change in EB1 level compared to DMSO treated cells. This was also the case for a combination of 10 µM tubacin and 10 µM SFN or 15 µM SFN treated ARPE-19 cells, which showed no effect on EB1 expression (Figure 4.33, a).

EB1 comet circularity was investigated by using ImageJ software. The results revealed no significant difference in comet circularity in 10 µM tubacin treated ARPE-19 cells compared to DMSO treated cells (Figure 4.33, b). Two-tail unpaired t-tests were used to compare the statistical significance of differences between the two groups. Fluorescence intensity analysis was utilised to quantify EB1 lattice association. This intensity of EB1 was measured along random selected microtubules (as described in section 4.3.6). Results revealed a significant increase in EB1 association along the microtubules in 10 µM tunacin and 15 µM SFN treated ARPE-19 cells, but not with 10 µM tubacin and 10 µM SFN, as compared to DMSO treated cells. This was assessed by one-way ANOVA with Tukey's multiple comparison (Figure 4.33, c).

The 10 µM tubacin treated PANC-1 cells showed that EB1 appeared as comets at the plus-ends of microtubules, similar to DMSO treated cells (Figure 4.34, a, b). No difference in EB1 comets was observed in 10 µM tubacin and 10 µM SFN

treated PANC-1 cells compared to DMSO treated cells, where EB1 was observed as comets at the plus-ends (Figure 4.34, c). However, a combination of 10 µM tubacin and 15 µM SFN treated PANC-1 cells caused a marked association between EB1 and microtubules lattice (Figure 4.34, d), similar to what was observed with 15 µM SFN treated PANC-1 cells (Figure 4.16). Western blots revealed that 10 µM tubacin treated PANC-1 cells showed no change in EB1 level compared to DMSO treated cells; this was the same with the combination of 10 µM tubacin and 10 µM SFN or 15 µM SFN treated PANC-1 cells (Figure 4.35, a).

Analyses of the EB1 comet circularity in 10 µM tubacin and combination of 10 µM tubacin and 10 µM SFN treated PANC-1 cells revealed no difference in comet shape compared to DMSO treated cells (Figure 4.35, b). The results were assessed by one-way ANOVA with Tukey's multiple comparison. EB1 lattice association was analysed by quantifying the fluorescence intensity. A combination of 10 µM tubacin and 15 µM SFN treated PANC-1 cells showed a significant increase in EB1 lattice intensity, compared to DMSO treated cells (Figure 4.25, c). Two-tail unpaired t-tests were used to compare the statistical significance of differences between the two groups.

4.3.14 Tubacin only treatment has no effect on EB2 localisation and expression in ARPE-19 and PANC-1 cells

SFN treatment affected EB2 expression and localisation in ARPE-19 and PANC-1 cells, with more cytoplasmic EB2 evident in SFN treated cells (Figures 4.19 and 20). Published data have shown that HDAC6 and EB2 are overexpressed in these PANC-1 cells (Abiatari et al., 2009, Li et al., 2014). Experiments were therefore performed to assess whether inhibition of HDAC6 by tubacin affects EB2 expression and localisation on microtubules in ARPE-19 and PANC-1 cells. Both

cell lines were seeded and treated with 10 µM tubacin or with a combination of 10 µM tubacin and 10 µM SFN or 15 µM SFN for 48 hours. Cells were immunolabelled for EB2 and α-tubulin and lysates were taken for western blotting. 10 µM tubacin treated ARPE-19 cells showed EB2 along the microtubule lattice and at plus-ends, with some free EB2 in the cytoplasm, similar to DMSO treated cells (Figure 36 a and b). The combination of 10 µM tubacin and 10 µM SFN or 15 µM SFN treated ARPE-19 cells revealed more EB2 in the cytoplasm, with just a few along the microtubule lattice (Figure 4.36, c and d).

The 10 µM tubacin treated PANC-1 cells revealed EB2 along the lattice and at the plus-ends of microtubules, with some in the cytoplasm similar to results observed in DMSO treated cells (Figure 4.37, a and b). The 10 µM tubacin and 10 µM SFN or 15 µM SFN treated PANC-1 cells revealed EB2 localised in the cytoplasm with some along the microtubule lattice (Figure 4.37, c and d). Western blots showed no changes in the levels of EB2 in all conditions (Figure 4.38).

4.3.15 Tubacin treatment does not lead to co-localisation of HDAC6 and microtubules

It has been reported that inhibition of HDAC6 increases the association between microtubules and HDAC6, which enhances microtubule stability. It has been suggested that this effect on microtubule dynamics is due to the association between microtubules and HDAC6, rather than the increase in acetylation of microtubules (Asthana et al., 2013). Experiments were therefore conducted to assess whether tubacin could affect HDAC6 association with microtubules in ARPE-19 and PANC-1 cells. Cells were seeded on coverslips, then treated with 10 µM tubacin or with a combination of 10 µM tubacin with 10 µM SFN or 15 µM SFN and incubated for 48 hours. Cells were immunolabelled against HDAC6 and

α-tubulin. DMSO treated cells revealed HDAC6 free in the cytoplasm and around the nucleus, with some along the microtubule lattice (Figure 4.39, a). The 10 µM tubacin treated ARPE-19 cells revealed no association between HDAC6 and the microtubule lattice, where HDAC6 was arranged in filament-like structure in the cytoplasm and around the nucleus (Figure 4.39, b). The combination of 10 µM tubacin and 10 µM SFN or 15 µM SFN treated ARPE-19 cells revealed HDAC6 arranged in filaments-like in the cytoplasm and around the nucleus, with some free in the cytoplasm (Figure 4.40, a and c). Again no evidence of co-localisation with microtubules. Similar results were observed in the 10 µM and 15 µM SFN treated cells (Figure 4.23).

DMSO treated PANC-1 cells showed HDAC6 diffuse in the cytoplasm and around the nucleus with no co-alignment between HDAC6 and microtubules (Figure 4.41, a). The 10 µM tubacin treated PANC-1 cells showed no clear association between HDAC6 and the microtubules lattice, but HDAC6 was appeared in filaments alignment in the cytoplasm and around the cell nucleus (Figure 4.41, b). The combinations of 10 µM tubacin and 10 µM SFN or 15 µM SFN treated PANC-1 cells revealed HDAC6 was mainly arranged in filament-like in the cytoplasm, with some concentrated around the nucleus and cell periphery, and there was no co-alignment between HDAC6 and microtubules lattice (Figure 4.42, a and b).

The filament-like organisation of HDAC6 observed in tubacin and tubacin and SFN treated cells will need further investigation to determing whether HDAC6 is co-localising with actin or intermediumte filaments.

Table 5: Chapter IV summary.

Experiments	Results
MTT assay (Cell viability)	• ≥ 30 µM SFN affects cell viability in ARPE-19 and PANC-1 cells
Morphological changes	• Increase in cell area with 10 and 15 µM SFN both cell lines
Cell migration (Speed and distance)	• 10 and 15 µM SFN cause decrease in migration speed in ARPE-19 cells but no effect in PANC-1 cells. • SFN reduced distance in ARPE-19 cells and most of treated PANC-1 cells also showed reduced distance.
SFN and microtubule organisation	• Increased microtubule bundles in ARPE-19 cells with 10 and 15 µM SFN. • Distinct bundles in PANC-1 cells with 15 µM SFN.
SFN and actin	ARPE-19: • Microtubule and actin co-alignment. • Loss of cortical actin with 15 µM SFN. PANC-1: • Stress fibres in centre increase and dorsal and fibres evident with 15 µM SFN and decrease in microspikes.
	ARPE-19: • EB1 lattice association with 10 and 15 µM SFN. • No change in comet circularity.

SFN and EB1	• Significant increase in fluorescence intensity along lattice. PANC-1: • Lattice evident in centre of cell in DMSO but also in periphery areas with 15 µM SFN. • No change in comet circularity. • Significant increase in fluorescent intensity along lattice with 15 µM SFN.
SFN and EB2	ARPE-19: • EB2 lattice association in DMSO and 2 µM SFN. • Cytoplasmic with 15 µM SFN. PANC-1: • Lattice association in DMSO. • Cytoplasmic with 15 µM SFN.
SFN and HDAC6	ARPE-19: • Some along microtubule lattice and in cytoplasm in DMSO and 2 µM SFN. • Cytoplasmic filament-like with 10 and 15 µM SFN. PANC-1: • Some along microtubule lattice and in cytoplasm and at cell membrane in control and 2 µM SFN. • Diffuse throughout cytoplasm with 10 and 15 µM SFN.
Tubacin and viability	• 10 µM tubacin (T) and 10 µM T + 10 or 15 µM SFN had no significant effect on cell viability.

Tubacin / T+SFN and cell area	• Significant increase in cell area in both cell lines.
Tubacin / T + SFN and acetylated tubulin	• Both immunolabelling and Western blots revealed marked increase in tubulin acetylation in both cell lines with 10 µM T and with 10 µM T + 10 or 15 µM SFN.
Tubacin / T + SFN and cell migration	ARPE-19: • Significant decrease in cell migration speeds for all conditions. PANC-1: • Only significant reduction in migration speed with 10 µM T + 15 µM SFN.
Tubacin / T + SFN and EB1	• No effect on EB1 localisation in both cell lines with tubacin alone. • T + 10 or 15 µM SFN shows extensive EB1 lattice association, confirmed by significant increase in fluorescence intensity in ARPE-19 and PANC-1. • No change in comet shape.
Tubacin / T + SFN and EB2	• Tubacin alone has no effect on EB2 localisation, but T + SFN T + SFN increases cytoplasmic EB2 in both cell lines.

Tubacin / T + SFN and HDAC6	• DMSO showed HDAC6 along microtubules and in cytoplasm. • Tubacin induced cytoplasmic HDAC6 to form filament-like structures that did not co-localise with microtubules. This more prominent with T + SFN.

4.4 Discussion

4.4.1 SFN caused an increase in cell area in ARPE-19 and PANC-1 cells

Our data revealed that ARPE-19 and PANC-1 cells treated with 30 µM SFN for 48 hours dramatically affected cell viability and caused cell death. The 10 and 15 µM SFN treated ARPE-19 and PANC-1 cells showed no significant effects on cell viability when treated for 48 hours. It is vital to determine the cytotoxic concentrations of SFN treatment that affect the viability of the cell lines. It has been previously found that the viability of breast cancer cells *in vitro* has been decreased by treating them with 25 µM SFN and incubating them for 48 hours (Jackson et al., 2007). Additionally, cell viability in human cancer colon cells was reduced by treatment with 15 µM SFN, but after incubation for 96 hours (Gamet-Payrastre et al., 2000).

However, SFN treated ARPE-19 and PANC-1 cells showed a significant increase in cell area. Fluorescent images were used to analyse cell area and results revealed a significant increase in cell area of 10 and 15 µM SFN treated AREP-19 and PANC-1 cells. Our results are compatible with other research, where an increase in cell area and decrease in cell migration with inhibition of HDAC6 by tubacin has been reported (Tran et al., 2007). These changes in cell area following SFN treatment suggest that SFN may have an effect on cell adhesion and possibly also cell proliferation, which could lead to affect on cell migration. Cell migration requires dynamic microtubules and dynamic focal adhesion (Kaverina et al., 2002), so any disturbance in focal adhesions dynamics causes an increase in their area which may lead to increase cell area and inhibits cell migration (Lauffenburger and Horwitz, 1996, Rodriguez et al., 2003).

4.4.2 SFN caused a dramatic decrease in ARPE-19 cell migration

Cell migration was studied for SFN treated ARPE-19 and PANC-1 cells. Experiments were performed to examine random cell migration for SFN treated ARPE-19 and PANC-1 cells. The 10 µM and 15 µM SFN treated ARPE-19 cells revealed a significant reduction in the speed of migrating cells. This is likely due to the observed alteration of microtubules, actin organisation and EB1 localisation caused by SFN treatment (see section 4.4.3). Moreover, this effect on migration speed may result from a change in the balance between dynamic and stable microtubules. This is related not only to changes in tubulin acetylation and sensitivity to cold treatment but also in changes to EB1 and EB2 microtubule localisation. EB1 was extensively associated with the microtubule lattice, with more cytoplasmic EB2 in SFN treated ARPE-19 cells. However, the 10 µM and 15 µM SFN treated PANC-1 cells showed no decrease in the speed of cell migration. This unexpected result may be due to EB2 being highly expressed in PANC-1 cells, which affects microtubule dynamics and leads to increased cell migration. It has been suggested that EB2 enhances microtubule dynamics and induces invasion in PANC-1 cells (Abiatari et al., 2009, Goldspink et al., 2013). Moreover, it has been reported that HDAC6 is overexpressed in pancreatic cancerous cells, where it leads to complete deacetylation of microtubules, regulates the microtubule dynamics and influences cell migration (Zhang et al., 2003, Huo et al., 2011, Li et al., 2011, Li et al., 2014, Yu et al., 2015). HDAC6 can also associate with end-binding proteins such as EB1 and HDAC6 has been reported to interact with EB1 at the plus-end of microtubules to regulate their dynamics and influence cell migration (Li et al., 2011). All these together suggest that the overexpression of EB2 and HDAC6 in PANC-1 cells may prevent SFN from causing a reduction in migration of PANC-1 cells.

4.4.3 SFN altered microtubule and actin organisation and resulted in EB1 decorating the microtubule lattice while EB2 became cytoplasmic

SFN treated ARPE-19 and PANC-1 cells revealed a marked increase in the cell area. However, only SFN treated ARPE-19 cells showed a decrease in cell migration. Our results showed that the microtubules appeared straighter and frequently formed bundles in 10 µM and 15 µM SFN treated ARPE-19 cells. Bundles of microtubules could also be observed in 15 µM SFN treated PANC-1 cells. Further work has revealed that actin filaments and microtubules co-aligned in SFN treated ARPE-19 cells, where actin filaments co-aligned with microtubule bundles. However, this was not the case for SFN treated PANC-1 cells.

To the best of our knowledge, co-alignment between microtubules and actin filaments has not been previously reported as a result in SFN treated cells. Co-alignment between actin filaments and microtubules was reported in EB2 depleted cells where EB1 and ACF7 association along the microtubules lattice enable links to actin filaments (Goldspink et al., 2013). Our results suggested a slight reduction in EB2 level in SFN treated ARPE-19 cells but not in PANC-1 cells, where it seems that there is an increase in EB2 expression with 15µm SFN. Further analysis will be needed to confirm these results and possibly using a different loading control as SFN may affect actin. In addition, EB2 localisation was affected in SFN treated cells. Control ARPE-19 cells showed EB2 localisation in patches along the microtubule lattice and at the plus-ends, as previously described (Komarova et al., 2009). EB2 localisation along the microtubule lattice was affected in ARPE-19 SFN treated cells, with EB2 found mainly diffuse in the cytoplasm and some along the lattice. SFN treated PANC-1 cells seemed to show even more diffuse EB2 in the cytoplasm. In a recent publication, it was observed that phosphorylation of EB2 can lead to EB2 disassociation from microtubules and release into the cytoplasm

(Iimori et al., 2016). This suggests that SFN may induce EB2 phosphorylation and this needs to be investigated further.

EB1 was also relocated from its classic comets at the plus-ends of microtubules to associate extensively with the microtubule lattice in SFN treated ARPE-19 and PANC-1 cells. This association of EB1 along the microtubule lattice was examined by fluorescence intensity analysis and showed a significance association along microtubules in 10 µM and 15 µM SFN treated ARPE-19 cells and with 15 µM SFN treated PANC-1 cells. However, no change was found in the level of EB1 expression, as suggested by Western blots results. It has been suggested that EB1 lattice binding enforces the lateral microtubule protofilament and enhances microtubule stability and bundle formation (Sandblad et al., 2006, des Georges et al., 2008, Vitre et al., 2008, Zhang et al., 2009). EB1 lattice binding requires this stabilisation of microtubules to facilitate its lattice binding; this was observed in stable microtubules by Taxol (Jordan et al., 1991, Jordan and Wilson, 2004). Increased GTP-tubulin along the microtubule lattice could also facilitate the EB1 binding lattice; in addition, the reduction of repulsive forces may contribute to this association (Dimitrov et al., 2008, Nakata et al., 2011, Buey et al., 2011). Thus, EB1 association along the microtubule lattice may increase the stability of microtubules, which could lead to reduction in cell migration.

The results revealed that there is a different response to SFN treatment between ARPE-19 and PANC-1 cells. SFN treated ARPE-19 showed a significant decrease in cell migration along with marked alternation in microtubules and actin filaments organisation. Microtubule bundles co-aligned with actin filaments were observed in SFN treated ARPE-19 cells. However, SFN treated PANC-1 cell showed no effect on migration or a co-alignment between actin filaments and microtubules; however, some microtubules formed bundles in 15 µM SFN treated cells. EB1 was extensively associated with microtubules in SFN treated ARPE-19 and PANC-1 cells. More cytoplasmic EB2 could be observed in SFN treated cells. This suggests

that SFN may phosphorylate EB2 and affect its localisation on microtubules (Iimori et al., 2016). SFN treated ARPE-19 cells showed a slight reduction in EB2 level, but SFN treated PANC-1cells did not show the same reduction in EB2 level. This suggests that these differences may occur because PANC-1 cells have highly expressed EB2 and HDAC6; this may prevent SFN effects on microtubule organisation, and may end with no marked effects on microtubule dynamics and stability and thus migration.

4.4.4 SFN treatment caused loss of HDAC6 localisation along microtubule lattices in ARPE-19 and PANC-1 cells

SFN has been shown to inhibit HDACs in a variety of cell types. Our study examined whether the localisation of HDAC6 was affected with treatment of SFN in ARPE-19 and PANC-1. It has been reported that SFN inhibits global HDAC activity in treated breast cancer cells (Pledgie-Tracy et al., 2007). Furthermore, it has been shown that inhibition of HDAC6 activity in human breast cancer cells by tubastatin A caused a co-localisation between HDAC6 and microtubules (Asthana et al., 2013). However, our study revealed loss of HDAC6 association along microtubules. Distinct filament-like puncta of HDAC6 were evident with 10 and 15 µM SFN in ARPE-19 cells. These puncta did not co-localise with microtubules.

4.4.5 Combination treatments of tubacin and SFN inhibited PANC-1 cell migration

A combination of two agents for cancer prevention and therapy has been used in various *in vitro* and *in vivo* cell lines. Each agent may have its own unique targets,

but also share some common targets. Therefore, sulforaphane and tubacin (a specific HDAC6 activity inhibitor) were used as a combination treatment in our study. This combination may enable suppression of cell migration and improve therapeutic efficacy. HDAC6 has been reported to be a microtubule-associated protein that deacetylates α-tubulin and regulates microtubule dynamics. It can associate with the plus-end of microtubules and form a cap, which facilitates the interaction with EB1 and Arp1 (Hubbert et al., 2002, Matsuyama et al., 2002, Zhang et al., 2003, Huo et al., 2011, Zilberman et al., 2009). Importantly, HDAC6 has been reported to be overexpressed in cancerous cells, such as ovarian cancer cells, prostate cancer cells and pancreatic cancer cells. Overexpression of HDAC6 causes complete deacetylation of microtubules and resulted in increased cell migration in cancer cells (Hubbert et al., 2002, Yang and Seto, 2008, Huo et al., 2011, Li et al., 2014).

We achieved one of our research aims, to decrease the speed of migration in PANC-1 cells by treating them with a combination of 15 µM SFN and 10 µM tubacin. In our experiments, we started by examining whether 10 µM tubacin alone can affect the speed of ARPE-19 migration. Data showed that tubacin significantly increased cell area and significantly decreased the speed of cell movement in ARPE-19. Moreover, 10 µM tubacin caused increased acetylation of microtubules with some bundle formation in ARPE-19 cells. This was also shown by Western blotting, with a high increase in acetylation tubulin in 10 µM tubacin treated ARPE-19 cells. Our results are compatible with other research, where an increase in cell area with inhibition of HDAC6 by tubacin has been reported (Tran et al., 2007). Furthermore, the total acetylation of microtubules was previously reported as a result of inhibition of HDAC6 activity by tubacin with different cells (Haggarty et al., 2003, Saji et al., 2005, Tran et al., 2007, Zilberman et al., 2009, Li et al., 2011, Asthana et al., 2013), along with a reduction in cell movement (Saji et al., 2005). However, while 10 µM tubacin treated PANC-1 cells did not show a marked decrease on cell

migration, there was an increase in acetylated microtubules without noticeable bundle formation. A combination of 10 µM tubacin and 10 µM SFN or 15µM SFN showed a significant decrease in the speed of cell migration in ARPE-19 cells (Figure 4.31), as also seen with SFN treatment alone. Importantly, 10 µM tubacin and 15 µM SFN treated PANC-1 cells revealed a dramatic reduction in the speed of cell migration, with a significant increase in cell area and increase in acetylated tubulin along with some bundle formation. It seems that this inhibition in cell migration may be due to the effect of SFN on EB1 and EB2 localisation, with EB1 associating along the microtubule lattice and EB2 appearing to have detached from the microtubules. SFN may lead to the phosphorylation of EB2 and this would cause loss of association between EB2 and microtubules. In addition, microtubules contribute to the delivery of essential adhesion turnover proteins such as MAP4K4 and HAX1 which are both interactors of EB2. Therefore, losing EB2 from microtubules may affect focal adhesion turnover ending with an increase in cell adhesion and thus cell area and consequently inhibiting cell migration. However, EB2 is overexpressed in PANC-1 cells so this may prevent SFN effect and some EB2 may remain associated with microtubules enabling delivery of MAP4K4 and HAX1 to focal adhesions and initiate disassembly. Tubacin inhibits HDAC6 activity that regulates microtubule dynamics and increases acetylated microtubules. A combination of SFN and tubacin is therefore likely to work together counteracting the effect of high EB2 and HDAC6 expression leading to suppression of cell migration in PANC-1 cells.

The 10 µM tubacin treated ARPE-19 and PANC-1 cells revealed EB1 as classic comets at the plus-end of the microtubules, with no difference in comet area. However, it has been reported that inhibition of HDAC6 can affect EB1 association with the microtubule plus-ends (Zilberman et al., 2009). A combination of 10 µM tubacin and 10 µM SFN or 15 µM SFN treated ARPE-19 cells revealed EB1 association along the microtubule lattice, and statistical analysis showed a

significant association between EB1 and the microtubule lattice. A significant association between EB1 and microtubules was observed in SFN alone in ARPE-19 cells. Meanwhile, a combination of 10 µM tubacin and 15 µM SFN treated PANC-1 cells showed an association between EB1 and the microtubule lattice, similar to 15 µM SFN treated PANC-1 cells. Thus, it seems that this effect on EB1 localisation is due to SFN rather than inhibition of HDAC6 activity by tubacin. EB1 binding along the microtubule lattice has been noticed previously by Goldspink et al. (2013) who suggested it is related to an increase in microtubule stability and bundling formation. It was also observed in cells depleted of EB2.

Tubacin alone or a combination of tubacin and SFN-treated ARPE-19 and PANC-1 cells revealed more free EB2 in the cell cytoplasm with some along the microtubule lattice. However, western blots showed no decrease in EB2 level in tubacin or the combination of tubacin and SFN treated PANC-1 cells. Loss of EB2 microtubule association suggests that SFN may phosphorylate EB2 and lead to EB2 dispersed in the cytoplasm rather than remain localised along the microtubule lattices. This will then enable EB1 to decorate the length of the microtubules, as noticed in SFN treated ARPE-19 and PANC-1 cells. It has been reported that phosphorylated EB2 reduces its affinity for microtubules and leads to EB2 detachment from microtubules (Iimori et al., 2016).

In addition, 10 µM tubacin and a combination of 10 µM tubacin and 10 µM or 15 µM SFN treated ARPE-19 and PANC-1 cells showed no co-localisation between HDAC6 and microtubules, but there was an observation of filament-like organisation in tubacin and tubacin and SFN treated cells. The filament-like organisation of HDAC6 observed in tubacin and tubacin and SFN treated cells will need further investigation to determent whether HDAC6 is co-localising with actin of intermediumte filaments. A different observation was made in TAS and tubastatin A (HDAC6 inhibitor) treated human breast cancer cells, where HDAC6 co-aligned with microtubules with suppressed dynamic instability and delayed the

depolymerisation of the microtubules (Asthana et al., 2013). Inhibition of HDAC6 increases the level of acetylated microtubules along with the effect of SFN and tubacin on EB2 and EB1 localisation and expression, where it was associated along microtubules with more free EB2 in the cytoplasm. This seems due to phosphorylation or depletion of EB2 as a result of SFN. All these together may play an important role in inhibiting microtubule dynamics or becoming more stable, and dramatically decreasing cell migration.

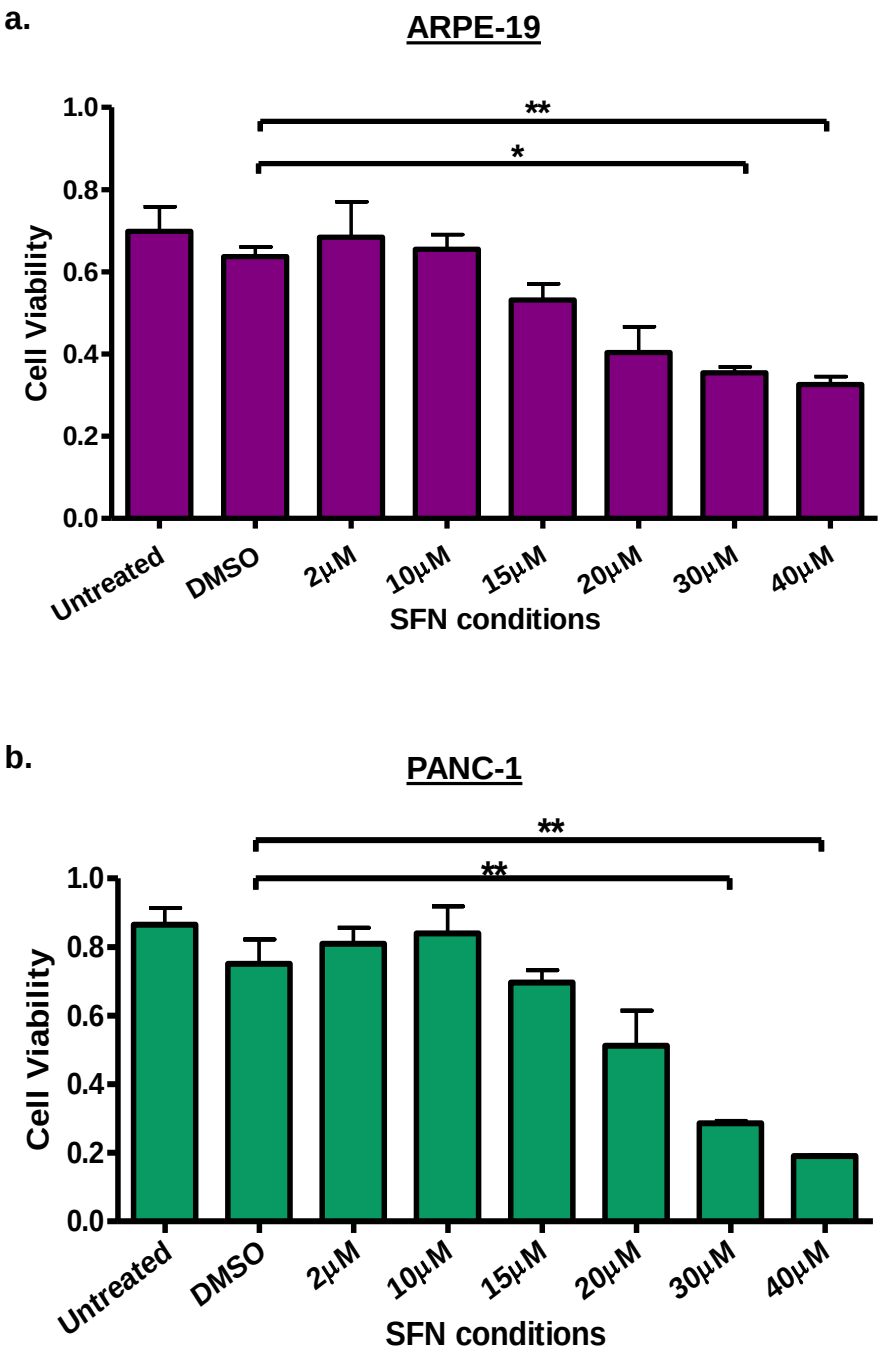

Figure 4.1 SFN ≥ 30μM decreases cell viability in ARPE-19 and PANC-1 cells

Cell viability was examined with a MTT assay, which is based on the reduction of yellow tetrazole to purple formazan in living cells. The results illustrate that 30 and 40μM SFN significantly decreased ARPE-91 and PANC-1 cell viability. Statistical analysis was compared to DMSO using one-way ANOVA with Tukey multiple comparison test, [*P<0.01 & **P<0.001].

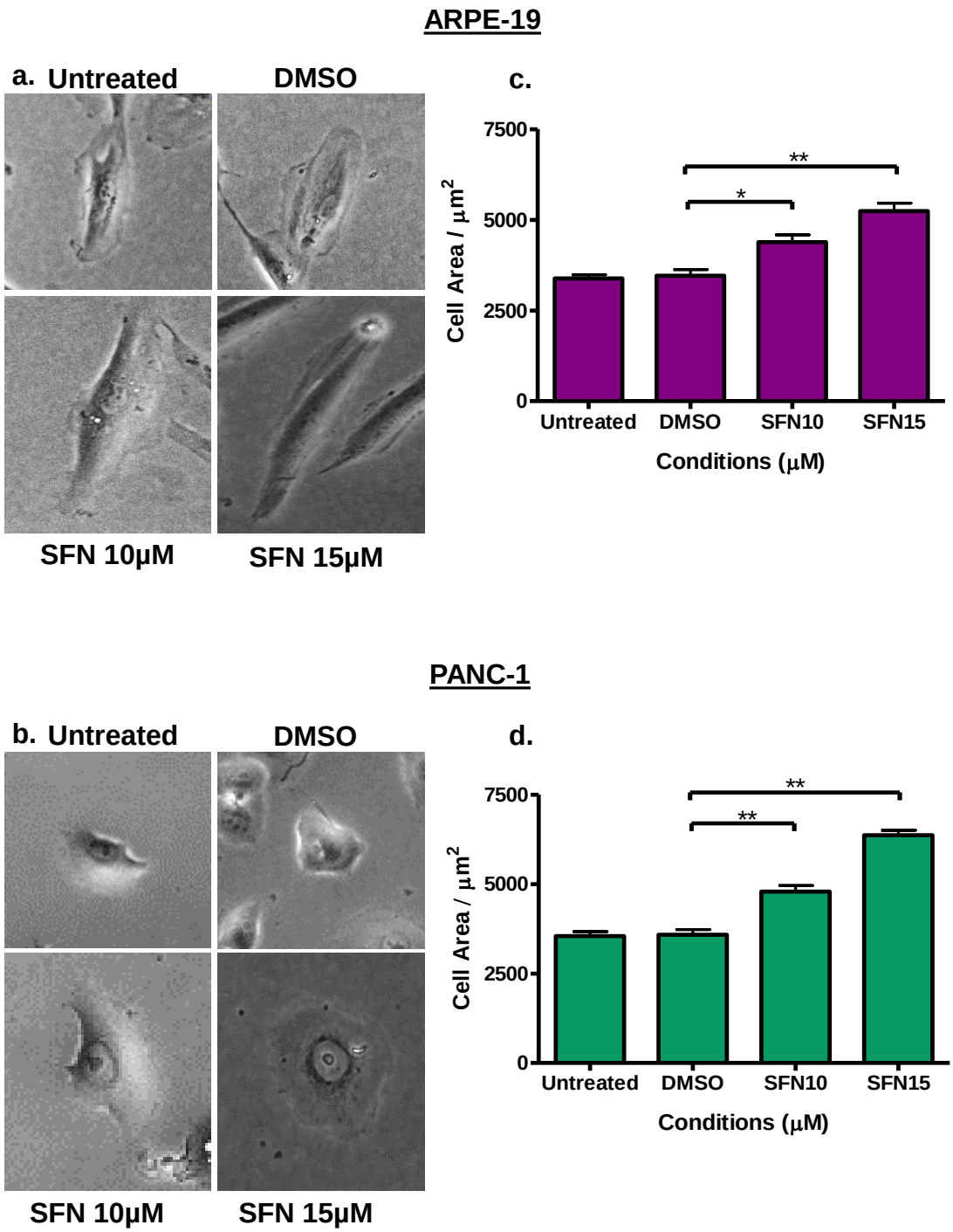

Figure 4.2 SFN at 10 and 15µM affects cell size and morphology in ARPE-19 and PANC-1 cells

Cells were seeded and treated with different concentrations of SFN or DMSO for 48 h. Selected cells from frames from live imaging recording (a, b), show morphological changes in treated cells size. Live-images were used to analyse cell area by using FIJ (Image J) software. c, d) The size of SFN treated cells significantly increased compared to DMSO. Cell size statistical analysis determined compared to DMSO, statistical significance assessed by one-way ANOVA with Tukey's multiple comparison test, [*P<0.05 & **P<0.001], n=65.

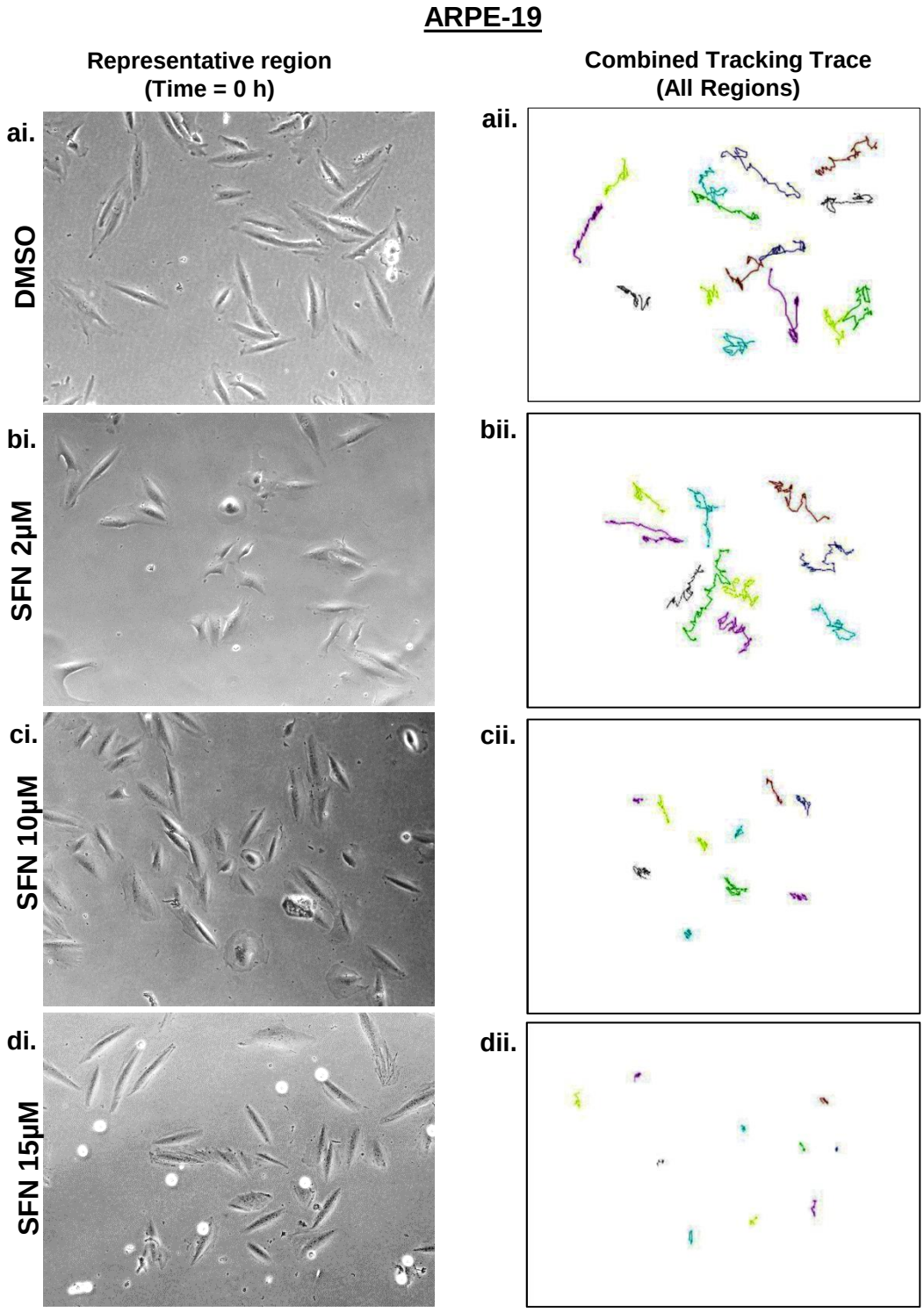

Figure 4.3 Single cell tracking of ARPE-19 cells
Cells treated with DMSO or different concentrations of SFN (2, 10 and 15 µM) were seeded into 24 a well plate and imaged by widefield time-lapse microscopy for 16 h, and frames were taken every 10 minutes. Selective representative fields of cells at t=0 are shown in ai, bi, ci, di. 10 cells were analysed from each of 20 regions (40 cells total); cells position was tracked at each time point for each cell to give a trace of position over the time-course and combined to produce the combined tracking trace illustrated (aii, bii, cii, dii), with the different coloured lines representing individual cell track. All scale bars =100µm.

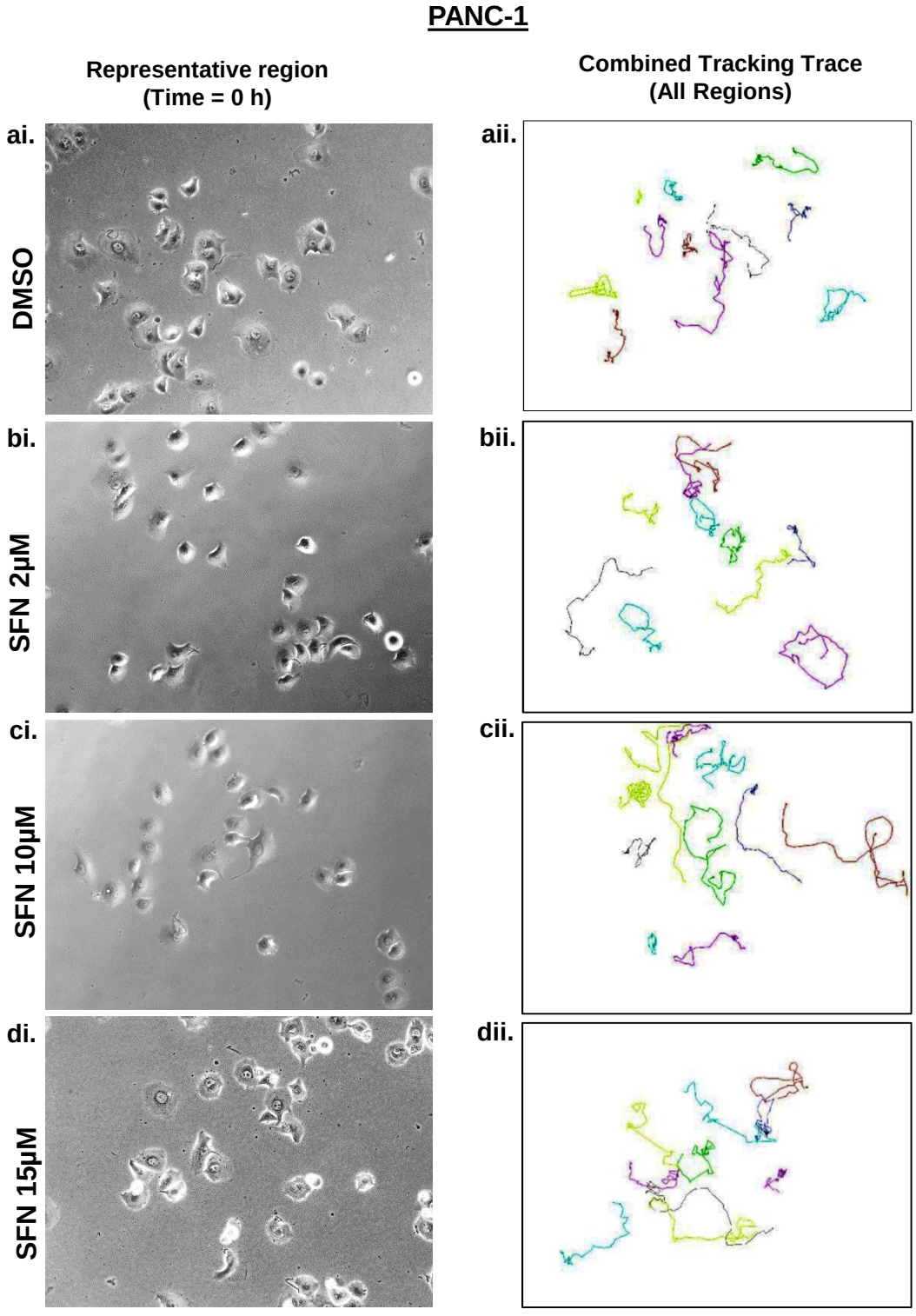

Figure 4.4 Single cell tracking of PANC-1 cells
Cells treated with DMSO or different concentrations of SFN (2, 10 and 15 µM) were seeded into 24 a well plate and imaged by widefield time-lapse microscopy for 16 h, and frames were taken every 10 minutes. Selective representative fields of cells at t=0 are shown in ai, bi, ci, di. 10 cells were analysed from each of 20 regions (40 cells total); cells position was tracked at each time point for each cell to give a trace of position over the time-course and combined to produce the combined tracking trace illustrated (aii, bii, cii, dii), with coloured lines representing individual cell track. All scale bars =100µm.

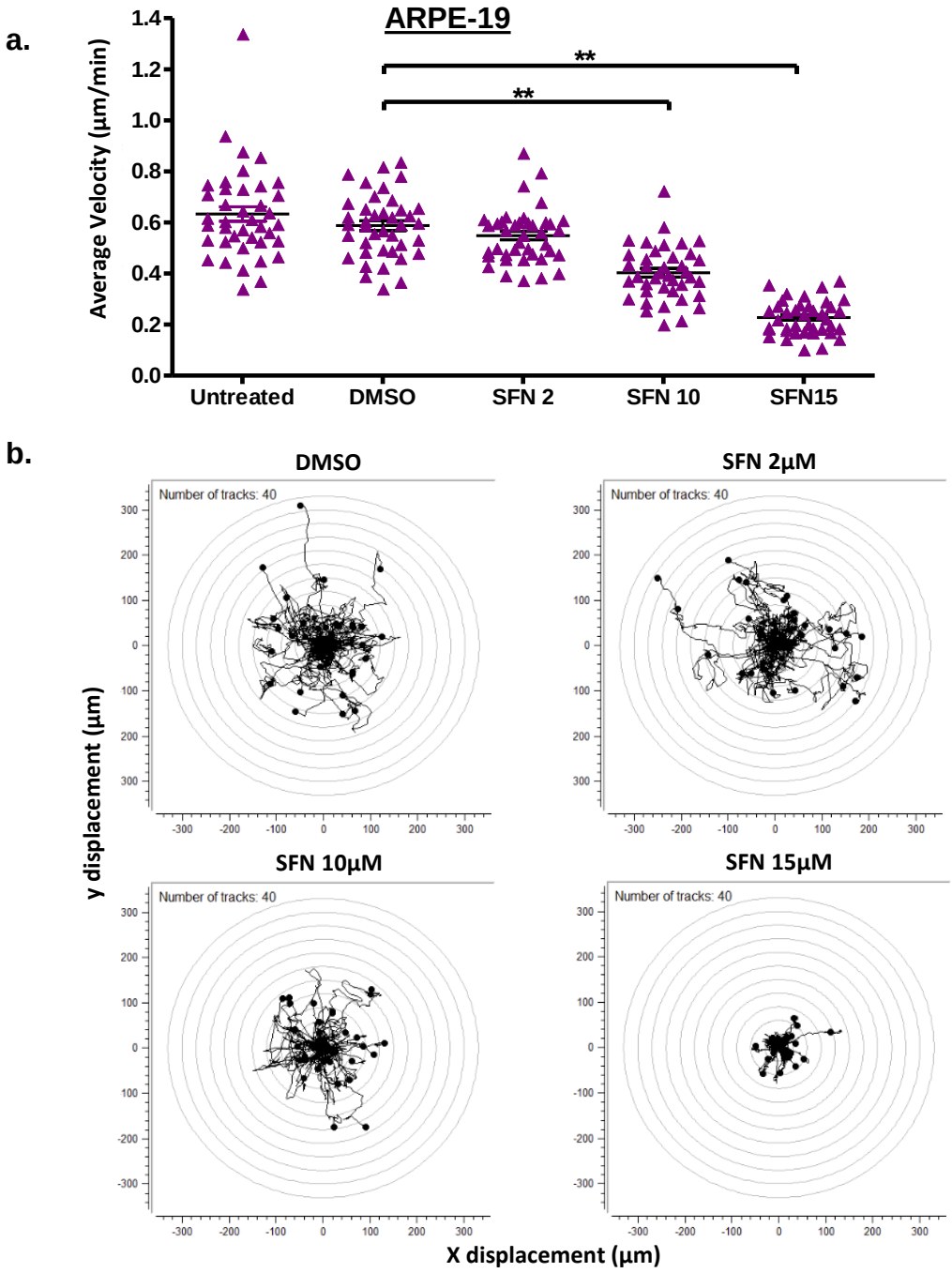

Figure 4.5 SFN causes decreased speed and spread of random migration in ARPE-19 cells

Cells were treated with SFN for 48 h. Cells were seeded sparsely into 24 well plate and imaged by widefield time lapse microscopy for a 16 h period beginning 32 h post initial treated, with frames taken every 10 minutes. 40 cells for each treatment were analysed. The position of each cell was tracked in FIJI (ImageJ) software for each time-point across the time-course. a) From these data, the average velocity for each cell across the time was calculated and plotted. Analysis by one-way ANOVA with Tukey's multiple comparison test shows a significant decrease in cell velocity with SFN 10 and 15 µM compared to DMSO [P<0.001]. b) Spider graph show the distance of individual cells during migration and reveal a decrease in spread with both 10 and 15µM SFN. SFN treated cells travel short distance compared to DMSO treated cells.

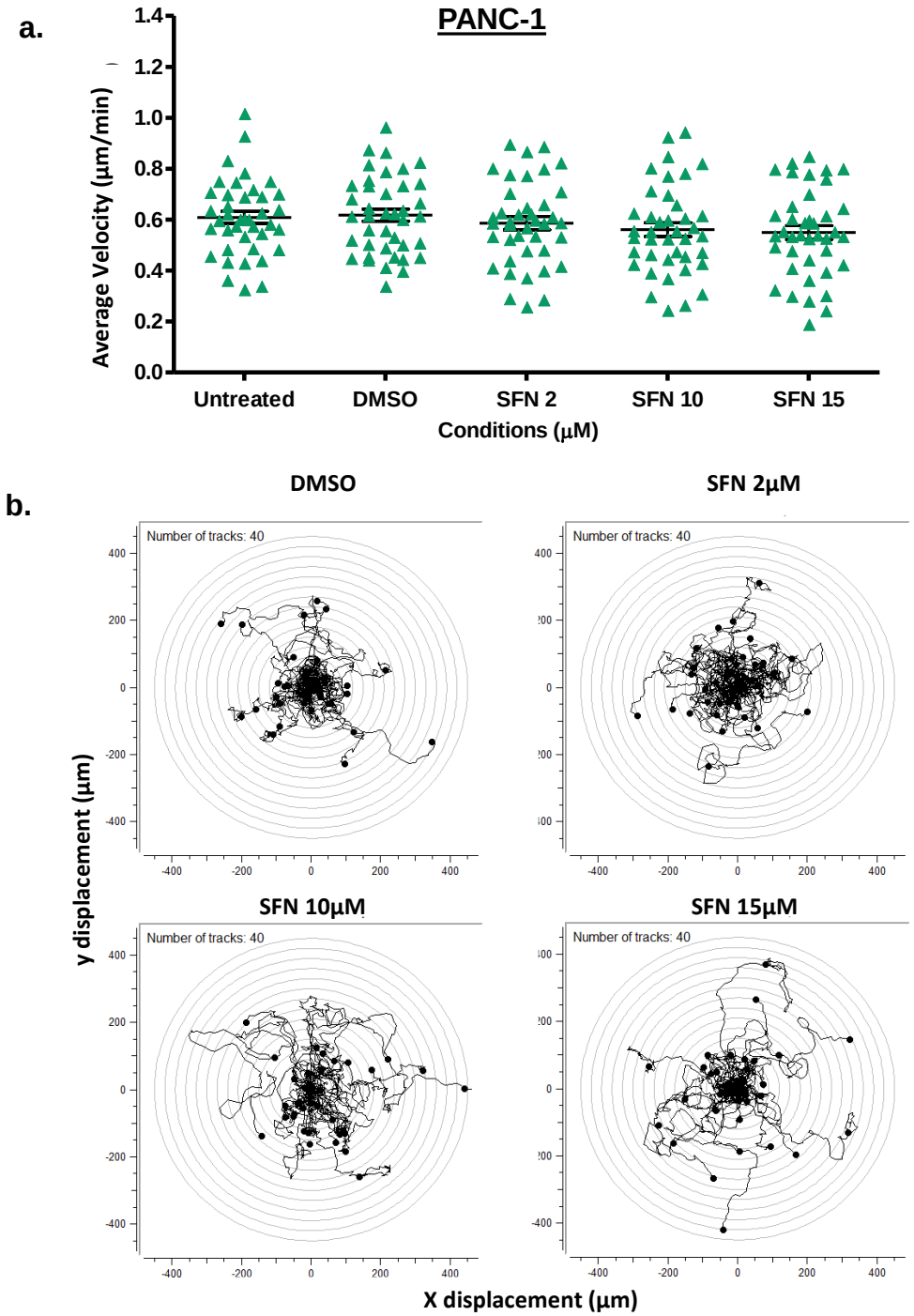

Figure 4.6 SFN did not affect the speed and spread of random migration in PANC-1 cells

Cells were treated with SFN for 48 h. Cells were seeded sparsely into 24 well plate and imaged by widefield time lapse microscopy for a 16 h period beginning 32 h post initial treated, with frames taken every 10 minutes. 40 cells for each treatment were analysed. The position of each cell was tracked in FIJI (ImageJ) software for each time-point across the time-course. a) From these data, the average velocity for each cell across the time-period was calculated and plotted. Analysis by one-way ANOVA with Tukey's multiple comparison test showed no significant decrease in cell velocity with SFN 10 and 15 µM compared to DMSO [P<0.001]. b) Spider graph show the distance of individual cells migration and show no marked differences in spread with few cells appear travel more in 15µM SFN. Generally, SFN and DMSO treated cells travel similar distance.

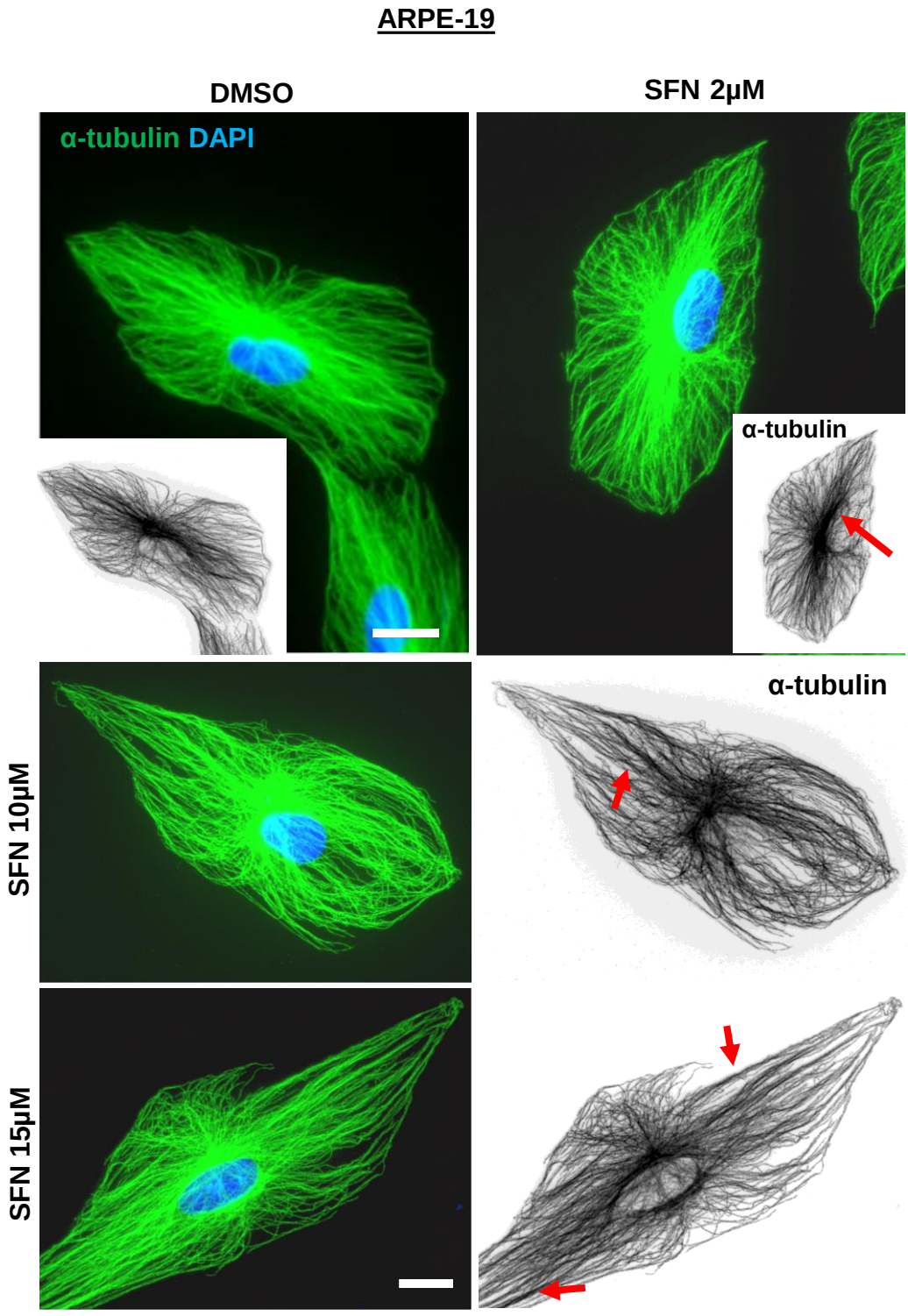

Figure 4.7 SFN affects microtubule organisation in ARPE-19 cells
Cells were treated with different concentrations of SFN and DMSO for 48 h. Cells were immnolabelled for a-tubulin (green, invert) and DAPI (blue). DMSO and 2µM SFN treated cells show a classic radial array of microtubules focused on the centre of the cell. 10µM and 15µM SFN treated cells show more microtubule bundles formation (arrows). Scale bars = 10µm.

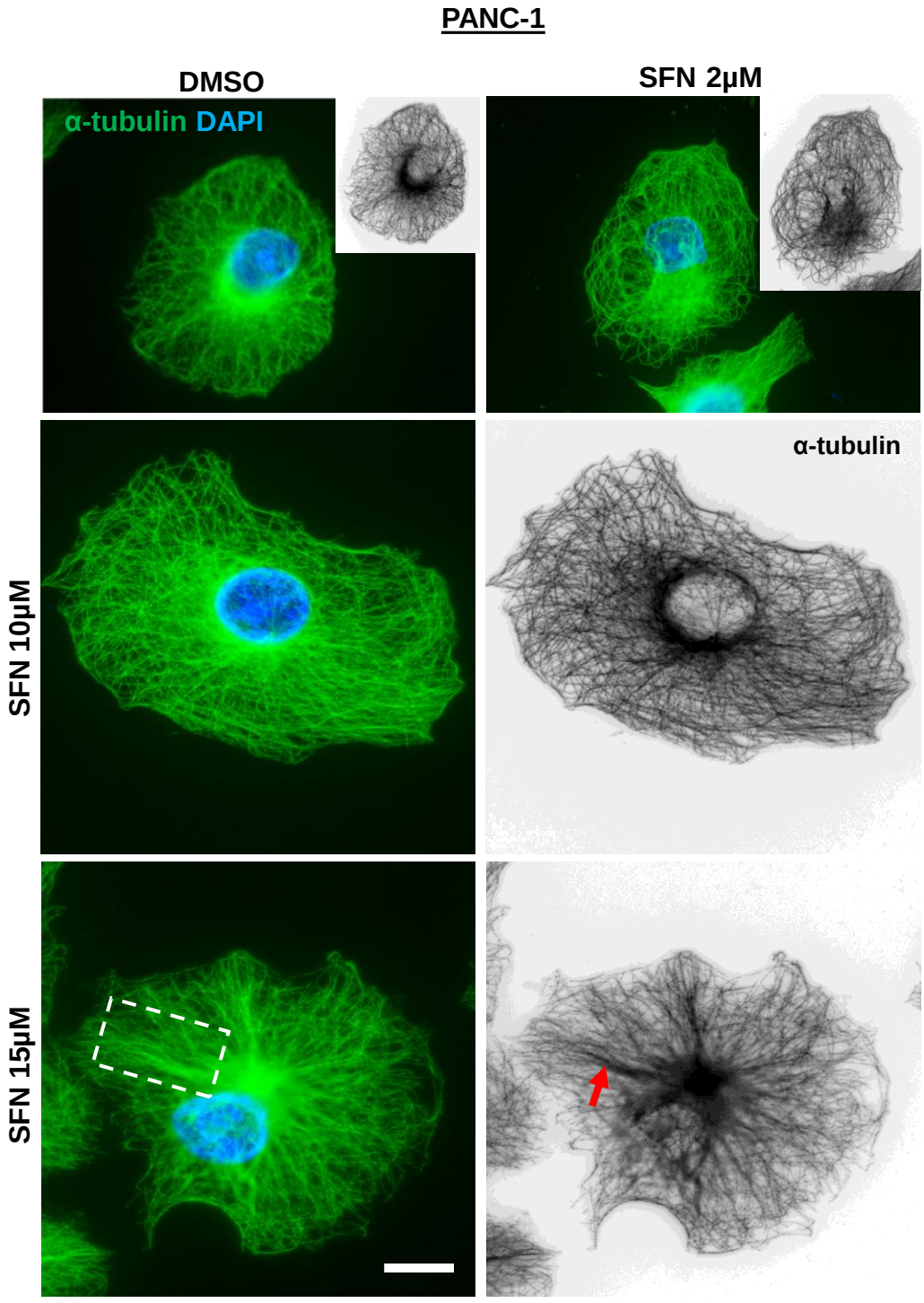

Figure 4.8 SFN affects microtubule organisation in PANC-1 cells
Cells were treated with different concentrations of SFN and DMSO for 48 h. Cells were then immnolabelled for a-tubulin (green, invert) and DAPI (blue). DMSO treated cell shows disorganised microtubules focused in the centre of the cell and elongated towards cell periphery. 2μM and 10μM SFN treated cells reveal similar microtubule pattern to DMSO treated cell. However, 15μM SFN treated cell reveals some cells forming straight and bundled microtubules (arrows). Scale bars = 10μm.

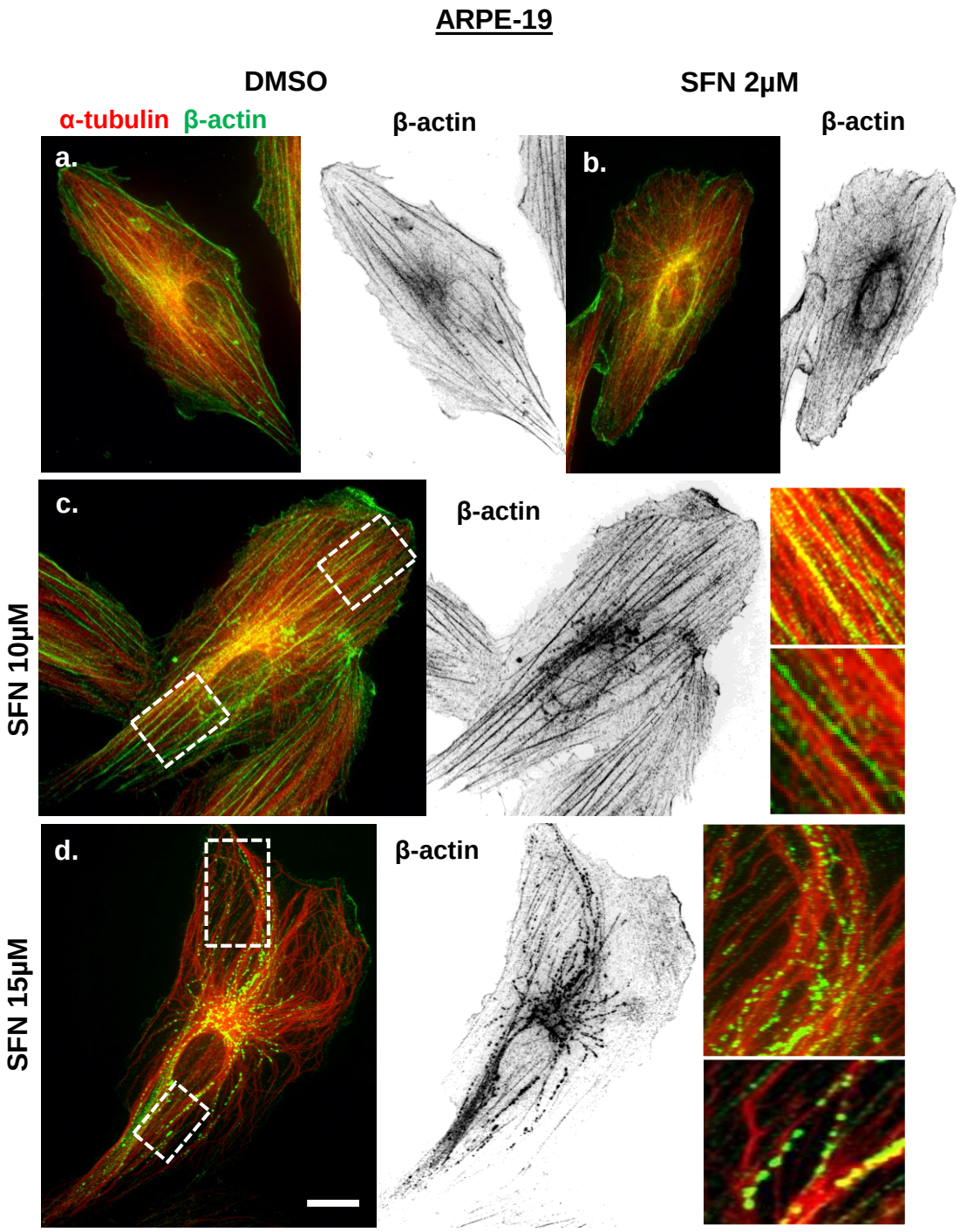

Figure 4.9 SFN causes actin filaments disorganisation and co-alignment with microtubules in ARPE-19 cells
Cells were immunolabelled for microtubules (α-tubulin; red) and actin (β-actin, green, invert). a) DMSO treated cell shows actin located at cell edges and forming lamellipodium with some actin filaments running parallel to long axis of in cell body, and (b) 2μM SFN treated cell shows similar organisation. 10μM SFN treated cell reveals actin filaments are co-aligned with microtubules (enlarged boxed). 15μM SFN treated shows actin filaments are accumulated and co-aligned with microtubules. The dotted appearance of β-actin suggests of breakdown actin filaments (enlarged boxed). Scale bars = 10μm.

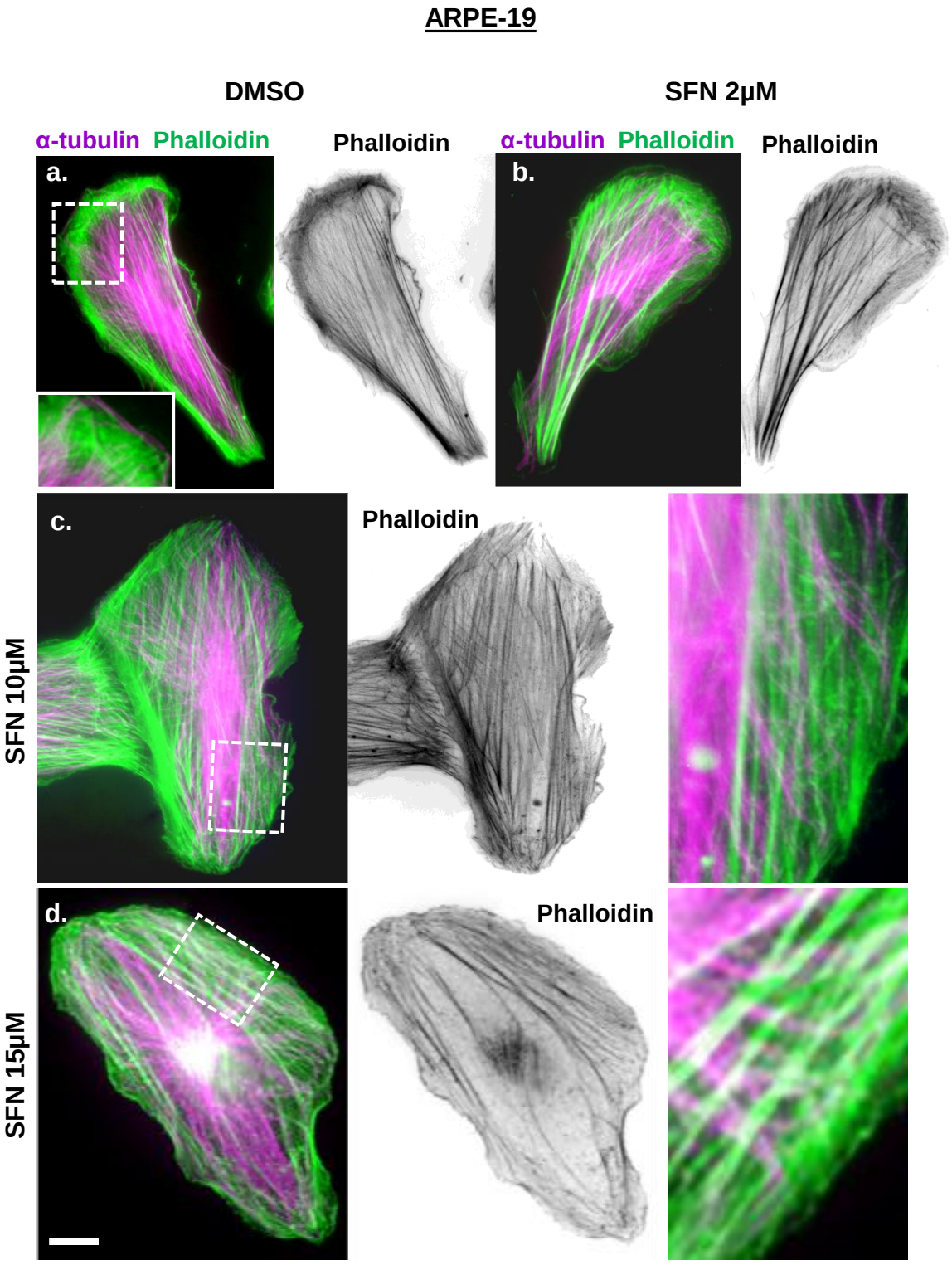

Figure 4.10 Stress fibres organisation in SFN treated ARPE-19 cells
Cells were immunolabelled for microtubules (α-tubulin; purple) and actin filaments (phalloidin, green, invert). a) DMSO treated cell shows stress fibres running parallel in the cell centre and actin at periphery, and 2µM SFN treated cell shows similar organisation (b). c) 10µM SFN treated cell reveals an increase of stress fibres (enlarged boxed). d) 15µM SFN treated cell shows an increase of stress fibres but with a decrease of cortical actin (enlarged boxed). Scale bars = 10µm.

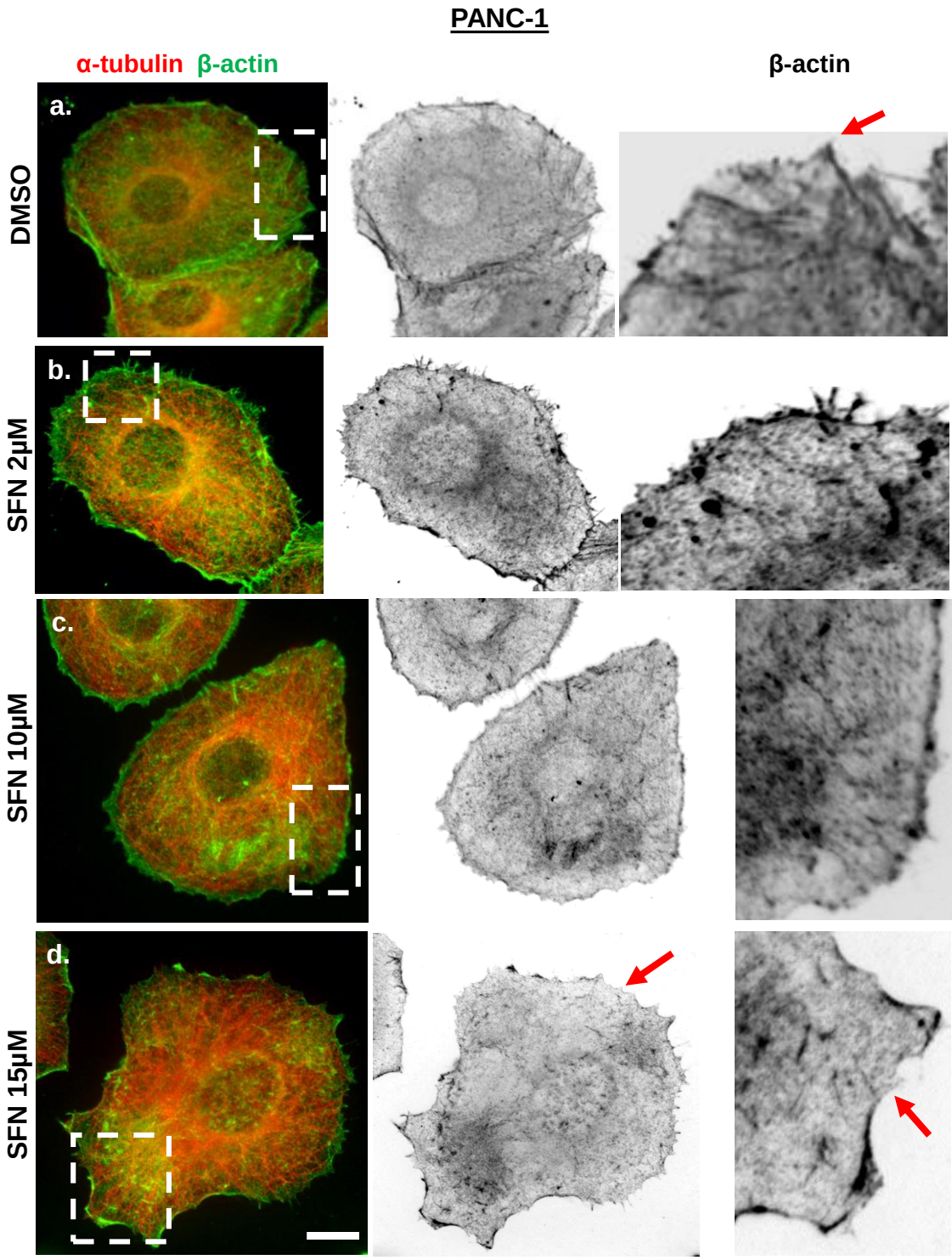

Figure 4.11 Effects of SFN on actin organisation in PANC-1 cells
Cells were immunolabelled for microtubules (α-tubulin; red) and actin (β-actin, green, invert). a) DMSO treated cell shows actin filaments at the cell periphery with microspike at the front of the cell (boxed region, arrow). b) 2μM SFN treated cell shows actin filaments at the cell periphery. c) 10μM and 15μM treated cell reveals disorganised actin filaments with some accumulated actin in cell with some reduction of cortical actin (boxed region, arrow). Scale bars = 10μm.

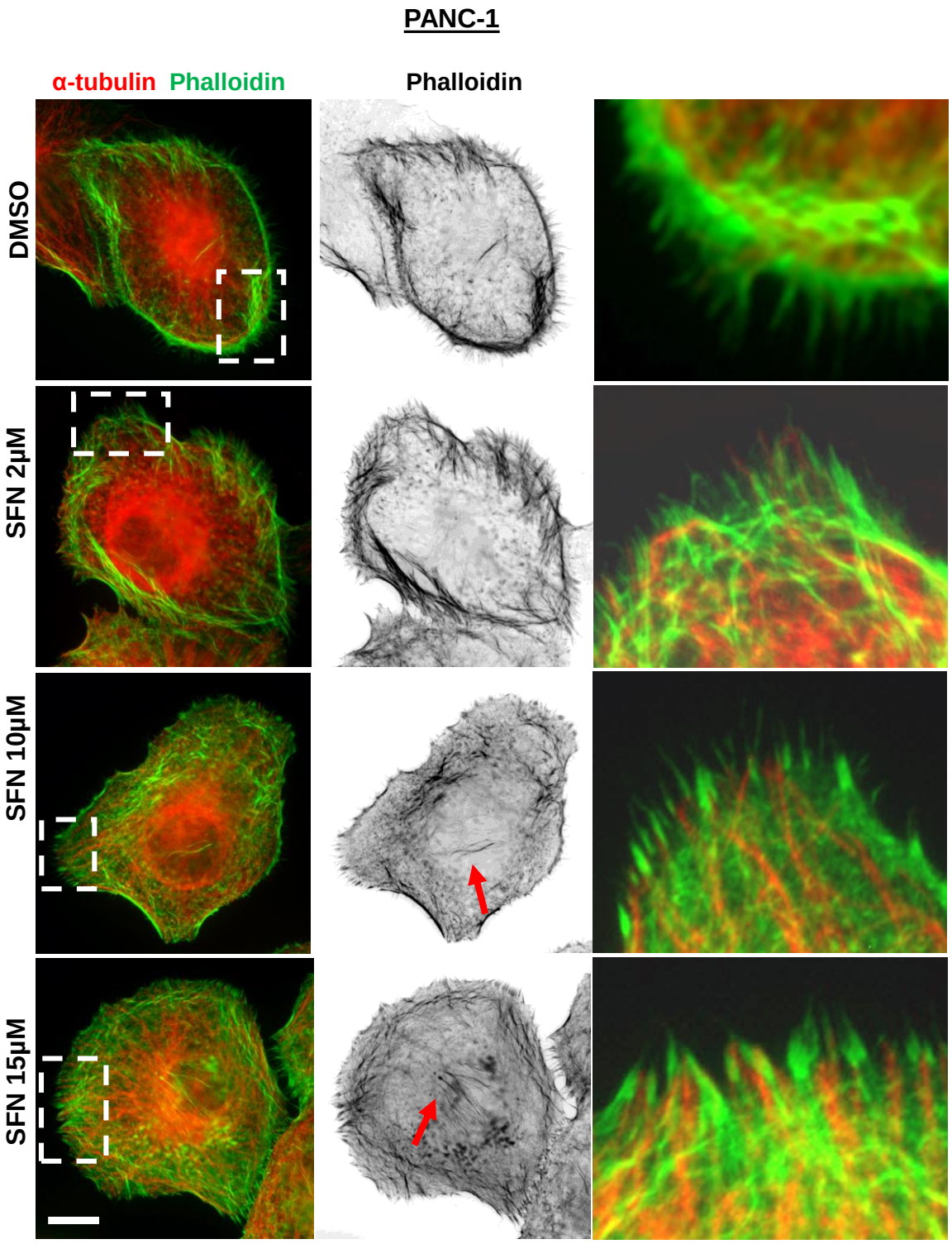

Figure 4.12 Stress fibre organisation in SFN treated PANC-1 cells
Cells were immunolabelled for microtubules (α-tubulin; red) and stained for actin filaments (Phalloidin, green, invert). a, b) DMSO and 2µM SFN treated cells reveal actin fibres close to periphery with filopodia and microspikes at the very front of the leading (boxed region). c, d) 10µM and 15µM treated cells show some stress fibres in the cell body with some decrease in microspikes at the front edge (arrows, boxed region). Scale bars = 10µm.

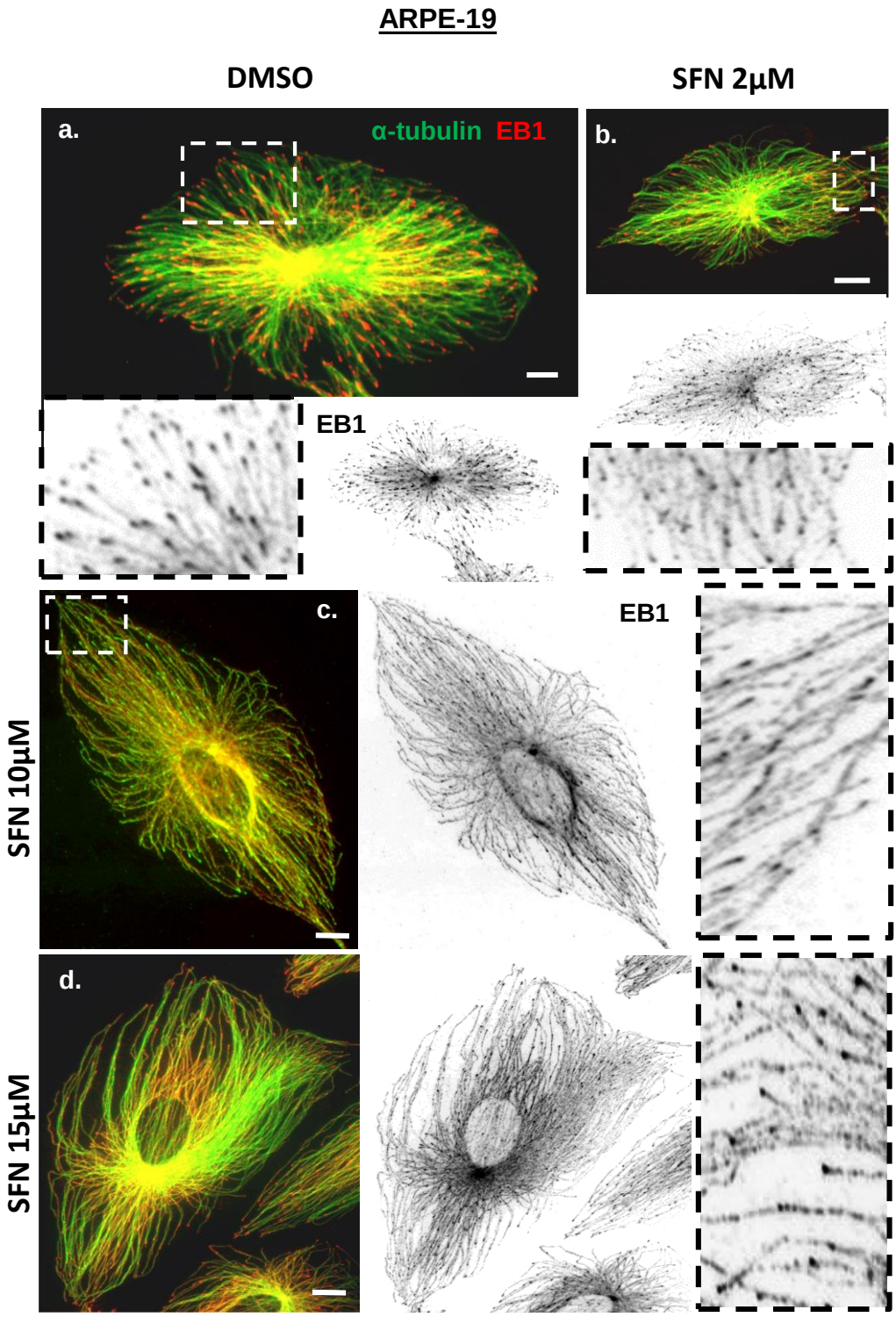

Figure 4.13 EB1 localisation in SFN treated ARPE-19 cells
Cells were immunolabelled for EB1 (red, inverted) and α-tubulin (green), and images were taken with Widefield fluorescence microscopy. a and b) DMSO and SFN 2µM treated cells show EB1 as classic comets at microtubule plus-ends. 10 and 15µM SFN treated cells reveal an extensive association between EB1 and microtubules, with EB1 binding along the microtubules lattice and with a distinct accumulation at the plus-ends (boxed region) (c and d). Scale bars = 10µm.

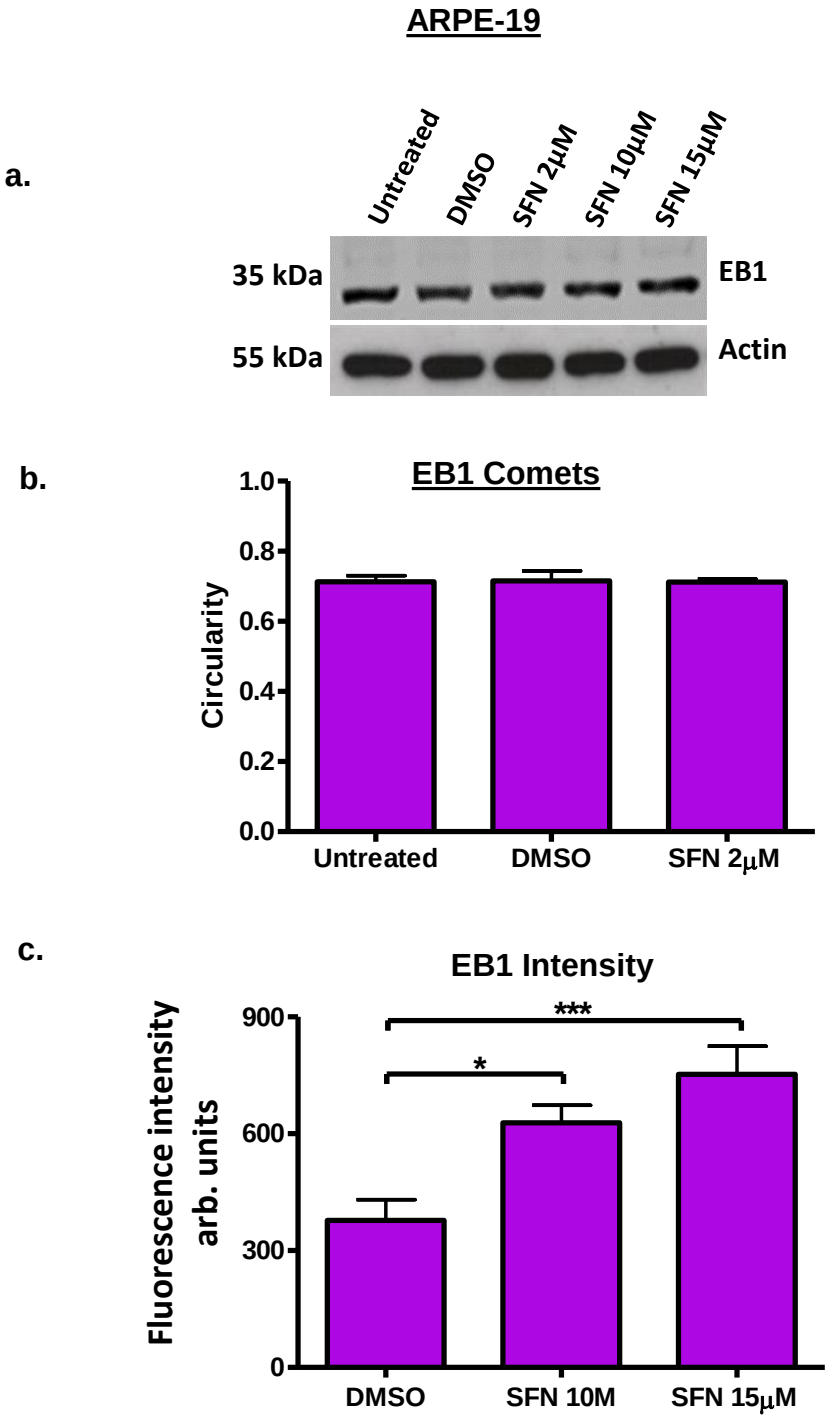

Figure 4.14 EB1 expression and comet analysis in SFN treated ARPE-19
Cells were treated with different concentrations of SFN for 48 h. a) Western blot result shows no change in the levels of EB1 in all concentrations. b) The analysis of EB1 comets shape shows no significant difference in EB1 comets circularity between the 2μM SFN AND DMSO treated cells. c) Fluorescence intensity analysis was used to quantify EB1 lattice association. The analysis of EB1 lattice association for 10 and 15μM SNF treated cells shows a dramatic increase in EB1 intensity along the microtubule lattice compared to DMSO treated cells. Significance was assessed by one-way ANOVA with Tukey's multiple comparisons test), $P<0.05$ & $P<0.001$.

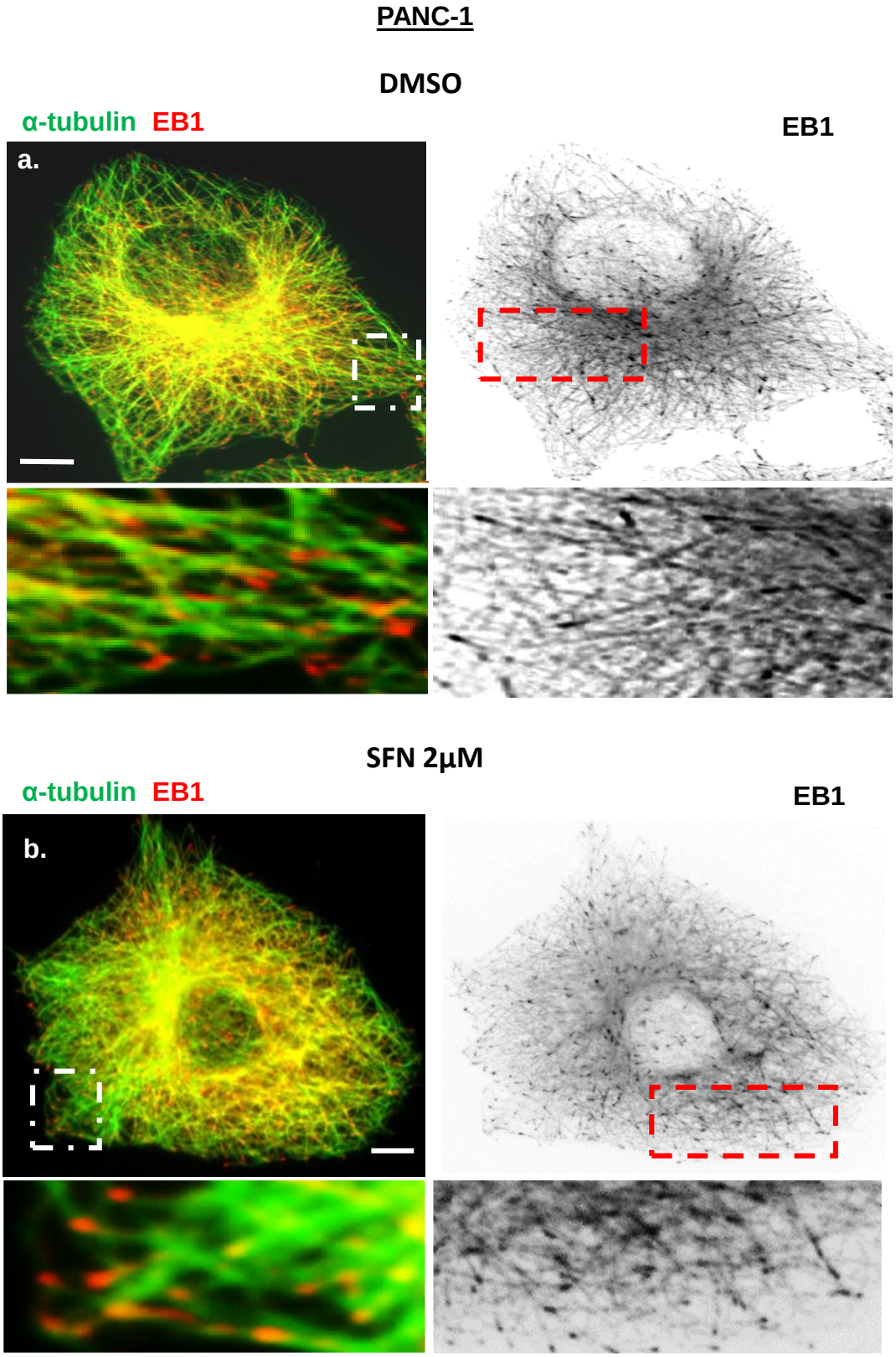

Figure 4.15 EB1 localisation in SFN treated PANC-1 cells
Cells were immunolabelled for EB1 (red, inverted) and α-tubulin (green). a) The fluorescence image for DMSO treated cell shows EB1 as classic comets at microtubules plus-ends with some lattice association in the centre of the cell. b) 2μM treated cell reveals EB1 accumulated at the plus-ends of microtubules as comets (boxed region). Scale bars = 10μm.

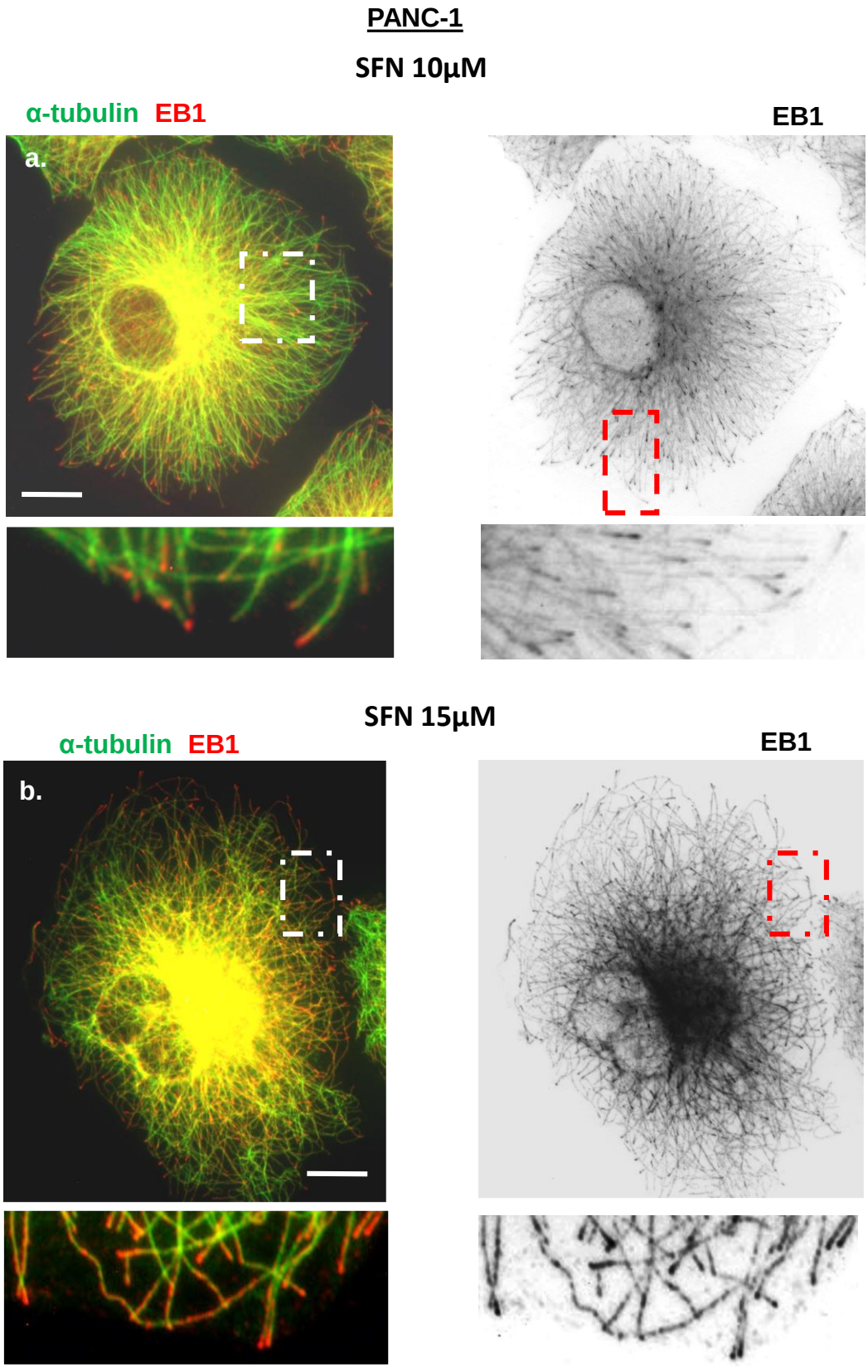

Figure 4.16 EB1 localisation in SFN treated PANC-1 cells
Cells were immunolabelled for EB1 (red, inverted) and α-tubulin (green). a) 10µM SFN treated cell shows EB1 as comets at microtubules plus-ends (boxed region). b) 15µM SFN treated cell reveals an extensive association between EB1 and the microtubule lattice (boxed region). Scale bars = 10µm.

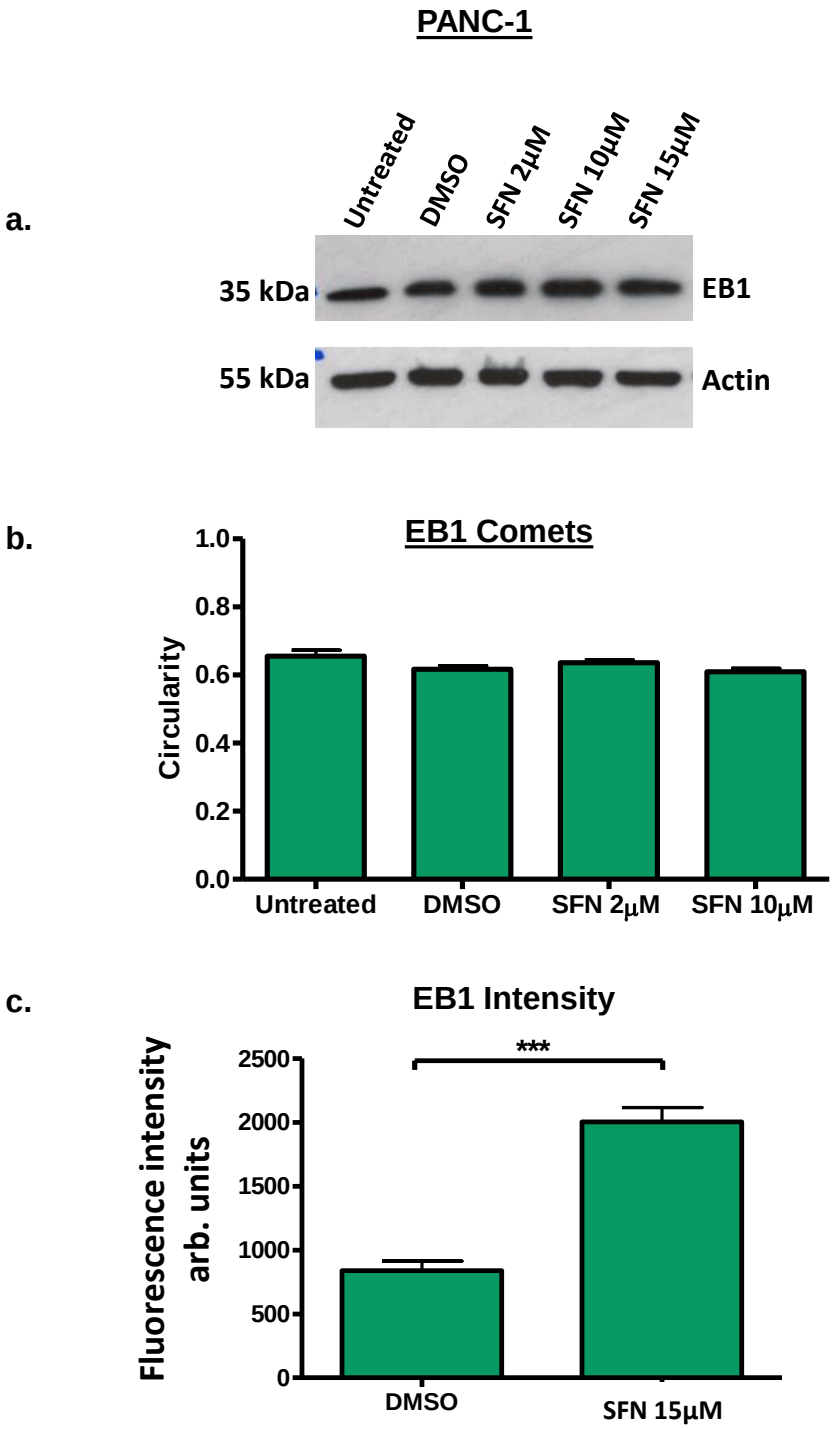

Figure 4.17 EB1 expression and comet analysis in PANC-1 cells
Cells were treated with different concentrations of SFN for 48 h. a) Western blot result suggests no change in the level of EB1 expression in all conditions. b) The analysis of EB1 comets shape reveals no significant difference in EB1 comets circularity between all conditions, (one-way ANOVA with Tukey's multiple comparisons test). c) Fluorescence intensity analysis was used to quantify EB1 lattice association. The analysis of EB1 lattice association for 15μM SNF treated cells show a significant increase in intensity along the microtubule lattice compared to DMSO treated cells. Significance was assessed by unpaired t-test), $P<0.001$.

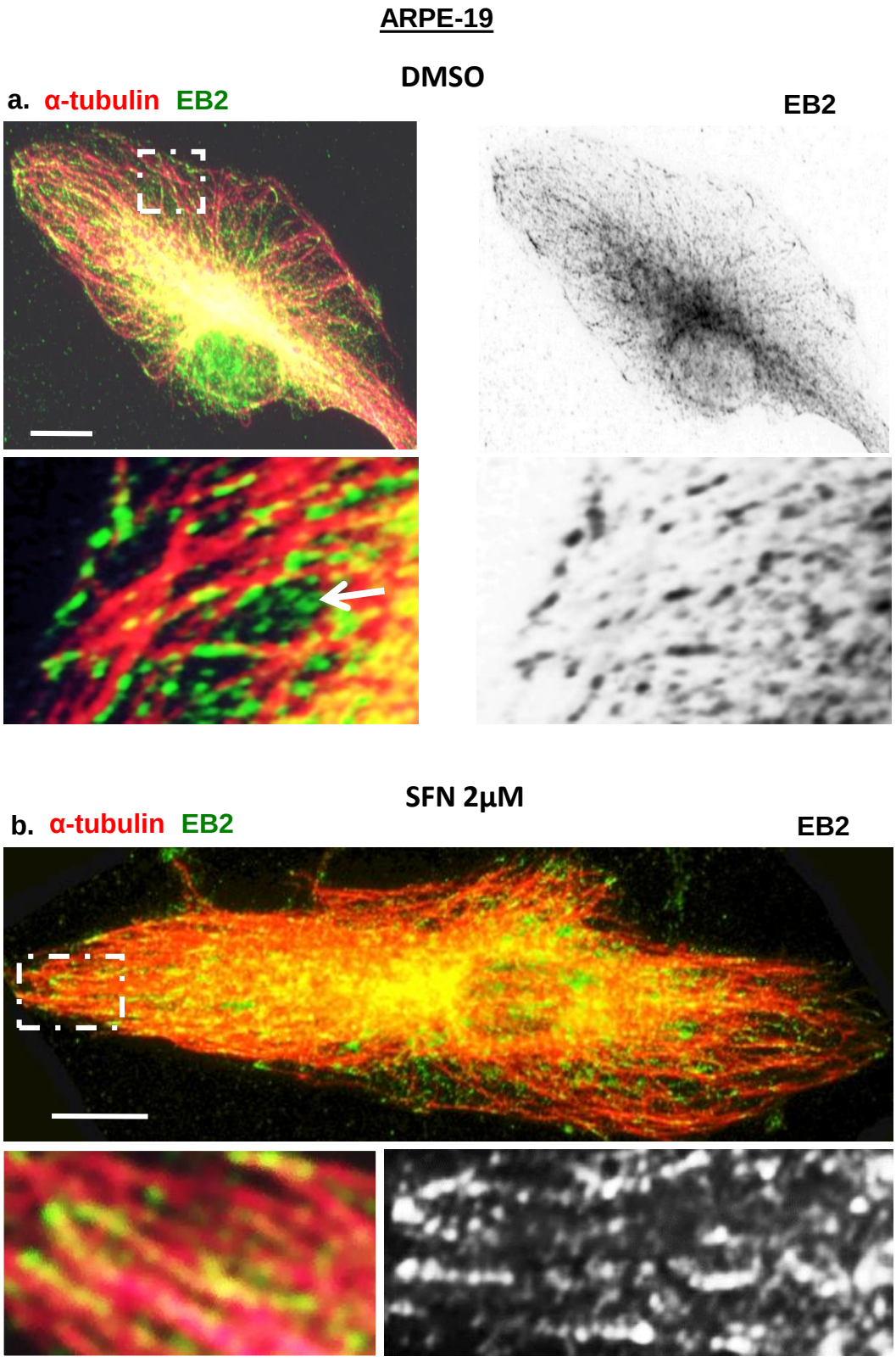

Figure 4.18 EB2 localisation in SFN treated ARPE-19 cells
Widefield fluorescent images of cells immunolabelled for α-tubulin (red) and EB2 (green, inverted). a) DMSO treated cell shows location of EB2 along the lattice with some at the plus-ends of microtubules, with few free in the cytoplasm (arrow, boxed region). b) 2µM SFN treated cell reveals EB2 mainly along the microtubule lattice and plus-ends (boxed region). Scale bars = 10µm.

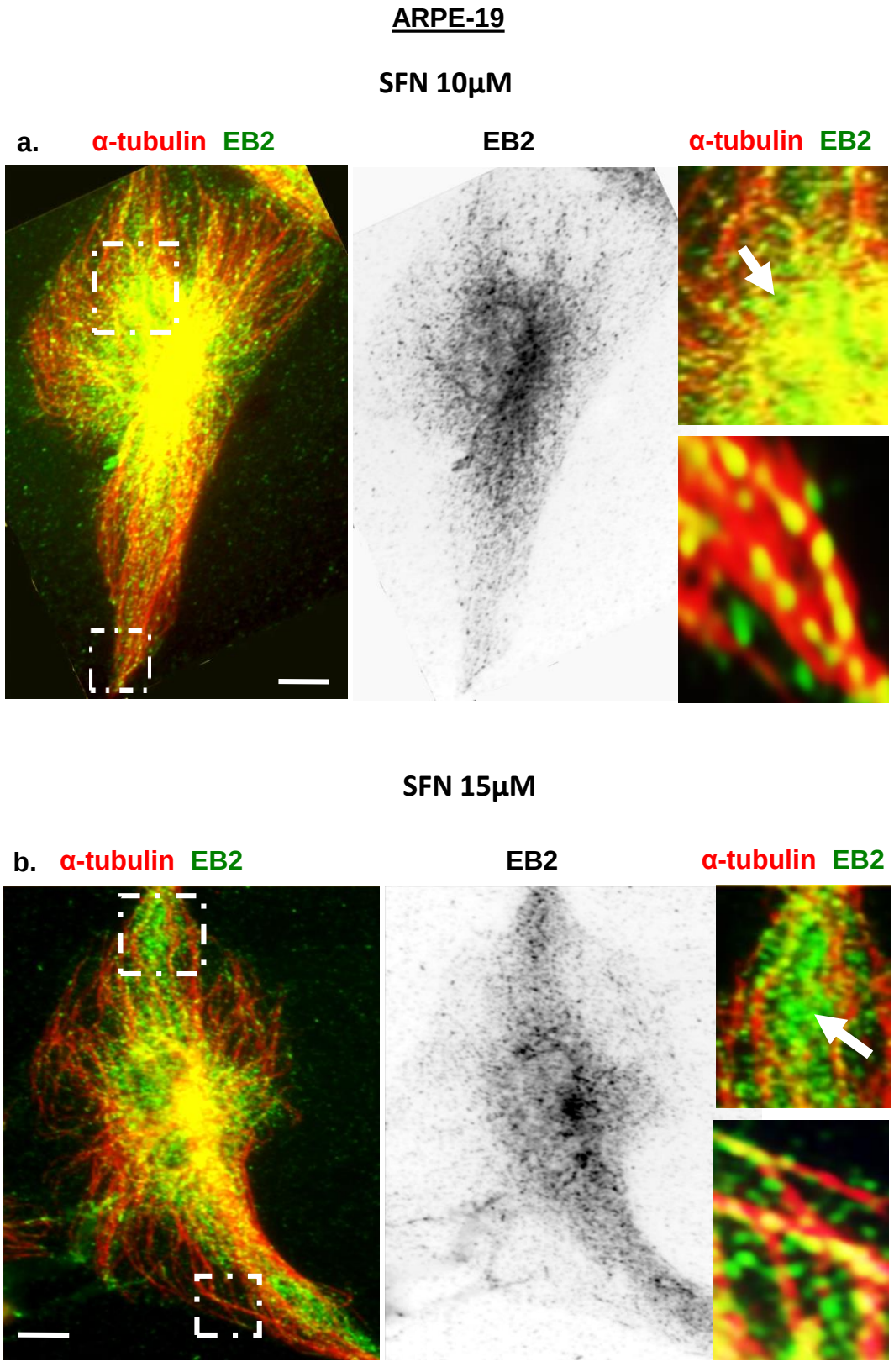

Figure 4.19 EB2 localisation in SFN treated ARPE-19 cells
Cells were immunolabelled for α-tubulin (red) and EB2 (green, inverted). a and b)10µM and 15µM SFN treated cells reveal more cytoplasmic EB2 (arrows) with few along the microtubules lattice and plus-ends (boxed region). Scale bars = 10µm.

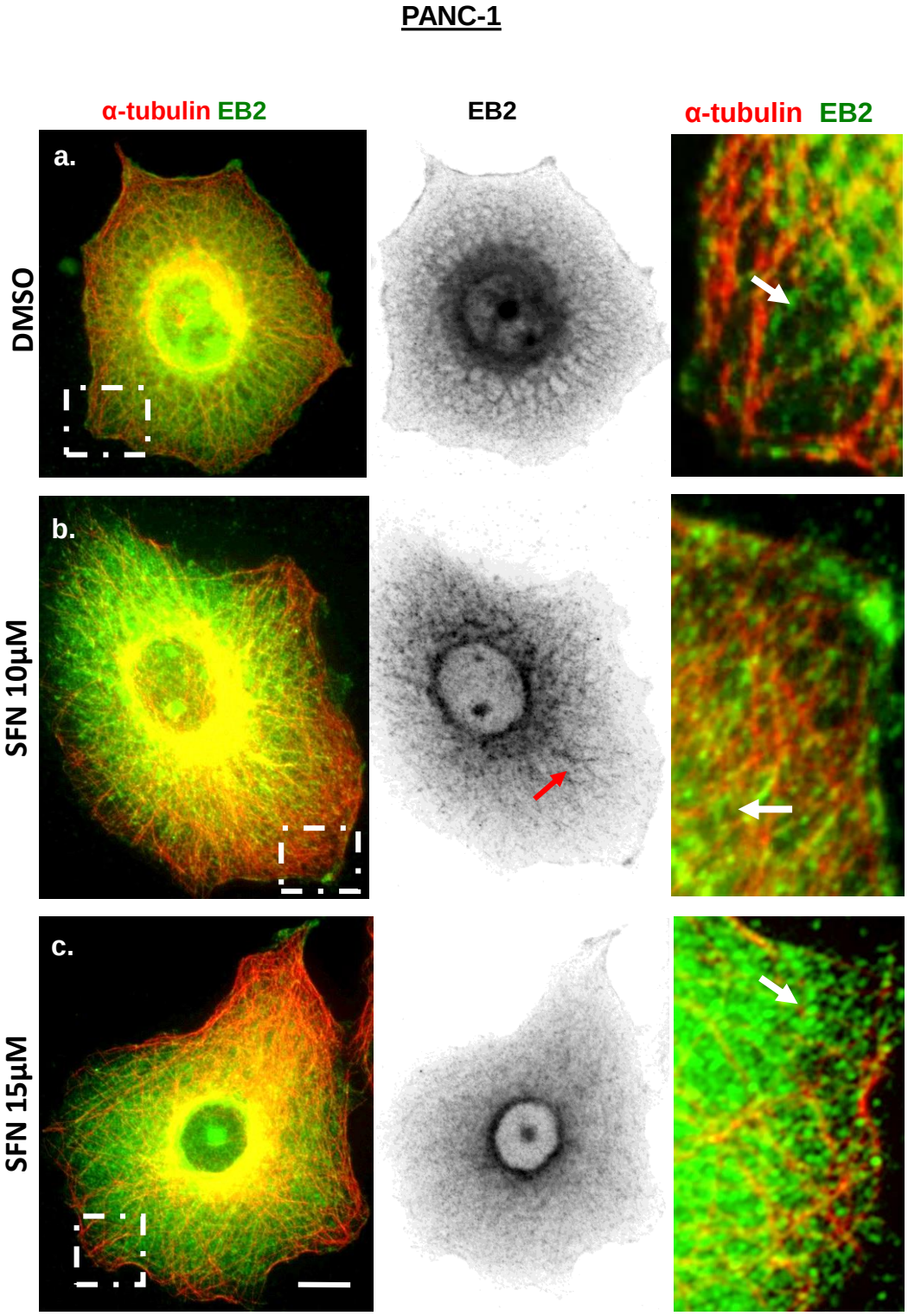

Figure 4.20 EB2 localisation in SFN treated PANC-1 cells
Cells were immunolabelled for α-tubulin (red) and EB2 (green, inverted) and treated with SFN and DMSO for 48 h. a) DMSO treated cell shows EB2 associated along the microtubules lattice with some at the cytoplasm (boxed region , arrows).10 and 15µM SFN treated cells reveal more free EB2 in the cytoplasm (arrows) with some along the lattice (boxed region and arrows) (b & c). Scale bars= 10µm.

a. **ARPE-19**

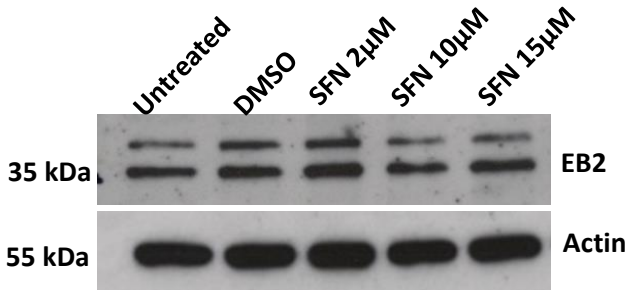

b. **PANC-1**

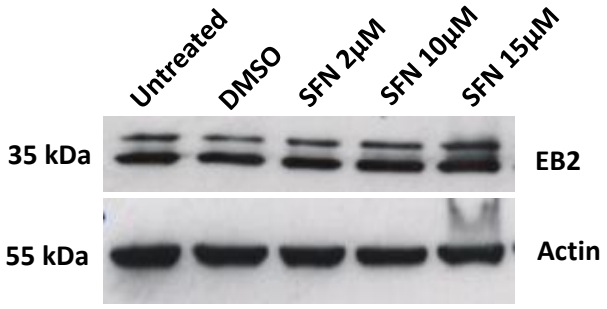

Figure 4.21 EB2 expression in SFN treated ARPE-19 and PANC-1 cells
Western blot were used to investigate the level of EB2 expression in SFN treated cells. a) Western blot result shows a slight decrease in upper band of 10 and 15µM SFN compare to DMSO treated cells. b) In contract, western blot for PANC-1 cells reveals slight increased in the level of EB2 expression in SFN treated cells compared to DMSO treated cells.

ARPE-19

DMSO

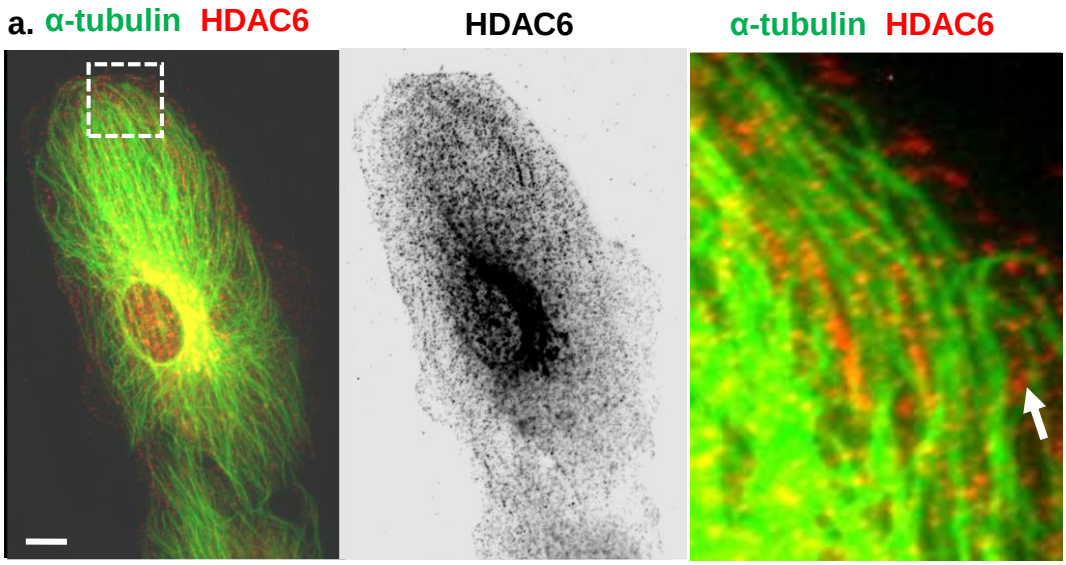

SFN 2µM

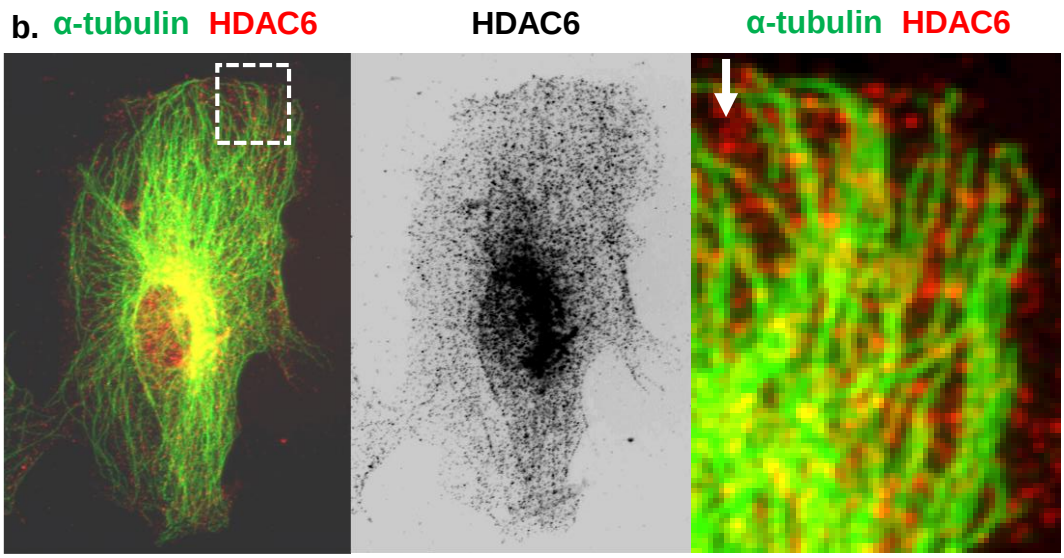

Figure 4.22 HDAC6 localisation in SFN treated ARPE-19 cells
Cells were immunolabelled for α-tubulin (green) and HDAC6 (red, invert). a) DMSO treated cell reveals HDAC6 free in the cytoplasm (arrow) and around the nucleus with some along the microtubule lattice. b) 2µM SFN treated cell shows HDAC6 mainly in the cytoplasm (arrow) with some along lattice (boxed region). All scale bars = 10µm.

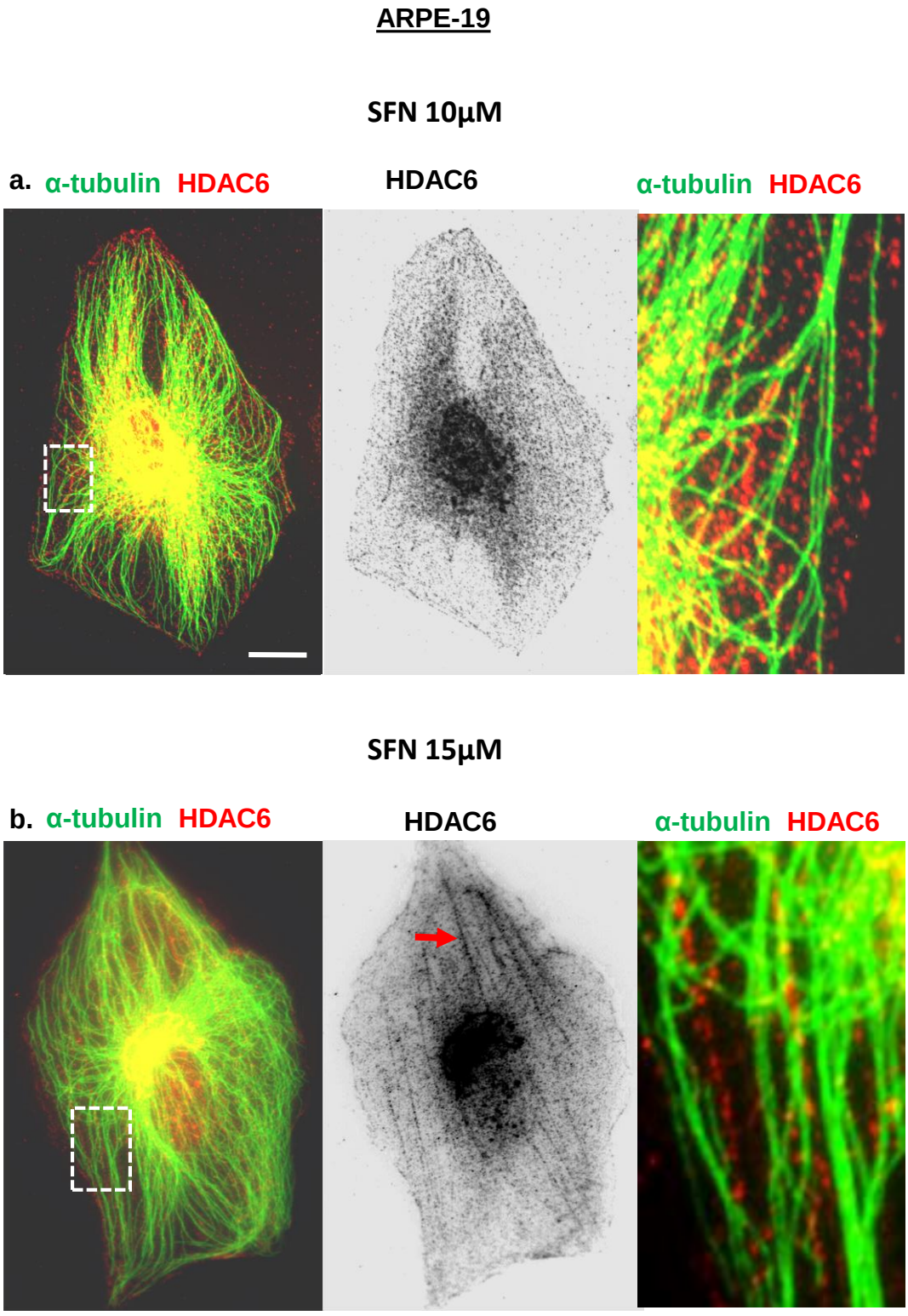

Figure 4.23 HDAC6 localisation in SFN treated ARPE-19 cells
Cells were immunolabelled for α-tubulin (green) and HDAC6 (red, invert). a) 10µM SFN treated cell reveals HDAC6 mainly in the cytoplasm and around the nucleus with no much evidence of association along the microtubules lattice (boxed region). b) 15µM SFN treated cell shows some filament-like of HDAC6 in the cytoplasm (arrow) and free in the cytoplasm, with no much evidence of association along the microtubules lattice. All scale bars = 10µm.

PANC-1

DMSO

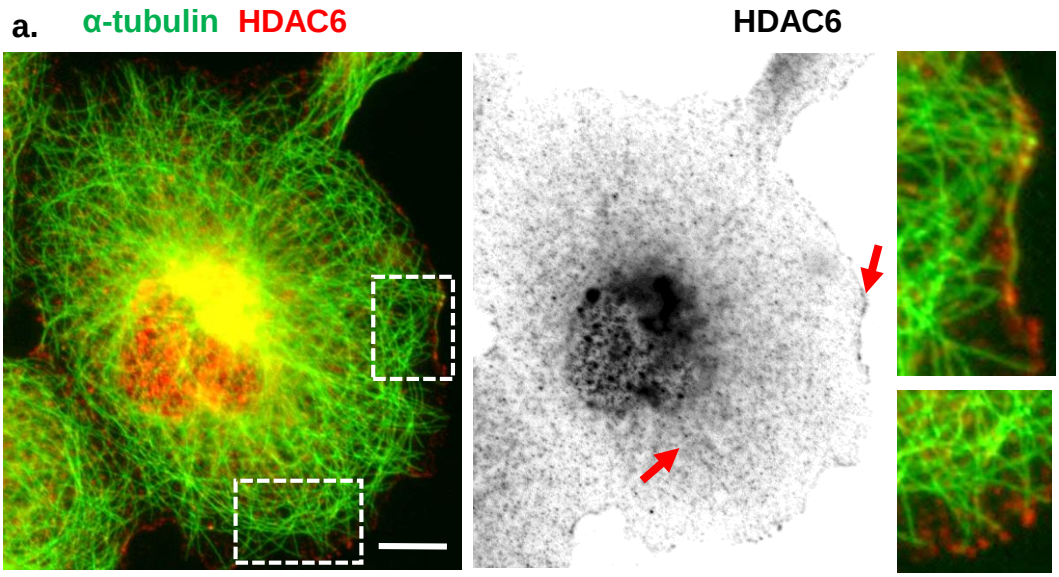

SFN 2µM

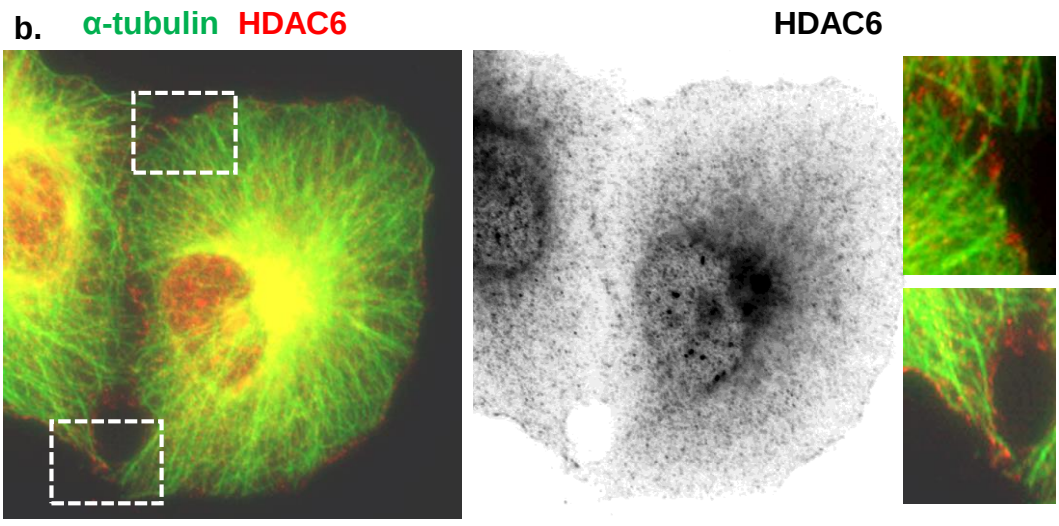

Figure 4.24 HDAC6 localisation in SFN treated PANC-1 cells
Cells immunolabelled for α-tubulin (green) and HDAC6 (red, invert). a) DMSO treated cell reveals HDAC6 mainly diffused in the cytoplasm and around the nucleus also some association along the microtubules and the periphery (arrows). Similar observation is found in 2µM SFN treated cell, where HDAC6 is free in the cytoplasm and around the nucleus, with no association along the microtubules lattice (boxed region) (b). All scale bars = 10µm.

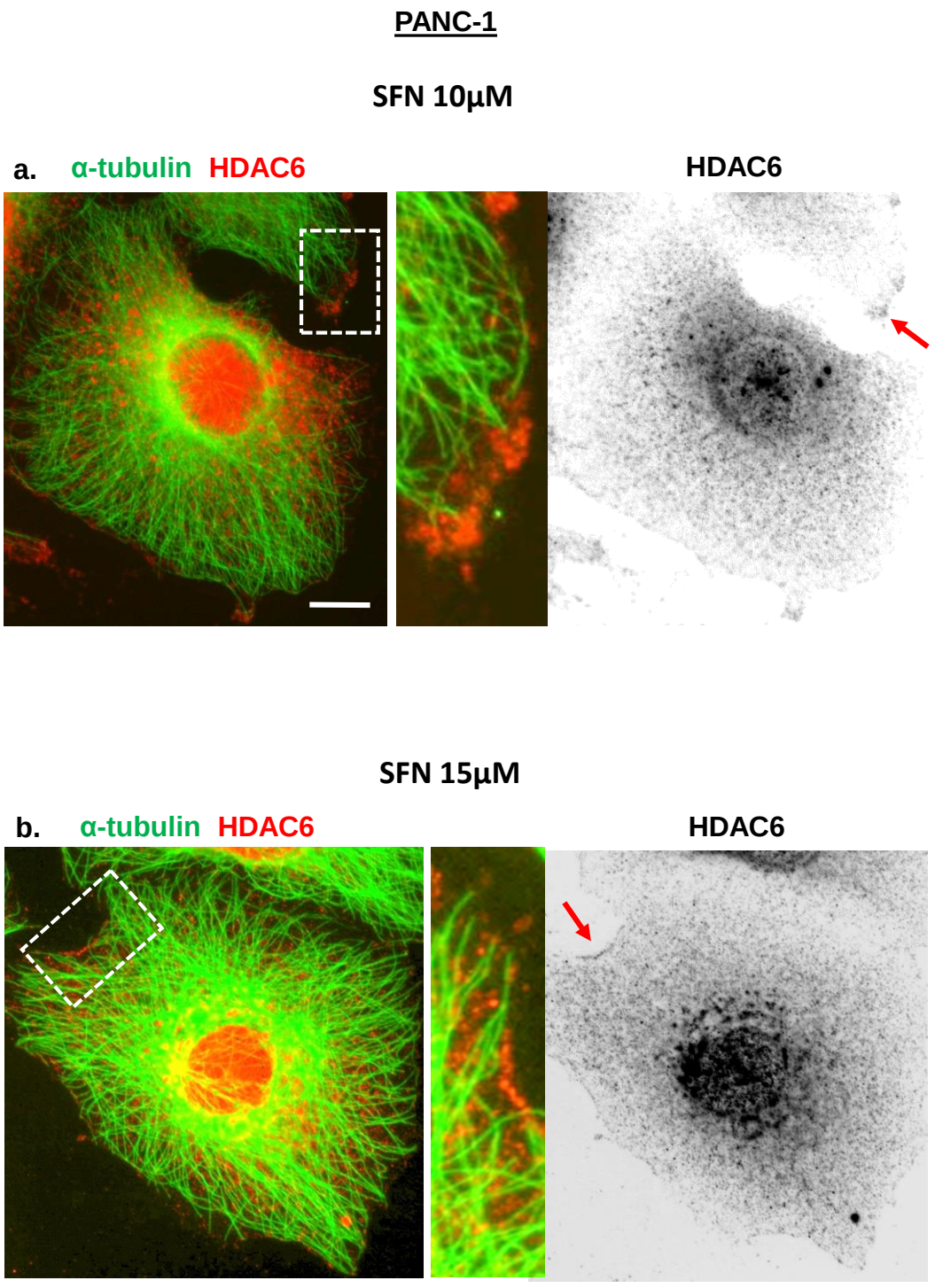

Figure 4.25 HDAC6 localisation in SFN treated PANC-1 cells
Cells were immunolabelled for α-tubulin (green) and HDAC6 (red, invert). The 10 and 15µM SFN treated cells show no association between HDAC6 and microtubules lattice. However, there is some marked accumulation in cell periphery (arrow) and around the nucleus and free in the cytoplasm (boxed region) (a and b). All scale bars = 10µm.

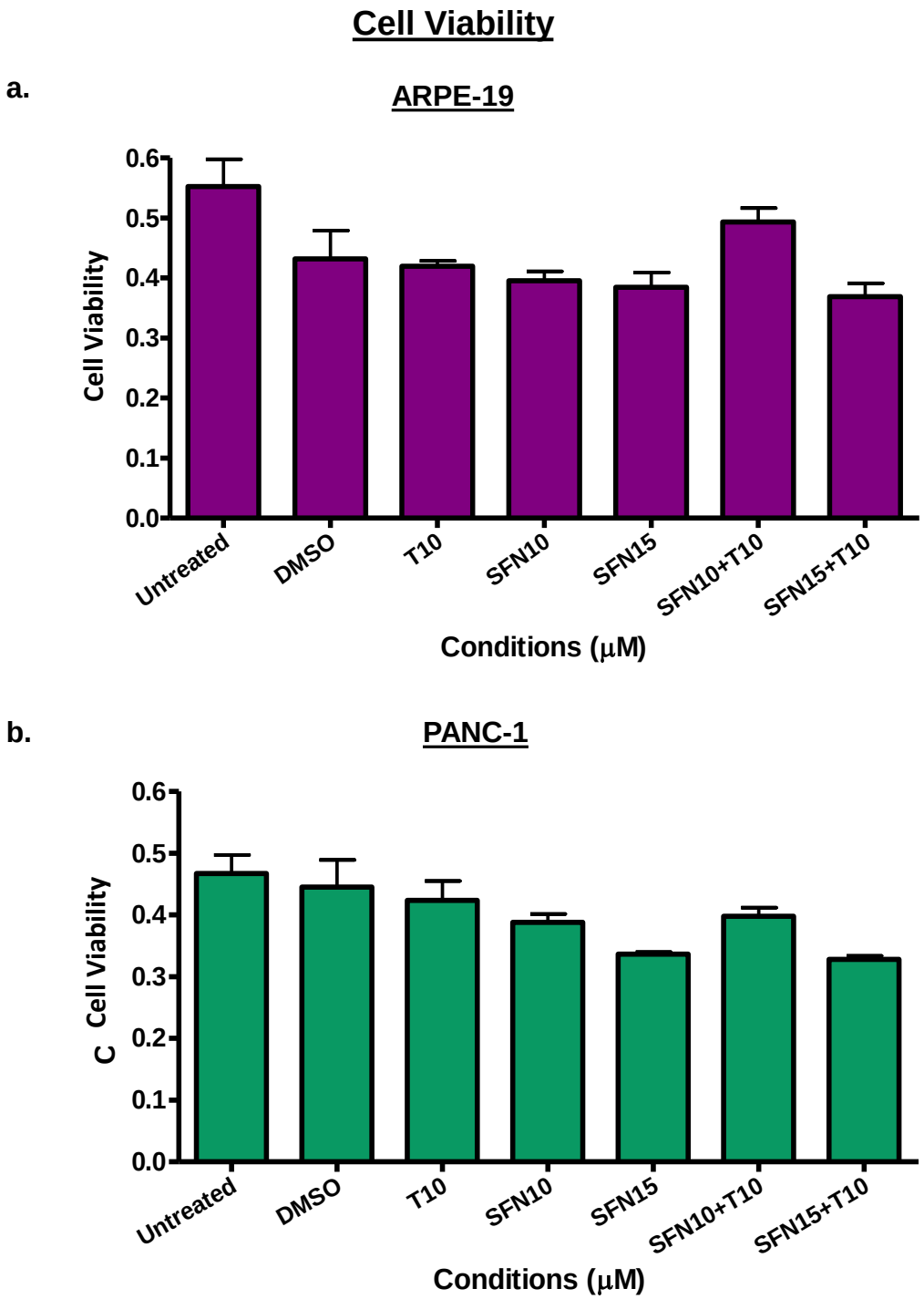

Figure 4.26 Tubacin at 10μM and combination of tubacin and 10μM or 15μM SFN has no significant effect on cell viability in ARPE-19 and PANC-1 cells
Cell viability was examined by MTT assay, which based on the reduction of yellow tetrazole to purple formazan in living cells. The results reveal no Effects on cell viability in 10μM tubacin and a combination with 10μM tubacin and 10μM or 15μM treated ARPE-19 cells (a). 10μM tubacin and combinations of 10μM tubacin and 10μM or 15μM treated PANC-1 cells show no Effects on the cell viability compared to DMSO treated cells and untreated (b). Statistical analysis determined compared to DMSO, using one-way ANOVA with Tukey's multiple comparison test.

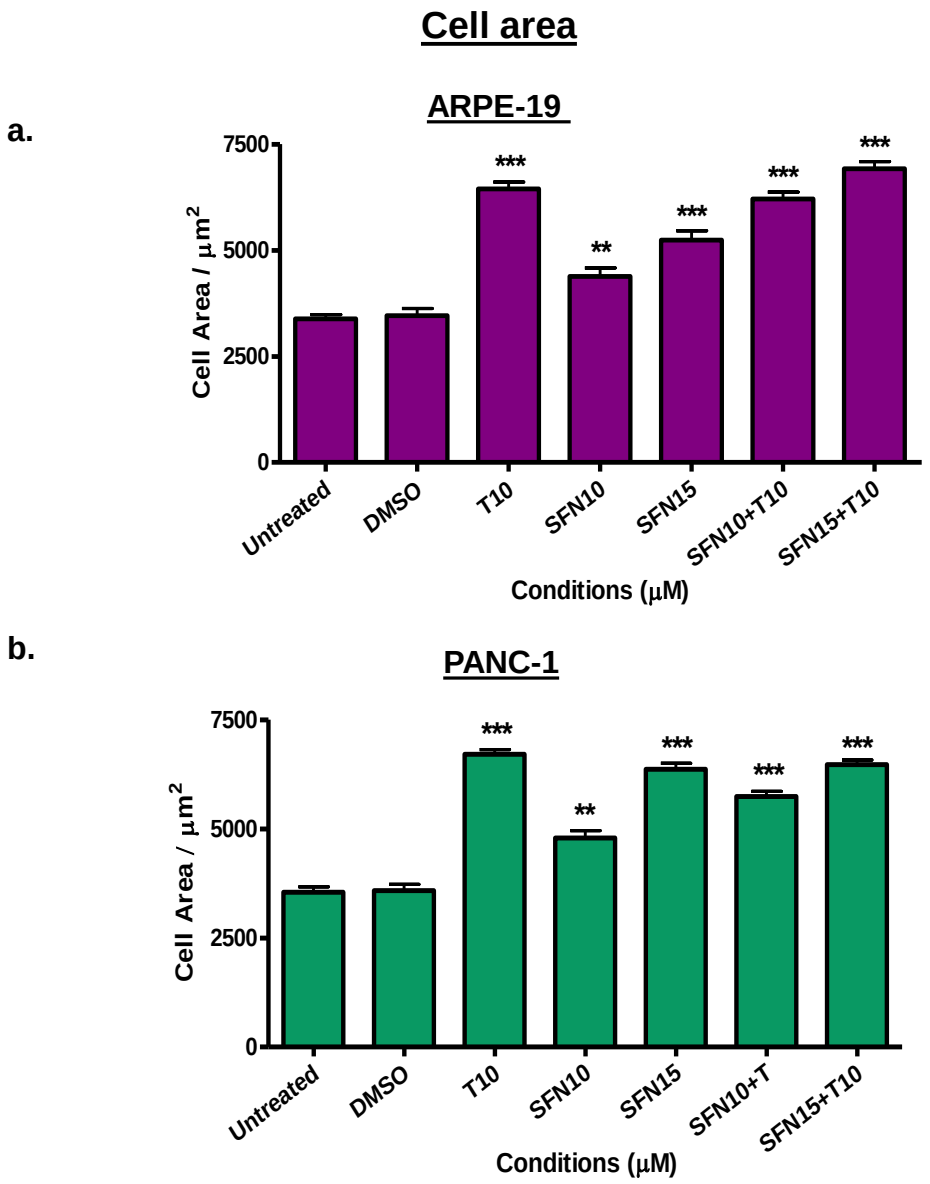

	ARPE-19	PANC-1
T vs 10µM SFN	P<0.001	P<0.001
T vs 15µM SFN	P<0.001	P<0.05
T vs 10µM T + 10µM SFN	P>0.05	P<0.001
T vs 10µM T + 15µM SFN	P>0.05	P>0.05

Figure 4.27 Relative size of ARPE-19 and PANC-1 cells in the absence of active HDAC6

Cells were treated with 10µM tubacin or combination of 10µM tubacin and 10µM or 15µM SFN and incubated for 48 h. Cell area were measured by using image J. Results of both cell lines show that, inhibition HDAC6 by tubacin causes a significant increase in cell area compare to DMSO cell. The combination of tubacin and SFN shows also a significant increase in cell area, as well as with SFN treatment alone. Statistical analysis using one-way ANOVA with Tukey's multiple comparison test, [P<0.00], n=65.

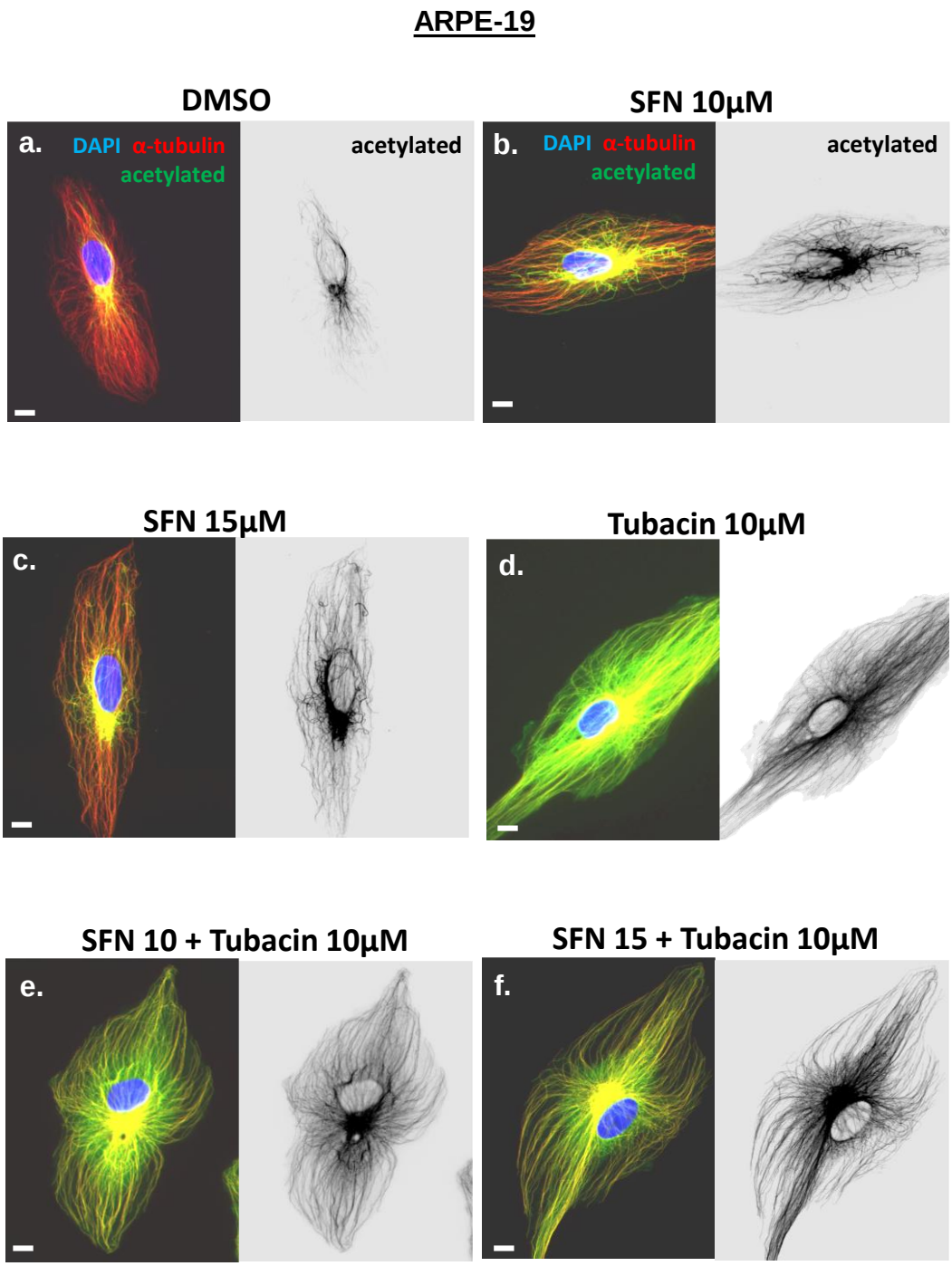

Figure 4.28 The Effects of tubacin on microtubule acetylation in ARPE-19

Cells were stained for acetylated α-tubulin (green, inverted) and α-tubulin (red) DAPI (blue). a) In DMSO treated cell, acetylated α-tubulin is mostly incorporated into scattered microtubule segments. b) In 10µM tubacin treated cell, all microtubules appear acetylated. c) 10µM SFN treated cell shows acetylated microtubules at the central of the cell with some segments near cell periphery. d) 15µM SFN treated cell shows more long segments of acetylated microtubules in the cell body. The combination of tubacin and SFN treatment show all microtubules are acetylated (e-f). Scale bars = 10µm.

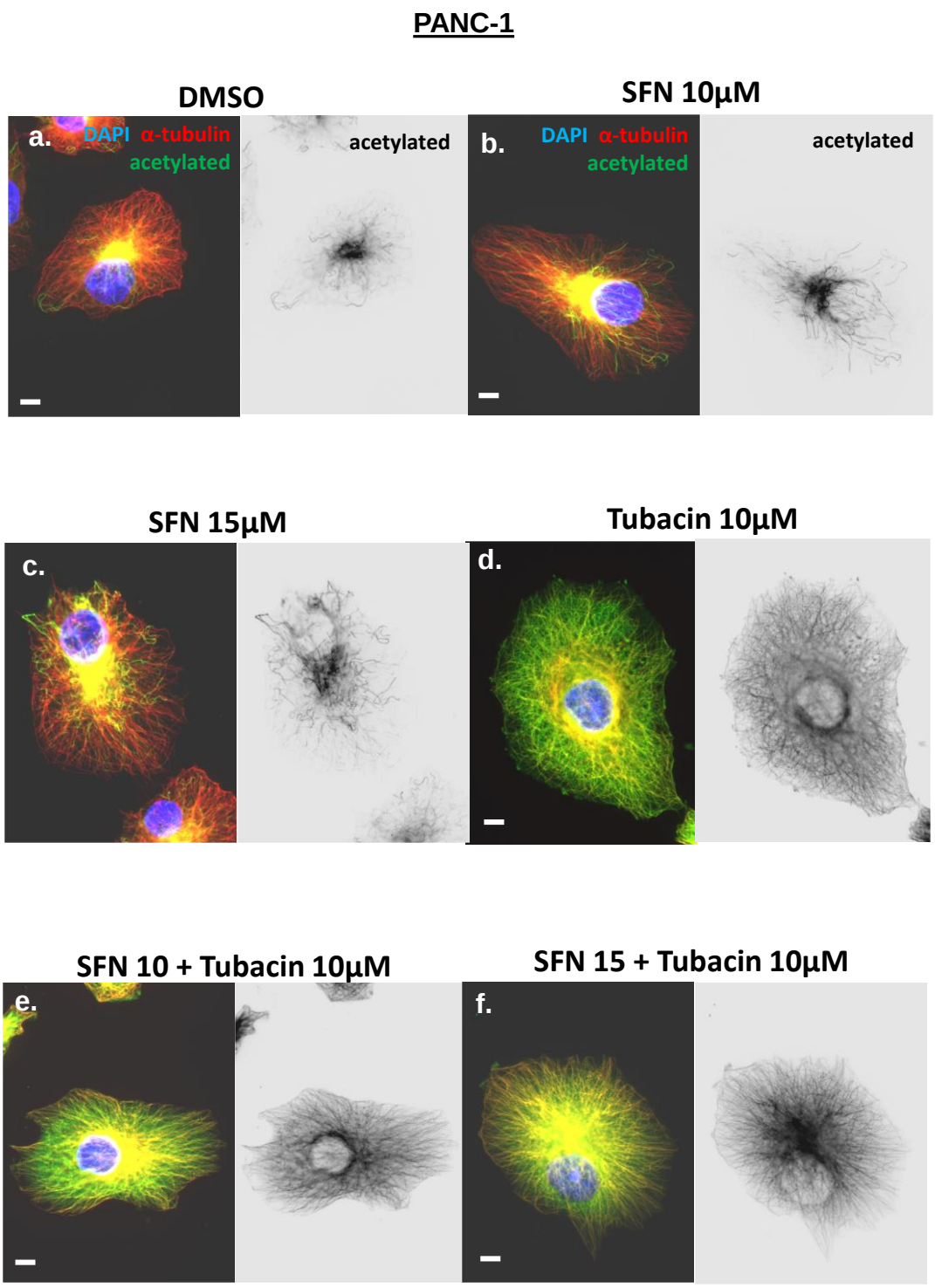

Figure 4.29 The Effects of tubacin om microtubule acetylation in PANC-1

Cells were labelled for acetylated α-tubulin (green, inverted) and α-tubulin (red) DAPI (blue). a) DMSO treated cell shows small segments of acetylated α-tubulin along microtubules. b) 10µM tubacin, treated cell shows that all microtubules consist of acetylated α-tubulin. c) 10µM SFN treated cell shows acetylated microtubules at the centre of the cell with some segments near cell periphery. b) 15µM SFN treated cell shows longer segments of acetylated microtubules. A combination of tubacin and SFN treatment produces acetylated microtubules (e-f). Scale bars = 10µm.

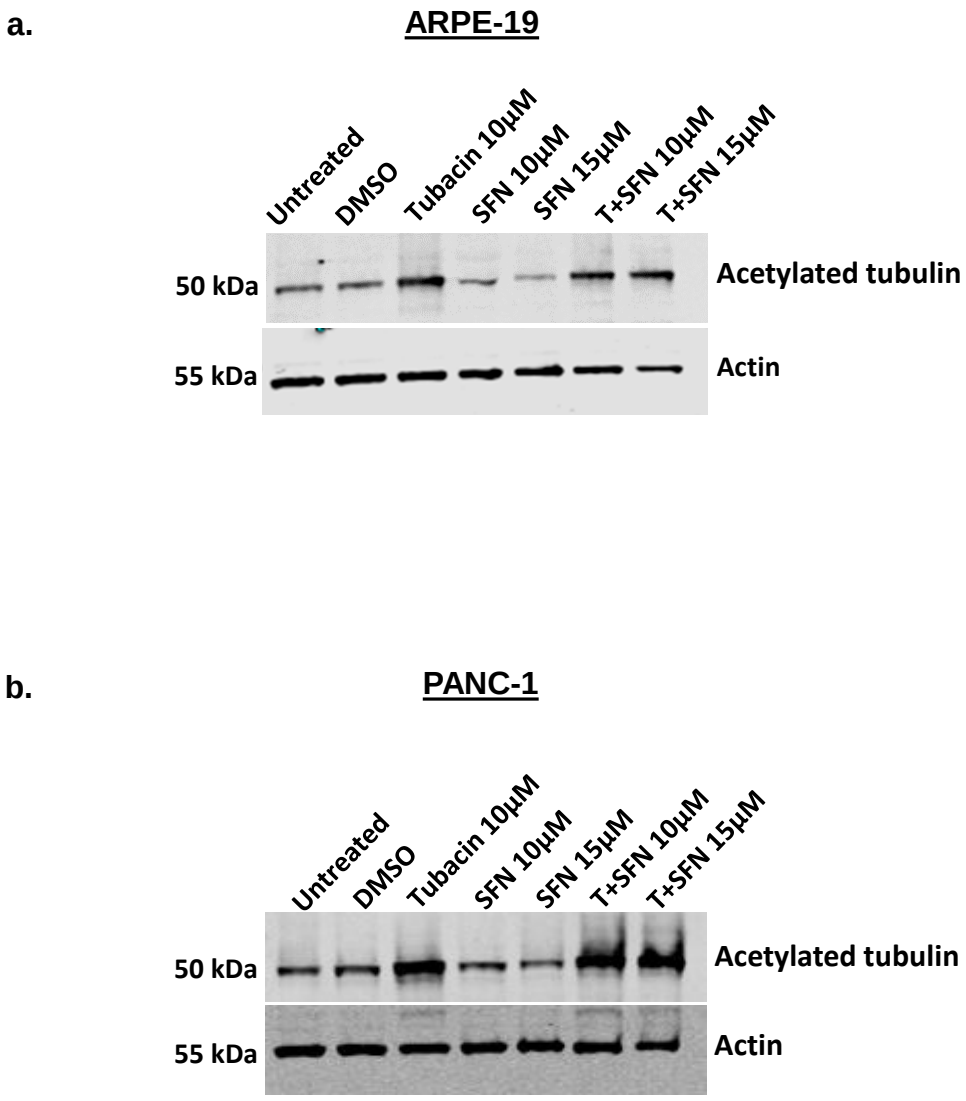

Figure 4.30 The Effects of tubacin and a combination of tubacin and SFN on microtubule acetylation in ARPE-19 and PANC-1 cells

Western blot of lysates was used for untreated, DMSO, tubacin, SFN (10 &15μM), and combination of 10μM tubacin and SFN (10 &15μM). a) ARPE-19 cells show high level of acetylated α-tubulin in 10μM tubucin and in a combination of tubacin and SFN treated cells. The 10 and 15μM SFN treated ARPE-19 cells show a slight reduction in acetylation levels compared to DMSO. b) The 10μM tubacin and a combination of 10μM tubacin and 10μM or 15μM SFN treated PANC-1 cells reveal an increase in the level of expression of acetylated tubulin compared to DMSO treated cells.

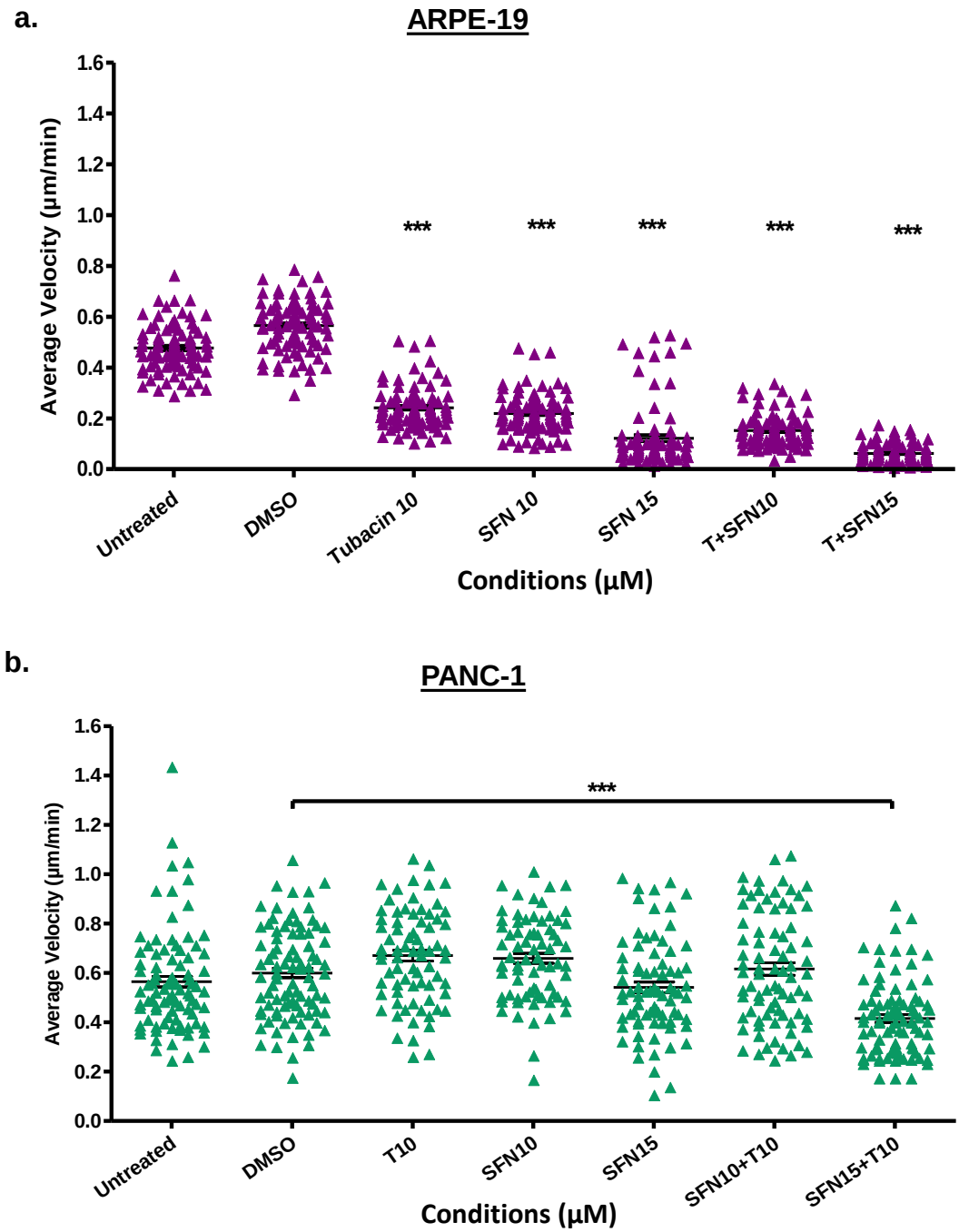

Figure 4.31 A combination of tubacin and SFN causes a reduction in speed of cell migration in ARPE-19 and PANC-1 cells

Cells were treated with tubacin & SFN for 48 h. Cells imaged by widefield time-lapse microscopy for a 16 h period beginning 32 h post initial treatment, with frames taken every 10 minutes. a) The 10µM tubacin, SFN (10 and 15µM), and combinations of 10µM tubcain and 10 or 15µM SFN treated ARPE-19 cells show a significant decrease in the average velocity compared to DMSO treated cells. b) The 10µM tubacin, SFN (10 and 15µM), and combinations of 10µM tubcain and 10µM SFN treated PANC-1 cells reveal no significant decrease in the average velocity compared to DMSO treated cells. The combination of tubacin and 15µM SFN shows a significant reduction in the average cell velocity compared to DMSO treated cells. Significance was assessed by one-way ANOVA with Tukey's multiple comparison test, $P<0.0001$, n=90.

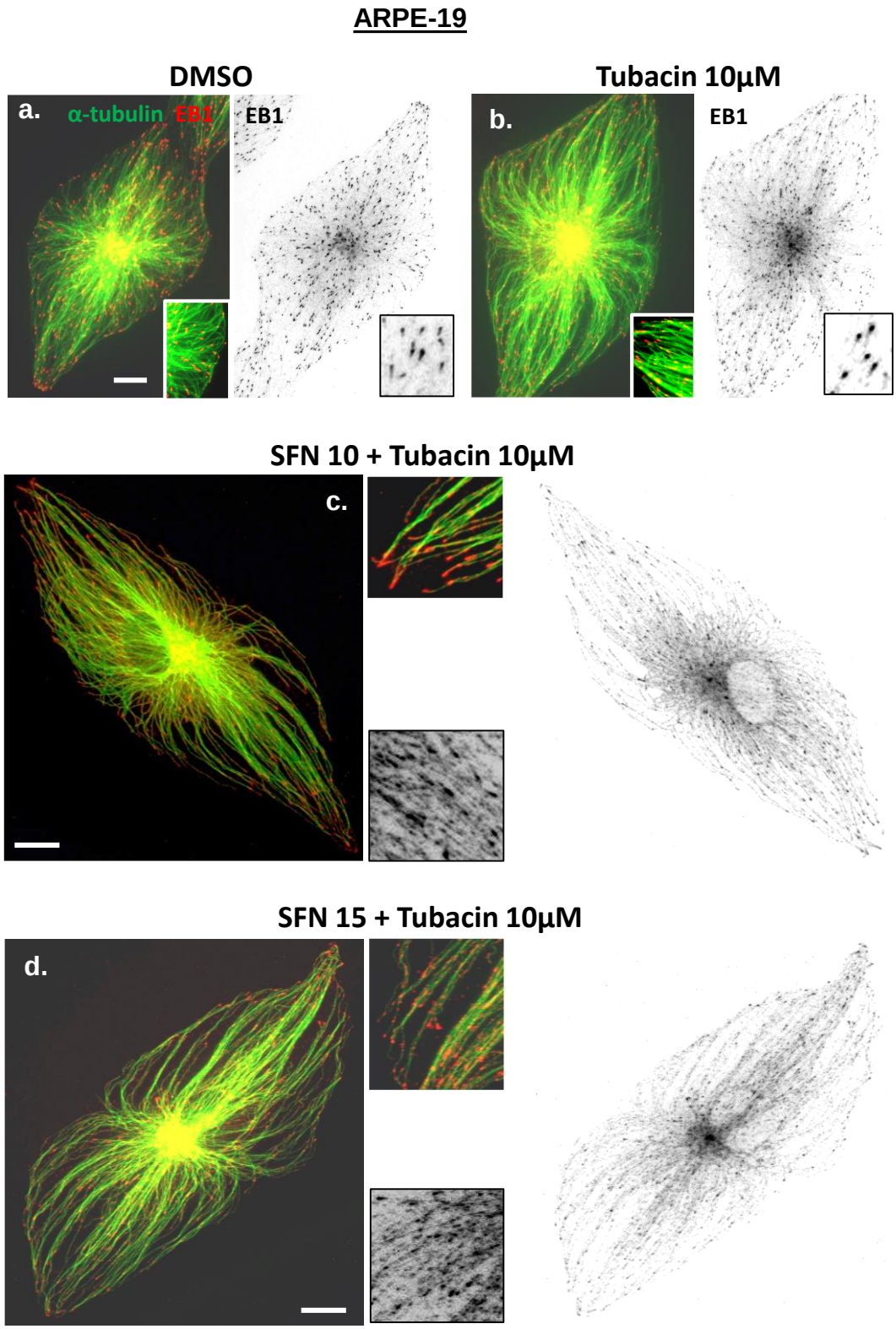

Figure 4.32 EB1 localisation in tubacin and combinations of tubacin and SFN treated ARPE-19 cells

Cells were immunolabelled for microtubules (α-tubulin; green) and EB1 (red, invert). a) EB1 appears as classic comets at plus-ends of microtubules in DMSO treated cells. b) The 10 µM tubacin treated cell shows EB1 at the plus-ends of microtubules as comets (boxed region). A combination of tubacin and SFN treated cells reveals an extensive association between EB1 and microtubules lattice and very few at plus-ends (boxed region) (c and d). Scale bars = 10µm.

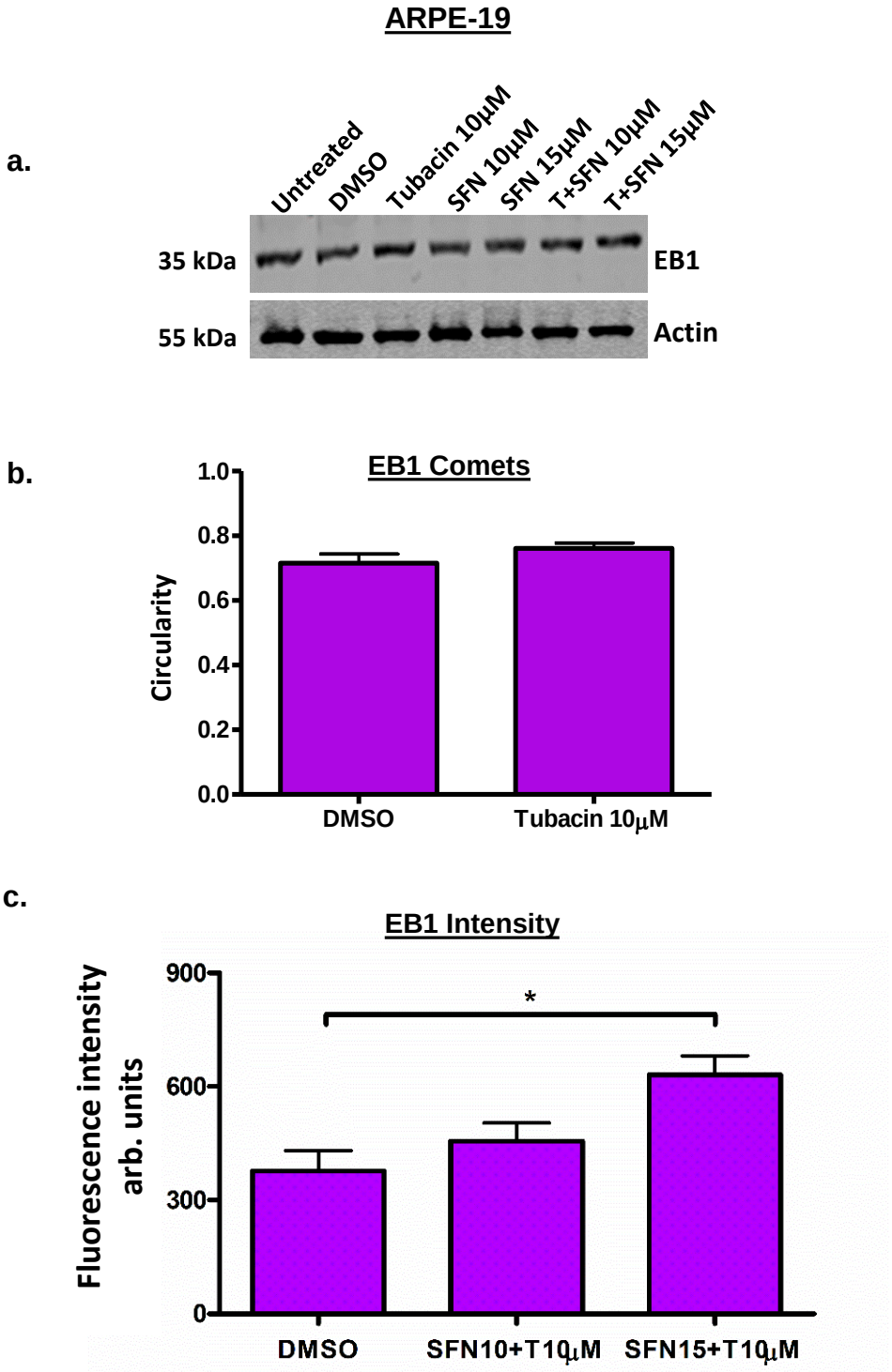

Figure 4.33 EB1 expression and comet analysis in tubacin and in combinations of tubacin and SFN treated ARPE-19 cells

Cells were treated with tubacin and SFN for 48 h. a) Western blot reveals no effect on the levels of EB1 expression in all conditions. b) The analysis of EB1 comet shape shows no significant difference in EB1 comets circularity between DMSO and 10μM tubacin treated cells. c) Fluorescence intensity analysis was used to quantify EB1 lattice association in DMSO, 10μM tubacin and a combination 10μM tubacin and 10 or 15μM SFN. Results show a significant increase in EB1 intensity in 10μM tubacin and 15μM SFN treated cells compared to DMSO treated cells. One-way ANOVA with Tukey's multiple comparisons test, $P<0.01$.

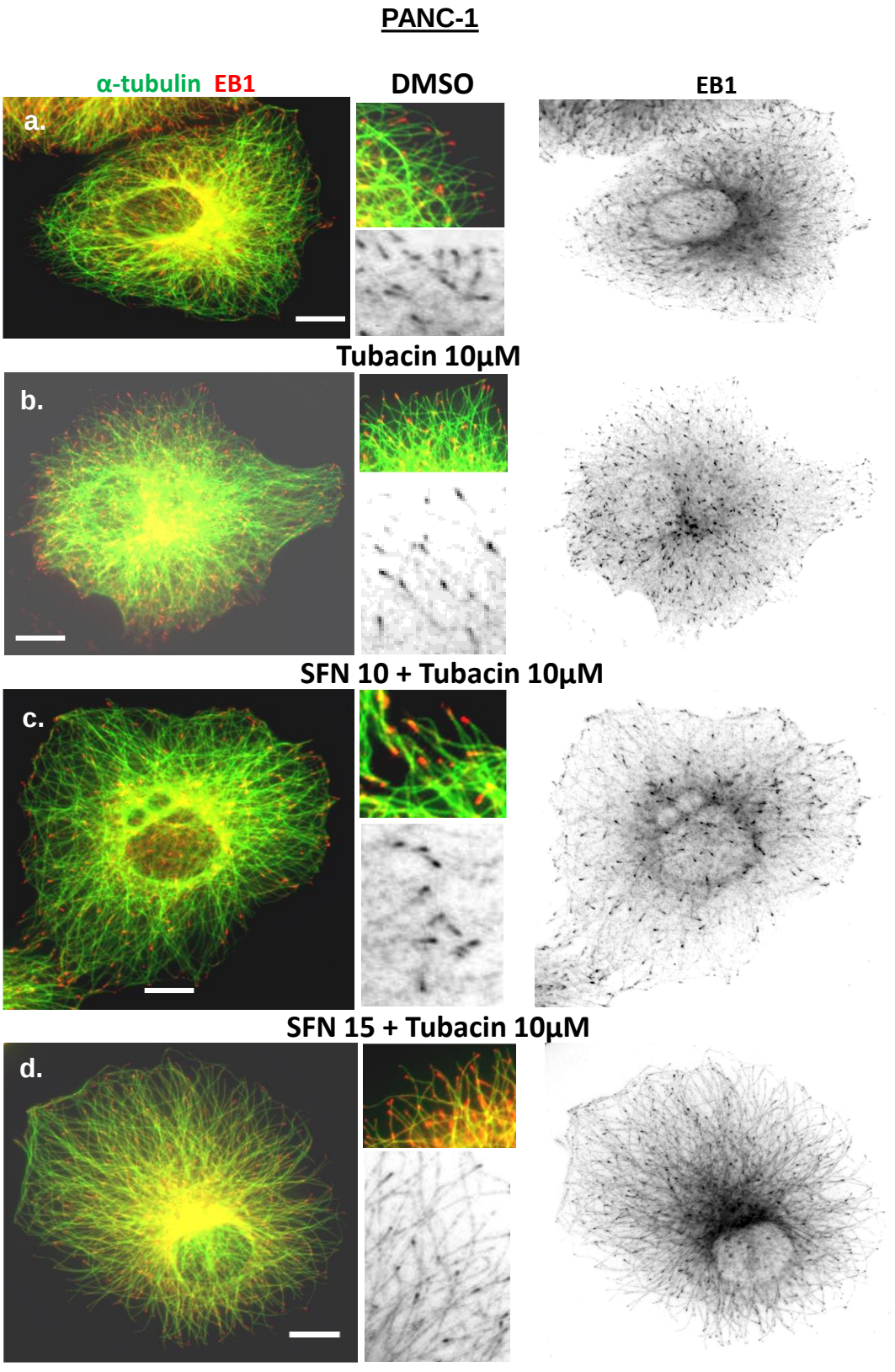

Figure 4.34 EB1 localisation in tubacin treated PANC-1 cells
Cells were immunolabelled for microtubules (α-tubulin; green) and EB1 (red, invert). a) In DMSO treated cells, EB1 appears as classic comets at plus-ends of microtubules. b) The 10 µM tubacin treated cell shows EB1 at plus-end of microtubules (boxed region), as well in tubacin &10µM SFN (c). d) A combination of 10µM tubacin and 15µM SFN treated cell reveals EB1 associated extensively along microtubules lattice (boxed region). Scale bars=10µm.

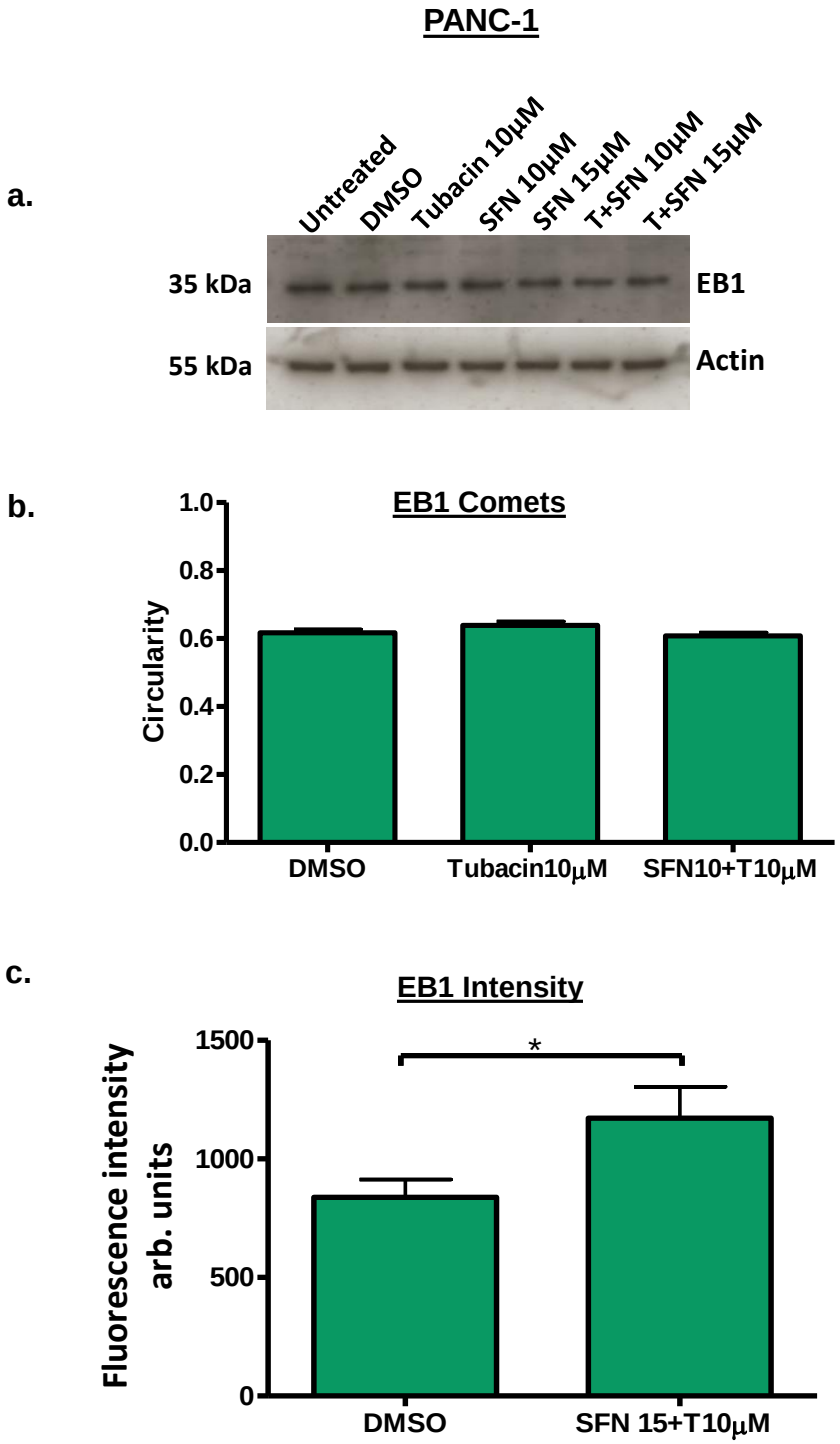

Figure 4.35 EB1 expression and comets analysis in tubacin and in combinations of tubacin and SFN treated PANC-1 cells

Cells were treated with tubacin and SFN for 48 h. a) Western blot reveals no marked Effects on the levels of EB1 in all conditions. b) The analysis of EB1 comets shape shows no significant difference in EB1 comet circularity between all conditions. c) Fluorescence intensity analysis was used to quantify EB1 lattice association in DMSO treated cells and a combination 10μM tubacin and 15μM SFN. Results show a significant increase in intensity compared to DMSO treated cells, $P<0.01$. One-way ANOVA with Tukey's multiple comparisons test.

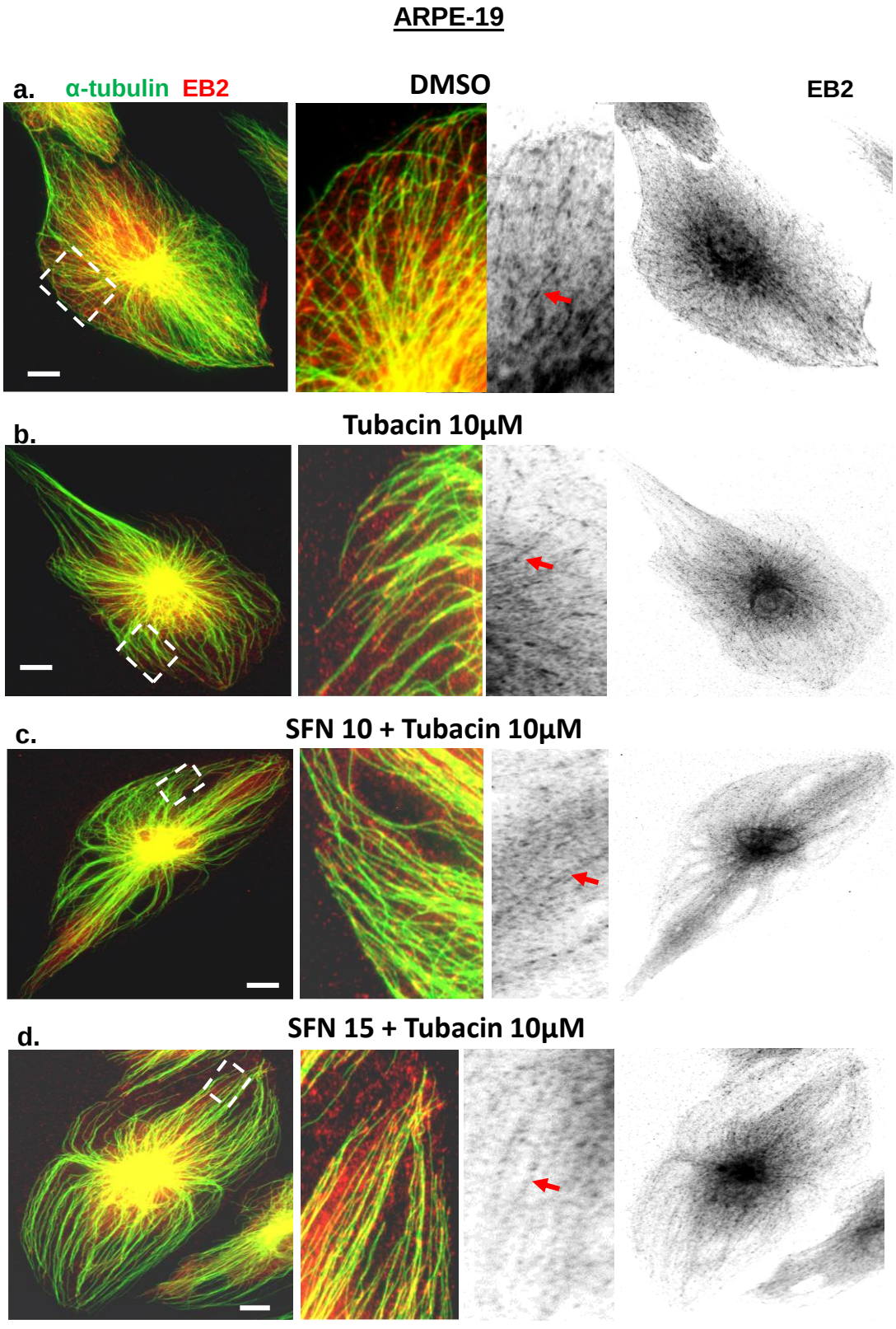

Figure 4.36 EB2 localisation in tubacin treated ARPE-19 cells
Cells were immunolabelled for α-tubulin (green) and EB2 (red, invert). a) DMSO treated cell shows EB2 along microtubules lattice (arrow) and at the cytoplasm (boxed region). b) 10µM tubacin treated cell shows some EB2 along the lattice and at the cytoplasm (arrows and boxed region). 10µM tubacin and 10µM or 15µM SFN treated cells reveal EB2 mainly in the cytoplasm with few EB2 along the lattice (arrows) (c and d) (boxed region). All scale bars = 10µm.

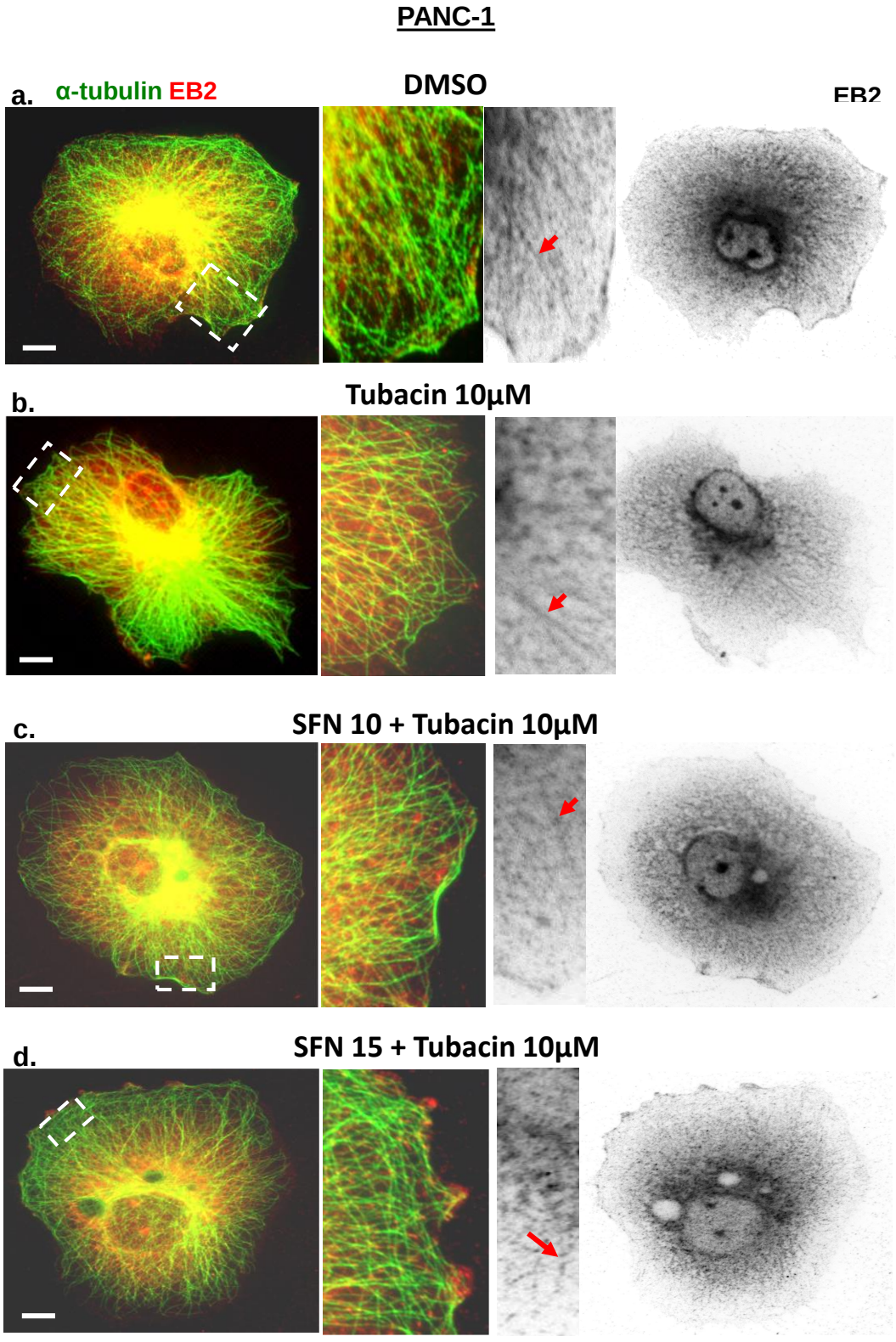

Figure 4.37 EB2 localisation in tubacin treated PANC-1 cells
Cells were immunolabelled for α-tubulin (green) and EB2 (red, invert). a) DMSO treated cell shows EB2 along microtubules lattice and at the cytoplasm (arrows and boxed region). b) 10µM tubacin treated cell shows EB2 along the lattice and with some in the cytoplasm (arrows and boxed region). 10µM tubacin and 10µM or 15µM SFN treated cells reveal EB2 mainly in the cytoplasm with few EB2 along the lattice (c and d) (arrows and boxed region). All scale bars = 10µm.

PANC-1

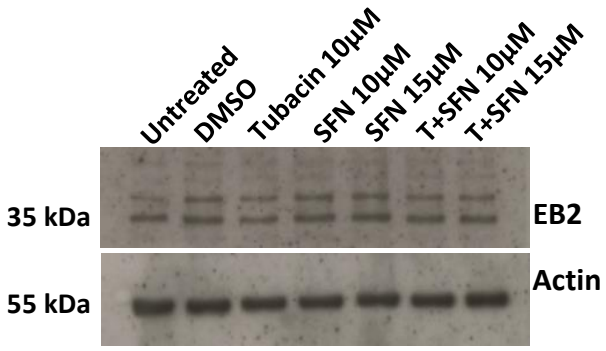

Figure 4.38 EB2 expression in tubacin treated PANC-1 cells
Western blots of PANC-1 lysates for 10μM tubacin and 10μM tubacin and 10μM or 15μM SFN. Result shows no changes on the level of EB2 expression in a combination of 10μM tubacin and 10μM or 15μM SFN treated cells, and also in 10 or 15μM SFN treated cells compared to DMSO treated cells.

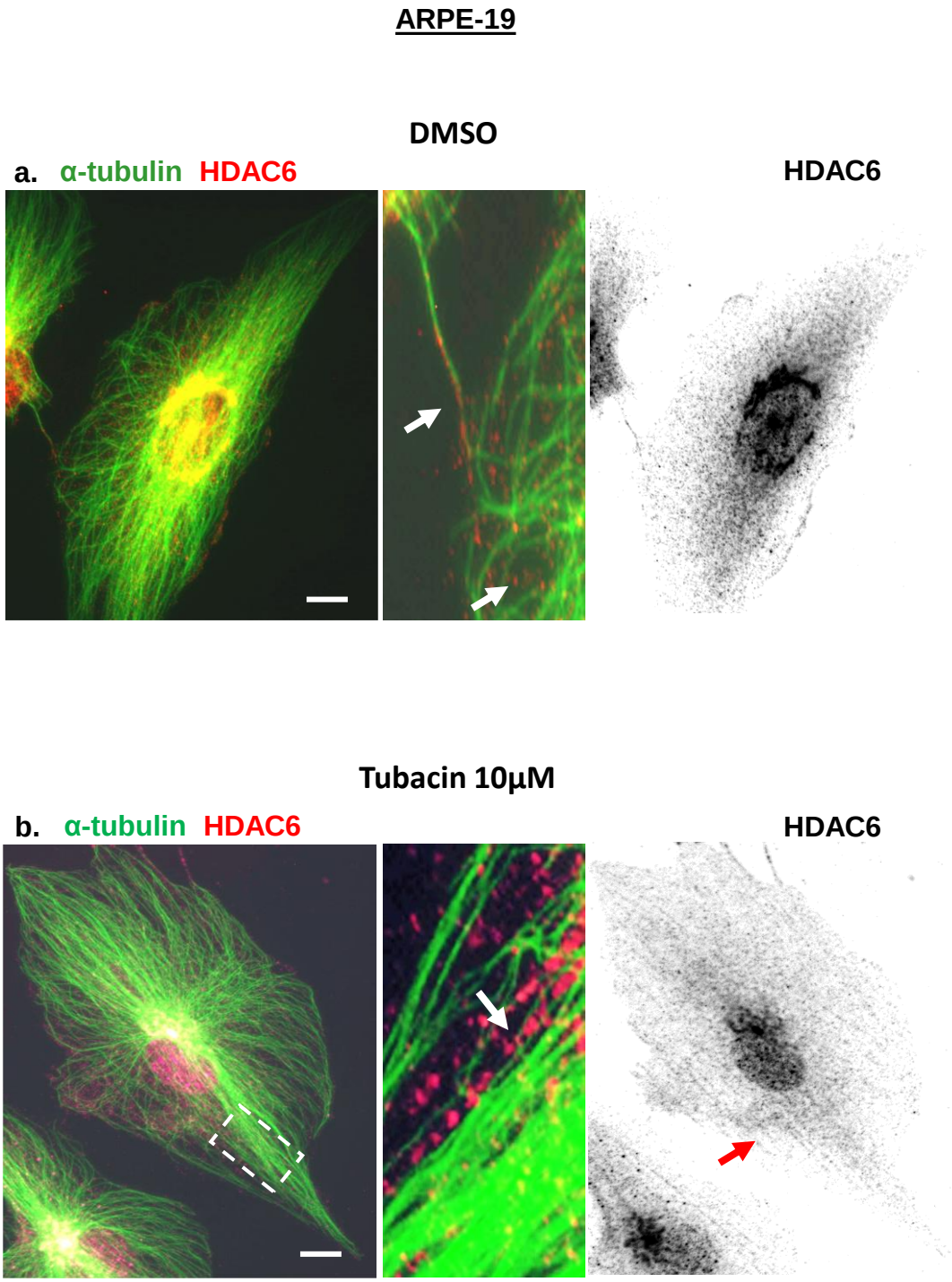

Figure 4.39 HDAC6 localisation in tubacin treated ARPE-19 cells
Cells were immunolabelled for α-tubulin (green) and HDAC6 (red, invert). a) DMSO treated cell shows HDAC6 localised in the cytoplasm (arrow) with some along microtubules lattice (arrow) and around the nucleus. b) 10µM tubacin treated cell shows no co-localisation between HDAC6 and microtubules, with HDAC6 arranged in filaments-like organisation in the cytoplasm (arrows) and around the nucleus. All scale bars = 10µm.

ARPE-19

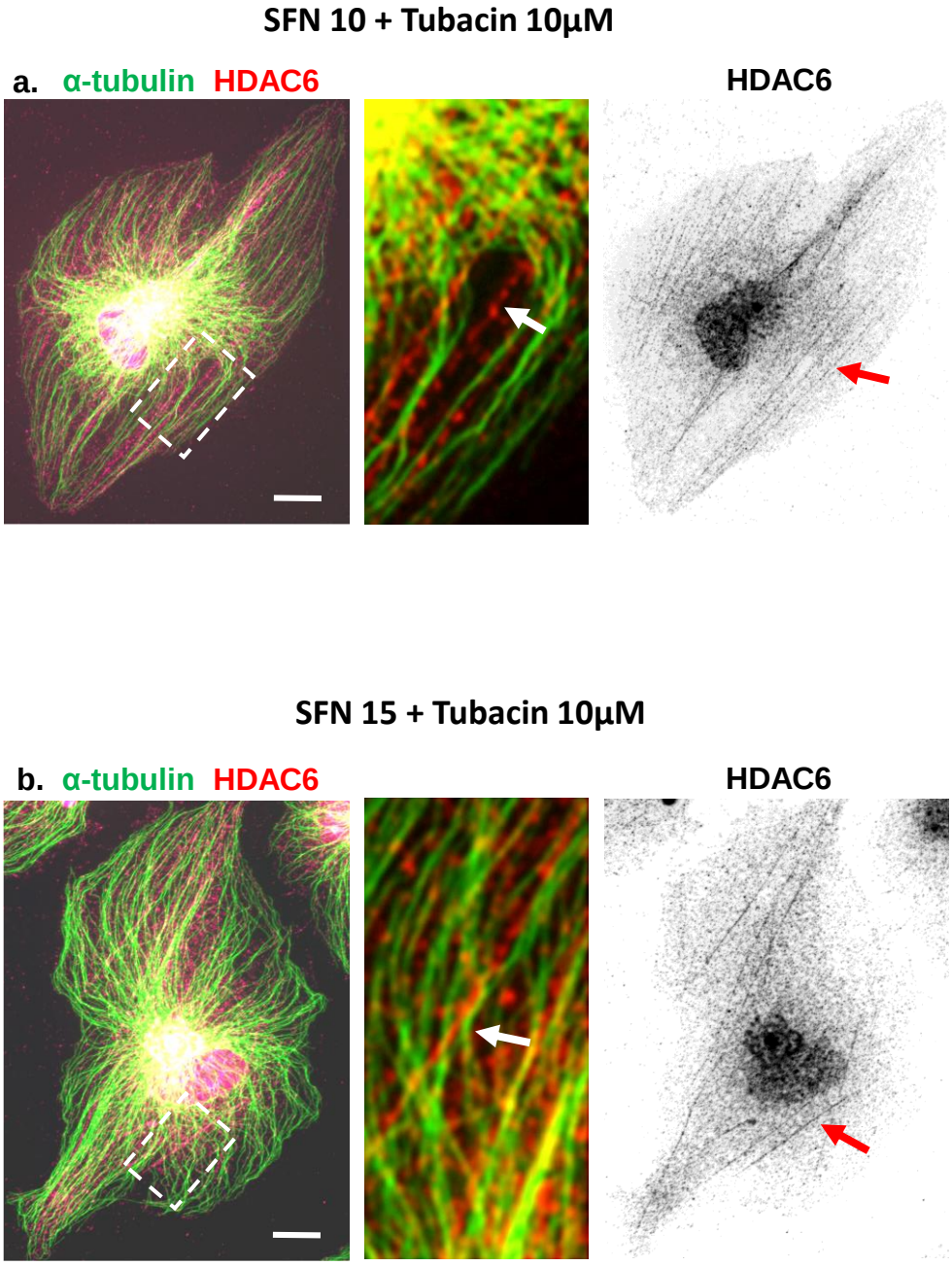

Figure 4.40 HDAC6 localisation in tubacin treated ARPE-19 cells
Cells were immunolabelled for α-tubulin (green) and HDAC6 (red, invert). 10µM tubacin and 10µM or 15µM SFN treated cells reveal HDAC6 arranged in filament-like structure in the cytoplasm (arrows) and around the nucleus but with no co-localisation with microtubules (arrows and boxed region) (a & b). All scale bars = 10µm.

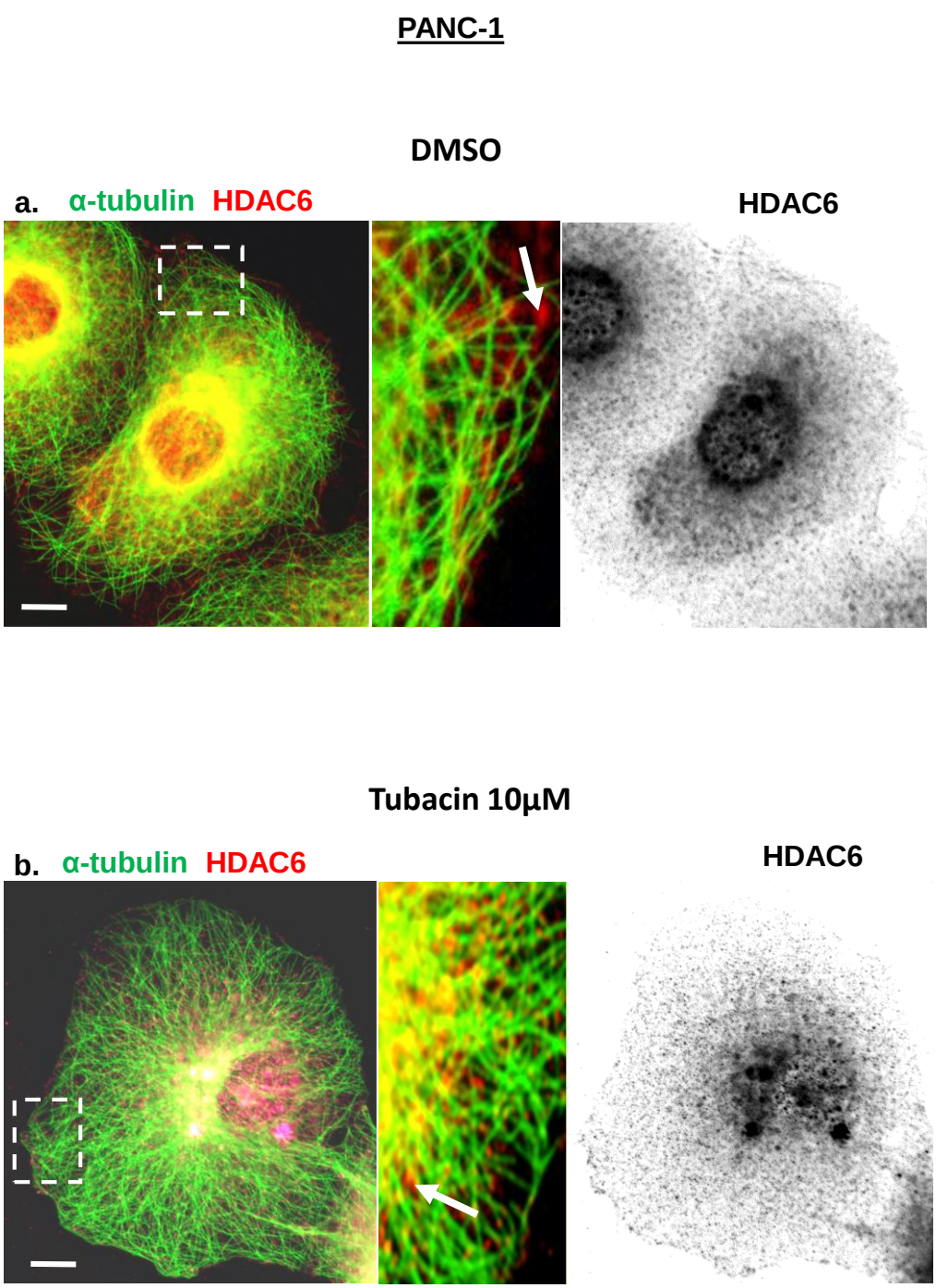

Figure 4.41 HDAC6 localisation in tubacin treated PANC-1 cells
Cells were immunolabelled for α-tubulin (green) and HDAC6 (red, invert). a) DMSO treated cell shows diffuse HDAC6 in the cytoplasm (arrow) and around the nucleus with no co-localisation between HDAC6 and microtubules (boxed region). 10µM tubacin treated cell reveals no co-localisation between HDAC6 and microtubules with most of HDAC6 in the cytoplasm (arrows and boxed region). All scale bars = 10µm.

PANC-1

SFN 10 + Tubacin 10µM

a. **α-tubulin** **HDAC6** **HDAC6**

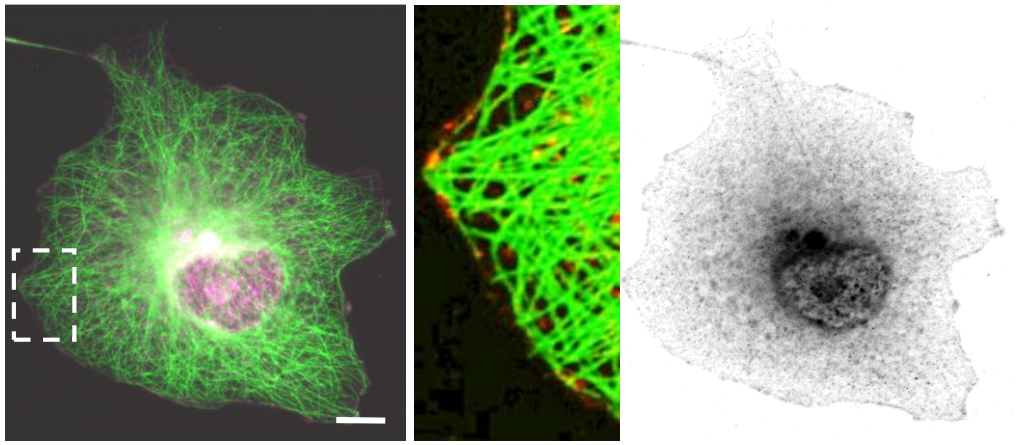

SFN 15 + Tubacin 10µM

b. **α-tubulin** **HDAC6** **HDAC6**

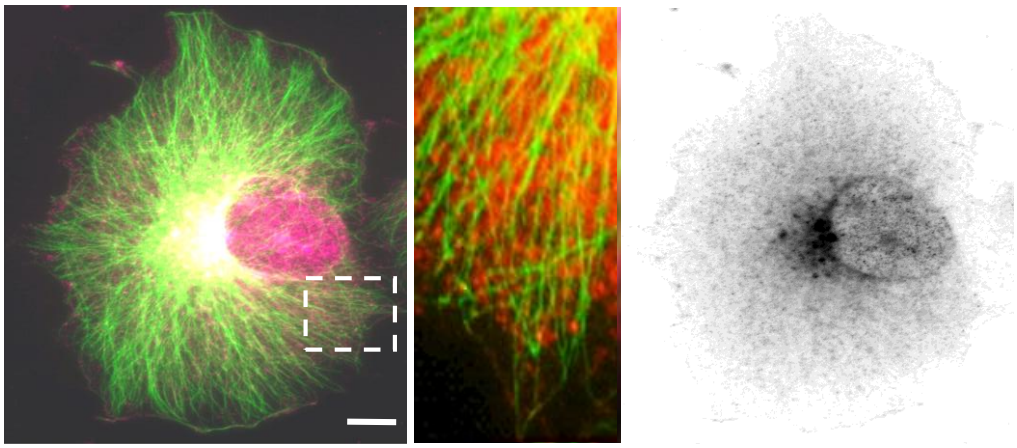

Figure 4.42 HDAC6 localisation in tubacin treated PANC-1 cells
Cells were immunolabelled for α-tubulin (green) and HDAC6 (red, invert). 10 µM tubacin with 10 µM or 15 µM SFN treated cells reveal HDAC6 was mainly dispersed in the cytoplasm with some concentrated around the nucleus and cell periphery. There is no co-localisation between HDAC6 and microtubules (boxed region). All scale bars = 10µm.

Chapter V: Sulforaphane Treatment and Microtubule Dynamics and Stability

5.1 Overview

The purpose of this chapter is to investigate microtubule dynamics and stability in SFN-treated cells and to determine whether treatment can affect focal adhesion dynamics and turnover. This chapter starts by introducing what is already known about the effect of SFN on microtubule dynamics and focal adhesion dynamics in cancer cells. Then, start presents the effect of SFN on acetylation and detyrosination, microtubule stability and cold treatment. In addition, this chapter shows the effect of SFN on microtubule dynamics and focal adhesion turnover. Finally, the chapter ends with a summary and discussion of the results.

5.2 Introduction

The dynamic instability of microtubules enables cells to rapidly reorganise the microtubule cytoskeleton into various cellular patterns that suit particular functions, such as cell polarisation, cell division and migration (Mitchison and Kirschner, 1984, Gelfand and Bershadsky, 1991, Howard and Hyman, 2003, Hawkins et al., 2010). This instability is an essential behaviour of microtubule subunits, which are heterodimers of α/β-tubulin, and is regulated by a multitude of microtubule-associated proteins. Some of these proteins accumulate at the growing end of microtubules, while others bind along the microtubule lattice (Valiron et al., 2001, Heald and Nogales, 2002, Burbank and Mitchison, 2006, Nogales and Wang, 2006). For example, plus-end-tracking proteins, such as EB1, APC, CLIP 170, CLASP, and dynactin complex, play important roles in regulating microtubule dynamics (Akhmanova et al., 2001, Akhmanova and Hoogenraad, 2005, Patel et al., 2012, Akhmanova and Steinmetz, 2015, Nehlig et al., 2017). These +TIPs can also influence microtubule interaction with other cellular structures, such as actin,

and focal adhesions (Kaverina et al., 2002, Mimori-Kiyosue et al., 2005, Chhabra and Higgs, 2007).

The post-translation modification of tubulin is an important mechanism via which microtubule dynamics are controlled. It allows microtubules to assume distinct properties and roles within the overall network (Verhey and Gaertig, 2007, Garnham and Roll-Mecak, 2012, Yu et al., 2015). Generally, there are two distinct populations among undifferentiated cells during interphase: the majority are tyrosinated, and a small and distinct subset are detyrosinated (Gundersen et al., 1984). Tyrosinated microtubules are mostly dynamic, while detyrosination has been linked to stable long-lived microtubules and is used as a marker for microtubule stability. The removal of tyrosine (Glu-Tur) from the C-terminal of α-tubulin occurs on the outer surface of the microtubules (Gundersen et al., 1984, Webster et al., 1987, Bulinski and Gundersen, 1991). Acetylation is another type of tubulin modification, which occurs on lysine 40, located in the luminal face of the microtubule (L'Hernault and Rosenbaum, 1985, Bulinski and Gundersen, 1991, Janke and Bulinski, 2012). The exact effects of tubulin acetylation are still not fully understood, but it most commonly associated with stable microtubules. Acetylation is reversible, and there are two types of microtubule deacetylase, HDAC6 (Hubbert et al., 2002) and SIRT2, which can function independently (North et al., 2003).

Tubulin undergoes modifications when polymerised into microtubules, and the reversible reaction occurs mainly in depolymerised microtubule subunits (Westermann and Weber, 2003). Therefore, several types of post-translational tubulin modifications accumulate in stable (long-lived) microtubules (Hammond et al., 2008). It was further shown that tyrosine residues in tubulin play a vital role in recruiting certain proteins to the plus-end of microtubules, such as CLIP-170 and $p150^{Glued}$, which are known to help regulate microtubule dynamics. Therefore, detyrosination affects microtubule behaviour by altering the affinity of microtubules to specific proteins that regulate their dynamics and stability

(Akhmanova et al., 2001, Akhmanova and Hoogenraad, 2005). Similarly, the acetylation of tubulin has been utilised to identify stable microtubules because it leads to reduced microtubule dynamics (Piperno et al., 1987, Webster and Borisy, 1989). Moreover, it has been reported that acetylation can affect the binding of microtubules to certain motor proteins, such as kinesin-1 (Reed et al., 2006, Dompierre et al., 2007, Janke and Bulinski, 2011, Garnham and Roll-Mecak, 2012). At the same time, other studies have shown that the acetylation of tubulin does not affect microtubule dynamics (Haggarty et al., 2003, Palazzo et al., 2003, Zhang et al., 2008, Asthana et al., 2013). In neurones, it has been suggested that acetyltransferase and the acetyltransferase complex can acetylate tubulin (Creppe et al., 2009). It is not clear whether this is the case in ARPE-19 and PANC-1. Meanwhile, the molecules that facilitate the reverse reaction, deacetylation, which include HDAC6 and SIRT2 (class III NAD-dependent histone deacetylase), have been identified in several studies (Hubbert et al., 2002, Matsuyama et al., 2002, North et al., 2003, Zhang et al., 2003).

One of the main questions in this project is whether SFN can inhibit microtubule dynamics and increase stability. It has been suggested that SFN can suppress microtubule dynamic instability and decrease turnover in various cancer cells, such as human breast cancer cells, affecting individual growth and shrinkage rates (Azarenko et al., 2008). However, prior dynamic instability analysis was only based on four microtubules (Azarenko et al., 2008). Additionally, SFN treatment leads to changes in post-translational tubulin modifications, including increased tubulin acetylation. Concentrations ≥15 μM SFN promotes acetylated tubulin in human breast cancer and prostate cancer cells. Meanwhile, concentrations ≥ 50 μM SFN in human breast cancer cells showed completely depolymerised microtubules (Azarenko et al., 2008, Gibbs et al., 2009, Clarke et al., 2011). Interestingly, a recent study by Dickinson (2014) showed that 15 μM SFN decreased the level of

acetylated tubulin; this was observed *in vitro* in SFN-treated human skin keratinocytes (HaCaT) after 48 hours of incubation (Dickinson et al., 2015).

Cell migration is a vital process for wound healing, developmental morphogenesis and tumour metastasis. This process requires the combined activities of the cytoskeleton, cell membrane and extracellular matrix (ECM) (Lauffenburger and Horwitz, 1996, Rodriguez et al., 2003). Focal adhesions are organelles that play an important role in cell migration. Focal adhesion disassembly requires dynamic microtubules, where microtubules have been observed at peripheral focal adhesions and contribute to promote adhesion disassembly (Kaverina et al., 2002). Focal adhesion site enlarged when microtubules were disassembled by nocodazole, which means that dynamic microtubules are crucial for focal adhesion disassembly (Kaverina et al., 2002, Krylyshkina et al., 2002). Additionally, it has been shown that ACF7 regulates focal adhesion dynamics, with the absence of ACF7 leading to stabilised actin filaments and a focal adhesion network, and preventing the targeting of microtubules along actin filaments reaching to focal adhesion sites (Wu et al., 2008). Recent studies have shown that dynamic microtubules can increase focal adhesion turnover by delivering proteins that are essential for disassembly. This occurs via the interaction of kinase kinase kinase kinase 4 (MAP4K4, disassembly protein) and EB2. The knockout of MAP4K4 stabilises focal adhesion and impairs cell movement (Yue et al., 2014).

One important aspect of the phenotype observed following SFN treatment in ARPE-19 cells was the apparent reorganisation of microtubules into bundles that were co-aligned with actin filaments (Chapter 4). The appearance of microtubules bundles in cells is indicative of stabilised microtubules, suggesting that SFN may be involved in influencing the stability of the microtubule population. Stable microtubules have been correlated with an accumulation of post-translational tubulin modifications, such as acetylation and detyrosination. It has been shown that SFN treatment alters post-translational tubulin modifications, increasing

tubulin acetylation and stable microtubules. This was also observed in breast cancer and prostate cancer cells (Azarenko et al., 2008, Clarke et al., 2011). Therefore, it is important to analyse acetylation and detyrosination level and expression in SFN treated ARPE-19 and PANC-1 cells.

Another essential change noted in cells treated with SFN was a significant increase in cell area with a dramatic decrease in ARPE-19 cell migration (Chapter 4). Successful cell migration requires a balance between stable and dynamic microtubules and dynamic focal adhesion, with dynamic microtubules contributing to the regulation of focal adhesion dynamics and turnover (Kaverina et al., 2002). Thus, any decrease in microtubule dynamics leads to a change in the state of focal adhesion turnover, which leads to reduced cell migration and increases cell area. It is therefore important to study focal adhesion dynamics and turnover in SFN treated cells and determine whether SFN induced changes in microtubules have dramatic effects on cell migration and whether the increase in the area of cells treated with SFN is associated with changes in focal adhesion dynamics and turnover.

5.3 Results

5.3.1 SFN treated ARPE-19 but not PANC-1 cells express more acetylated microtubules

ARPE-19 and PANC-1 cells were grown on glass coverslips and treated with 10 or 15 µM SFN for 48 hours, with DMSO being used as a control, and then fixed with -20^{o} C methanol for five minutes. Cells were then immunolabelled for acetylated tubulin and α-tubulin. DMSO and SFN treated ARPE-19 cells expressed acetylated tubulin. The DMSO treated ARPE-19 cells revealed few acetylated microtubules around the centre of the cell, with only small acetylated segments along these microtubules, which was similar to the results for the untreated ARPE-19 cells (Figure 5.1). However, the 10 µM and 15 µM SFN treated ARPE-19 cells showed prominent acetylation along the length of other curly microtubules extending from the centre of the cell towards the cell periphery, where curly microtubules are commonly observed with acetylated microtubules. Distinct bundles of acetylated microtubules were also evident in the 15 µM SFN treated ARPE-19 cells (Figure 5.1). The amount of acetylated tubulin as a percentage of total tubulin in ARPE-19 cells was accessed following SFN treatment was analysed using ImageJ. Ten immunolabeled cells for acetylated tubulin and α-tubulin were used for this analysis (as described in 2.10). The 10 µM and 15 µM SFN treated ARPE-19 cells revealed a significant increase in the total area of acetylated microtubules as compared to DMSO treated cells (Figure 5.2, a). Western blot suggested that there was a slight increase in the level of acetylated tubulin expression in 10 µM and 15 µM SFN treated ARPE-19 cells compared to DMSO treated cells (Figure 5.2, b).

This marked increased in acetylated microtubules suggests an increase in microtubule stability. This was tested in SFN treated ARPE-19 cells via cold treatment. The incubation of cells on ice causes depolymerisation of microtubules

with only stable microtubules being resistant to the cold and remaining polymerised. The incubation of DMSO treated cells on ice for 15 minutes showed that most of microtubules had depolymerised. In contrast, 10 µM SFN treated ARPE-19 cells revealed a marked number of stable microtubules, and 15 µM SFN treated ARPE-19 cells showed a further increase in number of stable microtubules. These remaining microtubules were resistant to cold and thus more stable (Figure 5.3).

In PANC-1 cells, acetylated tubulin was also observed in DMSO and SFN treated cells. DMSO treated cells showed a few acetylated microtubules concentrated in the cell centre and along small subsections of the microtubules. The 10 µM and 15 µM SFN treated PANC-1 cells had prominent acetylated microtubules around the cell centre and long acetylated segments along the microtubules (Figure 5.4). Analysis of the acetylated tubulin area revealed no significant increase in the percentage of total area of acetylated microtubule in 10 µM and 15 µM SFN treated PANC-1 cells, compared to DMSO treated cells (Figure 5.5, a). Western blots suggested that there was no change in the levels of acetylated tubulin in 10 µM and 15 µM SFN treated PANC-1 cells, compared with DMSO treated cells (Figure 5.5, c). The cold treatment experiment suggested that untreated and DMSO treated PANC-1 cells had some stable microtubules (Figure 5.6). The 10 µM and 15 µM SFN treated PANC-1 cells underwent little change. Networks of stable microtubules could be observed around the nucleus and in the cytoplasm, suggesting no marked increase in microtubule stability in SFN treated PANC-1 cells (Figure 5.6).

5.3.2 SFN treated ARPE-19 but not PANC-1 cells reveal an increase in detyrosinated tubulin

To assess whether the expression of detyrosinated tubulin was affected by SFN treatment, ARPE-19 and PANC-1 cells were seeded on glass coverslips, incubated overnight and then treated with 10 µM or 15 µM SFN and incubated for 48 hours. SFN and DMSO treated ARPE-19 and PANC-1 cells were fixed and immunolabelled for tyrosinated and detyrosinated tubulin. DMSO treated ARPE-19 cells had mostly tyrosinated microtubules, along with few detyrosinated microtubules. These few detyrosinated microtubules were concentrated in the cell centre and a few small segments along the microtubules (Figure 5.7). Similar observations were made in 10 µM SFN treated ARPE-19 cells. However, 15 µM SFN treated ARPE-19 cells revealed extensive detyrosinated bundles of microtubules that were composed of straight detyrosinated microtubules that exbended from the cell centre toward the periphery (Figure 5.7).

DMSO treated and 10 µM and 15 µM SFN treated PANC-1 cells showed minimal expression of detyrosinated tubulin. This suggests that SFN does not increase expression of detyrosinated tubulin in PANC-1 cells (Figure 5.8).

5.3.3 SFN treatment affects microtubule dynamics in ARPE-19 cells

To assess the effect of SFN treatment on microtubule dynamics, GFP-CLIP-170 comet dynamics were analysed in SFN treated ARPE-19 and PANC-1 cells. Cells were grown in glass-bottomed dishes and incubated overnight. Cells were then treated with 10 and 15 µM SFN and incubated for 48 hours. For each concentration, cells expressing GFP-CLIP-170 were imaged using live time-lapse fluorescence

microscopy for three minutes, with frames taken every three seconds, yielding 60 frames in total. GFP-CLIP-170 comets were followed using the automated tracking software U-Track, originally packaged as plusTipTracker (Applegate et al., 2011). All post-tracking analysis was conducted using MATLAB, as described in chapter 4.13. Importantly, it must be noted that stable microtubules cannot be identified via this method. GFP-CLIP-170 may cause an increase in microtubule rescue.

U-Track analysis of GFP-CLIP-170 comets over a three-minute period, every three seconds, showed GFP-CLIP-170 comets with lines presenting different phases, growing (red), shrinking (yellow) and pausing (blue) (Figure 5.9, Movie S17, S18 and S19). CLIP-170 tracking images suggested that SFN may affect microtubules length. Analysis of GFP-CLIP-170 comets in the ARPE-19 cells treated with 10 µM and 15 µM SFN revealed a significant decrease in the average comet's speed. The DMSO treated ARPE-19 cells revealed an average CLIP-170 comet speed of 14.6 µm min^{-1}. In contrast, the 10 µM and 15 µM SFN treated ARPE-19 cells showed average CLIP-170 comet speeds of 9.9 µm min^{-1} and 9.05 µm min^{-1}, respectively (Figure 5.10, a). Furthermore, analysis of mean growth length of microtubules in DMSO and SFN treated ARPE-19 cells showed that 10 µM and 15 µM SFN treated cells had significantly decreased CLIP-170 growth lengths compared to DMSO treated cells (Figure 5.10, b, Movies S20, S21 and S22).

The microtubule dynamics in PANC-1 cells were analysed in the same way as those in ARPE-19 cells. U-Track analysis of GFP-CLIP-170 comets over three-minutes period with growing (red), shrinking (yellow) and pausing (blue) (Figure 5.11). The 10 µM and 15 µM SFN treated PANC-1 cells revealed no significant difference in comet speed compared to DMSO treated cells (Figure 5.12, a). Moreover, 10 µM and 15 µM SFN treated PANC-1 cells showed no changes in the comet growth length compared to DMSO treated cells (Figure 5.12).

The results revealed that SFN treatment decrease significantly microtubule dynamics in AREP-19, however, no significant reduction was observed in SFN treated PANC-1 cells.

5.3.4 SFN treatment increases focal adhesion area AREP-19 cells

To assess whether SFN treatment affects focal adhesion area and turnover, ARPE-19 and PANC-1 cells were seeded on glass coverslips and incubated overnight. These cells were then treated with 10 µM and 15 µM SFN, incubated for 48 hours and immunolabelled for focal adhesion kinase (FAK) and microtubules. DMSO treated ARPE-19 cells revealed focal adhesions at the cell edge, along with some focal adhesions in the cell body. Treatments with 10 µM and 15 µM SFN in ARPE-19 cells showed more FAK in the centre of the cell, along with some adhesions at the cell periphery (Figure 5.13).

In contrast, DMSO treated PANC-1 cells showed focal adhesions at the cell periphery, along with some FAK staining that was diffuse in the cytoplasm. The 10 µM and 15 µM SFN treated PANC-1 cells revealed more dispersed FAK (Figure 14).

Focal adhesion images were analysed using imageJ software. AREP-19 and PANC-1 cells were grown on glass coverslips, treated with SFN for 48 hours, then with GFP-paxillin construct for four hours and fixed. The adhesion areas in the AREP-19 and PANC-1 cells were assessed. GFP-paxillin images revealed focal adhesions at the cell periphery and in cell body in DMSO and SFN treated ARPE-19 cells (Figure 5.15, a), while they localised mainly at the cell periphery in DMSO and SFN treated PANC-1 cells (Figure 5.16, a). The surface area of the cell

including all focal adhesions were quantified. To obtain the percentage of focal adhesion area in the cells, the total focal adhesion area was divided by the total area of the cell. The mean focal adhesions area was also analysed in the cells.

The results illustrated that 15µM SFN treated ARPE-19 cells had a significant increase in the percentage of total adhesion area of focal adhesion compared to the DMSO treated cells (Figure 5.15, b). In contrast, the 10 µM and 15 µM SFN treated PANC-1 cells showed no significant increase in total focal adhesion area or in the average area of focal adhesion compared to the DMSO treated cells (Figure 5.16, b and c).

5.3.5 SFN treatment and focal adhesion dynamics in ARPE-19 and PANC-1 cells

To investigate whether SFN treatment has an effect on focal adhesion turnover, ARPE-19 and PANC-1 cells were grown in glass-bottom dishes and incubated overnight. The following day, these cells were treated with 10 µM or 15 µM SFN and incubated for 48 hours. The ARPE-19 and PANC-1 cells were then transfected with GFP-paxillin, incubated for four hours, given fresh medium and then incubated for a total of 48 hours. Adhesion dynamics was then analysed in live in ARPE-19 and PANC-1 cells expressing GFP-paxillin using FRAP (fluorescence recovery after photobleaching). Confocal microscopy (Zeiss LSM510 META scanning confocal microscope) was used for the live imaging in ARPE-19 and PANC-1 cells expressing GFP-paxillin, every three-seconds over a three-minute period (as described in Material and Methods, 2.8.3). The fluorescence mean recovery after FRAP was measured with time needed to return to the full recovery (as described in Material and Methods, 2.14). As illustrated in Figure 5.17 and 5.18 for DMSO and SFN treated ARPE-19 and PANC-1 cells, where focal adhesions

underwent to FRAP over three-minutes (Figure 5.17 and 5.18, Movies S23, S24, S25, S26, S27 and S28).

The results showed no significant difference in the percentage of the mean recovery between DMSO and SFN treated AREP-19 cells (Figure 5.19, a). DMSO treated cells showed that the percentage of mean recovery reached about 58% within 33 Meanwhile, 10 and 15 µM SFN treated cells revealed that the percentage of mean recovery reached about 53% and 58% within 36 and 42 respectively (Figure 5.19, b). However, none of the three conditions of treated cells showed a fully recovery after photobleaching.

The 10 and 15 µM SFN treated PANC-1 cells revealed a significant increase in the percentage of the mean fluorescence GFP-paxillin recovery compared to DMSO cells (Figure 5.20, a). The results revealed that DMSO treated PANC-1 cells reached the percentage of the mean recovery around 50% within 42, while 10 and 15 µM SFN treated cells reached the percentage the mean recovery of 59% and 68% within 30 and one respectively. Increasingly, 10 and 15 µM SFN treated PANC-1 cells reached 46% and 40% within 10 seconds compared to DMSO treated cells, which reached the percentage of the mean recovery of 29% within 10 seconds (Figure 5.20, b). These FRAP studies suggested that there is no significant change in the focal adhesion dynamics in SFN treated ARPE-19 cells. However, there is a significant increase in the focal adhesion turnover in SFN treated PANC-1 cells.

Table 6: Chapter V summary

Experiments	Results
SFN and acetylated tubulin	ARPE-19: • Significant increase in the total area of acetylated microtubules • Western blot showed an increase in acetylated tubulin. • Cold treatment suggested marked increase in microtubule stability PANC-1: • No significant increase in the total area of acetylated microtubule • Western blot revealed no increase in acetylated tubulin. • Cold treatment suggested no marked increase in microtubule stability
SFN and microtubule dynamics	ARPE-19: • CLIP-170 comet analysis revealed a significant decrease in the average comet speed and in the length growth of MTs in SFN treated cells. PANC-1: • No significant decrease in the average of comets speed or in the growth length of MTs in SFN treated cells.

SFN and focal adhesion	ARPE-19: • Focal adhesion analysis showed a significant increase in the percentage of total focal adhesion area and in the average area in SFN treated cells. PANC-1: • Focal adhesion analysis revealed no significant increase in the average of total focal adhesion area or in the area of focal adhesion in SFN treated cells.
SFN and focal adhesion dynamics	ARPE-19: • FRAP analyses showed no significant effect on focal adhesion recovery between DMSO and SFN treated ARPE-19 cells, with no marked difference in recovery time. PANC-1: • FRAP analyses showed a significant increase in the mean of focal adhesion recovery in SFN treated cells, and SFN treated cell showed to recover faster compared to DNSO.

5.4 Discussion

5.4.1 SFN increases acetylated and detyrosinated microtubules and inhibits microtubule dynamics in ARPE-19 but not in PANC-1 cells

The analysis of acetylated microtubules revealed that SFN treated ARPE-19 cells expressed more acetylated tubulin. This was also suggested by analysing the acetylated microtubule area in SFN treated ARPE-19 cells, which it revealed a significant increase in acetylated area. Coupled with this, the microtubule bundles that formed in SFN treated ARPE-19 cells expressed more detyrosinated microtubules, which suggests stable microtubules. Further results demonstrated that cold treatment caused total depolymerisation of microtubules in DMSO treated ARPE-19 cells, whereas in SFN treated cells, several stable microtubules remained intact despite the cold treatment. Importantly, the CLIP-170 comet dynamic results showed a dramatic decrease in comet speed and growth length in SFN treated AREP-19 cells, which suggest that SFN may inhibit microtubule dynamics. These results are in line with those of other studies in which SFN treatment has been shown to suppress microtubule dynamics and growth rate, for example, in human breast cancer cells (Azarenko et al., 2008). However, here we base the microtubule dynamics analysis on a global read from entire cells and not just a few peripheral microtubules by Azarenko et al (2008). Moreover, SFN treatment has been shown to affect on microtubule post-translational modifications. Specifically, it caused an increase in acetylated microtubules and thus more stable microtubules in human breast cancer and prostate cancer cells (Azarenko et al., 2008, Gibbs et al., 2009, Clarke et al., 2011).

SFN treated PANC-1 cells revealed no marked changes in acetylation level and expression. This was also suggested by analysing acetylated area in SFN treated PANC-1 cells, where no significant increase in acetylated area was evident. Cold treatment results indicated similar stable microtubules can be observed in SFN and DMSO treated cells. It is likely that any acetylation induced by SFN in PANC-1 cells is counteracted by the high expression of HDAC6. The analysis of microtubule dynamics in SFN treated PANC-1 cells revealed they remained largely unchanged, with no significant alteration in comet speed or growth length of microtubules. These results are in line with our observations regarding cell migration, which revealed that SFN treated PANC-1 cells showed no significant difference in cell migration, which requires dynamic microtubules, as compared to DMSO treated cells.

To summarise, the overall capability of SFN to affect microtubule dynamics appears to be related to an increase in acetylated microtubules and thus microtubule stability (Piperno et al., 1987, Webster and Borisy, 1989). Furthermore, it has been shown that acetylated tubulin can influence the ability of motor proteins to associate with microtubules (Janke and Bulinski, 2011, Garnham and Roll-Mecak, 2012), which may affect cellular functions such as focal adhesion turnover and cell migration. In PANC-1 cells, SFN had a different effect, with no increase in acetylated microtubules being seen in treated cells and there thus being no effect on microtubule dynamics. Our suggestion is that this may be due to EB2 and HDAC6 being highly expressed in the PANC-1 cell line (Abiatari et al., 2009, Li et al., 2014), with the EB family being essential regulators of microtubule dynamics (Komarova et al., 2009). Moreover, depleting EB2 causes more stable microtubules and decreased microtubule dynamics (Goldspink et al., 2013), and HDAC6 deacetylates microtubules and increases microtubule dynamics (Li et al., 2011). All these together may prevent or minimise SFN effects on microtubule dynamics and stability in PANC-1 cells.

5.4.2 SFN treatment leads to increased focal adhesion area in ARPE-19 but not in PANC-1 cells

Microtubules are involved in two essential stages of cell motility, the first stage being the reorientation of cellular organelles towards the direction of movement (Gundersen and Bulinski, 1988) and the second stage being the regulation of focal adhesion dynamics and turnover (Kaverina et al., 1999). According to our results, one important observation made regarding SFN treated ARPE-19 and PANC-1 cells was a distinct increase in cell area (Chapter 4.3.2). Such an increase in cell size is likely to be related to focal adhesions, resulting in a decrease in cell migration (Lauffenburger and Horwitz, 1996, Rodriguez et al., 2003). It was critical, therefore, to investigate whether there was any evidence of effecting focal adhesions turnover in SFN treated cells. Focal adhesion areas was significantly increased in SFN treated ARPE-19 cells but not in PANC-1 cells. Focal adhesion dynamics are related to microtubule dynamics. Specifically, less dynamic microtubules can affect focal adhesion dynamics and turnover. As previously indicated, SFN treated ARPE-19 cells showed an increase in microtubule stability, which may affect focal adhesion states. Acetylated microtubules may cause an increase in transport of essential proteins to maintain their focal adhesion dynamics. It has been suggested that EB2 contributes to focal adhesion turnover by associating with essential proteins, such as HAX1 (HCLS1-asociated protein X-1) and MAP4K4, and knockdown of MAP4K4 results in focal adhesion stability (Yue et al., 2014, Liu et al., 2015). Thus, the reduced association between EB2 and the microtubule lattice in SFN treated cells may affect focal adhesion.

Overall, microtubule dynamics play a critical role in focal adhesion dynamics, and we suggest that SFN inhibits microtubule dynamics, which then may affect focal adhesion dynamics. Therefore, this may be one of the mechanisms via which SFN affects cell migration.

5.4.3 SFN treatment did not inhibit focal adhesion turnover

As we have previously shown that SFN treatment leads to an increase in total focal adhesion area in ARPE-19 cells and further investigations were performed regarding focal adhesion turnover. Focal adhesion turnover requires dynamic microtubules to ensure full and successful. Unexpectedly, our results showed no significant effect on the percentage of the mean focal adhesion recovery in SFN treated ARPE-19 cells compared to DMSO treated cells. However, SFN treated PANC-1 cells showed an increase in the percentage of the mean focal adhesion recovery. It seems that the focal adhesions in the SFN treated cells did not fully disassemble, with more focal adhesions being observed in the cell body. The reason for dynamics and turnover not being affected could be that SFN may affect GFP-paxillin expression in treated cells, which showed no full recovery of fluorescence after photobleaching in FRAP experiments.

To summarise, the overall ability of SFN to affect focal adhesion dynamics and turnover and how it may contribute to the overall cell migration process are not completely understood and further investigation is required.

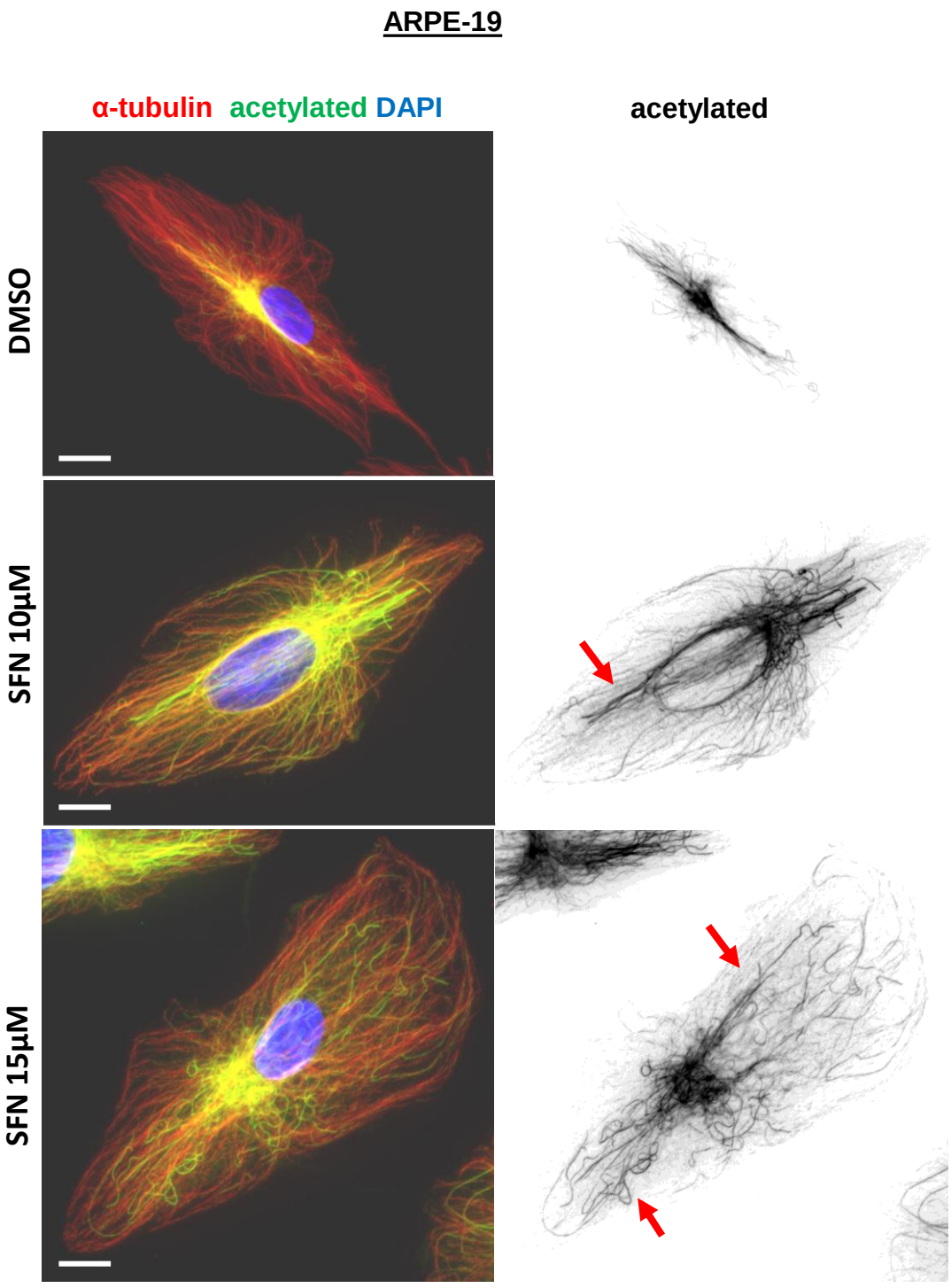

Figure 5.1 SFN treated ARPE-19 cells express acetylated tubulin along microtubules

Cells were Immunolabelled for microtubules (α-tubulin; red) and acetylated tubulin (green, invert) and DNA with DAPI. DMSO treated cell shows some acetylated microtubules mainly around the centre of the cell. 10 and 15µM SFN treated cells reveal extensive acetylation of curly microtubules that elongated from the centre of the cell towards the periphery. Scale bars=10µm.

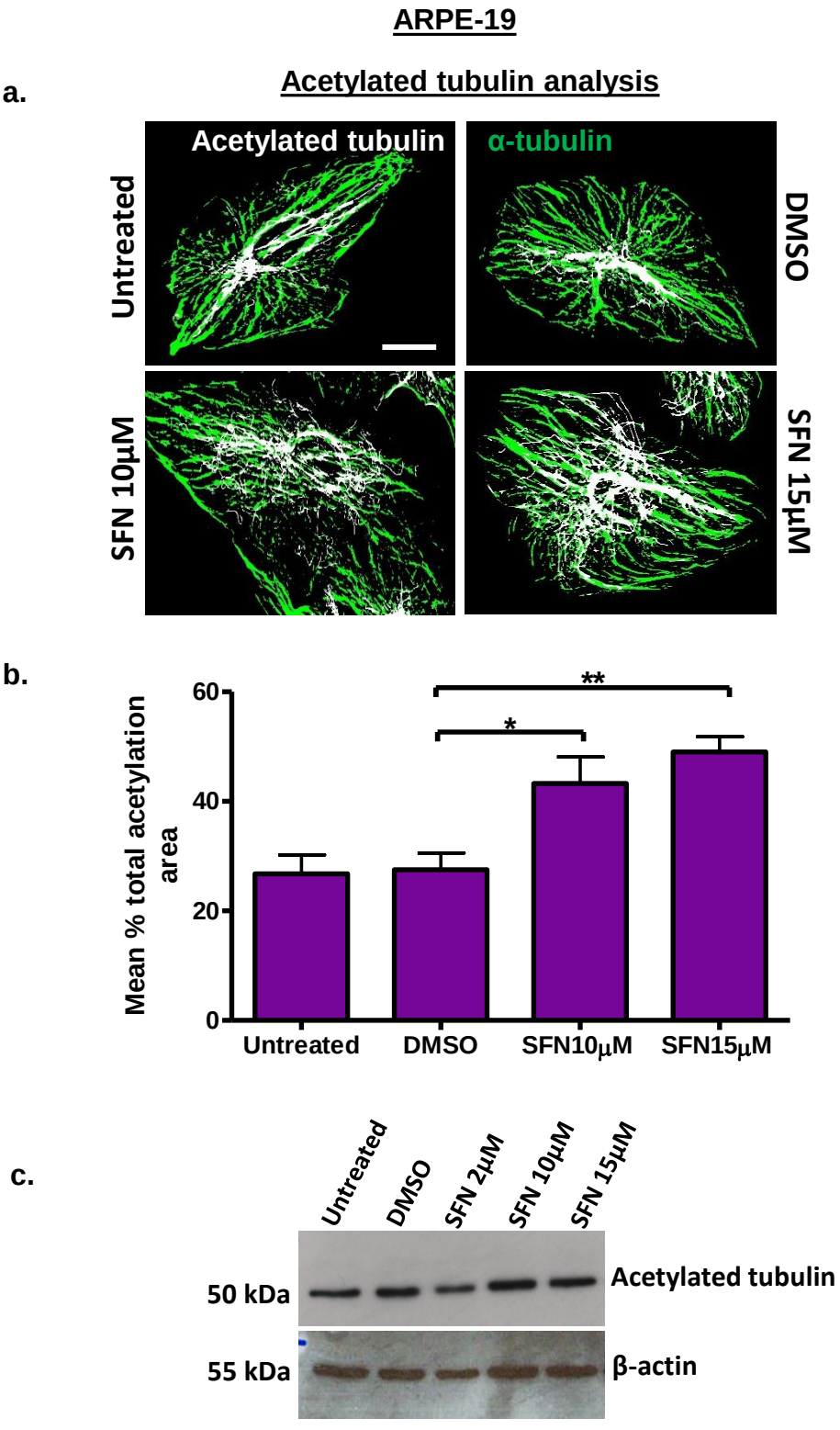

Figure 5.2 SFN increases acetylated microtubules in ARPE-19 cells
a) Images highlighting the areas of acetylated tubulin (white) compared to total α-tubulin area (green). b) Analysis of acetylated microtubule using ImageJ shows that 10 and 15μM SFN significantly increased the acetylated microtubule area compared to DMSO treated cells, N=20 [*P<0.05 & **P,0.001]. Scale bars=10μm. c) Western blots suggests a slight increase in acetylation levels in 10 and 15μM SFN treated ARP-19 cells compared to DMSO treated cells.

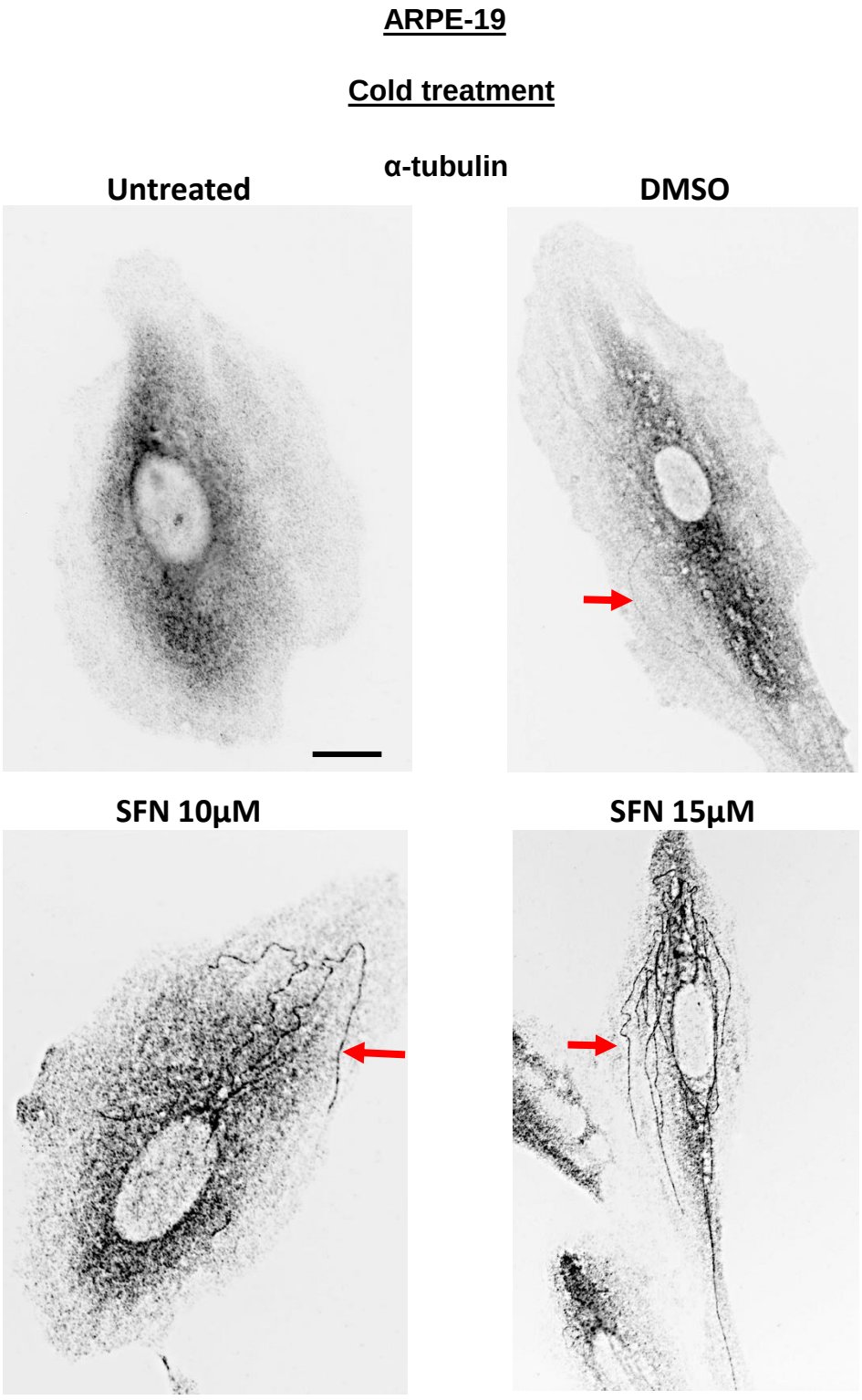

Figure 5.3 SFN stabilises microtubules against cold in ARPE-19 cells

Cells were treated with SFN (10 and 15µM) for 48 h. Cells were then incubated on ice for 15 mins, and fixed and immunolabelled for α-tubulin (inverted). Untreated cell shows that all microtubules have de depolymerised. DMSO treated cell reveals a few remaining microtubules (arrow). 10 and 15 µm SFN cells show an increase in remaining microtubules, suggesting an increase in stability in SFN treated cells (arrowed). Scale bars=10µm.

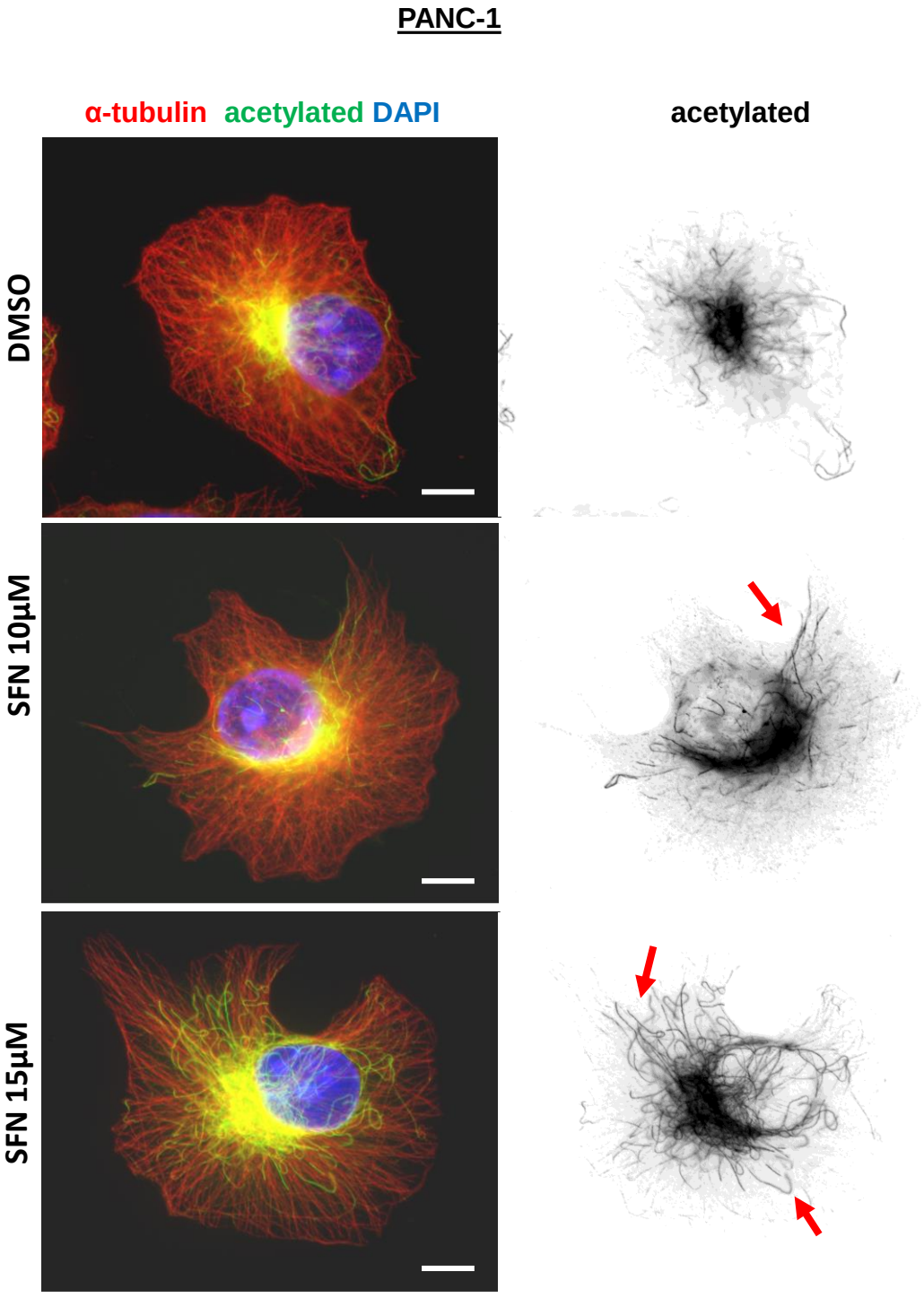

Figure 5.4 SFN treated PANC-1 cells express acetylated tubulin Cells were Immunolabelled for microtubules (α-tubulin; red) and acetylated tubulin (green, invert). DMSO treated cell shows acetylated microtubules localised at the centre of the cell with some extending to periphery. 10 and 15μM SFN treated cells reveal acetylated microtubules around the centre of the cell with more microtubules extending towards cell periphery (arrows). Scale bars=10μm.

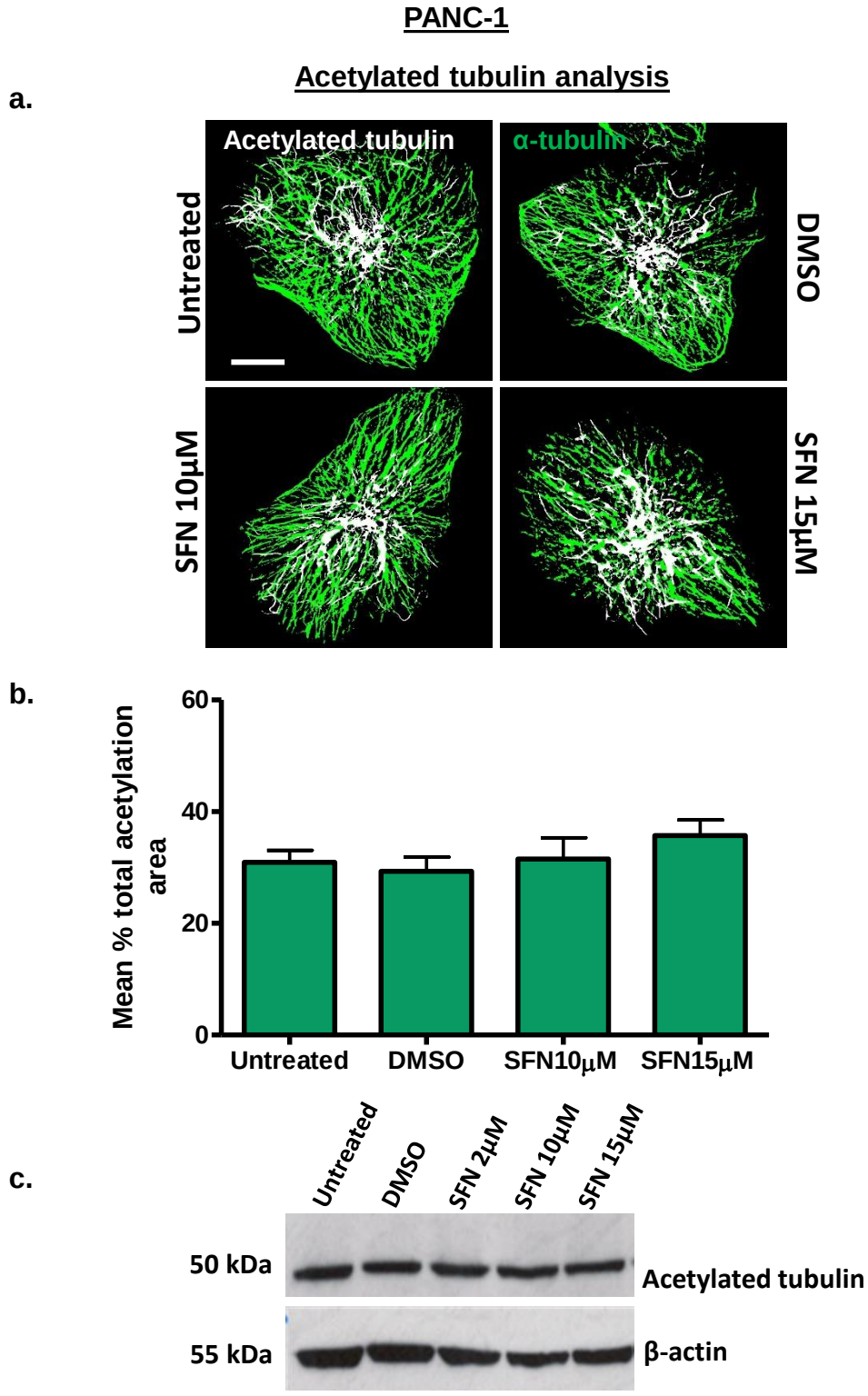

Figure 5.5 SFN treated PANC-1 cells shows no significant increase in acetylated microtubules expression

a) Images highlighting the areas of acetylated tubulin (white) compared to total α-tubulin area (green). b) Analyses of acetylated microtubule using ImageJ indicates that 10 and 15μM SFN treatment for 48 h results in no significant increase in acetylated microtubules area, compared to DMSO treated cells, N=20. Scale bars=10μm. b) Western blot suggests there is no change in acetylated tubulin levels in SFN treated cells compared to DMSO treated cells.

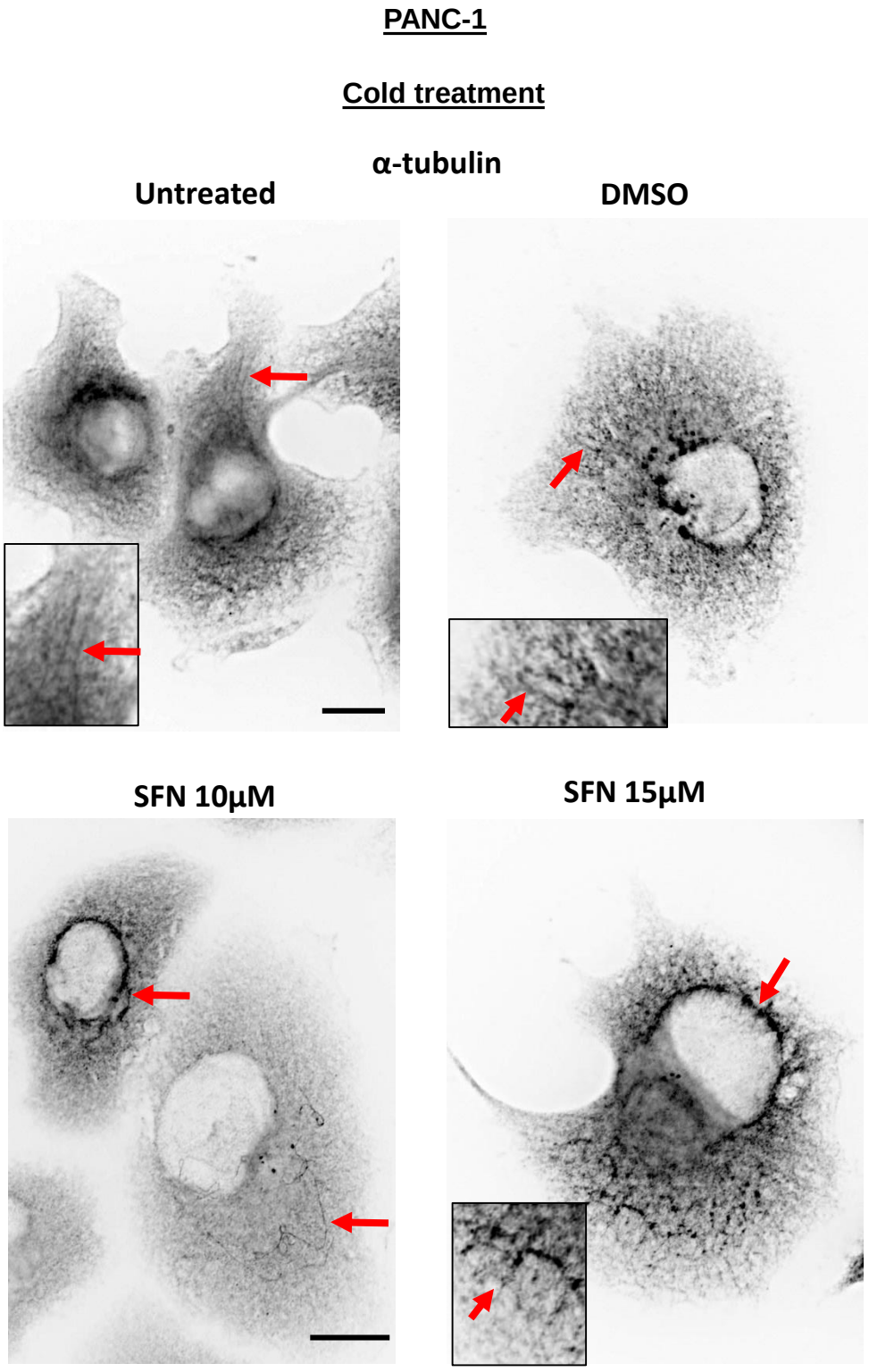

Figure 5.6 SFN treated PANC-1 cells shows no marked increase in stable microtubules against cold treatment

Cells were treated with 10 and 15µM SFN for 48h and then incubated on ice for 15 mins and immunolabelled for α-tubulin (inverted). Untreated and DMSO treated cells show a few stable microtubules (inset, arrows). 10 µM and 15 µM SFN treated cells reveal networks of stable microtubules around the nucleus and in the cytoplasm (inset, arrows), suggesting no marked increase in stability in SFN treated cells . Scale bars=10µm.

ARPE-19

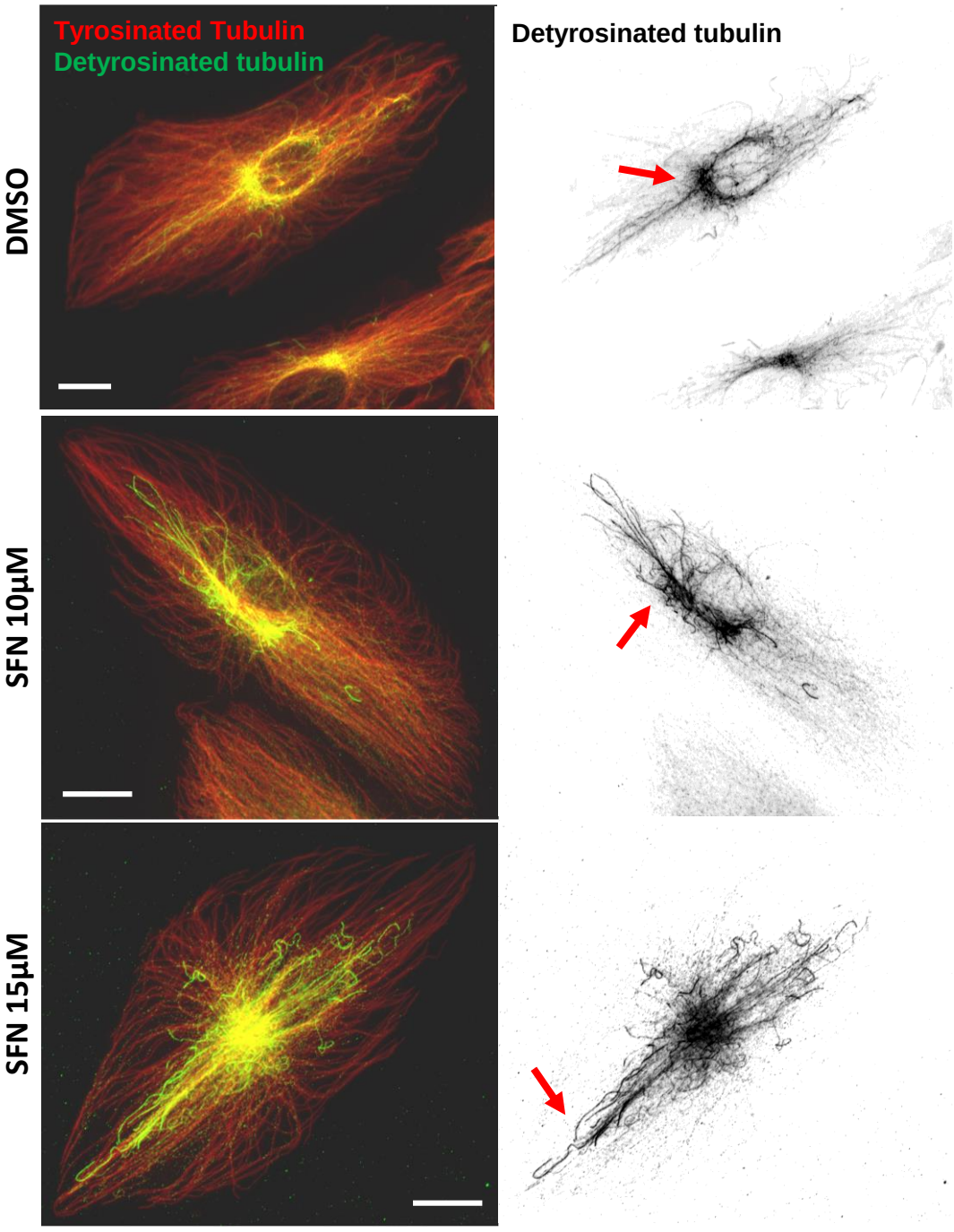

Figure 5.7 SFN treated ARPE-19 cells express detyrosinated tubulin in microtubule bundles

Cells Immunolabelled for tyrosinated tubulin (red) and detyrosinated tubulin (green, invert). DMSO treated cell reveals that most of microtubules were tyrosinated with some detyrosinated microtubules at the centre of the cell and along small segments. 10µM SFN treated cell shows a few detyrosinated microtubules similar to DMSO treated cell. 15µM treated cell reveals extensive detyrosinated microtubules bundles elongated from the centre of the cell to the periphery (arrowed), suggesting that SFN increases tubulin detyrosinated. Scale bars=10µm.

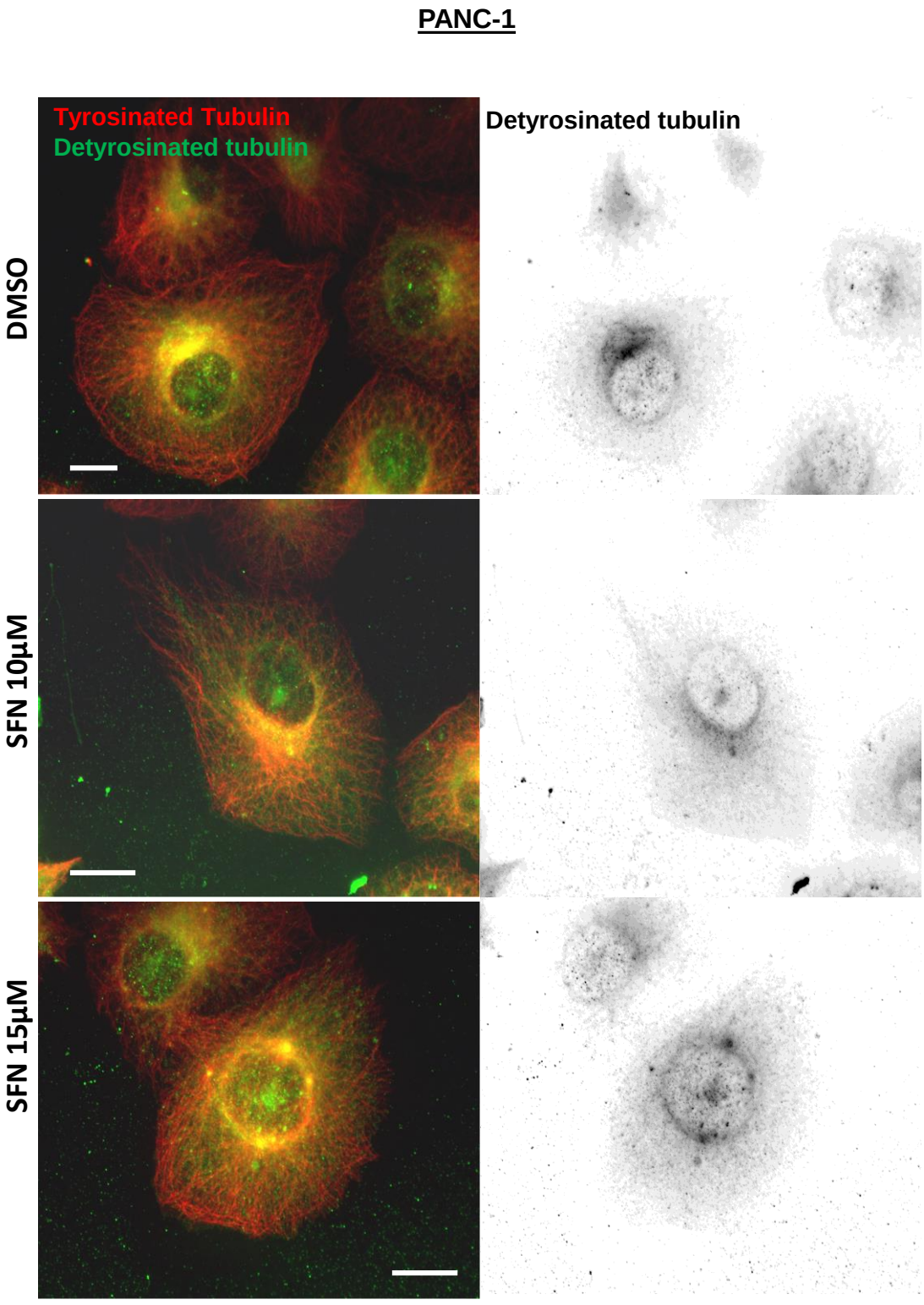

Figure 5.8 Detyrosinated tubulin is not expressed in PANC-1 cells Cells were immunolabelled for tyrosinated tubulin (red) and detyrosinated tubulin (green, invert). DMSO and SFN treated cells reveal minimal expression of detyrosinated tubulin. Scale bars=10µm.

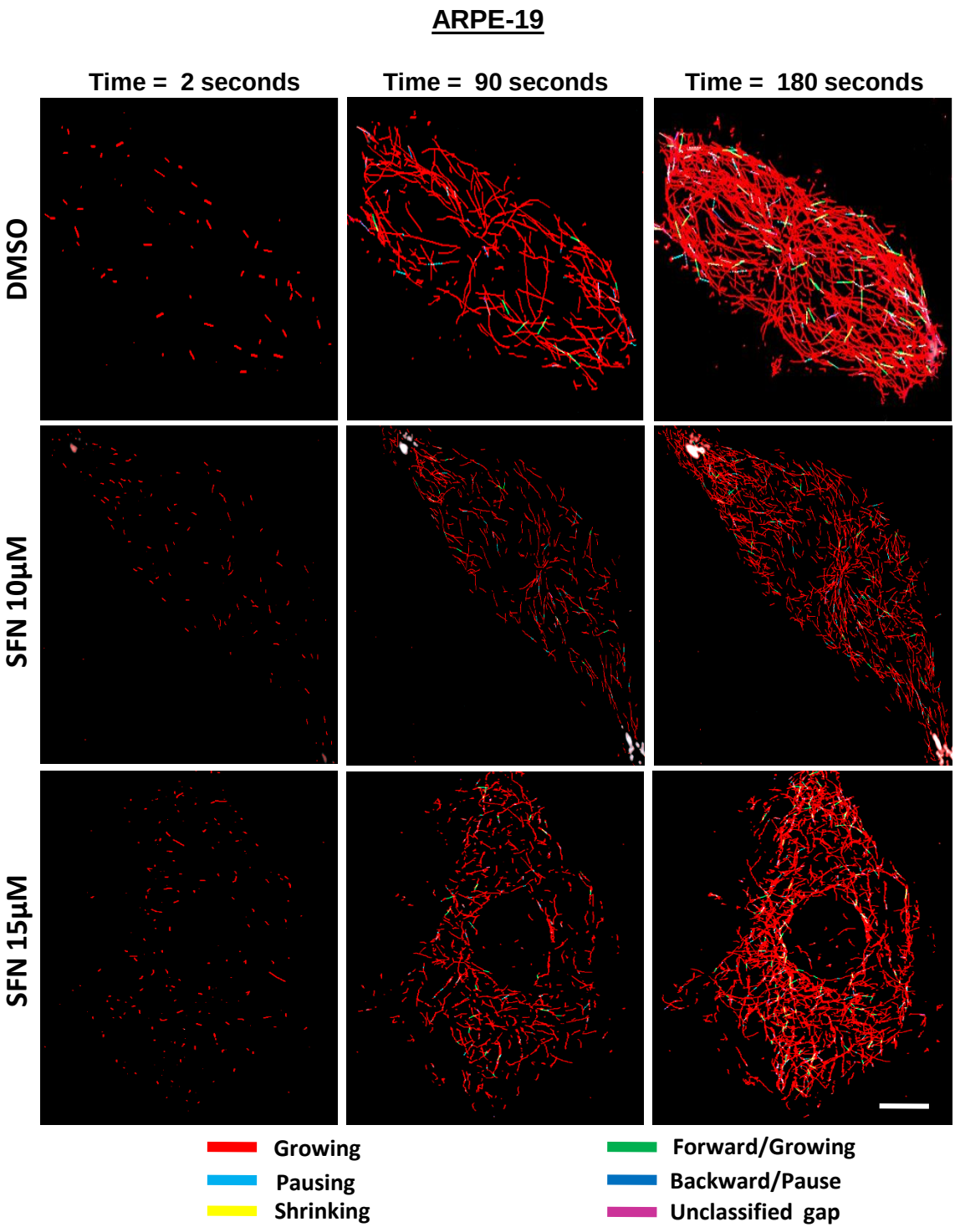

Figure 5.9 Microtubule dynamical tracking of ARPE-19 cells
Cells were imaged using live fluorescence microscopy for three minutes, and frames were taken every three seconds.
GFP-CLIP-170 comes in DMSO and 10 and 15µM SFN treated cells were live imaged and analysed using the automated tracking software U-Track. MATLAB was used to conduct all post-tracking analysis for microtubule dynamics, where coloured lines are presenting microtubules phases (red lines presents growing microtubules). DMSO treated cells show long dynamic microtubules. SFN treated cells reveals short dynamic microtubules, suggesting that SFN has an effect on microtubule dynamics. N=7, scale bars=10µm.

ARPE-19

a. **GFP-CLIP-170 comet speed**

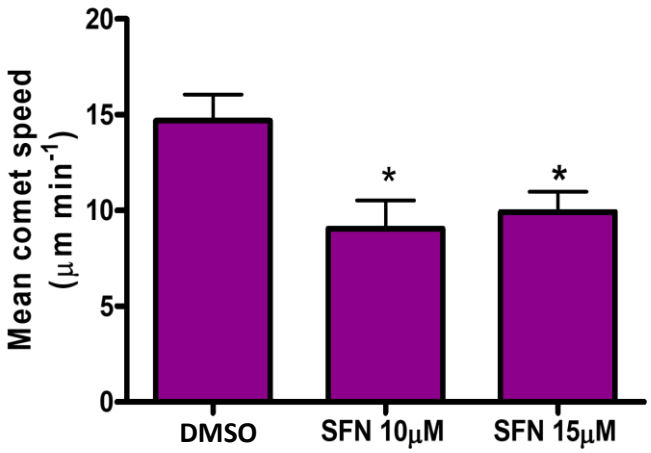

b. **GFP-CLIP-170 growth length**

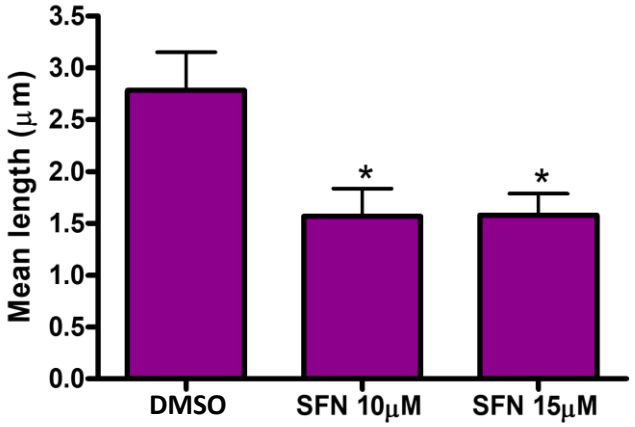

Figure 5.10 SFN treatment leads to decrease CLIP-170 comet velocity and growth events in ARPE-19 cells
GFP-CLIP-170 comets in DMSO and SFN treated cells were analysed to assess microtubule dynamics. a) 10 and 15μM SFN treated cells reveal a significant decrease in the mean comet speed compared to DMSO treated cells. b) the growth length of microtubules is significantly decreased in 10 and 15μM SFN treated cells compared to DMSO treated cells. Statistical significance assessed by one-way ANOVA with Tukey's multiple comparison test, [*P<0.05], n=7.

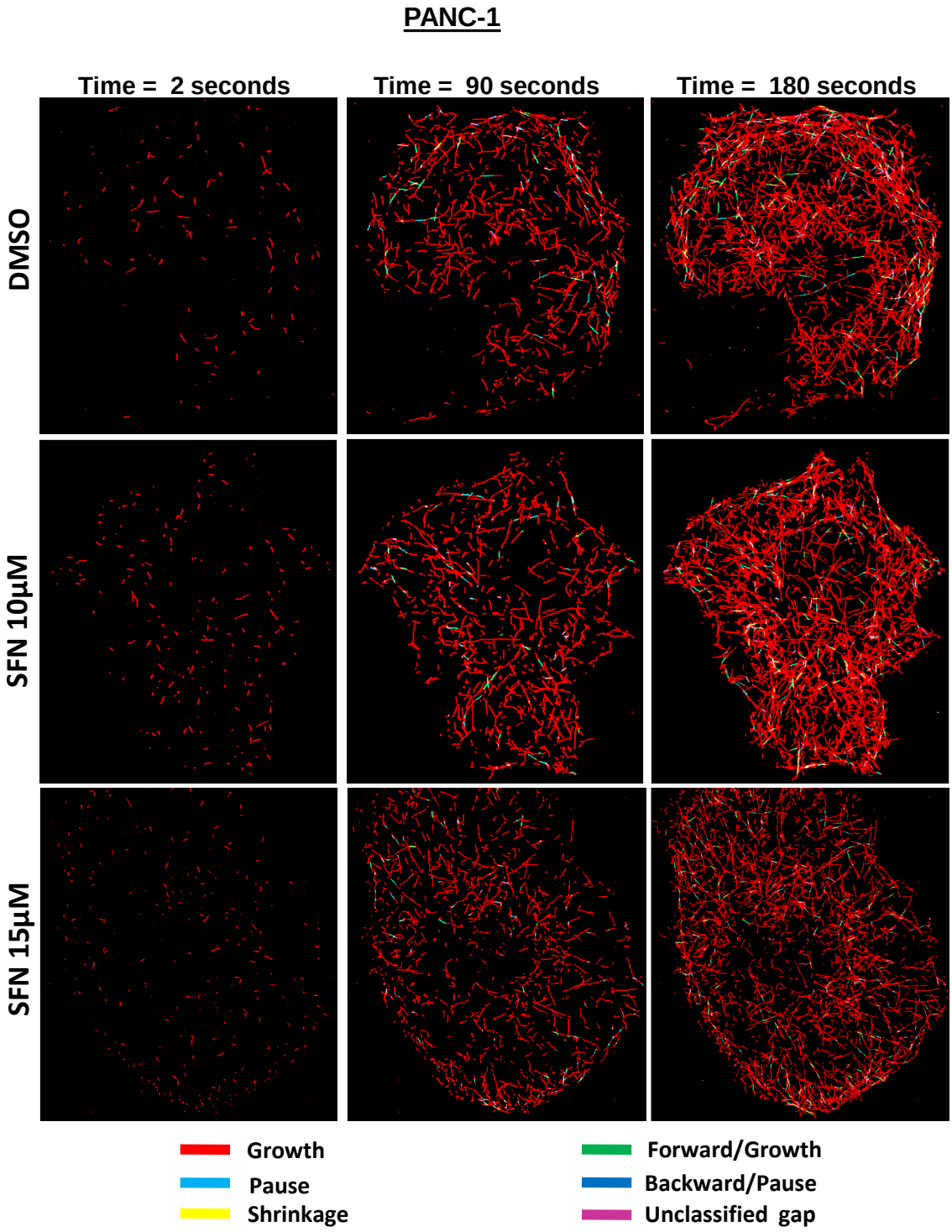

Figure 5.11 Microtubule dynamical tracking of PANC-1 cells
Cells were imaged using live time-lapse fluorescence microscopy for three minutes, and frames were taken every three seconds.
GFP-CLIP-170 comes in DMSO and 10 and 15µM SFN treated cells were live time-lapse imaged and analysed using the automated tracking software U-Track. MATLAB was used to conduct all post-tracking analysis for microtubule dynamics, where coloured lines are present microtubules behaviour (red lines presents growing microtubules). DMSO and SFN treated cells show no marked different in microtubules length, suggesting that SFN has no effects on microtubule dynamics. N=7, scale bars=10µm.

PANC-1

a.

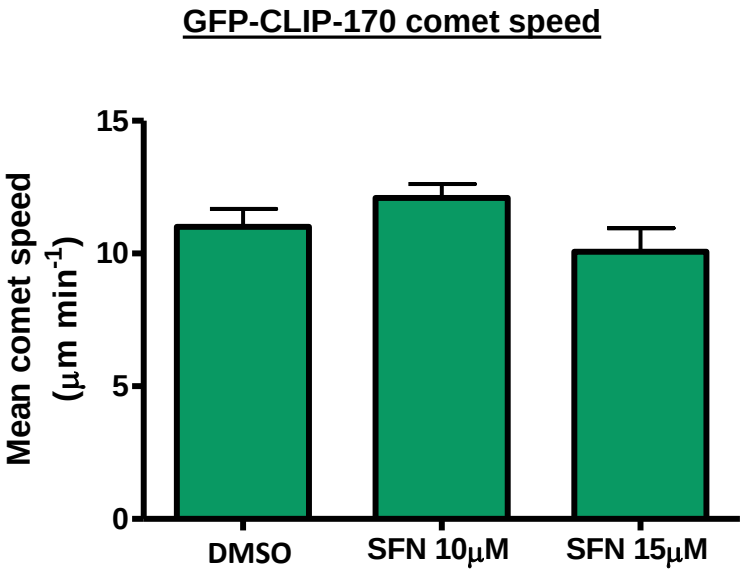

b.

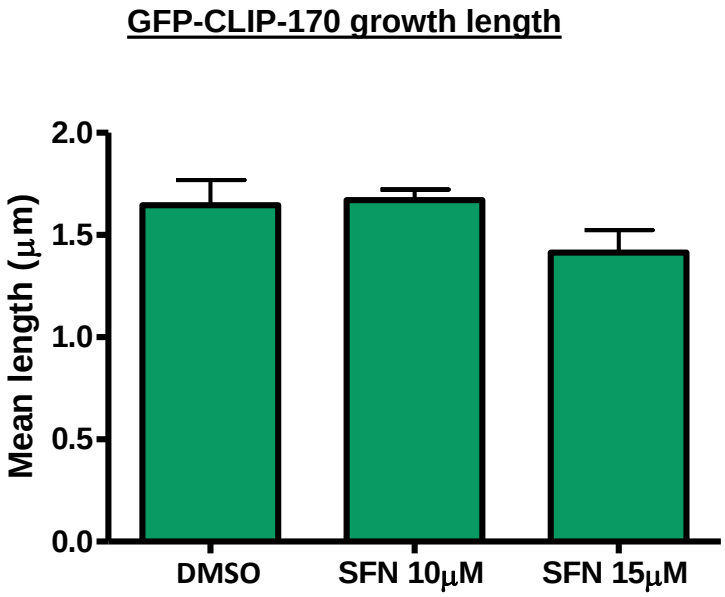

Figure 5.12 SFN treatment does not affect microtubule dynamics in PANC-1 cells

GFP-CLIP-170 comes in control and SFN treated cells was analysed to determined microtubules dynamics. a) 10 and 15μM SFN treated cells show no significant effect on the mean of comet speed compared to DMSO treated cells. b) the mean length of microtubules reveals no significant decrease in 10 and15μM SFN treated cells compared to DMSO treated cells. Statistical significance assessed by one-way ANOVA with Tukey's multiple comparison test, n=7.

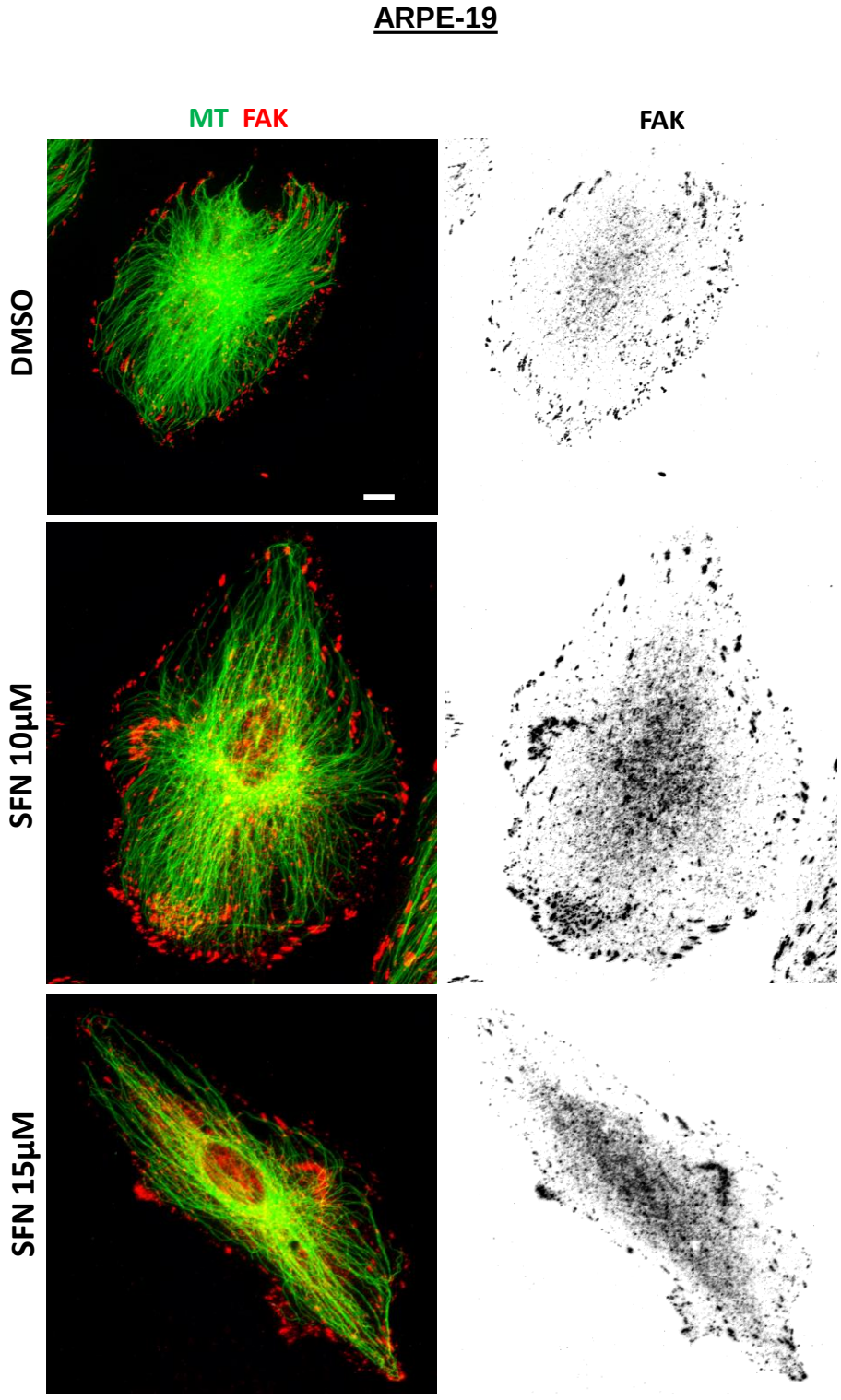

Figure 5.13 SFN treatment leads to spread more focal adhesion in ARPE-19 cells

Cells were immunelabelled for focal adhesion (FAK, red, invert) and microtubule (green). DMSO treated cell shows most of focal adhesions localised at cell periphery. In SFN treated cells, focal adhesion is mainly at cell periphery with some more in cell body in particular in 15µM SFN treated cells. Scale bars=10µm.

PANC-1

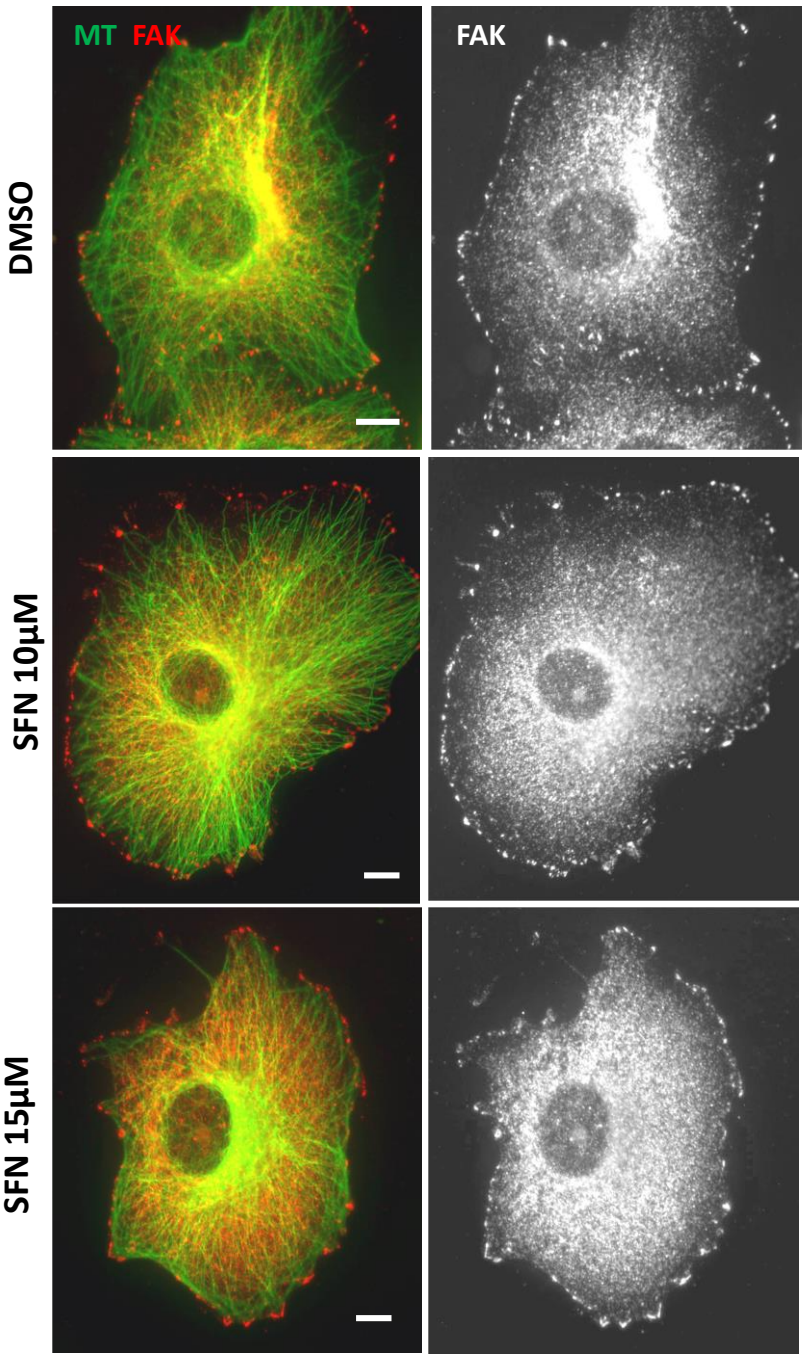

Figure 5.14 SFN treatment and focal adhesion localisation in PANC-1 cells

Cells were immunelabelled for focal adhesion (FAK, red) and microtubule (green). DMSO treated cell shows focal adhesions at cell periphery. In SFN treated cells, focal adhesion is mainly at cell periphery with some appear accumulated the periphery of 15µM SFN treated cells, suggesting no noticeable change in SFN treated cells. Scale bars=10µm.

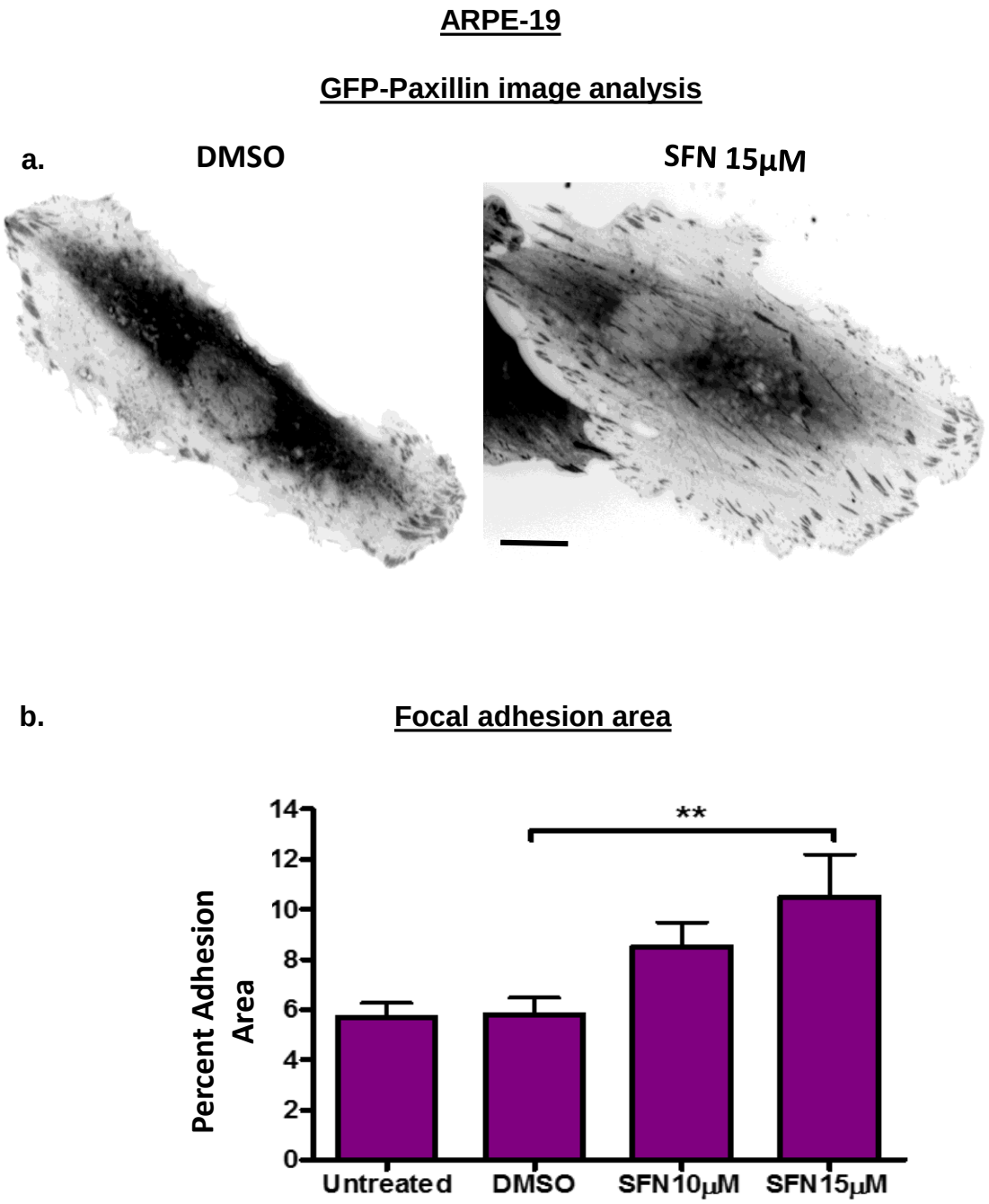

Figure 5.15 SFN treatment leads to increase adhesion area and size in ARPE-19 cells

a) GFP-Paxillin construct was added to cells, then live images were taken for quantitative analysis. b) 15µM SFN reveal a significant increase in focal adhesion area compared to DMSO treated cells. Statistical significance assessed by one-way ANOVA with Tukey's multiple comparison test, [**P<0.001], n=7. Scale bars=10µm.

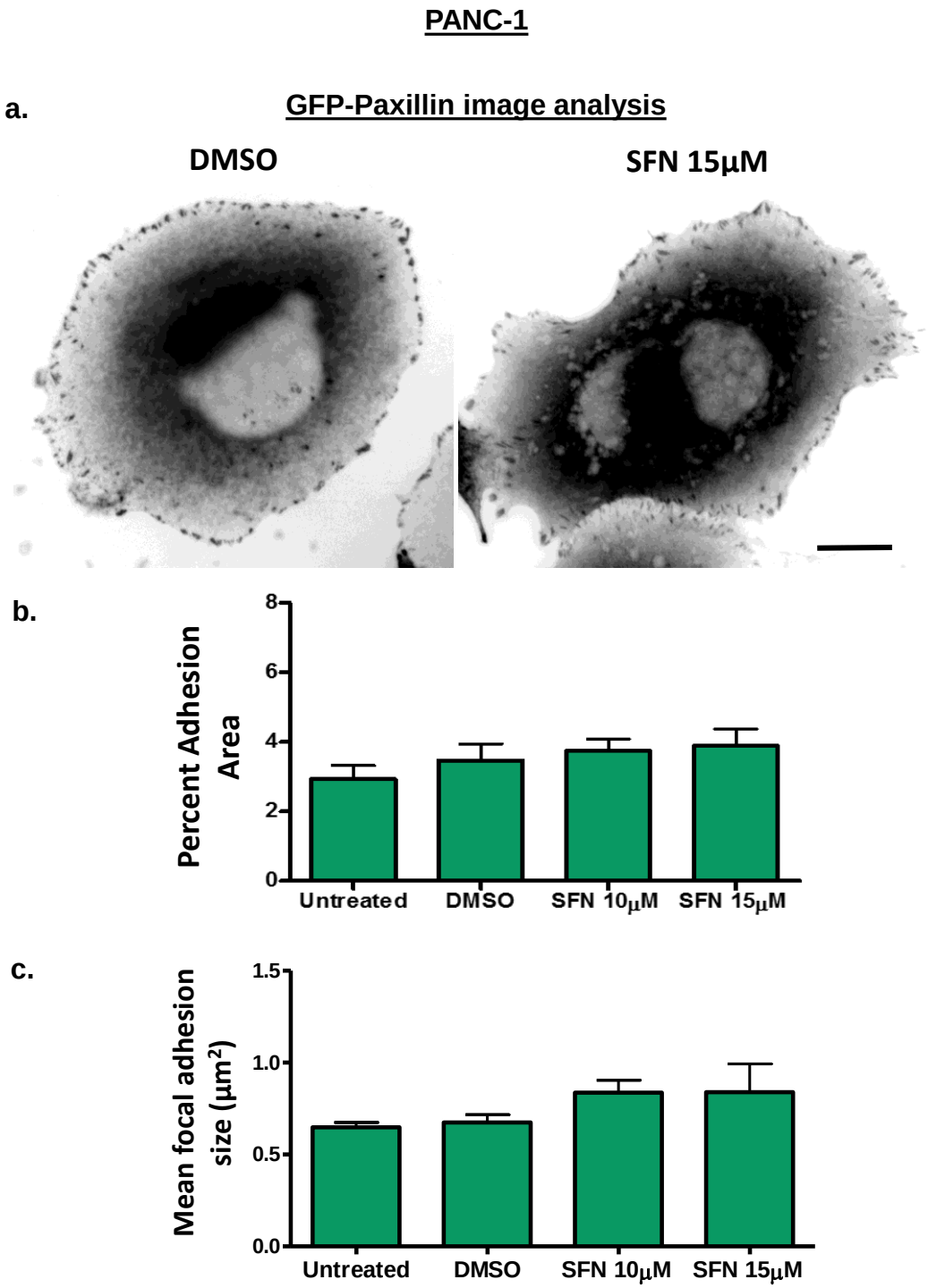

Figure 5.16 SFN treatment shows no effect on adhesion area or size in PANC-1 cell

a) GFP-Paxillin construct was added to cells, then live images were taken for quantitative analysis. b) 10 and 15µM treated SFN cells show no significant increase in adhesion area compared to DMSO treated cells. c) 10 and 15µM treated SFN cells reveal also no significant increase in the size of focal adhesions compared to DMSO treated cells. Statistical significance assessed by one-way ANOVA with Tukey's multiple comparison test, n=7. Scale bars=10µm.

ARPE-19

FRAP analyses of GFP-paxillin

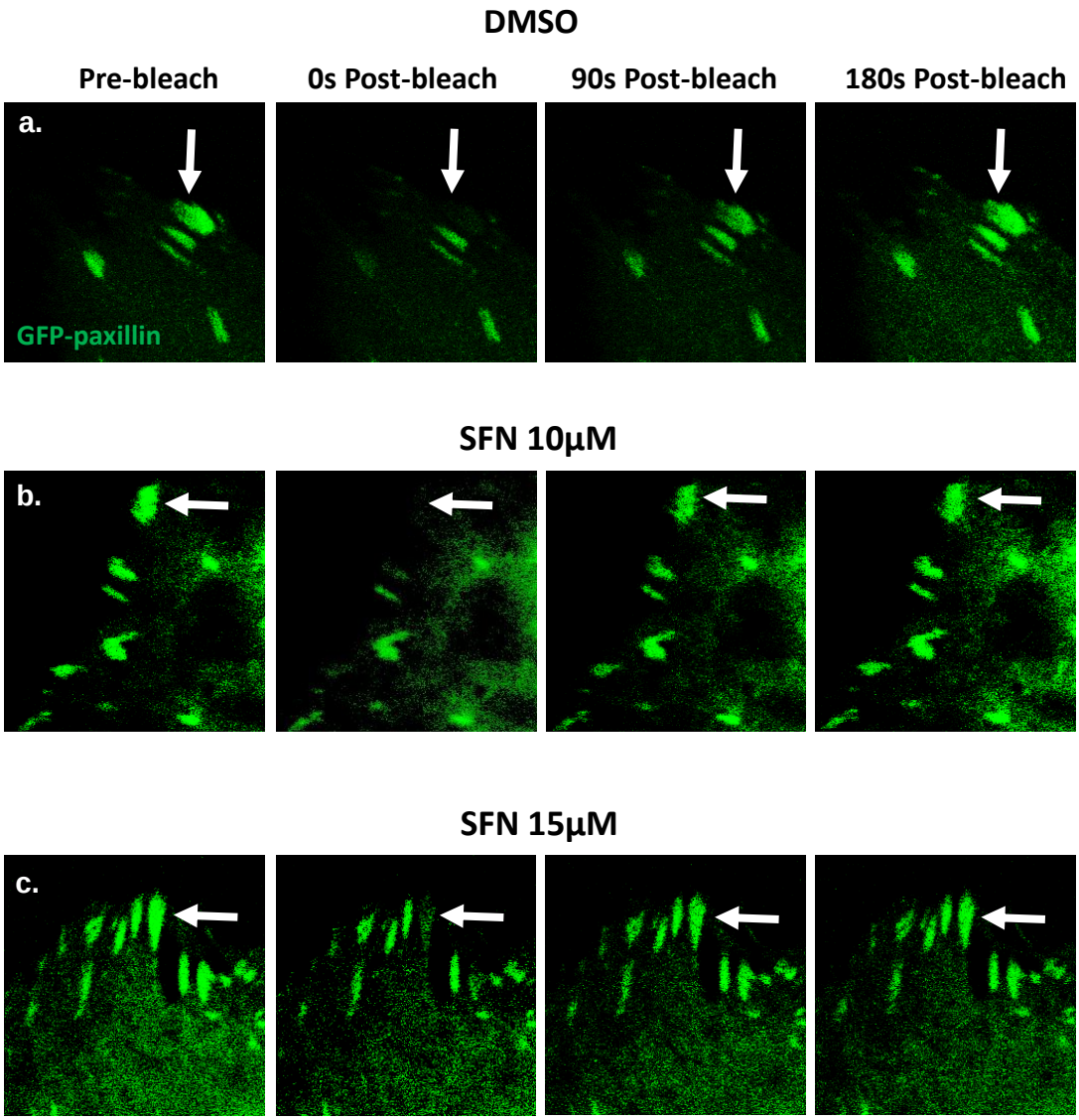

Figure 5.17 FRAP of GFP-paxillin at focal adhesion in ARPE-19 cells
Cells were treated with SFN and with GFP-paxillin construct. Live-confocal microscopy was used and selected focal adhesions were subjected to FRAP. Images from a time-lapse recording showing recovery of GFP-paxillin at the focal adhesion following photobleaching in DMSO and 10 and15µM SFN treated cells over three minutes (arrows).

PANC-1

FRAP analyses of GFP-paxillin

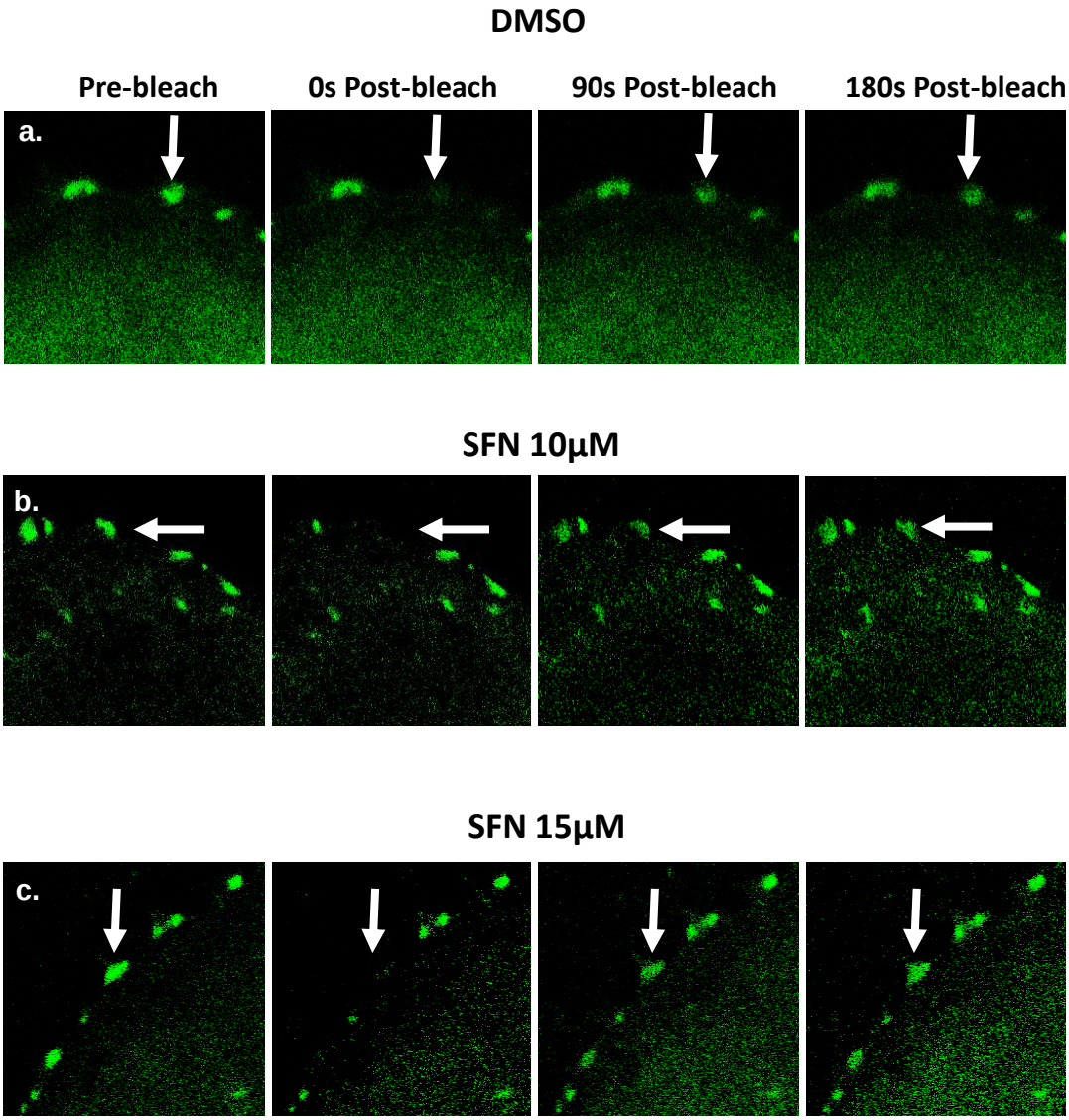

Figure 5.18 FRAP of GFP-paxillin at focal adhesion in PANC-1 cells
Cells were treated with SFN and with GFP-paxillin construct. Live-confocal microscopy was used and selected focal adhesions were subjected to FRAP. Images from a time-lapse recording showing recovery of GFP-paxillin at the focal adhesion following photobleaching in DMSO and 10 and µM SFN treated cells over three minutes (arrows).

ARPE-19

FRAP analyses of GFP-paxillin at focal adhesion

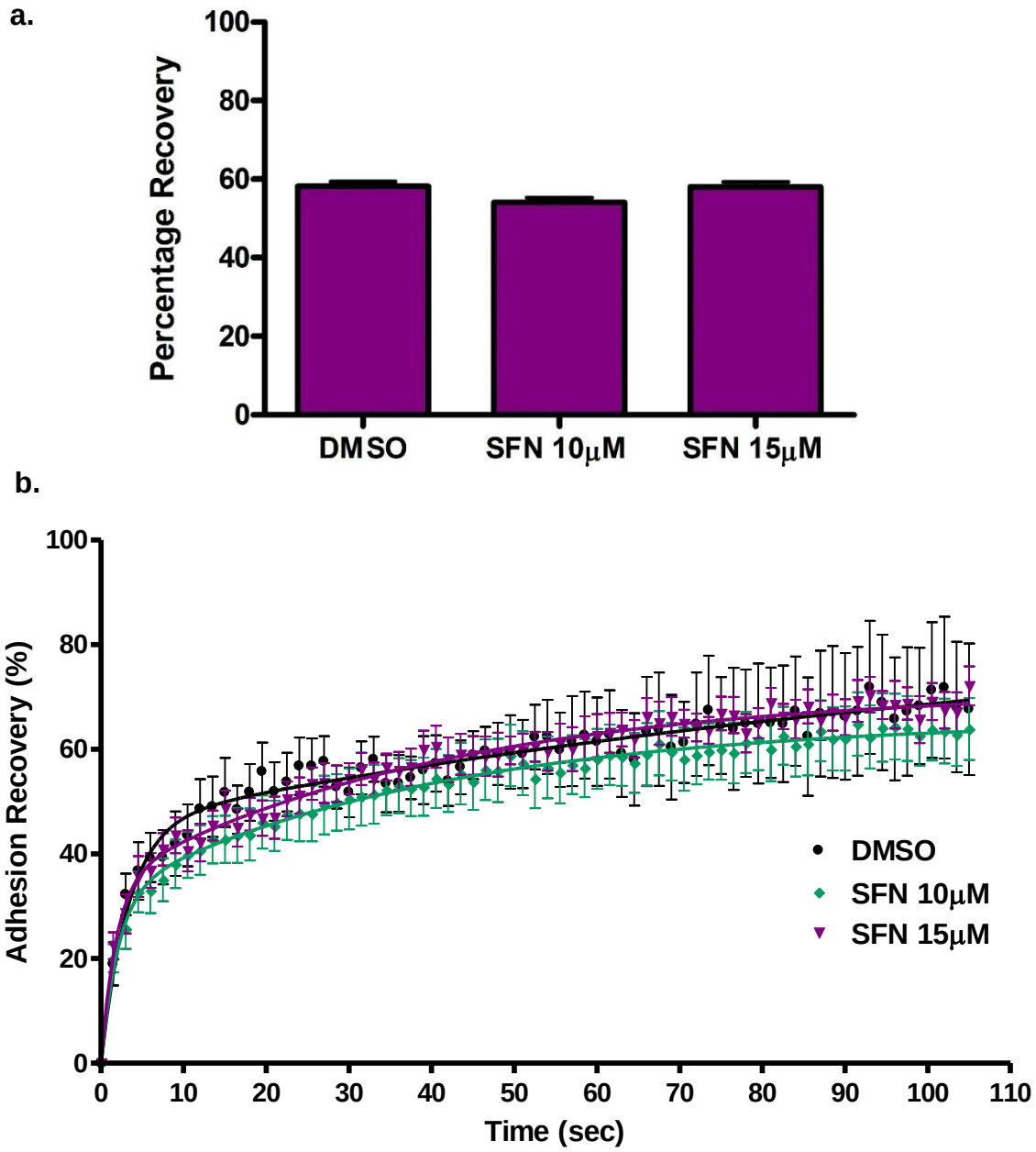

Figure 5.19 FRAP analyses of GFP-paxillin in ARPE-19 cells
Cells were treated with SFN for 48 h and with GFP-paxillin construct. Live-confocal microscopy was used and selected focal adhesions were subjected to FRAP. a) FRAP analyses illustrated there is no significant different in the percentage of the mean recovery between DMSO and 10 and 15µM SFN treated cells. b) FRAP results showed the fluorescence intensity during recovery following photobleaching of the DMSO (black) and 10µM (green) and 15µM (purple) SFN treated cells during experiment time, with no marked difference in the GFP-paxillin intensity during recovery following photobleaching, n=10.

PANC-1

FRAP analyses of GFP-paxillin at focal adhesion

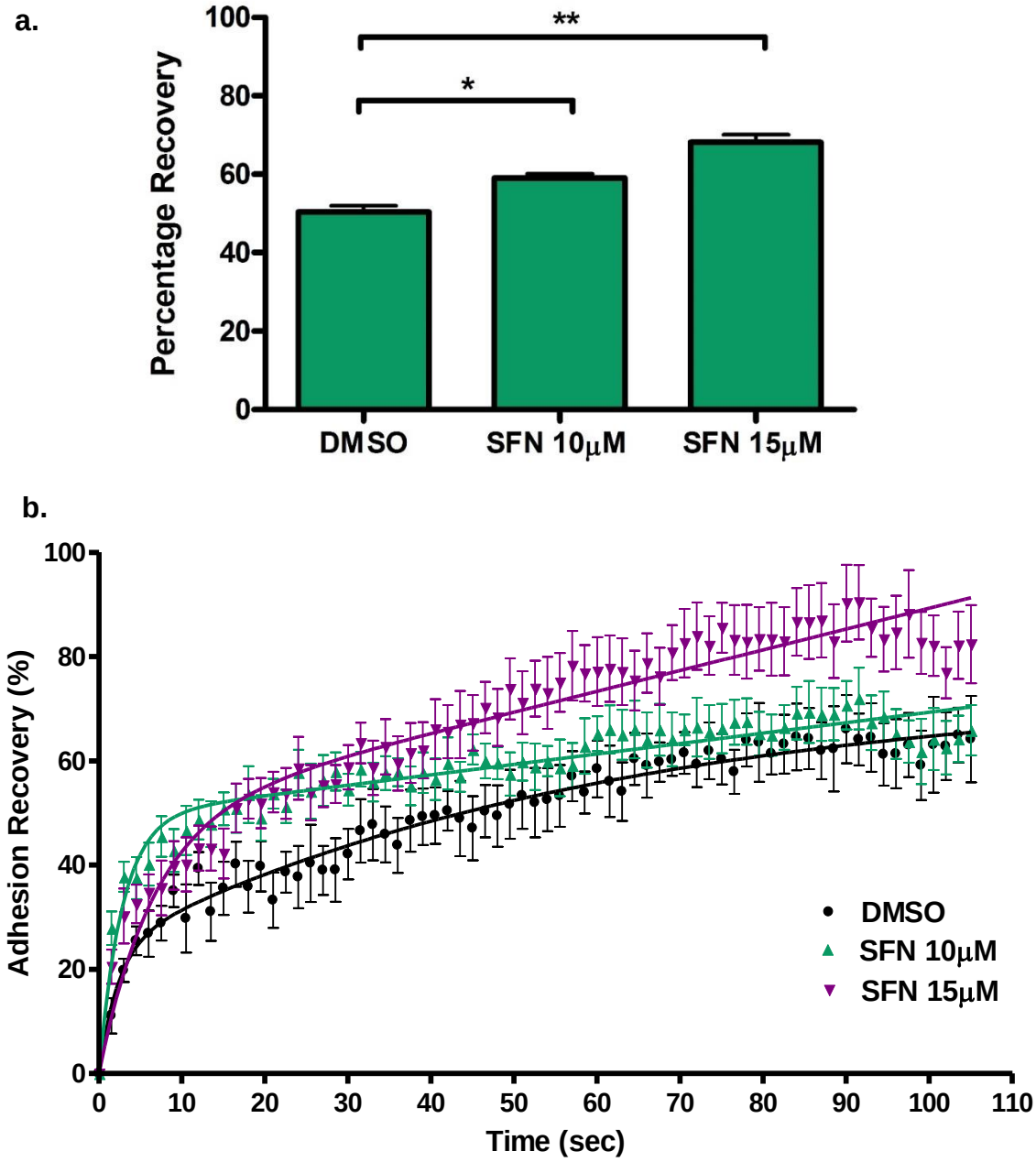

Figure 5.20 FRAP analyses of GFP-paxillin in PANC-1 cells
Cells were treated with SFN for 48 h and with GFP-paxillin construct. Live-confocal microscopy was used and selected focal adhesions were subjected to FRAP. a) FRAP analyses illustrates a significant increase in the percentage of the mean recovery in10 and 15μM SFN treated cells compared to DMSO. b) FRAP results showed the fluorescence intensity during recovery time following photobleaching of the DMSO (black) and 10 (green) and 15μM (purple) SFN treated cells during experiment time, with marked recovery at 10μM and 15μM SFN treated cells, n=10.

Chapter VI: General Discussion

6.1 Introduction

The microtubule cytoskeleton is one of the main targets for cancer research due to its dynamic instability, which allows microtubules to undergo the vital rearrangements required for various functions such as cell polarisation, division and migration. Microtubules along with other cytoskeletal elements play important roles in cell movement, generating distinct polarity and tracks for vesicle transport to the leading edge. They are also able to contribute to force production which is needed for movement. Dynamic instability allows the microtubules to explore the cytoplasm and make contact with cellular structures such as kinetochores or the cell cortex and regulate focal adhesion dynamics (Mitchison and Kirschner, 1984, Galjart and Perez, 2003, Howard and Hyman, 2003, Galjart, 2010, Li et al., 2011). Microtubule dynamics is tightly regulated by different groups of proteins, in particular the +TIP family of proteins. This family includes the EB family of proteins as well as HDAC6. EBs have an essential role in regulating microtubule dynamics, since they can interact with various other +TIPS as well as internal cell structures such as the cortex, organelles and the actin cytoskeleton (Vaughan, 2005, Lansbergen and Akhmanova, 2006). EBs can also associate along the microtubule lattice as a result of overexpression, which may affect the microtubule dynamics (Bu and Su, 2001, Goldspink et al., 2013). HDAC6 can associate with microtubule plus-ends and contribute to the regulation of microtubule dynamics. In addition, HDAC6 can promote and regulate cell motility, with overexpression of HDAC6 enhancing cell motility, while inhibition of its activity may impair cell movement (Pledgie-Tracy et al., 2007, Aldana-Masangkay and Sakamoto, 2010, Li et al., 2011, Li et al., 2014).

Due to these wide networks of microtubule-related proteins and their varying behaviour, it is interesting to investigate whether SFN could affect microtubule

organisation and dynamics in migrating epithelial cells both normal and cancerous, as well as its impact on EBs and HDAC6.

SFN is a promising potential cancer agent that is effective in different types of cancers, such as human prostate, colon and breast cancer (Jackson and Singletary, 2004, Gibbs et al., 2009, Clarke et al., 2011). SFN has been reported to affect microtubule behaviour, cell migration and mitosis. It has been reported that SFN reduces cell migration in ovarian cancer cells, but only in cytotoxic concentrations (Bryant et al., 2010). SFN also causes alterations in post-translational microtubule modifications and increases tubulin acetylation. This has been linked with stable microtubules, as reported in human breast and prostate cancer cells (Azarenko et al., 2008, Gibbs et al., 2009, Clarke et al., 2011).

There is thus a great desire to understand these actions, since they will likely lead to further development of effective drugs, especially for an aggressive cancer type such as pancreatic cancer, with patients expecting to survive for only five years after diagnosis. Pancreatic cancer, one of the most common diseases, is the most complicated epithelial cancers to treat since it is strongly resistant to current cancer treatment (Bardeesy and DePinho, 2002, Wang et al., 2011).

This project aimed to assess whether SFN will increase microtubule stability and decrease dynamics and whether SFN could induce a reduction in the speed of pancreatic cancer cell migration and normal epithelial cells. In addition, the project investigated whether SFN could affect the organisation of microtubules and actin filaments, as well as the localisation and expression of EBs and HDAC6. More generally, it also attempted to increase our knowledge of the effects of SFN treatment on cytoskeleton organisation and cell migration in cancer cells, thereby providing a better understanding of this process.

6.1.1 Research findings

The key findings of this project include the following:

1. SFN treatment dramatically reduced cell migration velocity in normal (ARPE-19) epithelial cells but not in PANC-1 cells (Chapter VI).

2. SFN treatment supressed microtubule dynamics (Chapter V), and caused a distinct phenotype with co-alignment between microtubules and actin filaments and EB1 relocated along the microtubule lattice resulting in the formation of microtubule bundles. These observations are in keeping with EB2 being cytoplasmic and thus allowing EB1 lattice association and microtubule bundle formation (Chapter IV).

3. SFN and tubacin together significantly reduced cell velocity of migration in pancreatic (Panc-1) cancer cells. Interestingly, no association between HDAC6 and microtubules was evident as previously reported (Hubbert et al., 2002) (Chapter IV).

4. SFN leads to an increase in focal adhesion size and area, with a significant increase in acetylated and detyrosinated microtubules and a marked increase in stable microtubules in normal (ARPE-19) epithelial cells. However, PANC-1 cells showed no increase in acetylated microtubules and stability, and also no different in focal adhesion size and area (Chapter V).

6.2 General discussion

SFN treatment showed a significant inhibition on cell migration in ARPE-19 epithelial cells but not in PANC-1 (pancreatic cancer cells) (Chapter IV). This significant reduction in cell migration in SFN treated ARPE-19 is likely to be due to the changes in the organisation of microtubules and actin filaments, as well as changes in the localisation of EB1 and EB2, where this may effect microtubules dynamics. SFN treated ARPE-19 cells showed alterations in the balance between dynamic and stable microtubules, with more acetylated and detyrosinated microtubules following SFN treatment. SFN has been reported to cause an increase in acetylation of microtubules in human breast and prostate cancer cells to result in decreased microtubule dynamics (Azarenko et al., 2008, Gibbs et al., 2009, Clarke et al., 2011). Tubulin acetylation and detyrosination are also known to be linked to stable microtubules (Kalebic et al., 2013, Sirajuddin et al., 2014, Yu et al., 2015). Our results also revealed, for the first time, co-alignment between microtubules and actin filaments as a result of SFN treatment, along with the formation of microtubule bundles (Chapter IV). This co-alignment has been reported in EB2-depleting cells with EB1 and ACF7 association along the microtubule lattice, which enables links to actin filaments (Goldspink et al., 2013).

Interestingly, SFN treatment leads to EB1 binding along the microtubule lattice and EB2 dispersal to the cytoplasm rather than along the lattice. The association between EB1 and the microtubule lattice suggests that EB1 lattice binding could enforce the lateral binding between microtubules protofilament, which may promote microtubule stability and also cause microtubule bundle formation (Sandblad et al., 2006, Vitre et al., 2008, Zhang et al., 2009, Goldspink et al., 2013).

SFN may indirectly cause phosphorylation of EB2 but future studies will be needed to confirm this. Studies have indicated that phosphorylation of EB2 by Aurora B or CDK1 on entry into mitosis leads to a decrease in the affinity of EB2 for microtubules and leads to EB2 release into the cytoplasm and this has been shown to be vital for normal mitosis progression (Iimori et al., 2016, Nehlig et al., 2017). SFN may thus induce EB2 phosphorylation at any stage of the cell cycle and lead to EB2 detachment from the microtubules lattice. A consequence of this could be that EB1 binds along the microtubule lattice. EB2 normally associates with the microtubule lattice and can bind and deliver MAP4K4 and HAX1 to focal adhesions, where MAP4K4 and HAX1 active IQSEC1 and Arf6 leading to focal adhesion turnover which is required for cell migration. Knockdown of EB2 has been shown to lead to focal adhesion stability and inhibit cell migration, as a result of undelivered MAP4K4 and HAX1 to focal adhesion and decrease focal adhesion turnover (Yue et al., 2014, Liu et al., 2015). EB2 has also been shown to be phosphorylated by CK2 causing a decrease in endothelial cell adhesion (Stenner et al., 2013). It is therefore possible that EB2 phosphorylation and detachment from the microtubule lattice could have a similar effect to EB2 depletion, with EB1 and ACF7 associating along the microtubule lattice and interacting with actin filaments causing their co-alignment (Goldspink et al., 2013). Further investigation of this would be very interesting.

In addition, SFN caused formation of microtubule bundles and an increase in ARPE-19 cell area. These results are compatible with other studies, where inhibition of HDAC6 in mouse embryonic fibroblast cells leads to increased adhesion area and decreased turnover with marked increase in cell area resulting in suppression of cell migration (Tran et al., 2007). These results suggest that all these

affects may play vital roles in the ARPE-19 cell migration mechanisms and reduce the speed of the cell migration.

Interestingly, SFN treated PANC-1 cells at concentration up to 15 μM did not show an effect on speed of cell migration or marked changes in microtubule organisation. However, EB1 was associated along the microtubule lattice and EB2 was found in the cytoplasm and along the microtubule lattice. These unexpected results may be due to the fact that EB2 and HDAC6 are highly expressed in PANC-1 cells, which may enhance microtubule dynamics and may lead to increased cell migration. EB2 is overexpressed and involved in the invasion in pancreatic cancer and HDAC6 causes complete deacetylation of microtubules and associates with EB1 and CLIP-170 at the plus-end to regulate microtubule dynamics that leads to increased cell migration (Hubbert et al., 2002, Matsuyama et al., 2002, Zhang et al., 2003, Abiatari et al., 2009, Zilberman et al., 2009, Clarke et al., 2011, Huo et al., 2011, Li et al., 2014, Ding et al., 2014, Ran et al., 2015).

The combination of the two treatments (SFN and tubacin) with distinct targets was used to achieve significant results. The combination of SFN and tubacin significantly decreased PANC-1 cancer cell migration (Chapter IV). To the best of our knowledge, this is the first time it has been reported that a combination of tubacin (a specific HDAC6 inhibitor) and SFN results in a dramatic reduction in the speed of pancreatic cancer cell migration, where tubacin or SFN alone did not affect PANC-1 cell migration. However, SFN showed an effect on EB1 and EB2 localisation, with extensive association between EB1 and microtubule lattice and with marked increase in cytoplasmic EB2. Interestingly, no effect on microtubule dynamics in PANC1 cells was observed although this should be investigated further. However, EB2 is overexpressed in PANC-1 cells and this may prevent SFN from causing total detachment of EB2 from the microtubule lattice and thus allow

some MAP4K4 delivery to focal adhesions. Additionally, HDAC6 is also overexpressed in PANC1 cells and it seems that SFN alone cannot counteract the activity of HDAC6. Tubacin was used to inhibit HDAC6 and in ARPE-19 cells 10μM tubacin caused a marked increase in cell area and a significant decrease in cell migration. However, tubacin alone was not sufficient to induce a decrease in cell migration in PANC-1 cells but a combination of tubacin and SFN led to reduced migration. This suggests that SFN and tubacin may work together affecting the localisation of the EBs and the activity of HDAC6 and combined they lead to a significant reduction in cell migration in PANC-1 cells.

We answered one of our research questions, namely, whether SFN treatment affects microtubule dynamics and stability in both normal and cancerous epithelial cells. Our results suggested that SFN inhibits microtubule growth in normal epithelial cells, as indicated by GFP-CLIP-170 dynamic analyses, with a significant reduction in average comet speed and growth length in SFN treated AREP-19 cells. However, SFN treated PANC-1 cells did not display a marked effect on microtubule growth length or speed. It has been reported that SFN supresses microtubule dynamics, with a significant reduction in microtubule growth rate in human breast cancer cells; however, only four microtubules were used to analyse microtubule dynamics, which is insufficient to deference significance (Azarenko et al., 2008). In addition, we found that the average area of acetylated microtubules increased dramatically in SFN treated ARPE-19 cells but not in PANC-1 cells. This was also suggested by cold treatment, where more stable microtubules were observed in SFN treated ARPE-19 cells. However, in PANC-1 cells, cold treatment resulted in the presence of stable microtubules without SFN treatment and no increase in stable microtubules in SFN treated PANC-1 cells compared to DMSO treated cells. Moreover, analysis of the average area of acetylated microtubules in SFN treated

PANC-1 cells revealed no significant increase in the area of acetylated microtubules. The results showed that SFN did not affect PANC-1 cell migration and this could be due to there is no marked decrease in microtubule dynamics in SFN treated PANC-1 cells. Western blot also suggested that there was an increase in the level of acetylated tubulin expression in SFN treated ARPE-19 cells but not in SFN treated PANC-1 cells.

The focal adhesion results revealed that the global focal adhesion area and individual size were significantly increased in the SFN treated ARPE-19 cells. Whereas, SFN treated PANC-1 cells showed no changes in focal adhesion global area or individual size. The focal adhesion recovery from FRAP results showed SFN had no effect on focal adhesion turnover in ARPE-19, but it increased focal adhesion dynamics in SFN treated PANC-1 cells. In general, further investigation is needed here to better understand the effect of SFN on focal adhesion dynamics and turnover.

To summarise, SFN treatment showed significant effects on microtubules and actin filaments organisation with marked co-alignment between actin filaments and bundle microtubules. It can suggested that this co-alignment is due to association between EB1 and ACF7, but this will need further investigation. EB2 could be phosphorylated by SFN treatment, as phosphorylation leads to EB2 detachment from the microtubules lattice and decreases focal adhesion turnover by affectting focal adhesion proteins (MAP4K4 and HAX1) delivery via EB2 (as been discussed early) (Yue et al., 2014, Liu et al., 2015). In addition, detachment of EB2 from microtubule may enhance more EB1 association along the lattice with marked microtubule bundles. This is similar to depleted EB2 effects with extensive association between EB1 and ACF7 (Goldspink et al., 2013). It seems that all these

results together lead to effect the mechanisms of migration and inhibit cell migration.

A suggested model of the possible mechanism of the effect of SFN on cell migration is shown in Figure 6.1. It is known that dynamic microtubules are guided to focal adhesions along actin filaments and cross-linking proteins, such as ACF7 (Kaverina et al., 1999, Wu et al., 2008). Microtubules can act as a track for the delivery of proteins that are essential for focal adhesion disassembly, with disassembly of focal adhesions being critical for cell movement. MAP4K4 is a focal adhesion regulator that associates indirectly with microtubules by binding to EB2, and its depletion leads to focal adhesion stabilisation and inhibition of migration. Microtubules can therefore deliver MAP4K4 to focal adhesions through binding to EB2. At the focal adhesion, MAP4K4 activates Arf6 via IQSEC1 and initiate focal adhesion disassembly (Yue et al., 2014, Liu et al., 2015). We propose that SFN may lead to the phosphorylation of EB2 causing EB2 to disassociate from microtubules. Cytoplasmic EB2 may in addition sequester MAP4K4/HAX1 and prevent the delivery of MAP4K4/HAX1 to focal adhesions. This would lead to a decrease in focal adhesion disassembly and turnover leading to suppression of cell migration.

Generation of a specific EB2 inhibitor may thus be of potential interest in the treatment of certain cancers in a similar way to HDAC6 inhibitors which have proved of clinical importance as anti-cancer agents (Haggarty et al., 2003).

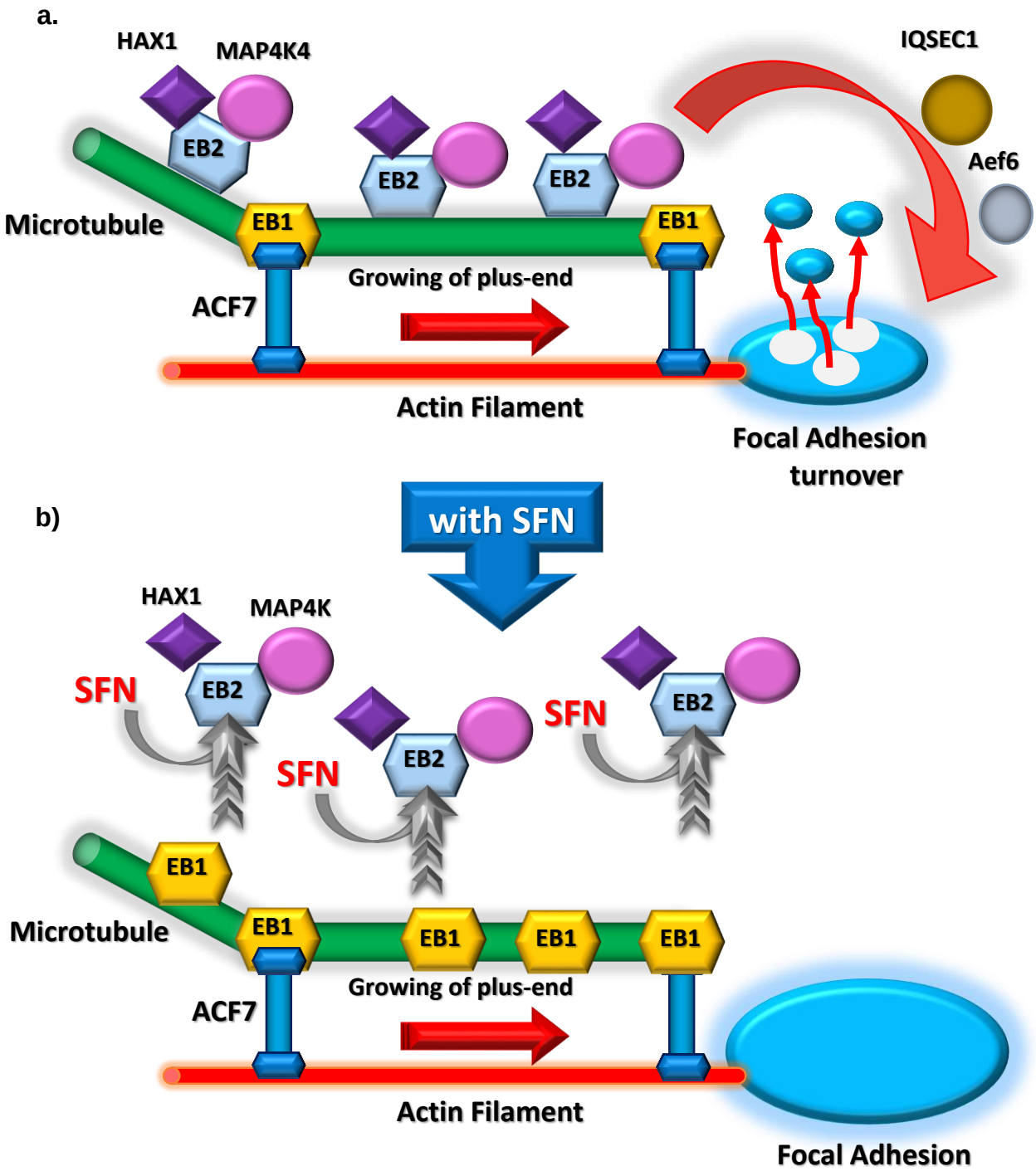

Figure 6.1 Model for SFN effects on cell migration

A working model for a possible mechanism by which SFN may effect cell migration. **a)** Dynamic microtubules target focal adhesions being guided along actin filaments by EB1/ACF7. This enables delivery of key disassembly components along microtubules to focal adhesions. MAP4K4 and HAX1 interact with EB2 and are delivered to focal adhesion. At the focal adhesion MAP4K4 activates IQSEC1 which activates Arf6 leading to integrin internalisation and focal adhesion disassembly. **b)** SFN may lead to phosphorylation of EB2 causing disassociation from microtubules. Cytoplasmic EB2 sequester MAP4K4/HAX1 and prevents their delivery to the focal adhesions, decreasing focal adhesion turnover and thus also cell migration. Detachment of EB2 from the microtubule lattice enable EB1 lattice association. Adapted from (Yue et al., 2014).

6.3 Future work

There remains several areas for future study, such as investigating whether SFN causes phosphorylation of EB2 and disassociation from the microtubules. This may provide a better understanding of the role of EB2 and the influence of SFN on microtubules and its interaction with other proteins. Furthermore, the co-alignment of actin filaments with microtubules as a result of SFN treatment must be investigated further, as to whether it is related to association with other proteins, such as ACF7 and EB1. It has been shown that ACF7 can bind to microtubules, EB1 and actin filaments (Goldspink et al., 2013). In depleted EB2 cells, EB1 was observed to bind along the microtubule lattice, recruiting ACF7 and facilitating microtubule bundle formation with co-alignment with actin filaments (Alves-Silva et al., 2012, Goldspink et al., 2013). The possible effects of SFN on ACF7 related to actin filaments and microtubules could also be investigated. This may provide a better understanding of the cell migration mechanism. In addition, HDAC6 and its association with EB1 may be interesting to study, as well as the possible association between HDAC6 and actin filaments or intermediate filaments with SFN treatment. In addition, microtubule bundle formation and microtubule and actin filament co-alignment needs further investigation by using transmission electron microscope (TEM).

Furthermore, SFN affects on focal adhesion turnover require additional investigation. Study has shown that the inhibition of HDAC6 leads to increase the focal adhesion area and inhibits focal adhesion turnover (Tran et al., 2007). Thus, it would be interesting to examine whether the combination of tubacin and SFN at low concentrations has the same effect on focal adhesion in cancerous epithelial cells. It would perhaps be most interesting, however, to investigate microtubule

dynamics in normal and cancer epithelial cells given both of these treatments, including whether this could affect protein delivery via microtubules. Other studies have revealed that dynamic microtubules and EB2 contribute to the delivery of essential focal adhesion disassembly proteins, such as MAP4K4 and HAX1 (Yue et al., 2014, Liu et al., 2015). Thus, SFN may affect the delivery of proteins that are essential for focal adhesion dynamics via its effect on EB2 localisation. This represents one possible mechanism by which SFN may affect focal adhesion dynamics. In addition, further investigation is needed to determine the effect of SFN in 3D model systems to observe whether it has similar effects on cell migration as in 2D.

Appendices

Appendix A: Reagents and Solutions

Western Blotting Solutions

Protein Lysis Buffer

In ddH2O:

50mM	HEPES	pH 7.5
50mM	NaCl	
1%	Triton X-100	
1mM	EDTA	
10%	Glycerol	

Sample Buffer

In ddH2O:

125mM	Tris-HCI at	pH 6.8
2%	SDS (Sodium dodecyl sulphate)	
0.02%	Bromophenol Blue	
20%	Glycerol	

Lower Gel Buffer (6%) (In final volume 250mls ddH2O)

200mls	ddH2O	
45.375 g	Tris (1.5M)	pH 6.8
1 g	SDS (0.4% w/v)	

Upper Gel Buffer (In final volume 250mls ddH2O)

200 mls	ddH2O	
15.125 g	Tris (500Mm)	pH 6.8
1 g	SDS (0.4% w/v)	

6% Lower Resolving Gel

Per gel (12ml total volume):

1.8ml 40%	Acrylamide (Sigma, Poole, Dorset)
3ml	Lower Gel Buffer
7.2ml	ddH2O
72µl 10%	Ammonium persulphate (Sigma, Poole, Dorset)
14µl	TEMED (N,N,N',N'Xtetramethylethylenediamine) (Sigma, Poole, Dorset)

8% Lower Resolving Gel

Per gel (12ml total volume):

2.4ml 40%	Acrylamide
3ml	Lower Gel Buffer
6.6ml	ddH2O
72µl 10%	Ammonium persulphate
14µl	TEMED

5% Upper Stacking Gel

Per gel (8ml total volume):

1ml 40%	Acrylamide
2ml	Upper Gel Buffer
5ml	ddH2O
72µl 10%	Ammonium persulphate
14µl	TEMED

10x SDS Running Buffer

In a final volume of 5l ddH20:

151g	Tris (250mM)
720g	Glycine (1.9M)
50g	SDS (1% w/v)

Transfer Buffer

In a final volume of 1l:

800ml	ddH2O	
2.9g	Glycine (39mM)	
5.8g	Tris (48mM)	adjusted to pH 8.3
0.375g	SDS (0.0375% w/v)	
200ml	Methanol (20% v/v)	

PBS-T

In a final volume of 200ml PBS:

100µl	Tween-20

Tris-HCl

In ddH20:

100mM	Tris	adjusted topH8.5 with Hydrochloric acid

ECL Solution A

In 10ml Tris-HCL, pH 8.5:

45µl	Coumaric acid (91mM stock solution: 0.15g in 10ml DMSO) (Sigma, Poole, Dorset)
100µl	Luminol (250mM stock solution: 0.44g in 10ml DMSO)

(Sigma, Poole, Dorset)

ECL Solution B

In 10ml Tris-HCL, pH 8.5:

6µl 30% Hydrogen peroxide solution

Appendix B: Supplementary Data

Movies

Chapter IV

Movie S1: Cell tracking in sub-confluent untreated ARPE-19 cells

Time-lapse movie of untreated ARPE-19 cells, where 10 cells were taken from eight different locations. For each cell, position was tracked from each frame for a 16-hour time-lapse experiment with images taken every 10-minutes using a x10 objective, and movies replayed at 10 frames per second. Position data for all cells were then combined, and ImageJ was used to prepare the traces.

Movie S2: Cell tracking in sub-confluent DMSO treated ARPE-19 cells

Time-lapse movie of DMSO treated cells, where 10 cells were taken from eight different locations. For each cell, position was tracked from each frame for a 16-hour time-lapse experiment with images taken every 10-minutes using a x10 objective, and movies replayed at 10 frames per second. Position data for all cells were then combined, and ImageJ was used to prepare the traces. Cells appeared to move generally similar to those in untreated cells.

Movie S3: Cell tracking in sub-confluent 2 µM SFN treated ARPE-19 cells

Time-lapse movie of 2 µM SFN treated cells, where 10 cells were taken from eight different locations. For each cell, position was tracked from each frame for a 16-hour time-lapse experiment with images taken every 10-minutes using a x10 objective, and movies replayed at 10 frames per second. Position data for all cells were then combined, and ImageJ was used to prepare the traces. Movie revealed no significant different in the speed of 2 µM SFN treated cells compared to DMSO cells.

Movie S4: Cell tracking in sub-confluent 10 µM SFN treated ARPE-19 cells

Time-lapse movie of 10 µM SFN treated cells, where 10 cells were taken from eight different locations. For each cell, position was tracked from each frame for a 16-hour time-lapse experiment with images taken every 10-minutes using a x10 objective, and movies replayed at 10 frames per second. Position data for all cells were then combined, and ImageJ was used to prepare the traces. Movie revealed a decrease in the speed of 10 µM SFN treated cells compared to DMSO cells.

Movie S5: Cell tracking in sub-confluent 15 µM SFN treated ARPE-19 cells

Time-lapse movie of 15 µM SFN treated cells, where 10 cells were taken from eight different locations. For each cell, position was tracked from each frame for a 16-hour time-lapse experiment with images taken every 10-minutes using a x10 objective, and movies replayed at 10 frames per second. Position data for all cells were then combined, and ImageJ was used to prepare the traces. Movie revealed a decrease in the speed of 15 µM SFN treated cells compared to DMSO cells.

Movie S6: Cell tracking in sub-confluent untreated PANC-1 cells

Time-lapse movie of untreated cells, where 10 cells were taken from eight different locations. For each cell, position was tracked from each frame for a 16-hour time-lapse experiment with images taken every 10-minutes using a x10 objective, and movies replayed at 10 frames per second. Position data for all cells were then combined, and ImageJ was used to prepare the traces.

Movie S7: Cell tracking in sub-confluent DMSO treated PANC-1 cells

Time-lapse movie of DMSO treated cells, where 10 cells were taken from eight different locations. For each cell, position was tracked from each frame for a 16-hour time-lapse experiment with images taken every 10-minutes using a x10 objective, and movies replayed at 10 frames per second. Position data for all cells were then combined, and ImageJ was used to prepare the traces. Cells appeared to move generally similar to those in untreated cells.

Movie S8: Cell tracking in sub-confluent 2 µM SFN treated PANC-1 cells

Time-lapse movie of 2 µM SFN treated cells, where 10 cells were taken from eight different locations. For each cell, position was tracked from each frame for a 16-hour time-lapse experiment with images taken every 10-minutes using a x10 objective, and movies replayed at 10 frames per second. Position data for all cells were then combined, and ImageJ was used to prepare the traces. Movie revealed no marked decrease in the speed of 2 µM SFN treated cells compared to DMSO cells.

Movie S9: Cell tracking in sub-confluent 10 µM SFN treated PANC-1 cells

Time-lapse movie of 10 µM SFN treated cells, where 10 cells were taken from eight different locations. For each cell, position was tracked from each frame for a 16-hour time-lapse experiment with images taken every 10-minutes using a x10 objective, and movies replayed at 10 frames per second. Position data for all cells were then combined, and ImageJ was used to prepare the traces. Movie revealed no marked decrease in the speed of 10 µM SFN treated cells compared to DMSO cells.

Movie S10: Cell tracking in sub-confluent 15 µM SFN treated PANC-1 cells

Time-lapse movie of 15 µM SFN treated cells, where 10 cells were taken from eight different locations. For each cell, position was tracked from each frame for a 16-hour time-lapse experiment with images taken every 10-minutes using a x10 objective, and movies replayed at 10 frames per second. Position data for all cells were then combined, and ImageJ was used to prepare the traces. Movie revealed no marked decrease in the speed of 15 µM SFN treated cells compared to DMSO cells.

Movie S11: Cell tracking in sub-confluent 10 µM tubacin treated ARPE-19 cells

Time-lapse movie of 10 µM tubacin treated cells, where 10 cells were taken from eight different locations. For each cell, position was tracked from each frame for a 16-hour time-lapse experiment with images taken every 10-minutes using a x10 objective, and movies replayed at 10 frames per second. Position data for all cells were then combined, and ImageJ was used to prepare the traces. Movie revealed a marked decrease in the speed of 10 µM tubacin treated cells compared to DMSO cells.

Movie S12: Cell tracking in sub-confluent 10 µM tubacin and 10 µM SFN treated ARPE-19 cells

Time-lapse movie of 10 µM tubacin and 10 µM SFN treated cells, where 10 cells were taken from eight different locations. For each cell, position was tracked from each frame for a 16-hour time-lapse experiment with images taken every 10-minutes using a x10 objective, and movies replayed at 10 frames per second. Position data for all cells were then combined, and ImageJ was used to prepare the traces. Movie revealed a marked decrease in the speed of 10 µM tubacin and 10 µM SFN treated cells compared to DMSO cells.

Movie S13: Cell tracking in sub-confluent 10 µM tubacin and 15 µM SFN treated ARPE-19 cells

Time-lapse movie of 10 µM tubacin and 15 µM SFN treated cells, where 10 cells were taken from eight different locations. For each cell, position was tracked from each frame for a 16-hour time-lapse experiment with images taken every 10-minutes using a x10 objective, and movies replayed at 10 frames per second. Position data for all cells were then combined, and ImageJ was used to prepare the traces. Movie revealed a marked decrease in the speed of 10 µM tubacin and 15 µM SFN treated cells compared to DMSO cells.

Movie S14: Cell tracking in sub-confluent 10 µM tubacin treated PANC-1 cells

Time-lapse movie of 10 µM tubacin treated cells, where 10 cells were taken from eight different locations. For each cell, position was tracked from each frame for a 16-hour time-lapse experiment with images taken every 10-minutes using a x10 objective, and movies replayed at 10 frames per second. Position data for all cells were then combined, and ImageJ was used to prepare the traces. Movie revealed no marked decrease in the speed of 10 µM tubacin treated cells compared to DMSO cells.

Movie S15: Cell tracking in sub-confluent 10 µM tubacin and 10 µM SFN treated PANC-1 cells

Time-lapse movie of 10 µM tubacin and 10 µM SFN treated cells, where 10 cells were taken from eight different locations. For each cell, position was tracked from each frame for a 16-hour time-lapse experiment with images taken every 10-minutes using a x10 objective, and movies replayed at 10 frames per second. Position data for all cells were then combined, and ImageJ was used to prepare the traces. Movie revealed no marked decrease in the speed of 10 µM tubacin and 10 µM SFN treated cells compared to DMSO cells.

Movie S16: Cell tracking in sub-confluent 10 µM tubacin and 15 µM SFN treated PANC-1 cells

Time-lapse movie of 10 µM tubacin and 15 µM SFN treated cells, where 10 cells were taken from eight different locations. For each cell, position was tracked from each frame for a 16-hour time-lapse experiment with images taken every 10-minutes using a x10 objective, and movies replayed at 10 frames per second. Position data for all cells were then combined, and ImageJ was used to prepare the traces. Movie revealed no marked decrease in the speed of 10 µM tubacin and 15 µM SFN treated cells compared to DMSO cells.

Chapter V

Movie S17: DMSO treated ARPE-19 GFP-CLIP-170 dynamics

Time-lapse of DMSO treated cell transiently expressing GFP-CLIP-170. Images were taken every three-seconds over three-minute period (60 frames in total) and replayed at 5 frames per second. The movie shows U-Track analysis of GFP-CLIP-170 comets over images period with growing (red), shrinking (yellow) and pausing (blue) microtubule highlighted.

Movie S18: 10 µM SFN treated ARPE-19 GFP-CLIP-170 dynamics

Time-lapse of 10 µM SFN treated cell transiently expressing GFP-CLIP-170. Images were taken every three-seconds over three-minute period (60 frames in total) and replayed at 5 frames per second. The movie shows U-Track analysis of GFP-CLIP-170 comets over images period with growing (red), shrinking (yellow) and pausing (blue) microtubule highlighted.

Movie S19: 15 µM SFN treated ARPE-19 GFP-CLIP-170 dynamics

Time-lapse of 15 µM SFN treated cell transiently expressing GFP-CLIP-170. Images were taken every three-seconds over three-minute period (60 frames in total) and replayed at 5 frames per second. The movie shows U-Track analysis of GFP-CLIP-170 comets over images period with growing (red), shrinking (yellow) and pausing (blue) microtubule highlighted.

Movie S20: DMSO SFN treated PANC-1 GFP-CLIP-170 dynamics

Time-lapse of DMSO treated cell transiently expressing GFP-CLIP-170. Images were taken every three-seconds over three-minute period (60 frames in total) and replayed at 5 frames per second. The movie shows U-Track analysis of GFP-CLIP-170 comets over images period with growing (red), shrinking (yellow) and pausing (blue) microtubule highlighted.

Movie S21: 10 µM SFN treated PANC-1 GFP-CLIP-170 dynamics

Time-lapse of 10 µM SFN treated cell transiently expressing GFP-CLIP-170. Images were taken every three-seconds over three-minute period (60 frames in total) and replayed at 5 frames per second. The movie shows U-Track analysis of GFP-CLIP-170 comets over images period with growing (red), shrinking (yellow) and pausing (blue) microtubule highlighted.

Movie S22: 15 µM SFN treated ARPE-19 GFP-CLIP-170 dynamics

Time-lapse of 15 µM SFN treated cell transiently expressing GFP-CLIP-170. Images were taken every three-seconds over three-minute period (60 frames in total) and replayed at 5 frames per second. The movie shows U-Track analysis of GFP-CLIP-170 comets over images period with growing (red), shrinking (yellow) and pausing (blue) microtubule highlighted.

Movie S23: DMSO treated ARPE-19 GFP-paxillan recovery after FRAP

Time-lapse of DMSO treated cell transiently expressing GFP-paxillan. Selected focal adhesion was subjected to FRAP (fluorescence recovery after photo-bleaching). Images were taken every three-seconds over three-minute period (60 frames in total) and replayed at 5 frames per second. The movie shows selected focal adhesion that subjected to FRAP and its recovery over 3 minutes period.

Movie S24: 10 µM SFN treated ARPE-19 GFP-paxillan recovery after FRAP

Time-lapse of 10 µM SFN treated cell transiently expressing GFP-paxillan. Selected focal adhesion was subjected to FRAP (fluorescence recovery after photo-bleaching). Images were taken every three-seconds over three-minute period (60 frames in total) and replayed at 5 frames per second. The movie shows selected focal adhesion that subjected to FRAP and its recovery over 3 minutes period.

Movie S25: 15 µM SFN treated ARPE-19 GFP-paxillan recovery after FRAP

Time-lapse of 15 µM SFN treated cell transiently expressing GFP-paxillan. Selected focal adhesion was subjected to FRAP (fluorescence recovery after photo-bleaching). Images were taken every three-seconds over three-minute period (60 frames in total) and replayed at 5 frames per second. The movie shows selected focal adhesion that subjected to FRAP and its recovery over 3 minutes period.

Movie S26: DMSO treated PANC-1 GFP-paxillan recovery after FRAP

Time-lapse of DMSO treated cell transiently expressing GFP-paxillan. Selected focal adhesion was subjected to FRAP (fluorescence recovery after photo-bleaching). Images were taken every three-seconds over three-minute period (60 frames in total) and replayed at 5 frames per second. The movie shows selected focal adhesion that subjected to FRAP and its recovery over 3 minutes period.

Movie S27: 10 µM SFN treated PANC-1 GFP-paxillan recovery after FRAP

Time-lapse of 10 µM SFN treated cell transiently expressing GFP-paxillan. Selected focal adhesion was subjected to FRAP (fluorescence recovery after photo-bleaching). Images were taken every three-seconds over three-minute period (60 frames in total) and replayed at 5 frames per second. The movie shows selected focal adhesion that subjected to FRAP and its recovery over 3 minutes period.

Movie S28: 15 µM SFN treated PANC-1 GFP-paxillan recovery after FRAP

Time-lapse of 15 µM SFN treated cell transiently expressing GFP-paxillan. Selected focal adhesion was subjected to FRAP (fluorescence recovery after photo-bleaching). Images were taken every three-seconds over three-minute period (60 frames in total) and replayed at 5 frames per second. The movie shows selected focal adhesion that subjected to FRAP and its recovery over 3-minutes period.

References

Abiatari, I., Gillen, S., Deoliveira, T., Klose, T., Bo, K., Giese, N. A., Friess, H. & Kleeff, J. 2009. The microtubule-associated protein MAPRE2 is involved in perineural invasion of pancreatic cancer cells. *Int J Oncol,* 35**,** 1111-6.

Akhmanova, A. & Hoogenraad, C. C. 2005. Microtubule plus-end-tracking proteins: mechanisms and functions. *Current opinion in cell biology,* 17**,** 47-54.

Akhmanova, A. & Hoogenraad, C. C. 2015. Microtubule minus-end-targeting proteins. *Current Biology,* 25**,** R162-R171.

Akhmanova, A., Hoogenraad, C. C., Drabek, K., Stepanova, T., Dortland, B., Verkerk, T., Vermeulen, W., Burgering, B. M., De Zeeuw, C. I., Grosveld, F. & Galjart, N. 2001. Clasps are CLIP-115 and -170 associating proteins involved in the regional regulation of microtubule dynamics in motile fibroblasts. *Cell,* 104**,** 923-35.

Akhmanova, A., Mausset-Bonnefont, A.-L., Van Cappellen, W., Keijzer, N., Hoogenraad, C. C., Stepanova, T., Drabek, K., Van Der Wees, J., Mommaas, M. & Onderwater, J. 2005. The microtubule plus-end-tracking protein CLIP-170 associates with the spermatid manchette and is essential for spermatogenesis. *Genes & development,* 19**,** 2501-2515.

Akhmanova, A. & Steinmetz, M. O. 2008. Tracking the ends: a dynamic protein network controls the fate of microtubule tips. *Nature reviews Molecular cell biology,* 9**,** 309-322.

Akhmanova, A. & Steinmetz, M. O. 2011. Microtubule end binding: EBs sense the guanine nucleotide state. *Current Biology,* 21**,** R283-R285.

Akhmanova, A. & Steinmetz, M. O. 2015. Control of microtubule organization and dynamics: two ends in the limelight. *Nature Reviews Molecular Cell Biology*.

Akhshi, T. K., Wernike, D. & Piekny, A. 2014. Microtubules and actin crosstalk in cell migration and division. *Cytoskeleton,* 71**,** 1-23.

Al-Bassam, J. & Chang, F. 2011. Regulation of microtubule dynamics by TOG-domain proteins XMAP215/Dis1 and CLASP. *Trends in cell biology,* 21**,** 604-614.

Al-Bassam, J., Kim, H., Brouhard, G., Van Oijen, A., Harrison, S. C. & Chang, F. 2010. CLASP promotes microtubule rescue by recruiting tubulin dimers to the microtubule. *Dev Cell,* 19**,** 245-58.

Aldana-Masangkay, G. I. & Sakamoto, K. M. 2010. The role of HDAC6 in cancer. *BioMed Research International,* 2011.

Alves-Silva, J., Sánchez-Soriano, N., Beaven, R., Klein, M., Parkin, J., Millard, T. H., Bellen, H. J., Venken, K. J., Ballestrem, C. & Kammerer, R. A. 2012. Spectraplakins promote microtubule-mediated axonal growth by functioning as structural microtubule-associated proteins and EB1-dependent+ TIPs (tip interacting proteins). *Journal of Neuroscience,* 32**,** 9143-9158.

Applegate, K. T., Besson, S., Matov, A., Bagonis, M. H., Jaqaman, K. & Danuser, G. 2011. plusTipTracker: quantitative image analysis software for the measurement of microtubule dynamics. *Journal of structural biology,* 176**,** 168-184.

Arao, S., Masumoto, A. & Otsuki, M. 2000. β1 integrins play an essential role in adhesion and invasion of pancreatic carcinoma cells. *Pancreas,* 20**,** 129-137.

Asthana, J., Kapoor, S., Mohan, R. & Panda, D. 2013. Inhibition of HDAC6 deacetylase activity increases its binding with microtubules and suppresses microtubule dynamic instability in MCF-7 cells. *Journal of Biological Chemistry,* 288**,** 22516-22526.

Azarenko, O., Okouneva, T., Singletary, K. W., Jordan, M. A. & Wilson, L. 2008. Suppression of microtubule dynamic instability and turnover in MCF7 breast cancer cells by sulforaphane. *Carcinogenesis,* 29**,** 2360-2368.

Bardeesy, N. & Depinho, R. A. 2002. Pancreatic cancer biology and genetics. *Nature Reviews Cancer,* 2**,** 897-909.

Barra, H., Arce, C., Rodriguez, J. & Caputto, R. 1973. Incorporation of phenylalanine as a single unit into rat brain protein: reciprocal inhibition by

phenylalanine and tyrosine of their respective incorporations. *Journal of neurochemistry,* 21**,** 1241-1251.

Bellett, G., Carter, J. M., Keynton, J., Goldspink, D., James, C., Moss, D. K. & Mogensen, M. M. 2009. Microtubule plus-end and minus-end capture at adherens junctions is involved in the assembly of apico-basal arrays in polarised epithelial cells. *Cell motility and the cytoskeleton,* 66**,** 893-908.

Berges, R., Baeza-Kallee, N., Tabouret, E., Chinot, O., Petit, M., Kruczynski, A., Figarella-Branger, D., Honore, S. & Braguer, D. 2014. End-binding 1 protein overexpression correlates with glioblastoma progression and sensitizes to Vinca-alkaloids in vitro and in vivo. *Oncotarget,* 5**,** 12769.

Bhat, K. M. & Setaluri, V. 2007. Microtubule-associated proteins as targets in cancer chemotherapy. *Clinical Cancer Research,* 13**,** 2849-2854.

Bieling, P., Laan, L., Schek, H., Munteanu, E. L., Sandblad, L., Dogterom, M., Brunner, D. & Surrey, T. 2007. Reconstitution of a microtubule plus-end tracking system in vitro. *Nature,* 450**,** 1100-1105.

Blanchoin, L., Boujemaa-Paterski, R., Sykes, C. & Plastino, J. 2014. Actin Dynamics, Architecture, and Mechanics in Cell Motility. *Physiological reviews,* 94**,** 235-263.

Bobinnec, Y., Khodjakov, A., Mir, L., Rieder, C., Edde, B. & Bornens, M. 1998. Centriole disassembly in vivo and its effect on centrosome structure and function in vertebrate cells. *The Journal of cell biology,* 143**,** 1575-1589.

Bond-Smith, G., Banga, N., Hammond, T. M. & Imber, C. J. 2012. Pancreatic adenocarcinoma. *Bmj,* 344**,** e2476.

Brinkley, B. 1985. Microtubule organizing centers. *Annual review of cell biology,* 1**,** 145-172.

Bryant, C. S., Kumar, S., Chamala, S., Shah, J., Pal, J., Haider, M., Seward, S., Qazi, A. M., Morris, R. & Semaan, A. 2010. Sulforaphane induces cell cycle arrest by protecting RB-E2F-1 complex in epithelial ovarian cancer cells. *Molecular Cancer,* 9**,** 1.

Bu, W. & Su, L.-K. 2001. Regulation of microtubule assembly by human EB1 family proteins. *Oncogene,* 20.

Bu, W. & Su, L.-K. 2001. Regulation of microtubule assembly by human EB1 family proteins. *Oncogene,* 20**,** 3185-3192.

Buey, R. M., Mohan, R., Leslie, K., Walzthoeni, T., Missimer, J. H., Menzel, A., Bjelić, S., Bargsten, K., Grigoriev, I. & Smal, I. 2011. Insights into EB1 structure and the role of its C-terminal domain for discriminating microtubule tips from the lattice. *Molecular biology of the cell,* 22**,** 2912-2923.

Bulinski, J. C. & Gundersen, G. G. 1991. Stabilization and post-translational modification of microtubules during cellular morphogenesis. *Bioessays,* 13**,** 285-293.

Burbank, K. S. & Mitchison, T. J. 2006. Microtubule dynamic instability. *Current Biology,* 16**,** R516-R517.

Burridge, K. & Guilluy, C. 2016. Focal adhesions, stress fibers and mechanical tension. *Experimental cell research,* 343**,** 14-20.

Burridge, K. & Wennerberg, K. 2004. Rho and Rac take center stage. *Cell,* 116**,** 167-179.

Busch, K. E. & Brunner, D. 2004. The microtubule plus end-tracking proteins mal3p and tip1p cooperate for cell-end targeting of interphase microtubules. *Current Biology,* 14**,** 548-559.

Carvalho, P., Tirnauer, J. S. & Pellman, D. 2003. Surfing on microtubule ends. *Trends in cell biology,* 13**,** 229-237.

Cassimeris, L. 2009. Microtubule assembly: lattice GTP to the rescue. *Current Biology,* 19**,** R174-R176.

Chambers, A. F., Groom, A. C. & Macdonald, I. C. 2002. Metastasis: dissemination and growth of cancer cells in metastatic sites. *Nature Reviews Cancer,* 2**,** 563-572.

Chang, Y.-C., Nalbant, P., Birkenfeld, J., Chang, Z.-F. & Bokoch, G. M. 2008. GEF-H1 couples nocodazole-induced microtubule disassembly to cell contractility via RhoA. *Molecular biology of the cell,* 19**,** 2147-2153.

Charafeddine, R. A., Nosanchuk, J. D. & Sharp, D. J. 2016. Targeting Microtubules for Wound Repair. *Advances in wound care,* 5**,** 444-454.

Chhabra, E. S. & Higgs, H. N. 2007. The many faces of actin: matching assembly factors with cellular structures. *Nature cell biology,* 9**,** 1110-1121.

Clarke, J. D., Hsu, A., Yu, Z., Dashwood, R. H. & Ho, E. 2011. Differential effects of sulforaphane on histone deacetylases, cell cycle arrest and apoptosis in normal prostate cells versus hyperplastic and cancerous prostate cells. *Molecular nutrition & food research,* 55**,** 999-1009.

Cohen, J. H., Kristal, A. R. & Stanford, J. L. 2000. Fruit and vegetable intakes and prostate cancer risk. *Journal of the National Cancer Institute,* 92**,** 61-68.

Cole, N. B. & Lippincott-Schwartz, J. 1995. Organization of organelles and membrane traffic by microtubules. *Current opinion in cell biology,* 7**,** 55-64.

Conde, C. & Caceres, A. 2009. Microtubule assembly, organization and dynamics in axons and dendrites. *Nat Rev Neurosci,* 10**,** 319-32.

Creppe, C., Malinouskaya, L., Volvert, M.-L., Gillard, M., Close, P., Malaise, O., Laguesse, S., Cornez, I., Rahmouni, S. & Ormenese, S. 2009. Elongator controls the migration and differentiation of cortical neurons through acetylation of α-tubulin. *Cell,* 136**,** 551-564.

Danen, E. H. 2013. Integrins: an overview of structural and functional aspects.

De Ruijter, A., Van Gennip, A., Caron, H., Kemp, S. & Van Kuilenburg, A. 2003. Histone deacetylases (HDACs): characterization of the classical HDAC family. *Biochem. J,* 370**,** 737-749.

Deer, E. L., Gonzalez-Hernandez, J., Coursen, J. D., Shea, J. E., Ngatia, J., Scaife, C. L., Firpo, M. A. & Mulvihill, S. J. 2010. Phenotype and genotype of pancreatic cancer cell lines. *Pancreas,* 39**,** 425-35.

Des Georges, A., Katsuki, M., Drummond, D. R., Osei, M., Cross, R. A. & Amos, L. A. 2008. Mal3, the Schizosaccharomyces pombe homolog of EB1, changes the microtubule lattice. *Nature structural & molecular biology,* 15**,** 1102-1108.

Desai, A. & Mitchison, T. J. 1997. Microtubule polymerization dynamics. *Annual review of cell and developmental biology,* 13**,** 83-117.

Di Magliano, M. P. & Logsdon, C. D. 2013. Roles for KRAS in pancreatic tumor development and progression. *Gastroenterology,* 144**,** 1220-1229.

Dickinson, S. E., Rusche, J. J., Bec, S. L., Horn, D. J., Janda, J., Rim, S. H., Smith, C. L. & Bowden, G. T. 2015. The effect of sulforaphane on histone deacetylase activity in keratinocytes: Differences between in vitro and in vivo analyses. *Molecular carcinogenesis,* 54**,** 1513-1520.

Dimitrov, A., Quesnoit, M., Moutel, S., Cantaloube, I., Poüs, C. & Perez, F. 2008. Detection of GTP-tubulin conformation in vivo reveals a role for GTP remnants in microtubule rescues. *Science,* 322**,** 1353-1356.

Ding, N., Ping, L., Feng, L., Zheng, X., Song, Y. & Zhu, J. 2014. Histone deacetylase 6 activity is critical for the metastasis of Burkitt's lymphoma cells. *Cancer Cell Int,* 14**,** 139.

Dixit, R., Barnett, B., Lazarus, J. E., Tokito, M., Goldman, Y. E. & Holzbaur, E. L. 2009. Microtubule plus-end tracking by CLIP-170 requires EB1. *Proceedings of the National Academy of Sciences,* 106**,** 492-497.

Dominguez, R. & Holmes, K. C. 2011. Actin structure and function. *Annu Rev Biophys,* 40**,** 169-86.

Dompierre, J. P., Godin, J. D., Charrin, B. C., Cordelières, F. P., King, S. J., Humbert, S. & Saudou, F. 2007. Histone deacetylase 6 inhibition compensates for the transport deficit in Huntington's disease by increasing tubulin acetylation. *The Journal of neuroscience,* 27**,** 3571-3583.

Dong, X., Liu, F., Sun, L., Liu, M., Li, D., Su, D., Zhu, Z., Dong, J. T., Fu, L. & Zhou, J. 2010. Oncogenic function of microtubule end-binding protein 1 in breast cancer. *The Journal of pathology,* 220**,** 361-369.

Drubin, D. G. & Nelson, W. J. 1996. Origins of cell polarity. *Cell,* 84**,** 335-344.

Duellberg, C., Cade, N. I., Holmes, D. & Surrey, T. 2016. The size of the EB cap determines instantaneous microtubule stability. *eLife,* 5**,** e13470.

Dzhindzhev, N. S., Rogers, S. L., Vale, R. D. & Ohkura, H. 2005. Distinct mechanisms govern the localisation of Drosophila CLIP-190 to unattached kinetochores and microtubule plus-ends. *J Cell Sci,* 118**,** 3781-90.

Elner, S. G. & Elner, V. M. 1996. The integrin superfamily and the eye. *Investigative ophthalmology & visual science,* 37**,** 696-701.

Etienne-Manneville, S. 2013. Microtubules in cell migration. *Annual review of cell and developmental biology,* 29**,** 471-499.

Fehon, R. G., Mcclatchey, A. I. & Bretscher, A. 2010. Organizing the cell cortex: the role of ERM proteins. *Nature reviews. Molecular cell biology,* 11**,** 276.

Fimognari, C. & Hrelia, P. 2007. Sulforaphane as a promising molecule for fighting cancer. *Mutation Research/Reviews in Mutation Research,* 635**,** 90-104.

Frixione, E. 2000. Recurring views on the structure and function of the cytoskeleton: a 300-year epic. *Cell motility and the cytoskeleton,* 46**,** 73-94.

Fuchs, E. & Cleveland, D. W. 1998. A structural scaffolding of intermediate filaments in health and disease. *Science,* 279**,** 514-519.

Fuchs, E. & Weber, K. 1994. Intermediate filaments: structure, dynamics, function and disease. *Annual review of biochemistry,* 63**,** 345-382.

Furness, D. N., Hackney, C. M. & Steyger, P. S. 1990. Organization of microtubules in cochlear hair cells. *Journal of electron microscopy technique,* 15**,** 261-279.

Galjart, N. 2005. CLIPs and CLASPs and cellular dynamics. *Nat Rev Mol Cell Biol,* 6**,** 487-98.

Galjart, N. 2010. Plus-end-tracking proteins and their interactions at microtubule ends. *Current Biology,* 20**,** R528-R537.

Galjart, N. & Perez, F. 2003. A plus-end raft to control microtubule dynamics and function. *Current opinion in cell biology,* 15**,** 48-53.

Gamet-Payrastre, L., Li, P., Lumeau, S., Cassar, G., Dupont, M.-A., Chevolleau, S., Gasc, N., Tulliez, J. & Tercé, F. 2000. Sulforaphane, a naturally

occurring isothiocyanate, induces cell cycle arrest and apoptosis in HT29 human colon cancer cells. *Cancer Research,* 60**,** 1426-1433.

Ganguly, A., Yang, H., Sharma, R., Patel, K. D. & Cabral, F. 2012. The role of microtubules and their dynamics in cell migration. *Journal of Biological Chemistry,* 287**,** 43359-43369.

Garnham, C. P. & Roll-Mecak, A. 2012. The chemical complexity of cellular microtubules: tubulin post-translational modification enzymes and their roles in tuning microtubule functions. *Cytoskeleton,* 69**,** 442-463.

Gasper, A. V., Al-Janobi, A., Smith, J. A., Bacon, J. R., Fortun, P., Atherton, C., Taylor, M. A., Hawkey, C. J., Barrett, D. A. & Mithen, R. F. 2005. Glutathione S-transferase M1 polymorphism and metabolism of sulforaphane from standard and high-glucosinolate broccoli. *The American journal of clinical nutrition,* 82**,** 1283-1291.

Gelfand, V. I. & Bershadsky, A. D. 1991. Microtubule dynamics: mechanism, regulation, and function. *Annual review of cell biology,* 7**,** 93-116.

Gibbs, A., Schwartzman, J., Deng, V. & Alumkal, J. 2009. Sulforaphane destabilizes the androgen receptor in prostate cancer cells by inactivating histone deacetylase 6. *Proceedings of the National Academy of Sciences,* 106**,** 16663-16668.

Goldspink, D. A., Gadsby, J. R., Bellett, G., Keynton, J., Tyrrell, B. J., Lund, E. K., Powell, P. P., Thomas, P. & Mogensen, M. M. 2013. The microtubule end-binding protein EB2 is a central regulator of microtubule reorganisation in apico-basal epithelial differentiation. *Journal of cell science,* 126**,** 4000-4014.

Goldspink, D. A., Rookyard, C., Tyrrell, B. J., Gadsby, J., Perkins, J., Lund, E. K., Galjart, N., Thomas, P., Wileman, T. & Mogensen, M. M. 2017. Ninein is essential for apico-basal microtubule formation and CLIP-170 facilitates its redeployment to non-centrosomal microtubule organizing centres. *Open Biology,* 7**,** 160274.

Goley, E. D. & Welch, M. D. 2006. The ARP2/3 complex: an actin nucleator comes of age. *Nature reviews Molecular cell biology,* 7**,** 713-726.

Gundersen, G. G. & Bulinski, J. C. 1988. Selective stabilization of microtubules oriented toward the direction of cell migration. *Proceedings of the National Academy of Sciences,* 85**,** 5946-5950.

Gundersen, G. G., Kalnoski, M. H. & Bulinski, J. C. 1984. Distinct populations of microtubules: tyrosinated and nontyrosinated alpha tubulin are distributed differently in vivo. *Cell,* 38**,** 779-789.

Haggarty, S. J., Koeller, K. M., Wong, J. C., Grozinger, C. M. & Schreiber, S. L. 2003. Domain-selective small-molecule inhibitor of histone deacetylase 6 (HDAC6)-mediated tubulin deacetylation. *Proceedings of the National Academy of Sciences,* 100**,** 4389-4394.

Haines, R. L. & Lane, E. B. 2012. Keratins and disease at a glance. *J Cell Sci,* 125**,** 3923-3928.

Hallak, M. E., Rodriguez, J., Barra, H. & Caputto, R. 1977. Release of tyrosine from tyrosinated tubulin. Some common factors that affect this process and the assembly of tubulin. *FEBS letters,* 73**,** 147-150.

Hammond, J. W., Cai, D. & Verhey, K. J. 2008. Tubulin modifications and their cellular functions. *Current opinion in cell biology,* 20**,** 71-76.

Hawkins, T., Mirigian, M., Yasar, M. S. & Ross, J. L. 2010. Mechanics of microtubules. *Journal of biomechanics,* 43**,** 23-30.

Hayashi, I., Wilde, A., Mal, T. K. & Ikura, M. 2005. Structural basis for the activation of microtubule assembly by the EB1 and p150 Glued complex. *Molecular cell,* 19**,** 449-460.

Heald, R. & Nogales, E. 2002. Microtubule dynamics. *Journal of Cell Science,* 115**,** 3-4.

Henty-Ridilla, J. L., Rankova, A., Eskin, J. A., Kenny, K. & Goode, B. L. 2016. Accelerated actin filament polymerization from microtubule plus ends. *Science,* 352**,** 1004-1009.

Herrmann, H. & Aebi, U. 2004. Intermediate filaments: molecular structure, assembly mechanism, and integration into functionally distinct intracellular scaffolds. *Annual review of biochemistry,* 73**,** 749-789.

Hezel, A. F., Kimmelman, A. C., Stanger, B. Z., Bardeesy, N. & Depinho, R. A. 2006. Genetics and biology of pancreatic ductal adenocarcinoma. *Genes & development,* 20**,** 1218-1249.

Honnappa, S., Gouveia, S. M., Weisbrich, A., Damberger, F. F., Bhavesh, N. S., Jawhari, H., Grigoriev, I., Van Rijssel, F. J., Buey, R. M. & Lawera, A. 2009. An EB1-binding motif acts as a microtubule tip localization signal. *Cell,* 138**,** 366-376.

Horwitz, R. & Webb, D. 2003. Cell migration. *Current Biology,* 13**,** R756-R759.

Houghton, C. A., Fassett, R. G. & Coombes, J. S. 2013. Sulforaphane: translational research from laboratory bench to clinic. *Nutr Rev,* 71**,** 709-26.

Howard, J. & Hyman, A. A. 2003. Dynamics and mechanics of the microtubule plus end. *Nature,* 422**,** 753-758.

Howard, J. & Hyman, A. A. 2007. Microtubule polymerases and depolymerases. *Current opinion in cell biology,* 19**,** 31-35.

Howard, J. & Hyman, A. A. 2009. Growth, fluctuation and switching at microtubule plus ends. *Nature Reviews Molecular Cell Biology,* 10**,** 569-574.

Hubbert, C., Guardiola, A., Shao, R., Kawaguchi, Y., Ito, A., Nixon, A., Yoshida, M., Wang, X.-F. & Yao, T.-P. 2002. HDAC6 is a microtubule-associated deacetylase. *Nature,* 417**,** 455-458.

Huo, L., Li, D., Sun, X., Shi, X., Karna, P., Yang, W., Liu, M., Qiao, W., Aneja, R. & Zhou, J. 2011. Regulation of Tat acetylation and transactivation activity by the microtubule-associated deacetylase HDAC6. *Journal of Biological Chemistry,* 286**,** 9280-9286.

Hynes, R. O. 1992. Integrins: versatility, modulation, and signaling in cell adhesion. *Cell,* 69**,** 11-25.

Iimori, M., Watanabe, S., Kiyonari, S., Matsuoka, K., Sakasai, R., Saeki, H., Oki, E., Kitao, H. & Maehara, Y. 2016. Phosphorylation of EB2 by Aurora B and CDK1 ensures mitotic progression and genome stability. *Nature communications,* 7.

Jackson, S. J. & Singletary, K. W. 2004. Sulforaphane inhibits human MCF-7 mammary cancer cell mitotic progression and tubulin polymerization. *The Journal of nutrition,* 134**,** 2229-2236.

Jackson, S. J., Singletary, K. W. & Venema, R. C. 2007. Sulforaphane suppresses angiogenesis and disrupts endothelial mitotic progression and microtubule polymerization. *Vascular pharmacology,* 46**,** 77-84.

Janke, C. & Bulinski, J. C. 2011. Post-translational regulation of the microtubule cytoskeleton: mechanisms and functions. *Nat Rev Mol Cell Biol,* 12**,** 773-86.

Janke, C. & Bulinski, J. C. 2012. Post-translational regulation of the microtubule cytoskeleton: mechanisms and functions. *Nature Reviews Molecular Cell Biology,* 13**,** 276-276.

Janke, C., Rogowski, K., Wloga, D., Regnard, C., Kajava, A. V., Strub, J.-M., Temurak, N., Van Dijk, J., Boucher, D. & Van Dorsselaer, A. 2005. Tubulin polyglutamylase enzymes are members of the TTL domain protein family. *Science,* 308**,** 1758-1762.

Job, D., Valiron, O. & Oakley, B. 2003. Microtubule nucleation. *Current opinion in cell biology,* 15**,** 111-117.

Jordan, M. A., Thrower, D. & Wilson, L. 1991. Mechanism of inhibition of cell proliferation by Vinca alkaloids. *Cancer research,* 51**,** 2212-2222.

Jordan, M. A. & Wilson, L. 2004. Microtubules as a target for anticancer drugs. *Nature Reviews Cancer,* 4**,** 253-265.

Kalebic, N., Sorrentino, S., Perlas, E., Bolasco, G., Martinez, C. & Heppenstall, P. A. 2013. αTAT1 is the major α-tubulin acetyltransferase in mice. *Nature communications,* 4.

Kaverina, I., Krylyshkina, O. & Small, J. V. 1999. Microtubule targeting of substrate contacts promotes their relaxation and dissociation. *The Journal of cell biology,* 146**,** 1033-1044.

Kaverina, I., Krylyshkina, O. & Small, J. V. 2002. Regulation of substrate adhesion dynamics during cell motility. *The international journal of biochemistry & cell biology,* 34**,** 746-761.

Kaverina, I. & Straube, A. Regulation of cell migration by dynamic microtubules. Seminars in cell & developmental biology, 2011. Elsevier, 968-974.

Kellogg, D. R., Moritz, M. & Alberts, B. M. 1994. The centrosome and cellular organization. *Annual review of biochemistry,* 63**,** 639-674.

Kollman, J. M., Merdes, A., Mourey, L. & Agard, D. A. 2011. Microtubule nucleation by γ-tubulin complexes. *Nature Reviews Molecular Cell Biology,* 12**,** 709-721.

Komarova, Y., De Groot, C. O., Grigoriev, I., Gouveia, S. M., Munteanu, E. L., Schober, J. M., Honnappa, S., Buey, R. M., Hoogenraad, C. C. & Dogterom, M. 2009. Mammalian end binding proteins control persistent microtubule growth. *The Journal of cell biology,* 184**,** 691-706.

Komarova, Y., Lansbergen, G., Galjart, N., Grosveld, F., Borisy, G. G. & Akhmanova, A. 2005. EB1 and EB3 control CLIP dissociation from the ends of growing microtubules. *Molecular biology of the cell,* 16**,** 5334-5345.

Kroboth, K., Newton, I. P., Kita, K., Dikovskaya, D., Zumbrunn, J., Waterman-Storer, C. M. & Näthke, I. S. 2007. Lack of adenomatous polyposis coli protein correlates with a decrease in cell migration and overall changes in microtubule stability. *Molecular biology of the cell,* 18**,** 910-918.

Krylyshkina, O., Kaverina, I., Kranewitter, W., Steffen, W., Alonso, M. C., Cross, R. A. & Small, J. V. 2002. Modulation of substrate adhesion dynamics via microtubule targeting requires kinesin-1. *The Journal of cell biology,* 156**,** 349-360.

Kumar, M., Mehra, S., Thakar, A., Shukla, N. K., Roychoudhary, A., Sharma, M. C., Ralhan, R. & Chauhan, S. S. 2016. End Binding 1 (EB1) overexpression in oral lesions and cancer: A biomarker of tumor progression and poor prognosis. *Clinica Chimica Acta,* 459**,** 45-52.

L'hernault, S. W. & Rosenbaum, J. L. 1985. Chlamydomonas alpha-tubulin is posttranslationally modified by acetylation on the epsilon-amino group of a lysine. *Biochemistry,* 24**,** 473-478.

Lane, E., Rugg, E., Navsaria, H., Leigh, I., Heagerty, A., Ishida-Yamamoto, A. & Eady, R. 1992. A mutation in the conserved helix termination peptide of keratin 5 in hereditary skin blistering. *Nature,* 356**,** 244-246.

Lansbergen, G. & Akhmanova, A. 2006. Microtubule plus end: a hub of cellular activities. *Traffic,* 7**,** 499-507.

Lansbergen, G., Grigoriev, I., Mimori-Kiyosue, Y., Ohtsuka, T., Higa, S., Kitajima, I., Demmers, J., Galjart, N., Houtsmuller, A. B., Grosveld, F. & Akhmanova, A. 2006. CLASPs attach microtubule plus ends to the cell cortex through a complex with LL5beta. *Dev Cell,* 11**,** 21-32.

Lappalainen, P. 2016. Actin-binding proteins: the long road to understanding the dynamic landscape of cellular actin networks. *Molecular biology of the cell,* 27**,** 2519-2522.

Lauffenburger, D. A. & Horwitz, A. F. 1996. Cell migration: a physically integrated molecular process. *Cell,* 84**,** 359-369.

Li, D., Sun, X., Zhang, L., Yan, B., Xie, S., Liu, R., Liu, M. & Zhou, J. 2014. Histone deacetylase 6 and cytoplasmic linker protein 170 function together to regulate the motility of pancreatic cancer cells. *Protein & cell,* 5**,** 214-223.

Li, D., Xie, K., Wolff, R. & Abbruzzese, J. L. 2004. Pancreatic cancer. *The Lancet,* 363**,** 1049-1057.

Li, D., Xie, S., Ren, Y., Huo, L., Gao, J., Cui, D., Liu, M. & Zhou, J. 2011. Microtubule-associated deacetylase HDAC6 promotes angiogenesis by regulating cell migration in an EB1-dependent manner. *Protein & cell,* 2**,** 150-160.

Li, L. & Yang, X.-J. 2015. Tubulin acetylation: responsible enzymes, biological functions and human diseases. *Cellular and Molecular Life Sciences,* 72**,** 4237-4255.

Li, W., Miki, T., Watanabe, T., Kakeno, M., Sugiyama, I., Kaibuchi, K. & Goshima, G. 2011. EB1 promotes microtubule dynamics by recruiting Sentin in Drosophila cells. *The Journal of cell biology,* 193**,** 973-983.

Liu, H., Yue, J., Huang, H., Gou, X., Chen, S.-Y., Zhao, Y. & Wu, X. 2015. Regulation of Focal Adhesion Dynamics and Cell Motility by the EB2 and Hax1 Protein Complex. *Journal of Biological Chemistry,* 290**,** 30771-30782.

Louie, R. K., Bahmanyar, S., Siemers, K. A., Votin, V., Chang, P., Stearns, T., Nelson, W. J. & Barth, A. I. 2004. Adenomatous polyposis coli and EB1 localize in close proximity of the mother centriole and EB1 is a functional component of centrosomes. *Journal of cell science,* 117**,** 1117-1128.

Louvet-Vallée, S. 2000. ERM proteins: from cellular architecture to cell signaling. *Biology of the Cell,* 92**,** 305-316.

Luo, Y., Li, D., Ran, J., Yan, B., Chen, J., Dong, X., Liu, Z., Liu, R., Zhou, J. & Liu, M. 2014. End-binding protein 1 stimulates paclitaxel sensitivity in breast cancer by promoting its actions toward microtubule assembly and stability. *Protein & cell,* 5**,** 469-479.

Maitra, A. & Hruban, R. H. 2008. Pancreatic cancer. *Annual review of pathology,* 3**,** 157.

Manna, T., Honnappa, S., Steinmetz, M. O. & Wilson, L. 2008. Suppression of microtubule dynamic instability by the+ TIP protein EB1 and its modulation by the CAP-Gly domain of p150glued. *Biochemistry,* 47**,** 779-786.

Matsuyama, A., Shimazu, T., Sumida, Y., Saito, A., Yoshimatsu, Y., Seigneurin-Berny, D., Osada, H., Komatsu, Y., Nishino, N. & Khochbin, S. 2002. In vivo destabilization of dynamic microtubules by HDAC6-mediated deacetylation. *The EMBO journal,* 21**,** 6820-6831.

Maurer, S. P., Bieling, P., Cope, J., Hoenger, A. & Surrey, T. 2011. GTPγS microtubules mimic the growing microtubule end structure recognized by end-binding proteins (EBs). *Proceedings of the National Academy of Sciences,* 108**,** 3988-3993.

Maurer, S. P., Fourniol, F. J., Bohner, G., Moores, C. A. & Surrey, T. 2012. EBs recognize a nucleotide-dependent structural cap at growing microtubule ends. *Cell,* 149**,** 371-382.

Mimori-Kiyosue, Y., Grigoriev, I., Lansbergen, G., Sasaki, H., Matsui, C., Severin, F., Galjart, N., Grosveld, F., Vorobjev, I. & Tsukita, S. 2005. CLASP1 and CLASP2 bind to EB1 and regulate microtubule plus-end dynamics at the cell cortex. *The Journal of cell biology,* 168**,** 141-153.

Mimori-Kiyosue, Y., Grigoriev, I., Sasaki, H., Matsui, C., Akhmanova, A., Tsukita, S. & Vorobjev, I. 2006. Mammalian CLASPs are required for mitotic

spindle organization and kinetochore alignment. *Genes to Cells,* 11**,** 845-857.

Mitchison, T. & Kirschner, M. 1984. Dynamic instability of microtubule growth. *nature,* 312**,** 237-242.

Mitchison, T. & Salmon, E. D. 2001. Mitosis: a history of division. *Nature cell biology,* 3**,** E17-E21.

Mogensen, M. M. 1999. Microtubule release and capture in epithelial cells. *Biology of the Cell,* 91**,** 331-341.

Mogensen, M. M., Mackie, J. B., Doxsey, S. J., Stearns, T. & Tucker, J. B. 1997. Centrosomal deployment of γ-tubulin and pericentrin: Evidence for a microtubule-nucleating domain and a minus-end docking domain in certain mouse epithelial cells. *Cytoskeleton,* 36**,** 276-290.

Moore, P. S., Beghelli, S., Zamboni, G. & Scarpa, A. 2003. Genetic abnormalities in pancreatic cancer. *Molecular cancer,* 2**,** 1.

Morrison, E., Wardleworth, B., Askham, J., Markham, A. & Meredith, D. 1998. EB1, a protein which interacts with the APC tumour suppressor, is associated with the microtubule cytoskeleton throughout the cell cycle. *Oncogene,* 17**,** 3471-3478.

Moss, D. K., Bellett, G., Carter, J. M., Liovic, M., Keynton, J., Prescott, A. R., Lane, E. B. & Mogensen, M. M. 2007. Ninein is released from the centrosome and moves bi-directionally along microtubules. *Journal of cell science,* 120**,** 3064-3074.

Müller-Reichert, T., Chrétien, D., Severin, F. & Hyman, A. A. 1998. Structural changes at microtubule ends accompanying GTP hydrolysis: information from a slowly hydrolyzable analogue of GTP, guanylyl (α, β) methylenediphosphonate. *Proceedings of the National Academy of Sciences,* 95**,** 3661-3666.

Myzak, M. C., Hardin, K., Wang, R., Dashwood, R. H. & Ho, E. 2006. Sulforaphane inhibits histone deacetylase activity in BPH-1, LnCaP and PC-3 prostate epithelial cells. *Carcinogenesis,* 27**,** 811-819.

Nakata, T., Niwa, S., Okada, Y., Perez, F. & Hirokawa, N. 2011. Preferential binding of a kinesin-1 motor to GTP-tubulin–rich microtubules underlies polarized vesicle transport. *The Journal of cell biology,* 194**,** 245-255.

Nehlig, A., Molina, A., Rodrigues-Ferreira, S., Honore, S. & Nahmias, C. 2017. Regulation of end-binding protein EB1 in the control of microtubule dynamics. *Cell Mol Life Sci*.

Nogales, E. 2000. Structural insights into microtubule function. *Annual review of biochemistry,* 69**,** 277-302.

Nogales, E. & Wang, H.-W. 2006. Structural intermediates in microtubule assembly and disassembly: how and why? *Current opinion in cell biology,* 18**,** 179-184.

Nogales, E. & Wang, H.-W. 2006. Structural mechanisms underlying nucleotide-dependent self-assembly of tubulin and its relatives. *Current opinion in structural biology,* 16**,** 221-229.

North, B. J., Marshall, B. L., Borra, M. T., Denu, J. M. & Verdin, E. 2003. The human Sir2 ortholog, SIRT2, is an NAD+-dependent tubulin deacetylase. *Molecular cell,* 11**,** 437-444.

Nurnberg, A., Kitzing, T. & Grosse, R. 2011. Nucleating actin for invasion. *Nat Rev Cancer,* 11**,** 177-87.

Palazzo, A., Ackerman, B. & Gundersen, G. G. 2003. Cell biology (communication arising): tubulin acetylation and cell motility. *Nature,* 421**,** 230-230.

Parsons, J. T., Horwitz, A. R. & Schwartz, M. A. 2010. Cell adhesion: integrating cytoskeletal dynamics and cellular tension. *Nature reviews Molecular cell biology,* 11**,** 633-643.

Patel, K., Nogales, E. & Heald, R. 2012. Multiple domains of human CLASP contribute to microtubule dynamics and organization in vitro and in Xenopus egg extracts. *Cytoskeleton (Hoboken),* 69**,** 155-65.

Perez, F., Diamantopoulos, G. S., Stalder, R. & Kreis, T. E. 1999. CLIP-170 highlights growing microtubule ends in vivo. *Cell,* 96**,** 517-27.

Peris, L., Wagenbach, M., Lafanechère, L., Brocard, J., Moore, A. T., Kozielski, F., Job, D., Wordeman, L. & Andrieux, A. 2009. Motor-dependent microtubule disassembly driven by tubulin tyrosination. *The Journal of cell biology,* 185**,** 1159-1166.

Piperno, G., Ledizet, M. & Chang, X. 1987. Microtubules containing acetylated alpha-tubulin in mammalian cells in culture. *The Journal of cell biology,* 104**,** 289-302.

Pledgie-Tracy, A., Sobolewski, M. D. & Davidson, N. E. 2007. Sulforaphane induces cell type–specific apoptosis in human breast cancer cell lines. *Molecular cancer therapeutics,* 6**,** 1013-1021.

Pollard, T. D. & Borisy, G. G. 2003. Cellular motility driven by assembly and disassembly of actin filaments. *Cell,* 112**,** 453-465.

Pollard, T. D. & Cooper, J. A. 2009. Actin, a central player in cell shape and movement. *Science,* 326**,** 1208-1212.

Proulx, S., Landreville, S., Guérin, S. L. & Salesse, C. 2004. Integrin α5 expression by the ARPE-19 cell line: comparison with primary RPE cultures and effect of growth medium on the α5 gene promoter strength. *Experimental eye research,* 79**,** 157-165.

Raftopoulou, M. & Hall, A. 2004. Cell migration: Rho GTPases lead the way. *Developmental biology,* 265**,** 23-32.

Ran, J., Yang, Y., Li, D., Liu, M. & Zhou, J. 2015. Deacetylation of α-tubulin and cortactin is required for HDAC6 to trigger ciliary disassembly. *Scientific reports,* 5.

Raynaud-Messina, B. & Merdes, A. 2007. γ-tubulin complexes and microtubule organization. *Current opinion in cell biology,* 19**,** 24-30.

Reed, N. A., Cai, D., Blasius, T. L., Jih, G. T., Meyhofer, E., Gaertig, J. & Verhey, K. J. 2006. Microtubule acetylation promotes kinesin-1 binding and transport. *Current biology,* 16**,** 2166-2172.

Rehberg, M. & Gräf, R. 2002. Dictyostelium EB1 is a genuine centrosomal component required for proper spindle formation. *Molecular biology of the cell,* 13**,** 2301-2310.

Rice, L. M., Montabana, E. A. & Agard, D. A. 2008. The lattice as allosteric effector: Structural studies of αβ-and γ-tubulin clarify the role of GTP in microtubule assembly. *Proceedings of the National Academy of Sciences,* 105**,** 5378-5383.

Ridley, A. J. 2001. Rho GTPases and cell migration. *Journal of cell science,* 114**,** 2713-2722.

Rodriguez, O. C., Schaefer, A. W., Mandato, C. A., Forscher, P., Bement, W. M. & Waterman-Storer, C. M. 2003. Conserved microtubule–actin interactions in cell movement and morphogenesis. *Nature cell biology,* 5**,** 599-609.

Rogers, S. L., Rogers, G. C., Sharp, D. J. & Vale, R. D. 2002. Drosophila EB1 is important for proper assembly, dynamics, and positioning of the mitotic spindle. *The Journal of cell biology,* 158**,** 873-884.

Rymut, S. M. & Kelley, T. J. 2015. Broader implications: biological and clinical significance of microtubule acetylation. *Cell Health and Cytoskeleton,* 7**,** 71-82.

Saji, S., Kawakami, M., Hayashi, S.-I., Yoshida, N., Hirose, M., Horiguchi, S.-I., Itoh, A., Funata, N., Schreiber, S. L. & Yoshida, M. 2005. Significance of HDAC6 regulation via estrogen signaling for cell motility and prognosis in estrogen receptor-positive breast cancer. *Oncogene,* 24**,** 4531.

Sandblad, L., Busch, K. E., Tittmann, P., Gross, H., Brunner, D. & Hoenger, A. 2006. The Schizosaccharomyces pombe EB1 homolog Mal3p binds and stabilizes the microtubule lattice seam. *Cell,* 127**,** 1415-1424.

Seetapun, D., Castle, B. T., Mcintyre, A. J., Tran, P. T. & Odde, D. J. 2012. Estimating the microtubule GTP cap size in vivo. *Current Biology,* 22**,** 1681-1687.

Siegel, R. L., Miller, K. D. & Jemal, A. 2016. Cancer statistics, 2016. *CA: a cancer journal for clinicians,* 66**,** 7-30.

Sirajuddin, M., Rice, L. M. & Vale, R. D. 2014. Regulation of microtubule motors by tubulin isotypes and post-translational modifications. *Nature cell biology,* 16**,** 335-344.

Slep, K. C. & Vale, R. D. 2007. Structural basis of microtubule plus end tracking by XMAP215, CLIP-170, and EB1. *Molecular cell,* 27**,** 976-991.

Sprague, B. L., Pego, R. L., Stavreva, D. A. & Mcnally, J. G. 2004. Analysis of binding reactions by fluorescence recovery after photobleaching. *Biophysical journal,* 86**,** 3473-3495.

Stehbens, S. & Wittmann, T. 2012. Targeting and transport: how microtubules control focal adhesion dynamics. *J Cell Biol,* 198**,** 481-9.

Stehbens, S. J., Paszek, M., Pemble, H., Ettinger, A., Gierke, S. & Wittmann, T. 2014. CLASPs link focal-adhesion-associated microtubule capture to localized exocytosis and adhesion site turnover. *Nat Cell Biol,* 16**,** 561-73.

Stenner, F., Liewen, H., Göttig, S., Henschler, R., Markuly, N., Kleber, S., Faust, M., Mischo, A., Bauer, S. & Zweifel, M. 2013. RP1 is a phosphorylation target of CK2 and is involved in cell adhesion. *PloS one,* 8**,** e67595.

Straub, F. 1943. Actin, ii. *Stud Inst Med Chem Univ Szeged,* 3**,** 23-37.

Su, L.-K., Burrell, M., Hill, D. E., Gyuris, J., Brent, R., Wiltshire, R., Trent, J., Vogelstein, B. & Kinzler, K. W. 1995. APC binds to the novel protein EB1. *Cancer research,* 55**,** 2972-2977.

Su, L.-K. & Qi, Y. 2001. Characterization of human MAPRE genes and their proteins. *Genomics,* 71**,** 142-149.

Szent-Györgyi, A. G. 1953. Meromyosins, the subunits of myosin. *Archives of biochemistry and biophysics,* 42**,** 305-320.

Thomas, G. E., Sreeja, J. S., Gireesh, K., Gupta, H. & Manna, T. K. 2015. + TIP EB1 downregulates paclitaxel-induced proliferation inhibition and apoptosis in breast cancer cells through inhibition of paclitaxel binding on microtubules. *International journal of oncology,* 46**,** 133-146.

Torre, L. A., Bray, F., Siegel, R. L., Ferlay, J., Lortet-Tieulent, J. & Jemal, A. 2015. Global cancer statistics, 2012. *CA: a cancer journal for clinicians,* 65**,** 87-108.

Traka, M. H., Saha, S., Huseby, S., Kopriva, S., Walley, P. G., Barker, G. C., Moore, J., Mero, G., Den Bosch, F. & Constant, H. 2013. Genetic regulation of glucoraphanin accumulation in Beneforté® broccoli. *New Phytologist,* 198**,** 1085-1095.

Tran, A. D.-A., Marmo, T. P., Salam, A. A., Che, S., Finkelstein, E., Kabarriti, R., Xenias, H. S., Mazitschek, R., Hubbert, C. & Kawaguchi, Y. 2007. HDAC6 deacetylation of tubulin modulates dynamics of cellular adhesions. *Journal of cell science,* 120**,** 1469-1479.

Tschumperlin, D. J. 2013. Fibroblasts and the ground they walk on. *Physiology,* 28**,** 380-390.

Valiron, O., Caudron, N. & Job, D. 2001. Microtubule dynamics. *Cellular and Molecular Life Sciences CMLS,* 58**,** 2069-2084.

Van Meerloo, J., Kaspers, G. J. & Cloos, J. 2011. Cell sensitivity assays: the MTT assay. *Cancer cell culture: methods and protocols***,** 237-245.

Vasiliev, J. M., Gelfand, I., Domnina, L., Ivanova, O. Y., Komm, S. & Olshevskaja, L. 1970. Effect of colcemid on the locomotory behaviour of fibroblasts. *Development,* 24**,** 625-640.

Vaughan, K. T. 2005. TIP maker and TIP marker; EB1 as a master controller of microtubule plus ends. *J Cell Biol,* 171**,** 197-200.

Verhey, K. J. & Gaertig, J. 2007. The tubulin code. *Cell cycle,* 6**,** 2152-2160.

Verhoeven, D. T., Goldbohm, R. A., Van Poppel, G., Verhagen, H. & Van Den Brandt, P. A. 1996. Epidemiological studies on brassica vegetables and cancer risk. *Cancer Epidemiology Biomarkers & Prevention,* 5**,** 733-748.

Vicente-Manzanares, M., Webb, D. J. & Horwitz, A. R. 2005. Cell migration at a glance. *Journal of Cell Science,* 118**,** 4917-4919.

Vinzenz, M., Nemethova, M., Schur, F., Mueller, J., Narita, A., Urban, E., Winkler, C., Schmeiser, C., Koestler, S. A. & Rottner, K. 2012. Actin branching in the initiation and maintenance of lamellipodia. *J Cell Sci,* 125**,** 2775-2785.

Vitre, B., Coquelle, F. M., Heichette, C., Garnier, C., Chrétien, D. & Arnal, I. 2008. EB1 regulates microtubule dynamics and tubulin sheet closure in vitro. *Nature cell biology,* 10**,** 415-421.

Wang, H.-W. & Nogales, E. 2005. Nucleotide-dependent bending flexibility of tubulin regulates microtubule assembly. *Nature,* 435**,** 911-915.

Wang, Z., Li, Y., Ahmad, A., Banerjee, S., Azmi, A. S., Kong, D. & Sarkar, F. H. 2011. Pancreatic cancer: understanding and overcoming chemoresistance. *Nature Reviews Gastroenterology and Hepatology,* 8**,** 27-33.

Webster, D. R. & Borisy, G. G. 1989. Microtubules are acetylated in domains that turn over slowly. *Journal of Cell Science,* 92**,** 57-65.

Webster, D. R., Gundersen, G. G., Bulinski, J. C. & Borisy, G. G. 1987. Differential turnover of tyrosinated and detyrosinated microtubules. *Proceedings of the National Academy of Sciences,* 84**,** 9040-9044.

Westermann, S. & Weber, K. 2003. Post-translational modifications regulate microtubule function. *Nature Reviews Molecular Cell Biology,* 4**,** 938-948.

Wiese, C. & Zheng, Y. 2006. Microtubule nucleation: γ-tubulin and beyond. *Journal of cell science,* 119**,** 4143-4153.

Wilbur, J. D. & Heald, R. 2013. Cryptic no longer: arrays of CLASP1 TOG domains. *Structure,* 21**,** 869-70.

Wojnacki, J., Quassollo, G., Marzolo, M.-P. & Cáceres, A. 2014. Rho GTPases at the crossroad of signaling networks in mammals: impact of Rho-GTPases on microtubule organization and dynamics. *Small GTPases,* 5**,** e28430.

Wolfenson, H., Henis, Y. I., Geiger, B. & Bershadsky, A. D. 2009. The heel and toe of the cell's foot: a multifaceted approach for understanding the structure and dynamics of focal adhesions. *Cell motility and the cytoskeleton,* 66**,** 1017-1029.

Wozniak, M. A., Modzelewska, K., Kwong, L. & Keely, P. J. 2004. Focal adhesion regulation of cell behavior. *Biochimica et Biophysica Acta (BBA)-Molecular Cell Research,* 1692**,** 103-119.

Wu, X., Kodama, A. & Fuchs, E. 2008. ACF7 regulates cytoskeletal-focal adhesion dynamics and migration and has ATPase activity. *Cell,* 135**,** 137-148.

Yan, X., Habedanck, R. & Nigg, E. A. 2006. A complex of two centrosomal proteins, CAP350 and FOP, cooperates with EB1 in microtubule anchoring. *Molecular biology of the cell,* 17**,** 634-644.

Yang, X.-J. & Seto, E. 2008. The Rpd3/Hda1 family of lysine deacetylases: from bacteria and yeast to mice and men. *Nature reviews Molecular cell biology,* 9**,** 206-218.

Yu, I., Garnham, C. P. & Roll-Mecak, A. 2015. Writing and reading the tubulin code. *Journal of Biological Chemistry,* 290**,** 17163-17172.

Yue, J., Xie, M., Gou, X., Lee, P., Schneider, M. D. & Wu, X. 2014. Microtubules regulate focal adhesion dynamics through MAP4K4. *Developmental cell,* 31**,** 572-585.

Zhang, T., Zaal, K. J., Sheridan, J., Mehta, A., Gundersen, G. G. & Ralston, E. 2009. Microtubule plus-end binding protein EB1 is necessary for muscle cell differentiation, elongation and fusion. *J Cell Sci,* 122**,** 1401-1409.

Zhang, Y., Kwon, S., Yamaguchi, T., Cubizolles, F., Rousseaux, S., Kneissel, M., Cao, C., Li, N., Cheng, H.-L. & Chua, K. 2008. Mice lacking histone deacetylase 6 have hyperacetylated tubulin but are viable and develop normally. *Molecular and cellular biology,* 28**,** 1688-1701.

Zhang, Y., Li, N., Caron, C., Matthias, G., Hess, D., Khochbin, S. & Matthias, P. 2003. HDAC-6 interacts with and deacetylates tubulin and microtubules in vivo. *The EMBO journal,* 22**,** 1168-1179.

Zheng, J., Furness, D., Duan, C., Miller, K. K., Edge, R. M., Chen, J., Homma, K., Hackney, C. M., Dallos, P. & Cheatham, M. A. 2013. Marshalin, a microtubule minus-end binding protein, regulates cytoskeletal structure in the organ of Corti. *Biology open,* 2**,** 1192-1202.

Zilberman, Y., Ballestrem, C., Carramusa, L., Mazitschek, R., Khochbin, S. & Bershadsky, A. 2009. Regulation of microtubule dynamics by inhibition of the tubulin deacetylase HDAC6. *Journal of cell science,* 122**,** 3531-3541.